

Methods to improve the PVD coatability of brass by using diffusion barriers.

LANGER, Bernd.

Available from the Sheffield Hallam University Research Archive (SHURA) at:

<http://shura.shu.ac.uk/19940/>

A Sheffield Hallam University thesis

This thesis is protected by copyright which belongs to the author.

The content must not be changed in any way or sold commercially in any format or medium without the formal permission of the author.

When referring to this work, full bibliographic details including the author, title, awarding institution and date of the thesis must be given.

Please visit <http://shura.shu.ac.uk/19940/> and <http://shura.shu.ac.uk/information.html> for further details about copyright and re-use permissions.

SHEFFIELD HALLAM UNIVERSITY LIBRARY
CITY CAMPUS POND STREET
SHEFFIELD S1 1WB

12005

101 493 608 X



BRN: 367729

Sheffield Hallam University
REFERENCE ONLY

ProQuest Number: 10697246

All rights reserved

INFORMATION TO ALL USERS

The quality of this reproduction is dependent upon the quality of the copy submitted.

In the unlikely event that the author did not send a complete manuscript and there are missing pages, these will be noted. Also, if material had to be removed, a note will indicate the deletion.



ProQuest 10697246

Published by ProQuest LLC (2017). Copyright of the Dissertation is held by the Author.

All rights reserved.

This work is protected against unauthorized copying under Title 17, United States Code
Microform Edition © ProQuest LLC.

ProQuest LLC.
789 East Eisenhower Parkway
P.O. Box 1346
Ann Arbor, MI 48106 – 1346

**Methods to improve the PVD coatability of brass by using
diffusion barriers**

Dipl.-Ing. (FH) Bernd Langer

A thesis submitted in partial fulfilment of the requirements of
Sheffield Hallam University
for the degree of Master of Philosophy

September 1995

Collaborating Organisations:
Fa. Wieland-Werke AG, Ulm/Donau, Germany
Freiberg University, Germany

This thesis is submitted to Sheffield Hallam University for the degree of Master of Philosophy.

The research was carried out during the period from September 1994 to September 1995 at the Materials Research Institute at the Sheffield Hallam University.

Post graduate courses in Crystallography, Electron microscopy and X-Ray techniques I and Surface Engineering I (PVD hard coatings) were attended at the Materials Research Institute at Sheffield Hallam University.

The results obtained during the course of this work are to the best of my knowledge original, except where reference is made to other work.

This thesis or any part, has not been submitted for a degree at any other university.

Sheffield, September 1995

Contents

	page
(i) Abstract Englisch	i
German	ii
(ii) Acknowledgements	iii
1) Introduction, Aims and Objectives	1
2) Literature Review	3
2.1) Substrate and Coating Materials	3
2.1.1) Substrate	3
2.1.2) Brasses	3
2.1.2.1) Structure	4
2.1.2.2) Mechanical Properties	4
2.1.2.3) Hot Forming Abilities	4
2.1.2.4) Cold Forming Abilities	5
2.1.2.5) Recrystallisation	5
2.1.2.6) Cutting Properties	5
2.1.3) Used Brass Substrate, Properties and Softening Behaviour ..	6
2.1.4) Evaporation of Zinc (Zn) Under Vacuum	8
2.1.5) Coatings	9
2.1.5.1) Intermediate Barrier Layers	9
2.1.5.1.1) Diffusion Barrier	10
2.1.5.1.2) Corrosion Resistance	11
2.1.5.1.3) Appearance	12
2.1.5.2) Electroplated Intermediate Layers	15
2.1.5.3) PVD Intermediate Layers	18
2.1.5.4) Used PVD Layer Systems	18
2.1.5.4.1) Aluminium (Al)	18
2.1.5.4.2) Niobium (Nb)	18
2.1.5.4.3) Aluminium-Niobium (Al-Nb) Sputter Alloy	19
2.1.5.4.4) Copper-Aluminium (Cu-Al) Alloy	19
2.2) Principles of Corrosion	21
2.2.1) Theory of Corrosion	21
2.2.2) Corrosion of PVD Systems	22
2.3) Principles of Diffusion	24
2.4) Physical Vapour Deposition	26
2.4.1) Coating Deposition from Vapour Phase	26
2.4.2) Physical Vapour Deposition PVD	27
2.4.3) Coating Methods	28
2.4.4) Magnetic Field	30
2.4.4.1) Magnetic Fields on the Target	30
2.4.4.1.1) Balanced and Unbalanced Sputtering Systems	30
2.4.4.1.2) Random and Steered Arc	31
2.4.4.2) Magnetic Fields in the Chamber	31

2.4.5)	The HTC 1000-4 ABS TM	33
2.4.5.1)	The Vacuum Chamber of the ABS TM System	33
2.4.5.2)	The Cathods	34
2.4.6)	Target and Substrate Cleaning in the PVD Chamber	36
2.4.6.1)	Target Cleaning	36
2.4.6.2)	Substrate Cleaning	37
2.4.6.2.1)	Argon Glow Discharge Mode	37
2.4.6.2.2)	Metal Ion Etching Mode	38
2.4.7)	Coating in the PVD Chamber	40
2.4.8)	Coating Growth and Structure Zone Models	41
2.5)	Test Methods	43
2.5.1)	Glow Discharge Spectroscopy	43
2.5.2)	Adhesion and Scratch Test	45
2.5.3)	Hardness	49
2.5.4)	Indentation Adhesion Test	51
2.5.5)	X-Ray Diffraction	52
2.5.6)	Corrosion Tests	53
3)	Experimental Techniques	55
3.1)	Diffusion Test	55
3.2)	Sample Preparation	57
3.2.1)	Grinding and Polishing	57
3.2.2)	Precleaning	58
3.3)	Cleaning in the PVD Chamber	60
3.3.1)	Argon Ion Etching	60
3.3.2)	Metal Ion Etching.....	60
3.3.3)	Combined Argon and Metal Ion Etching.....	60
3.4)	Coating Processes	61
3.4.1)	Aluminium Diffusion Barrier (Al)	62
3.4.2)	Aluminium-Niobium Diffusion Barrier (Al-Nb(X))	62
3.4.3)	Copper-Aluminium Diffusion Barrier (CuAl8)	63
3.4.4)	Copper-Aluminium-Niobium Diffusion Barrier (CuAl8-Nb(X))	63
3.4.5)	Niobium Coatings (Nb)	63
3.5)	Testing methods	65
3.5.1)	SO ₂ Corrosion Test	65
3.5.2)	NH ₃ Porosity Test	66
3.5.3)	Glow Discharge Optical Emission Spectroscopy GDOES	67
3.5.4)	Scratch Adhesion Test	69
3.5.5)	Indentation Adhesion Test	70
3.5.6)	Coating Thickness Determination	72
3.5.7)	X-Ray Diffraction XRD	74
3.5.8)	Scanning Electron Microscope SEM / EDX	77
3.5.9)	Metallography	78
3.5.10)	Roughness Measurement	78
3.5.11)	Micro Hardness Test	79
3.5.12)	Bending Test	79
3.5.13)	Colour Measurement	79

4)	Results	80
4.1)	Diffusion Test of Uncoated Brass Substrate	80
4.2)	Precleaning of the Brass Substrate	81
4.3)	Cleaning in the PVD Chamber	82
4.3.1)	Argon Ion Etching	82
4.3.2)	Metal Ion Etching	82
4.3.3)	Combined Argon and Metal Ion Etching	83
4.4)	Coating Processes	84
4.4.1)	Aluminium Diffusion Barrier (Al).....	85
4.4.2)	Aluminium-Niobium + Niobium (AlNb(X)+Nb)	89
4.4.3)	Copper-Aluminium Diffusion Barrier (CuAl8)	92
4.4.4)	Copper-Aluminium-Niobium + Niobium (CuAl8Nb(X)+Nb)	95
4.4.5)	Niobium Coatings (Nb)	99
5)	Discussion	103
	Conclusions	107
	References	108
6)	Figures and Tables	114
	Appendix	170
	Product Data Sheet Henkel P3 Galvaclean 62	171
	Product Data Sheet Henkel RST	172
	EXCEL Work Sheet (XRD)	178
	EXCEL Example (Nb)	185

ABSTRACT

Previous work involving PVD coatings on brass has used a combination of multilayers consisting of electroplated films like nickel or chromium and deposited decorative PVD coatings like TiN, TiAlN or ZrN systems. The disadvantages of these systems are the combination of wet electrochemistry and high tech vacuum processes. Furthermore the allergic reaction to nickel and the toxic nature of Cr(VI) must be considered.

There is a need for intermediate layers to 'seal-off' the brass in order to avoid the evaporation of zinc in vacuum using a diffusion barrier. Furthermore the intermediate layers are required to act as a corrosion barrier.

This thesis reports on the development of PVD coatings on heat sensitive brass substrate materials utilising ABSTTM technology with Al, CuAl8 and Nb targets as vapour sources.

The brass pretreatment includes careful grinding, polishing and cleaning steps as well as steered arc metal ion etching using the above target materials. The coatings are produced at temperatures between 100 and 250°C in the unbalanced magnetron mode, including layers made from Al, Al-Nb, CuAl8, CuAl8-Nb and Nb.

Scratch adhesion and Rockwell indentation tests are found not to be directly applicable to the system of soft brass and ductile coating(s). Therefore a new classification for both scratch and indentation tests was defined. The best adhesion was shown by the CuAl8 coatings on brass. Corrosion tests showed good results for the Al coatings and poor results for the pure Nb coatings directly applied on brass. The best corrosion result was obtained with a CuAl8-Nb layer system. This layer system also offers very good barrier behaviour concerning Zn diffusion.

Other investigations like Glow Discharge Optical Emission Spectroscopy (GDOES), Scanning Electron Microscopy (SEM) imaging, Transmission Electron Microscopy (TEM) and X-ray Diffraction (XRD) were undertaken to characterise the new coating systems for brass.

PVD-Schichten auf Messing werden bisher durch Kombination von galvanischen Zwischenbeschichtungen wie Nickel oder Chrom und dekorativen PVD-Schichten wie TiN, TiAlN oder ZrN hergestellt. Der Hauptnachteil liegt in der Kombination von naßchemischen Techniken und 'high-tech' Vakuumprozessen. Weiterhin müssen heutzutage die Allergieprobleme durch Nickel und die Toxizität von Cr(VI) in Betracht gezogen werden.

Mit den Zwischenschichten wird das Messing versiegelt, um eine Zinkausdampfung bedingt durch den Zinkdampfdruck im Vakuum durch eine Diffusionsbarriere zu verhindern. Weiterhin dienen die Zwischenschichten als Korrosionsbarrieren zwischen dem unedlen Substratwerkstoff Messing und den zum Teil sehr viel edleren dekorativen Schichten wie z.B. Niob. Niob selbst zeichnet sich durch eine hervorragende Korrosionsbeständigkeit aus.

Diese Arbeit berichtet von der Entwicklung von PVD-Schichten auf temperaturempfindlichen Messingsubstraten hergestellt durch die ABSTTM (Arc-bond-sputtering) Technologie. Die verwendeten Beschichtungsquellen sind Al, CuAl8 und Nb Targets.

Die Messingvorbereitung umfasst sorgfältiges Schleifen, Polieren und Reinigen, wie auch 'steered arc' Metall-Ionen Ätzen mit den oben genannten Targetmaterialien. Die Schichten wurden im Temperaturbereich zwischen 100 und 250 °C mithilfe des unbalancierten Magnetrons abgeschieden. Die produzierten Schichten umfassen Al, Al-Nb, CuAl8, CuAl8-Nb und reines Nb.

Es stellte sich heraus, daß der Ritz-Adhäsionstest und Rockwell-Eindrucktest nicht direkt bei dem System »weiches Messing« und duktile Schichten angewendet werden können. Deshalb wurde eine neue Klassifizierung für den Scratch- und Rockwell-Test definiert. Die beste Adhäsion zeigten die CuAl8-Schichten. Korrosionstests zeigten gute Ergebnisse für die Al-Schichten und schlechte Ergebnisse für direkt aufgebraute Nb-Schichten. Das beste Korrosionsergebnis zeigte ein CuAl8/Nb-Schichtsystem. Diese Kombination wies auch hervorragende Eigenschaften als Diffusionsbarriere gegen die Zinkausdampfung auf.

Andere Untersuchungsmethoden wie GDOES Element-Tiefen-Profilanalyse, Raster-elektronenmikroskopie, teilweise Transmissionselektronenmikroskopie und Röntgen-diffraktometrie wurden bei der Entwicklung von neuen Dünnschichtsystemen auf Messing angewendet.

Acknowledgements

I would like to thank my Director of Studies and Supervisor Prof. Dr. W.-D. Münz for his advice and encouragement.

I would like to thank Dr. Bögel, Mr H.-K. Knirsch and Mr R. Koch of Wieland-Werke AG for the commitment and advice concerning brass materials.

I would also like to thank Prof. Dr. Bergner of Freiberg University for advice concerning diffusion in brass materials.

Special thanks go to Mr. W. Kalb of Gesellschaft für Elektrometallurgie mbH for the CuAl8 target.

A very special thanks goes to Simon Yakan, who tried to show me the differences in English English and German English and polished my thesis.

The author would like to thank everyone who has been involved in the work towards this thesis, particularly the staff of the Materials Research Institute at Sheffield Hallam University.

The biggest very very special thanks are going to my luuvly wife Margit, who didn't have too much of me during this busy time.

1.0 Introduction

Maslow [1] defined the needs of human beings and developed the so called »satisfaction of needs pyramid«. He found that mankind first has to substantiate fundamental desires like eating, drinking and reproduction. After these three basic needs people try to maintain their level of comfort, claim a place to cultivate and grow plants and keep animals. People already had cult objects for ritualistic acts. They were largely made from gold and bronzes. Nowadays, peoples' life styles are characterised in industrial countries by guaranteed feeding, long life expectancy and good leisure amenities. It is now, even more, that the need arises for decorative articles, like jewellery, watches and other consumer goods.

The aim of the consumer goods industry is to produce valuable and valuable looking products, even for daily life. These increasingly competitive conditions placed demands on companies for advanced technologies. Contrary to the production of goods made from elements like gold, silver and titanium there are the methods of using cheaper substrate materials in combination with decorative ennoblement. A good example is the use of brass materials with applied electroplated coatings. Considering the rise of human illnesses like nickel allergy and excited by the growing demand of better coatings made with newly available coating techniques, physical vapour deposited (PVD) coatings are favourite candidates for the production of such decorative coatings. PVD refers to a class of plasma based coating techniques. Metals, alloys or chemical compounds are transferred into the vapour phase by thermal energy or particle bombardment in a high vacuum and condense onto the substrates. Using the PVD technique, not only decorative but also functional coatings can be produced. Important representatives of this family are corrosion barriers, wear resistant and hard coatings as well as high temperature coatings. It is important to optimise functional and aesthetic properties like resistance to corrosion, resistance to wear, good coating adhesion, control of colours and to avoid allergic reactions. Decorative coatings on brass find their applications in watch cases, spectacle frames, engineering components for use in videos and photographic apparatus, precision components in electromechanical applications and the writing tool industry. Physical vapour deposited (PVD) coatings are now being used in many sectors of industry on account of both their favourable wear and decorative properties [2, 3]. Thus hardwearing, gold coloured titanium nitride (TiN) coatings are widely used in the advanced machine tool industry on account of their wear properties and in the horological industry in the manufacture of good quality watches on account of their aesthetic appearance.

A limitation for the use of PVD coatings is that they show poor adhesion when applied directly to brass components. This is a significant limitation in the use of PVD coatings since many small components are manufactured from brass on account of its ready formability and machining properties. The problem of poor adhesion associated with

PVD coatings applied directly on brass is due to, (i) evaporation of zinc from the brass surface and (ii) the formation of zinc oxide at the substrate / coating interface during the course of the coating process.

The conventional approach to solving the problem is to "seal off" the brass surface using an electrodeposited coating. Coatings which have been used for this purpose include chromium, nickel and nickel-palladium deposits as well as duplex copper-nickel coatings [4, 5]. Unfortunately, the use of all these have some unfavourable aspect: Electroplated chromium is to be avoided from an environmental point of view as is that of nickel on account of its adverse allgenic properties. The use of electroplated copper has two drawbacks since when used alone it does not provide appropriate surface for PVD coatings and its use can lead to the diffusion of zinc from the brass substrate into the coating with the resulting formation of brittle copper-zinc intermetallic compounds. The intermetallics can then cause poor adhesion of the PVD coating.

An elegant solution to the problems associated with the use of PVD coatings on brass would be to form an intermediate barrier layer by the PVD process which would seal off the brass surface and prevent zinc diffusion from the substrate. This would not only solve the adhesion problem but eliminate the use of environmentally unfriendly wet electroplating steps. Two possible barrier coatings obtainable using PVD process appear worthy of consideration, either a thin aluminium or a copper-aluminium coating. The latter has the additional advantage that it has a gold colour when formed with the appropriate composition and might therefore act as a decorative coating on its own right.

Using the above approach it should be possible to develop multilayer coatings suitable for decorative purposes which could be formed on small 60:40 brass components. Typical coatings which might be formed using such a multi-stage process include Al/Nb, AlNb/Nb, CuAl8/Nb, CuAl8Nb/Nb and Nb coatings. The use of such decorative coatings would be subjected to their meeting the usual corrosion and compatibility tests associated with the particular sectors of industry where they are to be used, for example in watch and jewellery manufacture [6, 7].

The aims and objectives of the research would therefore be to deposit intermediate barrier PVD coatings onto brass components to seal-off the brass.

CHAPTER 2: Literature Review

2.1 Substrate and Coating Materials

Decorative hard coatings can be produced in various colours. The colour systems used are for example CrN_x (metallic grey), TiN_x (light yellow - gold colour - brownish yellow), TiC_xN_y (gold colour - reddish brown, adjustable to any gold colour tone), TiAlN (anthracite) and TiZrN_x (golden colours) [2]. To solve the natural tarnishing problem of brass, which leads to a decreasing reflectance, decorative ZrN coatings are used to obtain brass colours [8]. These decorative coatings have a high hardness, so that a coating thickness of 0.5 to 1 μm is sufficient to obtain the same life time as that obtained from a 20 μm thick electroplated gold coating [11]. Applying a coating that always contains pores and pinholes on a substrate means that the corrosion behaviour must be considered, especially if the potential difference is large.

2.1.1 Substrate

Decorative coatings on corrosive resistant substrate materials like titanium or austenitic chromium-nickel steels have been well known for years. These substrate materials have the disadvantage of extreme hardness, making it difficult to machine them like drilling, milling, grinding or polishing. The build-in of surface structures is extremely complex and makes it not economically viable. It is desirable to use soft substrate materials for better teeming, machining and surface finishing, although it is less corrosion resistance [9, 10]. Brass itself is softer than particles of dust [11] and is, without manipulation not usable for decorative purposes, but the surface properties are independent of the volume properties if a coating is applied.

2.1.2 Brasses (Cu-Zn Alloys)

Cu-Zn alloys ("brasses") are the most important group of the commercial copper alloys [12, 13]. They have both good cold-workability and machinability, combined with relatively high corrosion resistance. The designation "brass" relates to Cu-Zn alloys having more than 50 weight% Cu. Brasses may contain small amounts of other elements e.g. up to 4 % Pb, Ni and Sn. The phase diagram for the binary Cu-Zn system is shown in figure 6.57c. Three classes of brass are used commercially: the α -, $\alpha+\beta$ - and β brasses.

2.1.2.1 Structure



Figure 2.1: Structure of an α -brass, 100 x

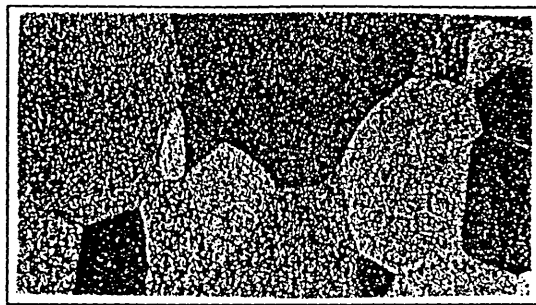


Figure 2.2: Structure of a β -brass, 100 x

A closer look at the Cu-Zn phase diagram (figure 6.57c) shows the increasing solubility for Zn in the fcc α -solid solution crystal. The bcc β -mixed crystal changes into the β' -phase below 460 °C. The cubic γ -phase is very brittle. The δ -, ϵ - and η -phases have a hexagonal lattice like pure Zn. Due to the brittleness of the brasses with the appearance of the γ -phase only alloys up to 50 % Zn are technically used. We distinguish the α -brasses (figure 2.1) with straight limited polygons and twinning bands and the β -brasses (figure 2.2) with no twinning bands.

2.1.2.2 Mechanical Properties

With increasing Zn content in the α -area the tensile strength and hardness increases slightly, whereas the ductility increases greatly. Contrary to this the tensile strength and hardness increases with the appearance of the β -phase, but the ductility decreases. The highest tensile strength is for pure β -brass.

2.1.2.3 Hot Forming Abilities

If the Pb concentration is less than 1 % in an (α + β)-brass and less than 0.02% in an α -brass the hot forming ability is very good. The reason for this is that β -mixed crystals can accommodate up to 1 % Pb whereas the α -mixed crystals can only hold a minimal amount. Hence the Pb is at the grain boundaries of α -brasses and makes it brittle at deforming temperatures above 329 °C. Forming under pressure from all sides like impact forging or extrusion moulding, the lead concentration has less influence. Bi, which is not at all soluble in α -brass makes hot forming impossible at a concentration of 0.005%.

2.1.2.4 Cold Forming Abilities

($\alpha+\beta$)-brass is not suitable but α -brass is very suitable for cold forming. The tensile strength increases greatly much but the ductility decreases significantly. For example the breaking elongation decreases in a cold forming process of a CuZn37 F 30 ($R_m = 300 \text{ N/mm}^2$) via the half hard and the hard into the spring hard condition from 45 % to 2 %.

2.1.2.5 Recrystallisation

The recrystallisation of brasses starts at higher temperatures than for Cu, despite the melting point being lower. Annealing to a special hardness is done at a temperature between 300 and 450 °C, annealing to eliminate the strain hardening completely between 450 and 600 °C. Figure 2.3 shows a recrystallisation diagram for CuZn37.

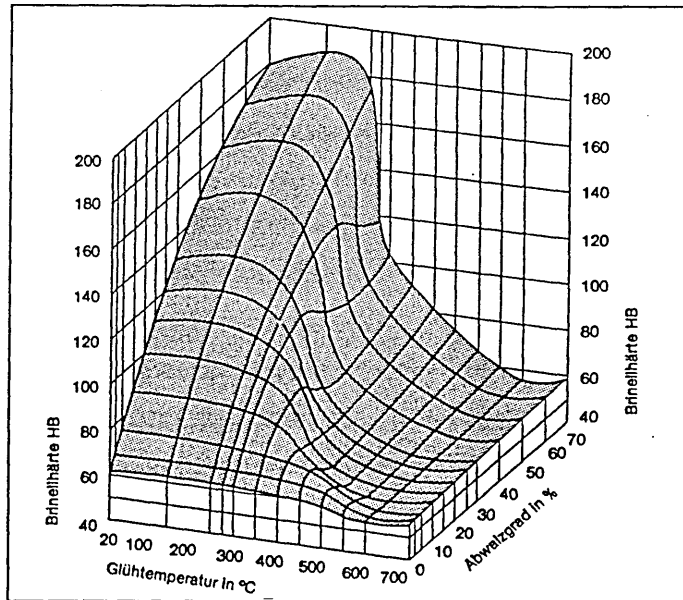


Figure 2.3: Recrystallisation diagram for CuZn37
[12]

2.1.2.6 Cutting Properties

Brasses are very suitable for rapid machining. ($\alpha+\beta$)-brasses are more suitable for rapid machining than β -brass. Only 0.01 % Pb leads to an improvement of the cutting property of α -brass, but deteriorates the hot forming properties. To make the removal of material on automates easier, up to 3 % Pb is alloyed into α - and ($\alpha+\beta$) -brasses. The finer the distribution of Pb, the better the effect.

2.1.3 Used Brass Substrate, Properties and Softening Behaviour

The substrate used in this work is 60:40 brass. The analysis was done using the X-Ray Fluorescence method (XRF) on a Philips PW2400 [14]. The result is shown in table 2.1.

element	Cu	Zn	Pb	Sn	Ni	Fe	Mg
conc. in mass %	61.6	36.52	1.52	0.103	0.06	0.17	0.015

Table 2.1: Analysis of the brass substrate

From the analysis this material can be recognised as CuZn36Pb1.5*, which is equivalent to the UK BS CZ118 / material number 2.0331 / USA UNS Nr. C34000**. The following properties are typical for this brass [12] (tables 2.2, 2.3 and 2.4):

Characteristic Quantities	Condition			
	soft	half hard	hard	spring hard
tensile strength R_m [N/mm ²]	340	400	490	550
tensile yield strength [N/mm ²]	130	300	450	520
elongation A_{10} [%]	50	30	12	3
hardness HB	75	115	140	160
shearing strength [N/mm ²]	250	300	330	
notched bar impact value [J/cm ²]	47			
modulus of elasticity [[kN/mm ²] = 110		modulus of torsional shear [kN/mm ²] = 39		

Table 2.2: Mechanical properties [12]

density [g/cm ³]	8.45
melting range [°C]	902-915
electrical conductivity [m/Ωmm ²]	14.7
average temp. coeff. of electrical resistance [K ⁻¹]	0.0014
caloric conductivity [W/mK]	113
thermal expansion coeff. [10 ⁻⁶ /K]	20.4

hot forming ability	good
cold forming ability	good
cutting property index (CuZn39Pb3 = 100)	80
polishable	good
electroplateable	very good
soft solderable	very good
hard solderable	moderate
weldability	
gas	qualified
inert gas	qualified
resistance	moderate
soft annealing temp. [°C]	450-650
relaxation temp. [°C]	200-300
hot forming temp. [°C]	750-800

Table 2.3: Physical properties

Table 2.4: Treatment properties

* following DIN 17 660 (copper wrought alloy Cu-Zn without additives, with lead additives, with further additives)

** UNS Unified Numbering System of the Copper Development Association CDA

This described alloy is mainly used if there is the need for metal removal and non-cutting shaping like pressing, bending or imprinting. Figure 2.4 shows the softening behaviour after cold deforming.

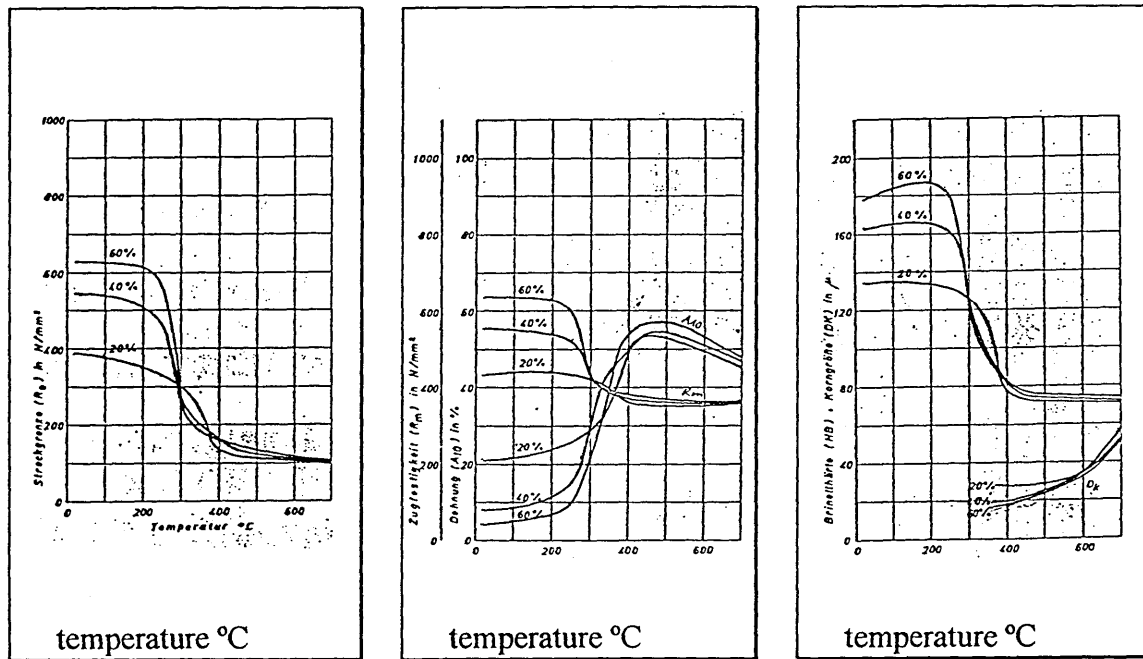


Figure 2.4: Softening behaviour at long time annealing (4 hours) after different cold deforming (20%, 40%, 60%)

(left) tensile yield strength $R_{p0.2}$
 (centre) tensile strength R_m / elongation A_{10}
 (right) hardness HB / grain size D_k

At temperatures greater than 250 °C to 300 °C all properties change dramatically. The hardness will increase to a maximum until this point, whereas R_m and $R_{p0.2}$ decreases slowly, afterwards rapidly to a minimum.

2.1.4 Evaporation of Zn Under Vacuum

The vapour pressure of Zn has been studied by several investigators and summarised by *Cominco* (1956) and a simple empirical equation developed [15].

$$\lg(p/1.33322) = (-6888/T) + 8.888 \quad \dots 1)$$

with vapour pressure p in mbar and temperature T in K.

Under conditions of high vacuum (10^{-5} to 10^{-6} mbar), metals begin to evaporate rapidly when the temperature rises to the point where the vapour pressure is higher than approximately 10^{-2} mbar [16]. The Zn vapour pressure at 200 °C is calculated with equation 1 to 2.79×10^{-6} mbar. Figure 2.5 shows the vapour pressure of several metals as a function of temperature. During the evaporation process, in equilibrium conditions, molecules are continuously passing from the condensed phase to the vapour phase, but at the same time, another stream of molecules is condensing out of the vapour and the two processes balance each other [16, 17].

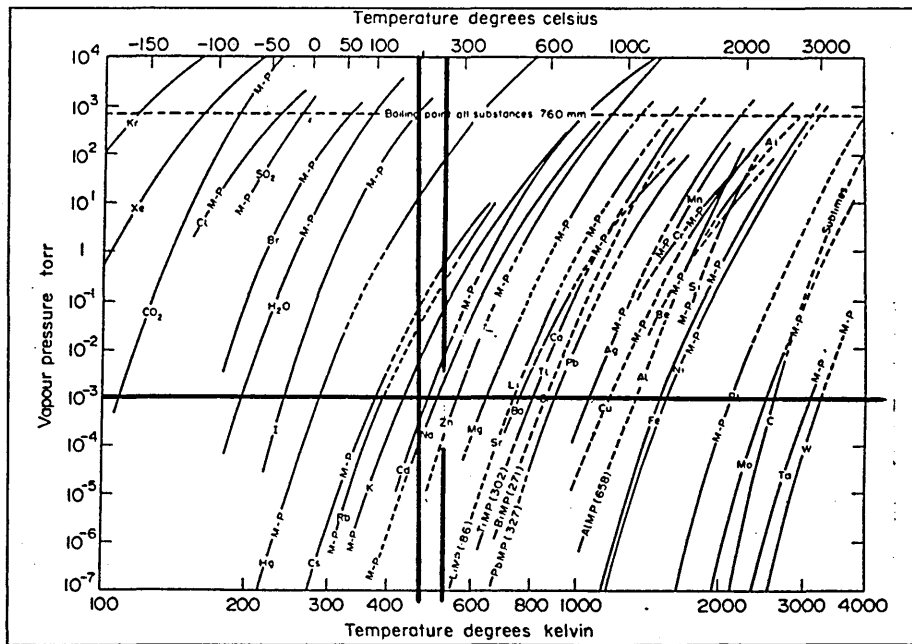


Figure 2.5: Vapour pressure data for several materials [16]

At a PVD total pressure of around 2.5×10^{-3} mbar evaporation of Zn is therefore negligible by keeping the temperature lower than 200 to 250 °C as the partial pressure of Zn is only 2.8×10^{-6} mbar. This area is marked in figure 2.5 with the bold lines.

2.1.5 Coatings

Decorative electroplated coatings are classified in a guideline of the "Deutsche Gesellschaft für Galvano- und Oberflächentechnik" [18]. The requirements include the corrosion resistance, wear and coating thickness. Up to now there are no guidelines available for hard decorative coatings, but these films have to cope at least with the electroplated alternative [19]. In contrast to electroplating processes, when coating three dimensional products by PVD there are problems with the microstructure and associated properties like colour, density and adhesion caused by different angle-of-incidence flux effects [20]. This problem can be partly overcome by substrate rotation (1 to 3 fold rotation).

Coatings applied on substrate surfaces can be distinguished as intermediate layers and decorative layers on top. Interesting PVD coatings for investigation are the carbides, nitrides and oxides of certain elements of the fourth to the sixth group of the periodic table of the elements, e.g. Ti, Zr, Hf, Nb, Ta, Cr, W and their alloys [9, 21]. The coating properties differ between bulk-, powder- and sputter alloys.

Decorative hard coatings are characterized by the following properties [2]:

- (i) controlled final colours (reproducible, uniform colour tone)
- (ii) resistance to wear
- (iii) resistance to corrosion
- (iv) cost effectiveness

In an ideal situation of hard decorative coatings there is no need for an intermediate layer. But to get coatings with low pore concentration and sufficient adhesion, multilayers are required. The single coatings have special functions such as: improvement of the adhesion, diffusion barrier, smoothing the surface, appearance [22], compensation of various thermal expansion coefficients and corrosion barrier [23].

2.1.5.1 Intermediate Barrier Layers

PVD coatings may not be applied directly to Zn or Cd containing substrate materials, because of the high vapour pressure of these elements. Therefore there is the need for intermediate barrier layers to vacuum tight seal these elements [24].

The intermediate barrier layer must have the following properties, which are explained below:

- diffusion barrier for Zn and Pb
- improvement or changing of the surface structure of the substrate material [10] and a good surface finish

-
- minimum of pores
 - integrity of the corrosion resistance of the entire system
 - low cost
 - no allergenic reaction
 - appropriate for following PVD processes [6]
 - adhesion of the undercoating to the substrate material
 - mechanical accommodation of the system PVD-layer / intermediate layer / substrate [9]

2.1.5.1.1 Diffusion Barrier

As already mentioned, one function of barrier layers is the prevention of diffusion. When coating brass by PVD there is the need for a diffusion barrier, because brass is a heat sensitive material. Interdiffusion occurs between base materials and the coating, resulting in the formation of intermetallic compound layers. Mainly in storage and operation, harmful elements, such as Zn, diffuse from the brass substrate to the coating and change the composition. The presence of Zn at the surface results in the formation of atmospheric corrosion products. The induced oxide films upon the surface affect properties, resulting in poor adhesion and discolouration of coatings directly deposited to brass. Consequently an intermediate barrier layer is used as a diffusion barrier to minimise this effect [25]. The deleterious effect of Zn diffusion can be reduced by thicker coatings as intermediate layers which inhibit diffusion [26].

An ideal diffusion barrier should avoid the interdiffusion between the brass substrate and the decorative top layer and should neither interact with the substrate material nor with the coating. The aims of a diffusion barrier layer are:

- (i) to avoid extreme diffusion zones [27]
- (ii) to reduce the the rate of growth of interfacial compound layers [25]
- (iii) to reduce the extent of diffusion into a coating [25]
- (iv) to avoid pores caused by the Kirkendall effect at high temperatures [27]

In reality there is always diffusion of substrate and coating material into the diffusion barrier and diffusion of the barrier layer material into the substrate and coating - depending on the diffusion barrier itself, the diffusion coefficients, the exposure time and temperature.

To act as a diffusion barrier, the barrier layer material should have the following properties

- (i) a high melting point compared to the diffusant
- (ii) a dense structure, if possible fcc or hex with an atomic packing density of 74%
- (iii) formation of intermetallic phases and miscibility gaps

R. Pinnel et al [28] investigated the mechanism of diffusion barriers by qualitative evaluation of frequently used nickel layers. Results demonstrated that the nickel layer retards but does not block the transport of the substrate material to the top coating. They found that the effectiveness of Ni in retarding the out-diffusion of Cu to an Au surface has its basis in the miscibility gap within the Au-Ni system. This restricted range of solid solubility which limits the concentration increase of Au in Ni and vice versa significantly affects the interdiffusion behaviour. The time necessary to diffuse Cu to the Au surface at a given temperature is longer with the Ni layer than without it. Finally, increasing the nickel thickness increases the time necessary for Cu penetration to the surface.

The reason for the miscibility gap within the system Au-Ni is the difference in the lattice parameter of 13.6 %. The limit of lattice parameter differences is $\pm 14\%$ [29], given by lattice stresses resulting in elongation and contraction caused by smaller or bigger substituted atoms. This effect increases with higher concentrations of the alloyed atoms. There is also an influence of the valence to the formation of mixed crystals and miscibility gaps.

2.1.5.1.2 Corrosion Resistance

It is reported that PVD coatings directly deposited on brass do not offer sufficient corrosion protection [20]. An anti-corrosive overlay and an underlying decorative coating would be the best solution for this problem, but anti-corrosive coatings deposited by PVD that are acceptable from engineering and economic view points do not yet exist [2]. Hence intermediate layers should offer a high corrosion resistance, which is closely connected with the surface quality of the substrate, and various coating defects like pinholes and pores. Depending on the choice of intermediate layer materials on brass and the decorative coating with respect to their electrochemical potential the coatings are more or less corrosion resistant. The density of the coating can be optimized by changing process parameters to minimize the quantity and quality of the defects. Especially the growth morphology is affected by factors like the substrate bias voltage. The growth rate of the coating and the substrate current density are known to be important [7, 23, 30]. PVD coatings offer a better corrosion resistance with increasing thickness and more fine-grained films. Ti-N ternary systems show a better corrosion behaviour when combined with Cr, Y or Pd. Al was found to deteriorate the corrosion resistance. It has been found that this is due to the structure and chemical composition changes [30].

2.1.5.1.3 Appearance

The appearance of the coatings is especially important for decorative purposes. This is mainly influenced by the substrate itself, the preparation including precleaning and the coating process, since it is reported that PVD coatings directly applied on brass have a matt appearance.

(i) substrate: To get the good quality surface necessary to produce valuable products, substrates made from special quality brasses (excluding recycled materials) are required. Recycled brass very often contains trace elements like Fe and Co, which lead to unsightly spots in electroplating and PVD. There is also the effect of the two brass phases α and β which are attacked differently by wet chemistry precleaning and ion etching processes, leading to a decreasing brilliance [20].

(ii) preparation and precleaning: Perfect substrate preparation and precleaning is essential for every process. Scratches and impurities like greases, oils, machining-, grinding- and polishing residues, thin oxide layers, adsorbed carbon hydrides and dust are often the origin of faults and coatings with bad qualities like reduced adhesion and pores in the coating. Corrosion will occur preferentially at these places [22]. Also important is that with increasing roughness of the substrate surface the brightness is decreasing, and only on perfect polished surfaces an optimum of brilliance is achievable [21]. Consequently there is the need for an individual precleaning program of the substrate, because the adhesion between the coating and the metal surface depends mainly on the interface morphology, the nucleation, chemical reactions and diffusion processes in the interface region. Generally alkaline baths serve for removal of oils, greases and other organic residues, whereas acid baths serve to pickle and activate the surface as well as to neutralize the alkaline residues. Degreaser should not contain silicates or borates because of a possible formation of films on copper alloys [31]. Between all baths a rinsing in deionised water is necessary to remove the residues of the prior cleaning step.

Pb is added to brass up to 3 wt% as chip breaker. It is known from literature that leaded brass is sometimes not appropriate for a following electroplating process, because the surface is smeared with Pb caused by the substrate preparation, leading to bad adhesion of the coating and bubbles. K.- H. Knirsch and H. Sick [32] investigated systematically the adhesion of electroplated Ni coatings on leaded brass depending on various mechanical preparation methods, precleaning steps and coating procedures. The adhesion test was performed as a bending test of tubes and an optical investigation of the delaminations occurred. The failure mechanism can be explained by smeared Pb. PbSO_4 formed by sulfates from the electrolytes and lead at the surface are found not to

be a failure reason. Therefore it seems to be important that sharp cutting tools are used to machine the substrate in order to avoid any smearing of Pb. Furthermore, a pickle step should be included in the precleaning to get rid of smeared lead, using HNO_3 or HBF_4 .

The atomiser test [22], which was described previously by K. Wittel in 1981, is able to examine the precleaning. The cleaned and cooled room temperature sample needs to be sprayed by an atomiser, until the surface is covered with a thin water film. Under the microscope small drops are visible, separated by smaller or bigger non wetted areas. Only if the entire area is covered with drops is the precleaning sufficient. At non wetted areas the activation of the surface is insufficient, leading to poor adhesion of the drops and the surface.

(iii) coating process: The structure to be obtained to get a shiny, bright surface is the transition zone T from the Thornton diagram. Hence it is important to investigate the appropriate process temperature depending on the applied bias voltage and chamber pressure (see chapter 2.4.8).

2.1.5.2 Electroplated Intermediate Layers

Satisfying results for intermediate layers on brass are, up to now, only achievable using a combination of electro plated and PVD layers, if there is the need for shiny coatings on rough surfaces with a long life time [4, 22]. A typical schematic process of combined electroplated intermediate layer and PVD decorative hard coating is given in Figure 2.6.

The samples have to be prepared mechanically, followed by a wet precleaning. To produce a clean and active metal surface, the oxids, greases, dirt such as dust and residues from grinding and polishing must be eliminated. The methods used for degreasing and cleaning are organic solvents or water based cold- and hot detergents, followed by chemical or electrolytic degreasing procedures [9, 10]. A galvanic barrier layer has to be applied, followed by a cleaning step prior to the PVD coating process.

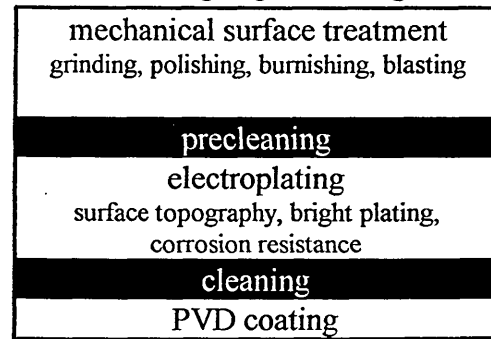


Figure 2.6: Schematic combined process

By electroplating, the surface structure can be changed in wide ranges, using the following features:

- (i) the structure and coating composition is given by the electrolyte composition [6]
- (ii) the surface roughness can be smoothed having a rather thick coating on scratched surfaces

The main disadvantages of electroplated intermediate layers and the use for combined electroplating and PVD coatings are:

- (i) Ni-coatings are passivating very fast, resulting in poor adhesion of PVD coatings [10]
- (ii) Electroplating processes can involve hazardous waste products
- (iii) Electroplating combined with PVD is a multistage process, including wet chemistry and high vacuum technology.
- (iv) Ni is known as a material causing allergical reactions.
- (v) metastable phases in coating systems can transform under heat influence, resulting in segregations and hence limiting the substrate temperature at a following process step [23].

Various types of electroplated intermediate layers were examined.

Ni: systems with hard coatings directly applied on Ni are not resistant for contact corrosion. Only at a coating thickness of around 20 μm are good results achievable. Having around 50 μm electroplated Ni the coatings become brittle, resulting in the loss of the decorative appearance of the coating [3, 22]. Ni causes allergies even when it is beneath a gold layer or a PVD coating with pin-holes [5].

Currentless Ni-P: Improvements of the corrosion resistance were made using Ni-P coatings [23]. Ni with 9 to 13 % P results in an amorphous structure of the barrier layer [33].

Ni + Cr: The behaviour is improved compared to the pure Ni. The Cr extends the time between the electroplating and the following PVD process, but the fine crack work in the Cr film cannot be covered by the PVD coating [22, 3]. NiCr has no satisfying corrosion resistance.

Ni + Au: This system has an excellent corrosion behaviour at an Au coating thickness of 1 to 2 μm . The main disadvantages are the very high costs and the bad mechanical behaviour of the soft gold film to the hard PVD coating [22].

Ni + Pd/Ni: excellent results are achieved having 5 to 7 μm Ni and 1 μm Ni/Pd. An explanation is the dense pinhole free coating and the electrochemical behaviour of the Pd/Ni coating [20, 22]. Also reported are 2 μm thick NiPd 20:80 coatings [23]. The hardness of these coatings of around 550 HV 0.1 is adopted very well to the PVD coating. NiPd can be coated directly by PVD using Ti-based materials [5].

Cr: Brass substrate with electroplated Cr shows a good resistance in all corrosion tests. Having a decorative PVD TiN on top overlaid with an 0.1 μm Au, the system failed in all corrosion tests because of the big difference in the electrochemical potential (Cr: + 0.74 V, TiN: + 1.3 V), leading to an anodic dissolving of the Cr coating [22]. A main drawback is the use of hazardous Cr (VI).

Co, Fe: Since Ni is already used as a barrier, Kay et al investigated diffusion barriers on brass made from metals of similar nature like Co [34, 35] and Fe. For the system brass - diffusion barrier - Sn, Fe appears by far the best choice for a barrier layer [25].

CuSn(Zn): A new advanced layer system without allergy risk was investigated by U. Beck et al [5]. They refer to Ni free layers using CuSn(Zn) systems which are described by G. Hoffacker [89]. They offer a good corrosion resistance on brass, show a better metal distribution than Ni and have comparable properties with Ni. But there are still interface problems to the decorative PVD coating on top of the electroplated barrier layer.

Standard Coating System: The standard coating system on non corrosive resistance substrates is an electroplated coating system of Cu, Ni, and Cr. [22]. Recommended practice to prevent Zn diffusion is to electrodeposit at 2.5 μm barrier layer of Cu or Ni (BS 1872, 1984 and BS 6137, 1982).

2.1.5.3 PVD Intermediate Layers

The state of the art shows an improved corrosion resistance of PVD coated brass substrate using a PVD intermediate barrier, but the desired quality of electroplated intermediate layers could not be reached yet, especially for decorative parts with the manifold geometry. It is desirable to have a PVD intermediate layer, but:

- (i) it is up to now not possible at low temperatures $< 250\text{ }^{\circ}\text{C}$ to get a dense coating [10].
- (ii) it is not possible to smooth the surface roughness by PVD [4, 36]

The sputter technology is in special circumstances the appropriate technique to produce a PVD barrier layer, because the thermal influence is not as high. However, coating temperatures at around $300\text{ }^{\circ}\text{C}$ would lead to a dezincification preferable to the β phase, resulting in areas under the hard coating with a pore and sponge characteristic. The evaporating Zn would disturb the coating growth and change the composition of the film [20]. For decorative purposes, temperatures above $100\text{ }^{\circ}\text{C}$ for heat sensitive materials are used with success, but for a better process, controlling temperatures between 150 and $200\text{ }^{\circ}\text{C}$ are preferred [9, 37]. In this temperature range PVD coatings show a transition structure of the zone T in the Thornton diagramme. These coatings show a strongly orientated growth. The resulting micro pores can not be closed by the growing film because of the small coating thickness. Defects on the surface itself can also lead to pores or coating failures [22].

Depositing a barrier layer on brass substrate the bias power plays a key role. Two different contradictory effects must be considered (Figure 2.7):

- (i) with increasing bias power the structure of the growing film becomes denser. Energy is transferred onto the adatoms during the condensation state by ion bombardment, hence shadowing effects can be overcome by surface diffusion processes.
- (ii) With increasing bias power the increasing ion bombardment leads to a higher temperature of the brass substrate. At a critical temperature of 250 °C dezincification occurs which deteriorates the corrosion behaviour.

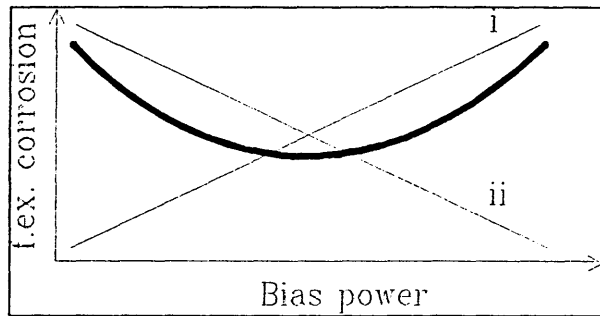


Figure 2.7: Effect of bias power

As the bold parabolic line shows, the result of both effects leads to a minimum in f.ex. corrosion attack, caused by the denser structure. Pure metal or an alloy seems to be the best corrosion barrier. The orientated structure is not as emphasised as in hard coatings (Thornton diagram) and metal coatings are much more ductile which is very important for parts with mechanical deformation [22].

Various types of PVD intermediate layers were examined:

Tantalum nitride: a tantalum nitride coating showed deep cracks in a bended test sample, leading to a massive corrosion attack of the substrate material [22].

Titanium: 2 to 4 µm Ti as a corrosion barrier showed good results in various corrosion tests. Only in the Kesternich test poor results were obtained [22]. The corrosion resistance was also further improved by a Ti interlayer between AISI 440 steel and 3 µm PVD TiN or 7 to 10 µm CVD TiN [30].

Cr: A Cr interlayer between AISI 304 steel and TiN hard coating was investigated to improve the corrosion resistance [30], but an improvement was only found in certain potential ranges.

The system CuZn39Pb3 / 1.5 µm Cr / 6 µm CrN was investigated [37]. Such coatings are of particular use for special corrosion resistance.

TiCr 65/35: known for high corrosion resistance and smoothing effect of Cr-alloys, this coating was tested as a barrier layer. The structure is expected to be denser because of the lower melting point than pure Ti. In summary, those coatings showed the best corrosion resistance [22].

Interrupted coating growth: to avoid or at least reduce the orientated structure of a growing film, after every 0.7 μm of a 2 μm thick pure Ti coating the process was interrupted and a high pressure etching process was done for five minutes. Another possible method used to get a denser coating was to increase the ionisation density and resulting the ion bombardment in the substrate area using closed field unbalanced magnetron. Those coatings showed a finer structure and an improved corrosion resistance [22].

Nickel: optimised Ni intermediate layers showed better results in corrosion tests than electroplated Ni/Pd-Ni coatings. It is unlikely that a decorative hard coating on top of such a Ni barrier is totally unabradable, leading to an allergic reaction [23].

TiN: provides high surface hardness, good chemical stability, good wear resistance and is acting as a diffusion barrier [38, 39].

Si_3N_4 and Ta coatings: are found to be good diffusion barriers to Cu [39].

Surface treatments: Plasma nitriding of the substrate prior to the coating worsened the overall corrosion performance, whilst plasma oxidizing caused a slight improvement [38].

Substrate treatments: PVD coating systems on annealed brass substrate with an almost Zn free surface as a result of the outdiffusion of Zn are used by a company in Switzerland with good success [Private communication: Multicoat SA, Zug, Switzerland].

TiPd 0.5%: The corrosion resistance was improved. The inert Pd is accumulating on the surface, but the thin coating will be destroyed [22].

Partly amorphous Al-based coating: [40] There is no need to preheat the substrate. The targets used are $\text{Al}_{62-85}\text{Ti}_{15-38}$ at-%, leading to (AlTi)N or $\text{Al}_{60-80}\text{Ta}_{20-40}$ at-%, leading to (AlTa)N. The coating changes from an aluminium based amorphous metal to a crystalline ceramic phase. Using an AlTi-target (Al.80%), the structure changes with the nitrogen pressure: N (0-0.02 Pa): Al crystals in amorphous matrix.

N (0.021-0.04 Pa): amorphous metal

N (>0.04 Pa): ceramic crystalline phase.

2.1.5.4 Used PVD Layer Systems

2.1.5.4.1 Aluminium (Al)

Table 2.5 shows the material specific values for Al.

Atomic number	13
Atomic weight	26.98
Atomic radius	1.82 Å
Crystal structure	fcc
lattice parameter	4.0494 Å
density	2.7 g/cm ³
melting temperature	660 °C

Table 2.5: Material specific values of Al

Physical properties: Silver white, very shiny light metal. Gloss let up in air through formation of a thin oxide layer. The metal is very soft and ductile.

Chemical properties: Very base, hence formation of Al₂O₃. Reduction of the oxide not possible with carbon, hence production through electrolysis in dry way. Al reacts heavily with HCl and NaOH, less with H₂SO₄, passive to HNO₃ in cold condition.

2.1.5.4.2 Niobium (Nb)

Table 2.6 shows the material specific values for Nb.

Atomic number	41
Atomic weight	92.91
Atomic radius	2.08 Å
Crystal structure	bcc
lattice parameter	3.3066 Å
density	8.55 g/cm ³
melting temperature	2467 °C

Cu / Mo / W / Ta / Nb
0.07 / 0.8 / 1 / 6 / 11
price comparison [13]

Table 2.6: Material specific values of Nb

Physical properties: white shiny metal. Nb has similar values for strength like steel.

Chemical properties: resistance to air. Attack only possible by HF and caustic alkali molten mass. The effects for acting as a corrosion barrier are given by the noble niobium(V)oxide Nb₂O₅, which are formed if exposed to an electrochemically active

environment. The oxides formed are electrically insulating, resulting in a kind of self healing effect [40].

Structure type: Nb is bcc and remains up to the melting point. It is known that Nb can have an allotrope modification with increasing nitrogen concentration as shown in figure 2.7. Nb can exist in thin films also in a fcc, tetragonal and hexagonal crystallographic structure.

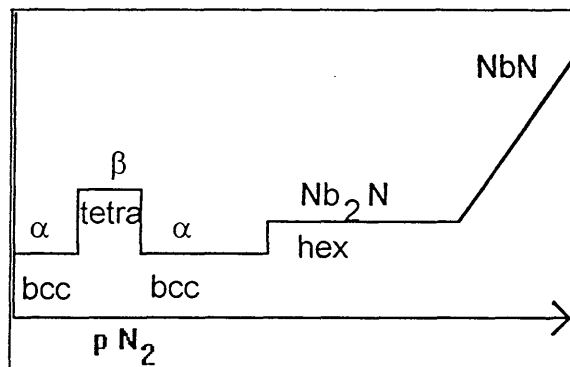


Figure 2.7: Crystallographic modifications of Nb with increasing N concentration

2.1.5.4.3 Aluminium - Niobium (Al-Nb) Sputter Alloy

The Al-Nb binary phase diagram is shown in figure 6.57a. Related to the difference in the lattice parameters of 18.34 % there are miscibility gaps, which resulting phases are listed in figure 6.57a. The valence of Al and Nb has no influence onto the formation of miscibility gaps, because they are both + 3.

The intermediate crystal types in the aluminium rich phase of the Al-Nb binary system were studied by G. Brauer. He found that the corresponding structure is NbAl_3 , having a tetragonal structure with the lattice constants $a = 5.247 \text{ \AA}$ and $c = 8.584 \text{ \AA}$ [41].

2.1.5.4.4 Copper - Aluminium (Cu-Al) Alloy

Copper-Aluminium alloys (aluminium bronze) is distinguished for its high corrosion resistance and high strength. They are used for acid resistance fittings and highly stressed valves. The traded Cu-Al alloys have an Al concentration of up to 14 wt%. The colour is changing from copper red to yellowish at around 10 wt% Al. The Cu-Al binary phase diagram is given in figure 6.57b.

Standardized aluminium bronzes include very often up to 4 % Fe to get a finer grain size and to increase the tensile strength, Ni, As and Si. Additional alloy elements are for example Co, which improves the already high selective corrosion resistance further more, or Sn, which improves the tarnish resistivity.

Aluminium bronzes are not electroplateable, because it is very difficult to remove the aluminium oxides from the surface. The oxides will lead to a bad adhesion of the coating.

The used CuAl target is a CuAl₁₈Fe₃ alloy (DIN 17 665, BS 2874 and 2875). The XRF analysis is given in table 6.2. The density is 7.7 kg/dm³, the melting temperature is between 1045 and 1060 °C, the electrical conductivity is 7.5 m/Ωmm² (at 20 °C), the thermal conductivity is 65 W/mK (at 20 °C), the thermal expansion coefficient is 17 · 10⁻⁶/K (at 20 to 250 °C) and the Youngs Modulus is 120 kN/mm². The alloy has a good corrosion resistance against sea water, sulphite alkaline solution and mineral acids [42].

2.2 Principles of Corrosion

2.2.1 Theory of Corrosion

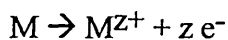
Corrosion is a major cause for materials failure. Hence corrosion protection is of major interest in surface engineering and targets mainly the following directions:

- to improve the materials
- to optimise the design of the equipment
- to improve the surface on a permanent (coatings, surface treatments etc.) or temporary basis (anodic / cathodic protection and external sources)

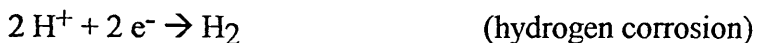
Corrosion is defined as an attack of a material by reaction with the adjacencies and the resulting reduction of properites (DIN 50 900). Usually this is an electrochemically reaction with liquid or gaseous media.

Corrosion damages can be distinguished in uniform area corrosion or non-uniform localised corrosion. The uniform area corrosion is not as dangerous, but the localised corrosion can attack at single places the material strongly and can go very deep [43].

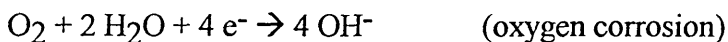
Electrochemical reactions are always connected with an interactive transformation within the material's existing chemical and electrical energy. The base metal transforms from the neutral atom by oxidation to a positive ion, whereas the nobel metal transforms from the positive ion by reduction to a neutral atom. The base metal is acting as a reducing agent, whereas the ions of the noble metal are acting as an oxidizing agent. The anodic reaction is the oxidation of the base metal. The anodic metal dissolving process is given by



The cathodic reaction is the reduction of hydrogen ions in acid atmosphere ($\text{pH} \leq 4$)



or the oxygen reduction in neutral or alkaline atmosphere



The interaction of the metal phase M and the ions in the solution M^{Z+} are leading to a potential difference, which is defined in the equilibrium by the Nernst equation. The voltage of the potential difference between the standard hydrogen electrode and a half element (metal / salt solution) is named standard potential of this element under standard conditions. The standard potential of the standard - hydrogen electrode is set to zero. The standard potentials referred to the standard hydrogen electrode are given in the electrochemical displacement series [44]. The metals with a positive standard potential are called noble, those with negative standard potential are called base.

In practice this displacement series is very inaccurate. Therefore Jehn et al developed a practical displacement series which gives the potentials of various metals in standard solutions [45].

The electrochemical corrosion involves at least one redox stage which has the specificity of electrochemical reactions, i.e. spatial separation of the oxidation / reduction half processes. Owing the energy non-uniformities at various points at an interface, induced by chemical, structural, stress and other local differences, these points adopt different electrochemical potentials. The driving power of electrochemical corrosion is the difference of electrochemical potentials of the used materials [6].

2.2.2 Corrosion of PVD Systems

PVD coatings are not totally dense, pore and pinhole free. It is largely the porosity which determines the resistance to corrosion or chemical attack of the coating - substrate combination. The corrosion behaviour of a coated material must be seen in the entire system (coating-substrate), even if the coating itself is corrosion resistant. The safety of the corrosion resistance of the entire coating system and the mechanical accommodation has to be seen in the inter-relationship.

As defined in DIN 50903, pores or cracks are gaps or separations observable in the deposit. They can be seen by eye or they are microscopically small and special procedures are necessary to observe them.

Chemical attack can be caused by H^+ , OH^- and Cl^- Ions and solved oxygen of the solution which is penetrating through the pores and pinholes to the substrate. The electrochemical behaviour can be distinguished in two different types: (i) local corrosion introduced by a galvanic element between an anodic substrate material and a noble cathodic coating and (ii) cathodic protection of the noble substrate material and anodic solution of the base coating. The corrosion appears mainly in the form of pittings (crevice corrosion, selective corrosion).

Figure 2.9 shows, in schematic form, the effect of pores on the corrosion of substrate and coating. The left hand diagram shows the effect of a pore in coating less noble than the brass substrate. In this case, a local galvanic couple is formed which cathodically protects the substrate metal, which cations of the overlaying deposit go into solution. The right hand diagram depicts a situation corresponding to a coating nobler than the substrate. Through pores in coatings there is a direct chemical attack of the substrate by the corrosive medium, resulting in formation of local elements and the appearance of corrosion [6].

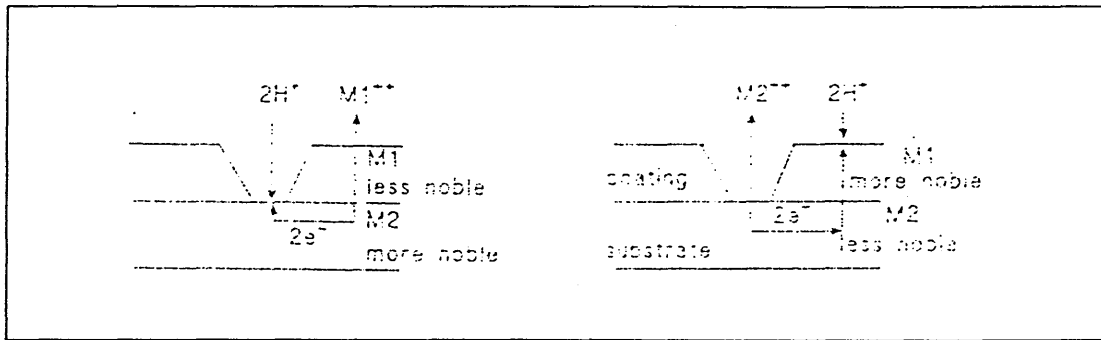


Figure 2.9: corrosion effect of pores, schematic [30]

Only layers deposited in a non-porous state can act as a corrosion barrier [44, 46]. There is a direct chemical attack of substrate material through pores in the coating, so that decorative hard coatings alone are no sufficient corrosion protection [6, 10]. Hence there is the need for an intermediate corrosion resistant layer [9, 10, 36, 47]. Galvanic intermediate layers have less porosity than PVD coatings and therefore offer a better corrosion resistance.

The potential difference between the base material and the noble coating has to be reduced by using a relative noble intermediate layer material. Alternatively the local corrosion attack of the substrate material has to be changed to an area corrosion attack of the intermediate layer [47].

2.3 Principles of Diffusion

Diffusion is defined as the temperature depending movement of atoms, ions and molecules in a static process [48]. The diffusion is responsible for mass transport phenomena in metallurgy. The diffusion in pure metals is named self diffusion. In this situation either a movement of vacancies or exchange of atoms occurs. Figure 2.10 shows the diffusion mechanisms.

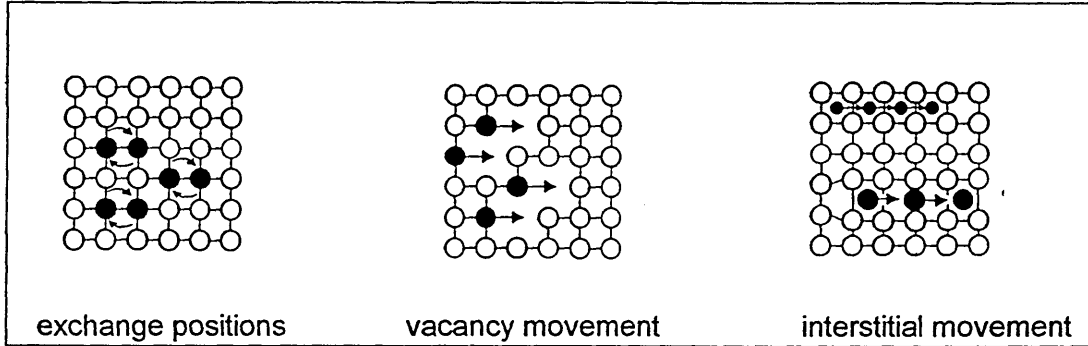


Figure 2.10: Diffusion mechanisms

Technically important is the diffusion in inhomogenous materials. The power for directional movement of atoms is difference in their concentrations. The mathematical relation that connects the concentration of the diffusing species with distance is Fick's law. Fick's first law states that the diffusion flux J is given by

$$J = -D(dC/dx) \quad \dots (2)$$

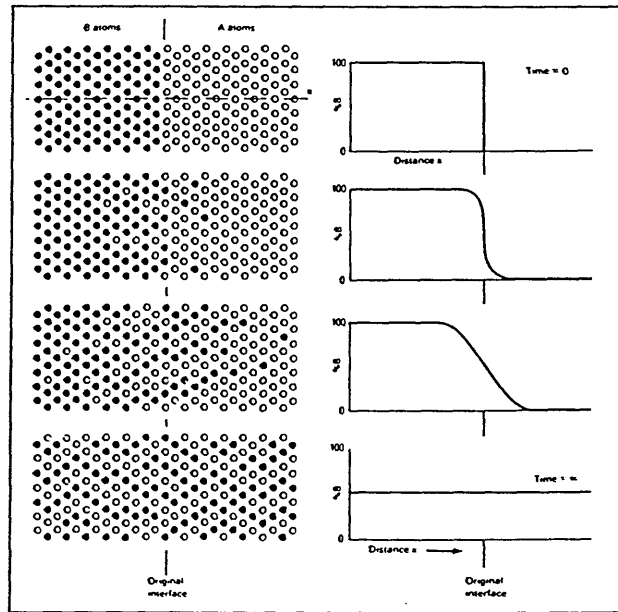


Figure 2.11: schematic diffusion process

where C is concentration and x is distance. D is the diffusion coefficient at a given temperature, but may be concentration-dependent. Figure 2.11 shows the schematic process of diffusion. As time progresses, mixing on the two sides occurs. At infinite time, complete mixing has been achieved. The effect of time t on the flux is incorporated in Fick's second law

$$\frac{dC}{dt} = D \frac{d^2C}{dx^2} \quad \dots (3)$$

The diffusion coefficient D is given by

$$D = D_0 e^{\left(\frac{-Q}{RT}\right)} \quad \dots(4)$$

where R is the ideal gas constant and Q is the activation energy for the diffusion process [49]. Figure 6.58 shows the interdiffusion coefficients for nonferrous metals [50].

The diffusion in the material can be distinguished in surface-, grain boundary- and volume diffusion. In surface diffusion, the atoms diffuse along the surface while in volume diffusion they spread uniformly over a wide front within the crystal lattice. In grain boundary diffusion the atoms move along the grain boundaries. This is undesirable in practice, because it is sometimes so intense that the grains of the base metal are completely surrounded [26]. Figure 2.12 shows as an example the diffusion behaviour for thorium in tungsten. The

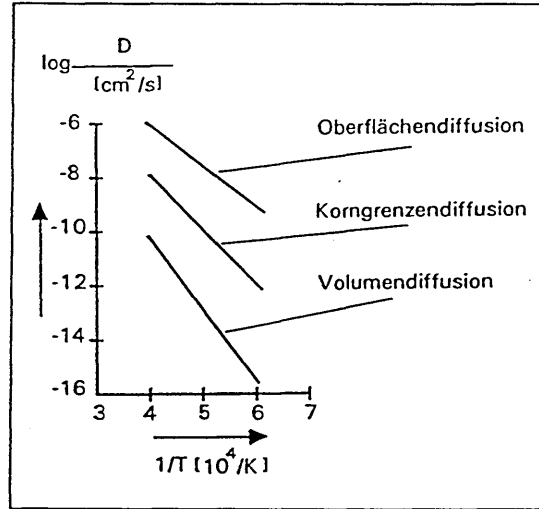


Figure 2.12: diffusion activities

volume diffusion activity is the lowest, followed by the grain boundary diffusion compared to the highest activity for the surface diffusion [27]. For pure metals the activation energy for surface- and volume diffusion increases proportionally with the melting point of the coating material.

Between metals which form solid solutions diffusion is not inhibited. Alloys of any composition can be formed by solid state diffusion. If two metals have only limited solubility in the solid state, the maximum alloy concentrations attainable by diffusion are represented by the saturation limit of the solid solutions. The probability of diffusion of metals is very low at room temperature. Only low melting metals can diffuse at room, or slightly elevated, temperatures [51].

Various kind of diffusion tests are mentioned in literature. The objectives of a diffusion anneal are to hold the sample at a constant temperature T for a time t in an atmosphere that does not change the chemistry of the sample, and to measure T accurately. Samples are annealed in oil bathes at low temperature ($T < 200^\circ \text{C}$) and in vacuum at high temperatures [52], hung in an air circulating oven at 170°C [25, 53] or in an furnace up to 750°C in air [28].

2.4 Physical Vapour Deposition

2.4.1 Coating Deposition from the Vapour Phase

The vapour deposition processes are subdivided in physical vapour deposition (PVD) and chemical vapour deposition (CVD). Typical deposition temperatures for PVD are between 100 and 500 °C at pressures between 10^{-8} to 10^{-1} mbar with a thickness range between 0.02 and 10 μm . The chemical reactions in CVD generally take place in the temperature range of 750 to 2200 °C at a pressure ranging from about 0.5 mbar to atmospheric pressure. The thickness ranges from 0.5 to 1000 μm .

The processes have several advantages and disadvantages relative to other competitive processes.

Advantages: + There is great versatility in the composition of coatings. Coatings can be produced with high purity, unusual micro structures and new crystallographic modifications.
+ Thin coatings (as low as a couple of nanometers thick) can be produced with extremely high adhesion at high deposition rates.
+ Most substrate materials which do not outgas and withstand deposition temperatures can be coated.
+ Substrate surface topography is reproduced, and generally no post finishing is required.

Disadvantages: - high capital costs and high processing costs are associated with vacuum systems.
- With certain exceptions, it is more difficult to deposit materials uniformly because of the line of sight problem
- CVD: toxic waste products (e.g. HCl)

Figure 2.13 enumerates the variants of deposition techniques which are based on vapour deposition [54, 55].

Vapour Deposition Techniques		
Physical Vapour Deposition		Chemical Vapour Deposition
Evaporation	Sputtering	
Direct	Ion Beam	
Reactive	Glow Discharge	
Arc: - random	Magnetron:	
- steered	- balanced	
	- unbalanced	
Ion Plating		

Figure 2.13 : Variants of deposition techniques

2.4.2 Physical Vapour Deposition

Physical Vapour deposition (PVD) is the choice of method for deposition of thin film coatings across a broad spectrum of industries. Products as diverse as cutting tools, architectural glass, in microelectronics, jewellery and optical discs are coated in large volumes using a variety of PVD techniques.

The term Physical Vapour Deposition refers to a group of thin film deposition processes in which a metal vapour flux is derived from a solid or molten source, transported through a low pressure environment and then deposited on a substrate [56].

The outstanding feature of PVD processes is the high flexibility. With regard to the coating materials there are almost no limits. The important advantage of PVD over CVD is that it can proceed at much lower temperatures. Virtually any metal, alloy, ceramic, intermetallic, and some polymeric-type materials and their mixtures can be easily deposited onto substrates of virtually any material which are stable at operating temperatures in the vacuum such as HSS, metals, ceramics, plastics and paper. The deposition temperature is variable over wide ranges and can be fitted to the particular situations; structure, density, roughness and hardness are some coating properties, which can be affected by the substrate temperature [57]. Substrates generally must be rotated for uniform coatings, because there is a directional flux from the targets to the substrate [55].

Physical vapour deposition consists of three major steps: (i) creation of a vapour phase species. (ii) transport from the source to the substrate. The vapour species are transported from the source to the substrate with or without collisions between atoms and molecules. During the transport, some of the vapour species may be ionised by creating a plasma. (iii) film growth on the surface. This process involves the condensation of the vapour species onto the substrate and subsequent formation of the film by nucleations and growth processes. The nucleation and growth processes can be strongly influenced by bombardment of the growing film by ionic species, resulting in a change in micro structure, composition, impurities and residual stress [58].

2.4.3 Coating Methods

Evaporation

The material to be deposited is melted in a resistively heated boat or crucible or by the heating action of either a high-current or a high voltage electron beam resulting in an atom flux. Using a cathodic arc results in a highly ionised flux. In any case, the material evaporates and forms a cloud of vapour which fills the deposition chamber. Condensation of this vapour onto the substrate produces the desired thin film. The atoms of the source material in the vapour phase have a very low energy, 0.2 to 0.6 eV, and, as a result do not produce highly adherent or dense films when condensed onto the substrate. Using an ionised flux and / or biased substrates the properties of the condensing films can be improved [55, 56].

Sputtering

When the surface of a material is bombarded with energetic particles, normally ions, one consequence is the "physical erosion of material" from the surface. This effect is known as *sputtering*. In a vacuum enclosure, backfilled with an inert sputtering gas to a pressure in the 10^{-1} Pa range, a potential is applied between two electrodes. Given a sufficiently high voltage, a gas discharge is established in the inter-electrode space. The discharge plasma is composed of equal numbers of gas ions and electrons. The gas ions, which carry a positive charge, are attracted to the negative electrode, or cathode. When these energetic ions arrive at the cathode surface, several events can occur. (i) The ions may simply be reflected from the surface, making no contribution to the sputtering process. (ii) The ions become imbedded in the substrate; this is the process of ion implantation. (iii) A near-surface atom is said to be sputtered from the surface when momentum transfer from the incoming ion is sufficient to cause the atom to be ejected from the surface. (iv) concurrent with these events is the emission of secondary electrons from the target. These secondaries are important in that they produce further ionisation of the sputtering gas, maintaining the discharge.

Since the source material remains solid, a sputtering cathode can be oriented to deposit in any direction. Sputtering is an intermediate energy process, depositing atoms with energies in the range 4.0 to 10.0 eV [56, 59].

Ion Plating

Ion plating is actually a hybrid concept based on the evaporation or sputtering mechanism coupled with a glow discharge [56, 58]. The definition of ion plating, given by W.-D. Münz (according to Bunshah) is: "Ion plating is an effect which occurs for the most part only on the substrate surface and is essentially independent of the source which generates the metal vapour. Under the action of energetic particles, the metal and gas atoms condense to cover denser and more adhesive surfaces. In this process an important role is played by the energy of the particles and their number in comparison with the number of condensing neutral metal and gas atoms ($v_i / v_o \geq 1$)" [60]. The vapour is charged positively and accelerated by a negative voltage applied to the substrate, named the bias voltage.

The effect of the bias voltage is as follows:

- (i) If the substrate is grounded, there is negligible ion bombardment of the growing film, resulting in no densification and poor coating qualities.
- (ii) Substrate with a floating potential leads to a self bias effect. The reason is the much higher velocity of the electrons compared to the ions, resulting in a higher bombardment of the substrate by electrons, charging the substrate to around -20 V.
- (iii) Low bias voltage (-50 to -500 V) leads to an ion bombardment of the growing film, resulting in an increases surface mobility of the coating atoms and ions. The effect is a densification of the film.
- (iv) Medium bias voltage (-500 to -3000 V) leads to an increased ion bombardment of the growing film. The resulting higher temperature reinforces the diffusion activity. There is also creation of lattice defects in the film.
- (v) High bias voltage of 3 kV and higher leads to ion implantation.

Ion plating techniques are the highest-energy deposition methods currently available. Particle arrival energies at the substrate can be of the order of several hundred eV.

2.4.4 Magnetic Fields

The effects of magnetic fields in sputter deposition technology are to increase (i) the particle energy, (ii) ionisation and (iii) ion density in the centre of a coating chamber where the substrate is located. Those magnetic fields are superpositioned rectangular to the electric fields.

2.4.4.1 Magnetic Fields on the Targets

2.4.4.1.1 Balanced and Unbalanced Sputtering Systems

In an ideal balanced system with conventional magnetron, the inner pole and outer pole magnets behind the targets are of equal strength, and so the field lines loop between them, returning via the steel yoke on which the magnets are fixed (Figure 2.14).

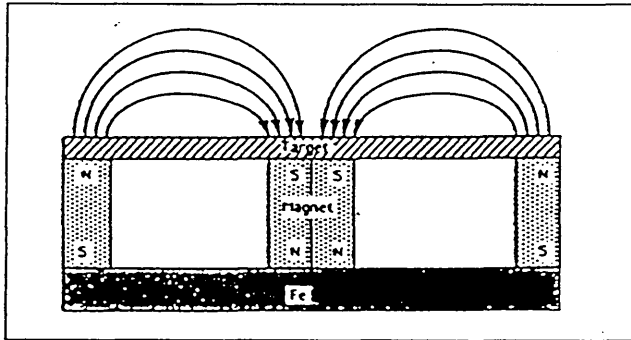


Figure 2.14: Balanced magnetron

By strengthening the inner or outer set of magnets, either with additional magnets or by using an electromagnetic coil, the magnetron becomes unbalanced (Figure 2.15). There are two unbalancing options:

- (i) strengthening the inner pole, resulting in increased secondary electron confinement and drawing the glow region in more tightly to the cathode (wrongly unbalanced),

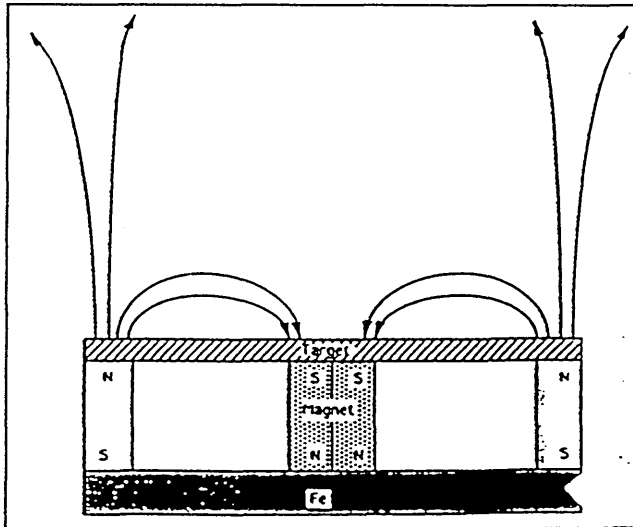


Figure 2.15: Unbalanced magnetron

- (ii) strengthening the outer pole, then the magnetic field lines, as well as looping on the cathode surface, curve away on all sides. Some of the secondary electrons follow these lines and are no longer confined to the cathode surface. The plasma glow is also expanded outward towards the substrate and considerably increases substrate bombardment intensity such that it is comparable with other high deposition rate techniques. The ability to vary the degree of unbalance of the magnetron by use of additional electromagnetic fields allows the ion flux at the substrate to be varied independently of sputter power and gas pressure.

2.4.4.1.2 Random and Steered Arc

The cathodic arc is a state of a discharge in low pressure with high current and low voltage. Depending on the applied magnetic field, various effects can be achieved:

(i) random arc: Having no magnetic field applied, the arc attacks the target in very small areas. This cathode spots are moving randomly over the target surface with a relatively long life time. The main disadvantage are droplets deposited on the substrate surface resulting in high surface roughness.

(ii) steered arc (confined arc): (U.S. Patent 3, 793.179 - 1974 L. P. Sablev and U.S. Patent 4, 673.477 - 1987 S. Ramalingam). A static magnetic field behind the target results in a confined arc, forcing the cathode spots to move around the target in defined closed tracks. The arc sits preferentially at the point on a cathode surface where the normal component of an applied magnetic field is zero [54]. There is also the possibility of a local variable magnetic field, leading the cathode spot on a track with variable diameter which may be circular or oval.

2.4.4.2 Magnetic Fields in the Chamber

When a pair of unbalanced magnetron cathodes are mounted in a vacuum chamber the arrangement of the magnets has a large effect on the plasma confinement and density polarisation. Two geometrical arrangements are generally possible:

(i) mirrored - like poles face each other, see Figure 2.16. The mirrored magnet configuration has no advantages and will reduce the degree of unbalancing by restricting the reach of the uncontained field lines to half the inter-cathode distance. Electrons follow the field lines and are lost. Research has shown that in a mirrored configuration, plasma density at the substrate is low and substrate bias current densities of less than 1 mA/cm^2

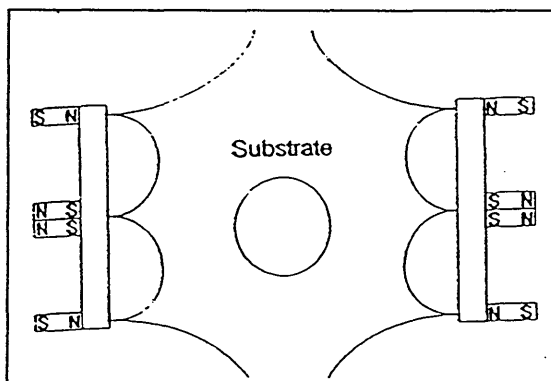


Figure 2.16: Mirrored magnet arrangement [61]

were achieved. However, if the distance of the magnetrons is short enough, eg. 12 cm, excellent deposition conditions for decorative coatings have been found [62, 63]. Batch type and inline coaters have been and are still built by Leibold AG using this principle. The technology is used in Europe, USA and Japan.

(ii) closed field - opposite poles face each other, see Figure 2.17. "Closed field" stands always in relation to the arrangements of several cathodes to each other. Only even numbers of cathodes may be used in an opposed arrangement without upsetting the repeating pattern. The opposed magnet configuration gives rise to field linking between the north and south outer poles of adjacent cathodes which serves to confine the escaped

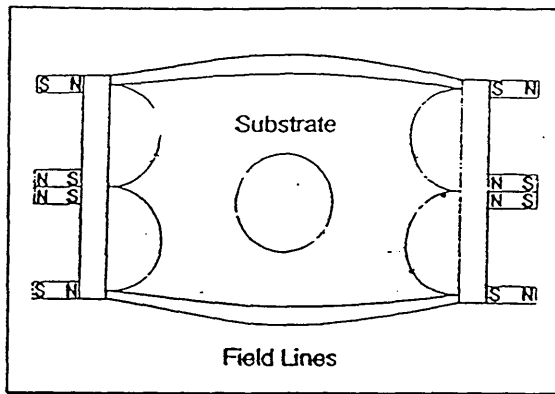


Figure 2.17: Closed field magnet arrangement [61]

secondary electrons and distribute them and the plasma intensity around the multi-cathode system. The increased travelling distance of the secondary electrons in front of the cathodes creates more ionisation events and result in increased sputtering. Also the closed magnetic field helps confine the plasma to the substrate region which enables changes in deposition conditions.

If the magnets were arranged in a closed-field configuration, where the field lines from one set of magnets were directly coupled with the other set, the substrate bias current density could be as high as 6 mA/cm^2 and high ionisation at the substrate could be achieved. The linking of the magnetic field lines resulted in excellent plasma confinement and allowed precise control of the deposition region. Four cathode units in unbalanced closed field geometry were found to offer a good practicable arrangement for the production of magnetron sputtered coatings (Figure 2.18).

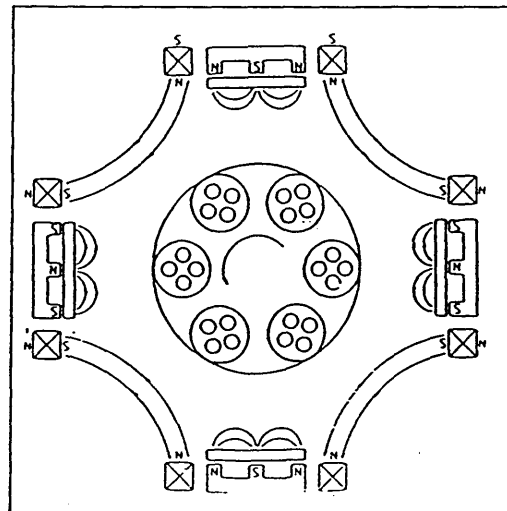


Figure 2.18: Cathode arrangement in the Hauzer ABS™ HTC-1000-4

2.4.5 The HTC 1000-4 ABS™

To get useful industrial TiN coatings, even at high distances between the substrate and the targets, the unbalanced magnetron is needed [64, 65]. Distinct differences in the micro structure (coating and interface) of TiN coatings were observed, depending on their method of etching pretreatment and coating. With the Hauzer HTC 1000-4 ABS™ it is possible to combine two different coating methods in a single system, the arc-etching and sputter coating - with the advantages of droplet minimisation by the Steered Arc™ principle during etching and the exemplary use of the Unbalanced Magnetron for coating. ABS stands for Arc Bond Sputtering. Pretreating of substrates with titanium ion etching offers better adhesion than argon ion etching.

2.4.5.1 The Vacuum Chamber of the ABS™ System

The vacuum chamber has an octagonal cross section, 1000 mm diagonal distance between the targets and a height of 1000 mm, giving a volume of 800 l. The walls are made from 25 mm thick stainless steel. The machine is equipped with two turbomolecular pumps with oil lubricant bearings and inert gas sealing, in combination using a roots pump and a rotary-vane pump. Figure 2.19 shows a schematic diagram of the vessel concept with doors open and closed.

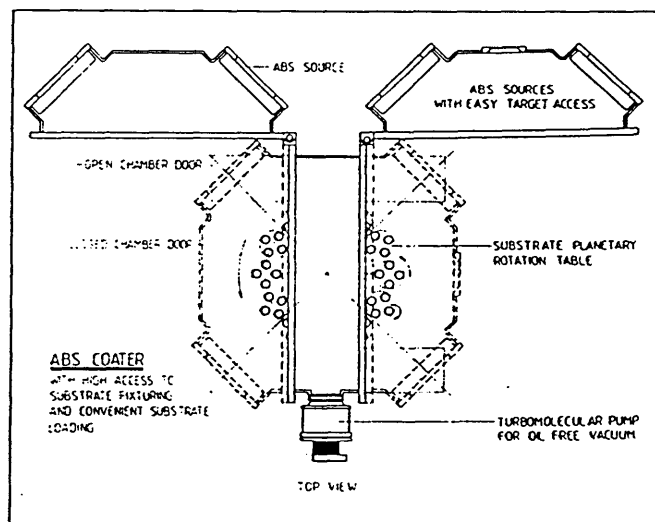


Figure 2.19: Vacuum Chamber open and closed

2.4.5.2 The Cathodes

The Arc-bond sputter system comprises four cathodes with targets 600 mm long and 190 mm wide, positioned at 90 ° to one another in the octagonal system. Each ABS cathode is connected to an individual power supply capable of delivering 80V / 100A in arc mode and 750V / 40A in magnetron mode. The cathodes accept powers of at least 10W/cm² for an adequate coating rate. Figure 2.20 shows the cathode with permanent and electromagnets. The permanent magnet material used is SmCo.

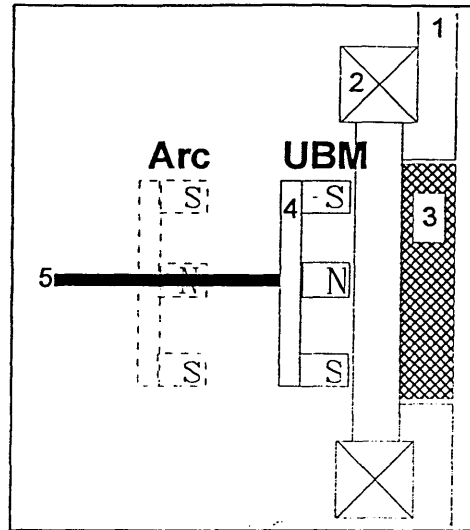


Figure 2.20: UBM / Arc cathode
[61]

The cathodes are surrounded by concentric electromagnetic coils, which can generate a magnetic field up to 10 000 ampere turns. With these magnetic coils the unbalancing effect can be adjusted. By moving the permanent magnets along the fixturing to around six cm away, the UBM cathode is converted to an arc cathode. When the magnets are this position the strength of the magnetic field is not as high as in the UBM mode. Figure 2.20 shows: (1) vacuum chamber, (2) electromagnetic coils, (3) target, (4) magnetic yoke and (5) fixturing.

The targets can be protected having moveable shutters in front. In UBM mode they avoid precoating of the substrate during the target cleaning step and in arc mode they avoid droplets reaching the substrate. The shutters have a floating potential, so that they do not reduce the amount of electrons and ions in the chamber. To optimise the efficiency of the shutters, they are positioned quite close to the targets.

Figure 2.21 shows the PVD machine.

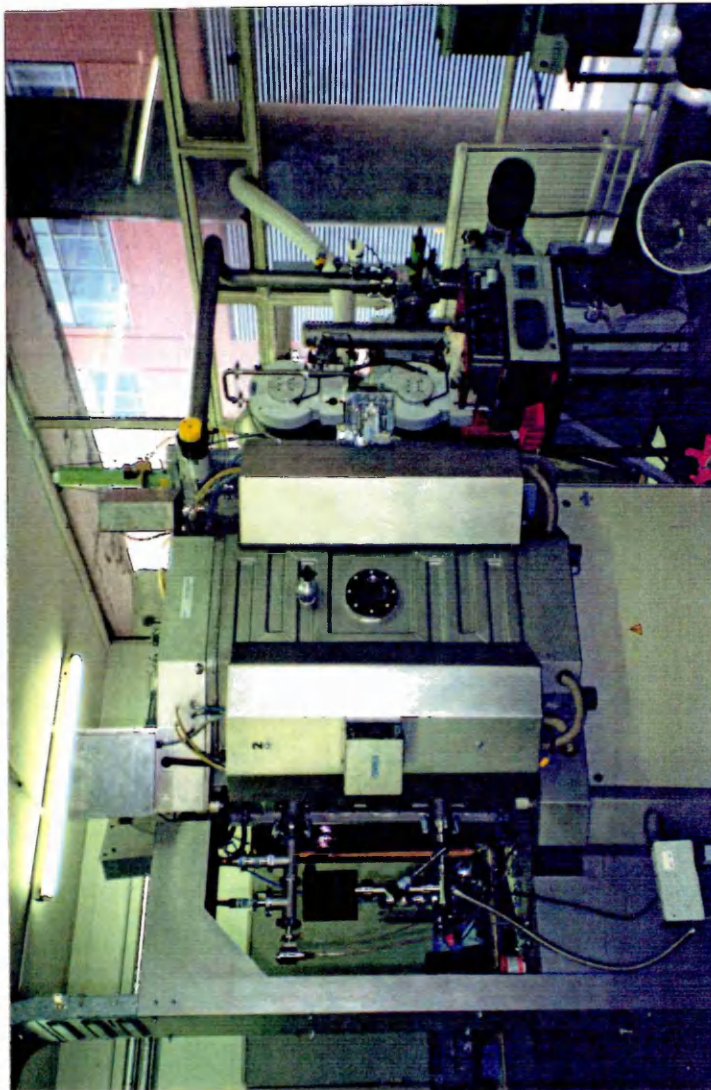


Figure 2.21: The Hauzer HTC 1000-4 ABS (coating chamber and control board)

2.4.6 Target and Substrate Cleaning in the PVD-Chamber

Before a coating procedure can be performed, there is the need to clean the targets and the substrates under vacuum conditions in the PVD-Chamber. Thin oxide layers, other chemical bonded molecules, water vapour, etc. on both targets and substrates can be removed using glow discharge and ion etching techniques.

2.4.6.1 Target Cleaning

Target cleaning is performed in glow discharge mode in a non reactive Ar-atmosphere. The shutters are closed to prevent a pre-coating of the substrate. This pre-coatings are non reproducible, non biased and porous coatings of poor quality. The target voltage is increased until a plasma is established. This condition is the actual cleaning process and should take around 15 minutes.

The positive argon ions (1) are accelerated to the negative target (2) and can cause the following reactions: Argon ions are reflected (3), target atoms are sputtered (4) or secondary electrons are emitted (5). The secondary electrons again produce more argon ions in front of the target, which reinforce these effects. Furthermore: (6) plasma, (7) shutter, (8) cathode, (9) substrate table. (Figure 2.22).

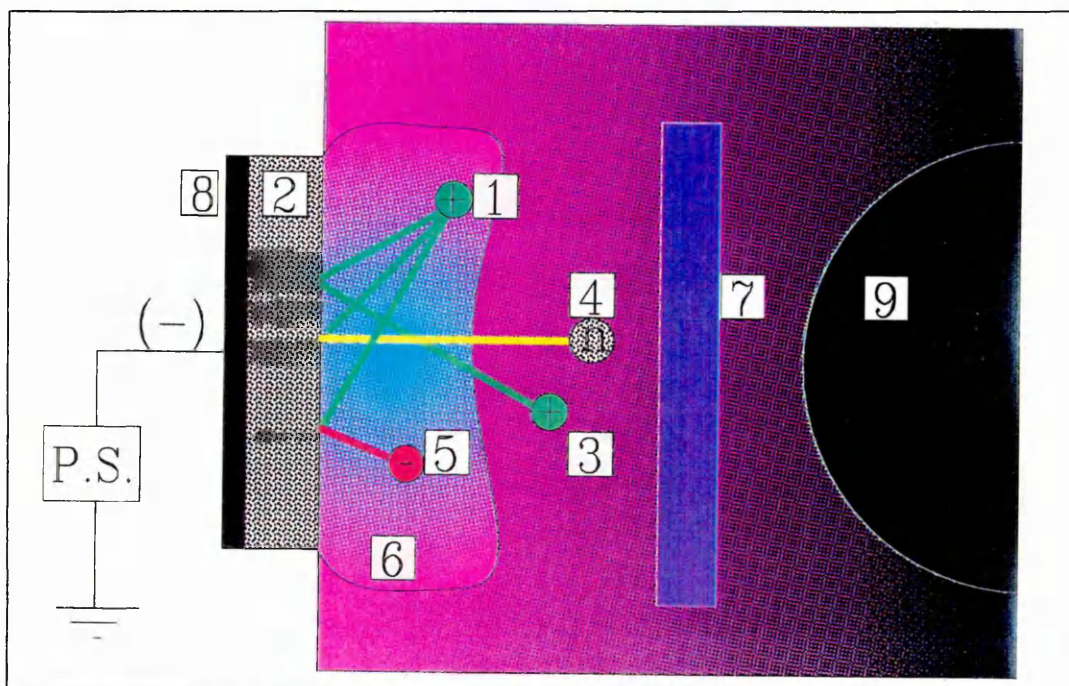


Figure 2.22: Target Cleaning in Glow Discharge Mode with Shutters closed

2.4.6.2 Substrate Cleaning

2.4.6.2.1 Argon Glow Discharge Mode

Substrate cleaning can be performed in *Glow Discharge Mode* (Argon Ion Etching) with the shutters open. A very weak plasma will be established at a target voltage of around -120 V, so that only electrons are emitted. If the target voltage would be increased to say -300 V, also metal atoms and metal ions (less than 1 %) would be emitted. The substrate bias voltage is important. The higher this voltage, the better the cleaning effect. The process parameters are a coil current of around 5 A on each target, an argon pressure of $2.5 \cdot 10^{-3}$ mbar and a bias voltage of -1200 V; the cleaning process should take at least 20 minutes. This coil current is reinforcing the cleaning effect of the substrate by densifying the plasma, which will be directed towards the substrates due to the closed magnetic field generated by the coils.

The positive argon ions (1) are accelerated by the negative cathode voltage (8) to the target (2) and by collision with the target material secondary electrons (5) will be emitted. They are moving, supported by the magnetic field of the coil current (3), to the substrate table and cause a lots of argon ions (11), which are accelerated at the very near surface (6) to the substrate (4) with the negative bias voltage (9). This bombardment of the argon ions is the cleaning procedure of the substrate. Furthermore: shutters (7), intense plasma (10). Figure 2.23:

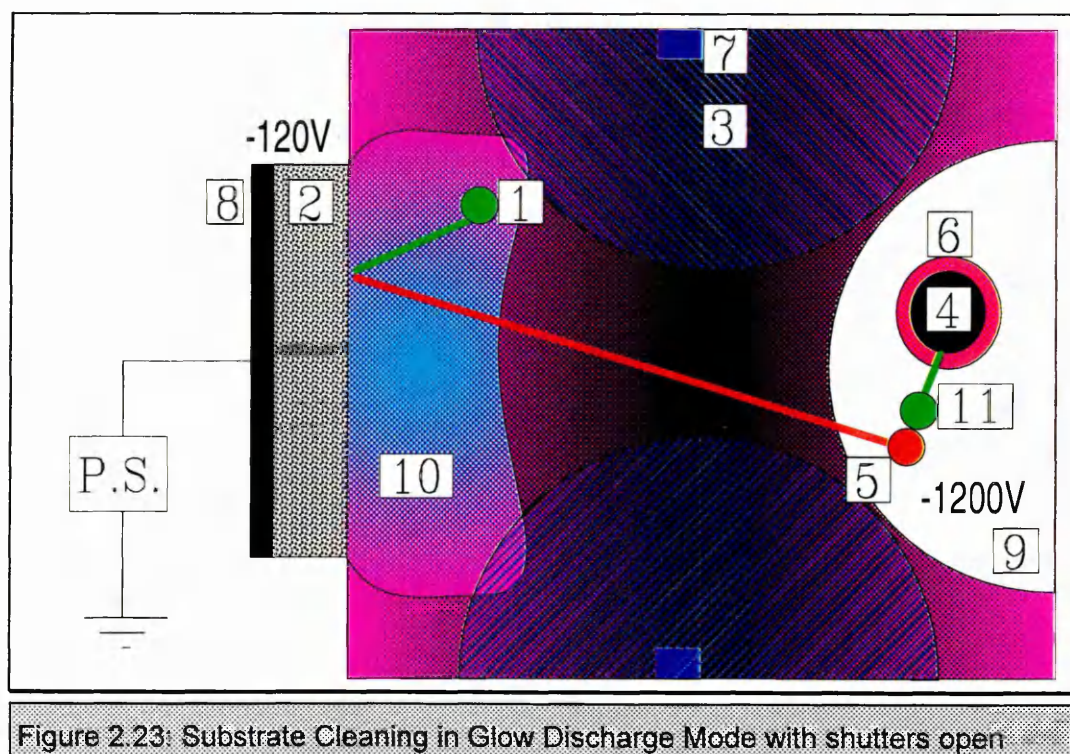


Figure 2.23: Substrate Cleaning in Glow Discharge Mode with shutters open

2.4.6.2.2 Metal Ion Etching Mode

Substrate cleaning can be performed in *Ion Etching Mode* (Metal Ion Etching). In contrast to Ar ion etching there are chemical reactions with the surface, whereas the Ar ions are inert. Furthermore ion implantation caused by multiple ionisation of the metal ions is found, resulting in a different interface and a better adhesion of the thin film.

By applying a high voltage pulse onto a wire which is surrounding the target using intelligent electronics an arc is ignited and runs on the target in steered mode. If the arc extinguishes, the electronics ignites a new arc. A bias voltage which is supplied to the substrate table accelerates the metal ions into the direction of the substrate. The bombardment of the metal ions onto the substrate surface is the cleaning process. Typical process parameters are -700 V bias voltage and an argon pressure of $2.5 \cdot 10^{-3}$ mbar.

(a) when the shutters are open (7) the arc spot (1) is running on the target (2). The high energy density produces a lot of metal ions (3), which are moving through the vacuum (10) to the substrate table with the negative bias voltage (5). As soon as the metal ions (3) come to the sheath (6) they will be accelerated to the substrate (4) and bombard it - which means a sputtering and therefore a cleaning of the surface. Furthermore: cathode (8), plasma (9). Figure 2.24. There is still the additional affect of argon ion etching.

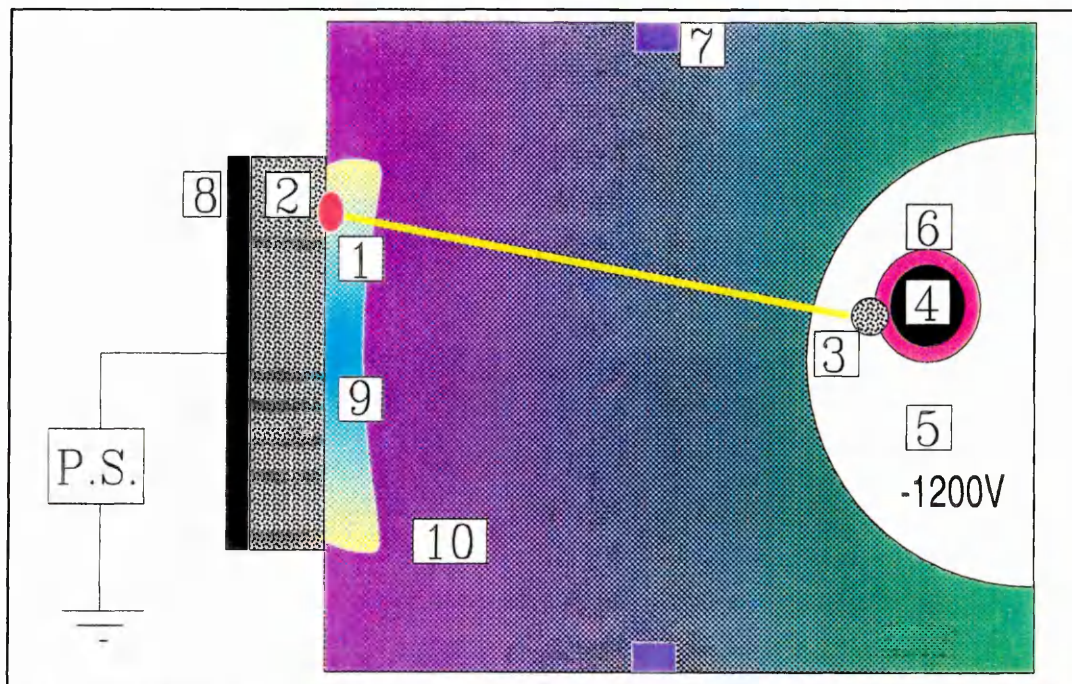


Figure 2.24: Metal Ion Etching in Ion Etching Mode with shutters open

(b) when the shutters are closed (7) the arc spot (1) is running on the target (2). The high energy density produces a lot of metal ions (3), which are moving through the vacuum (10). They are colliding with argon ions (12) and by this effect they are diverted around the shutters to the substrate table with the negative bias voltage (5). As soon as the metal ions (3) come to the sheath (6) they will be accelerated to the substrate (4) and bombard it - which means a cleaning of the surface. The shutters are closed, if there is the problem of droplets (11), they will be caught with the shutters so that they can not go to the substrate and destroy it by means of droplet deposition, resulting in a poor surface quality. Furthermore: cathode (8), plasma (9). Figure 2.25. There is still the additional affect of argon ion etching.

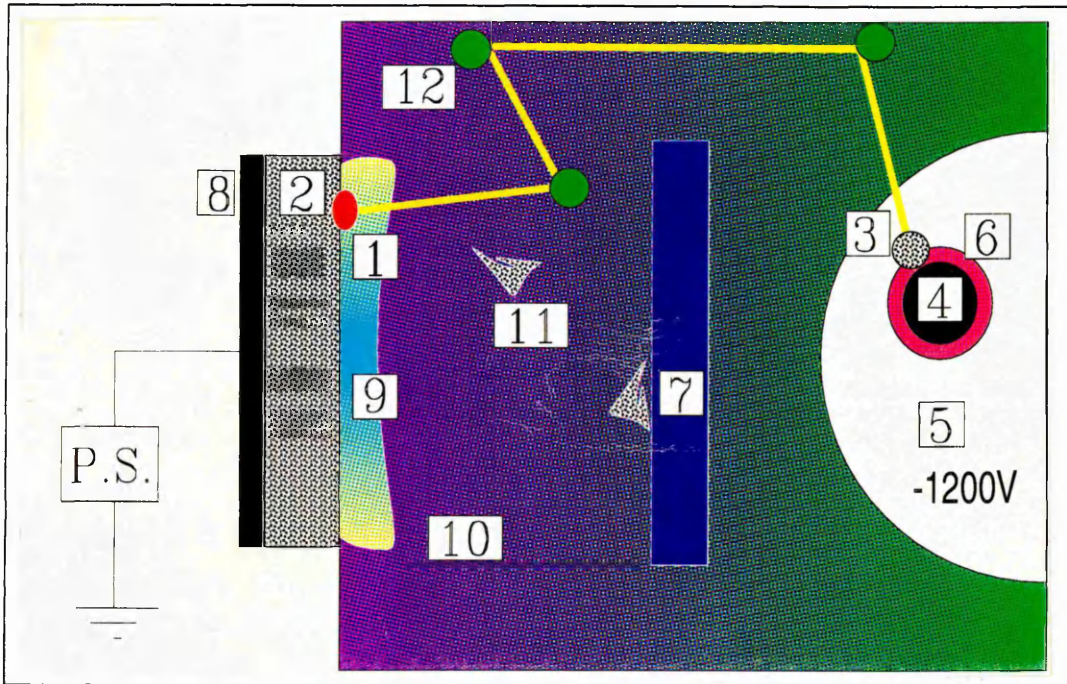


Figure 2.25: Metal Ion Etching in Ion Etching Mode with Shutters closed

Table 2.7 summarises the operational modes which are applied in the HTC 1000-4 and which are explained above.

	MODE		SHUTTERS	
	Glow Discharge	Ion Etching	open	closed
Target	✓			✓
Substrate	✓		✓	
		✓	✓	✓

Table 2.7: Target- and Substrate Cleaning combinations

2.4.7 Coating in the PVD-Chamber

Coating is performed in Coating Mode using unbalanced magnetron mode (UBM) with shutters open. The target voltage is increased until a plasma is established. This condition is the actual coating process.

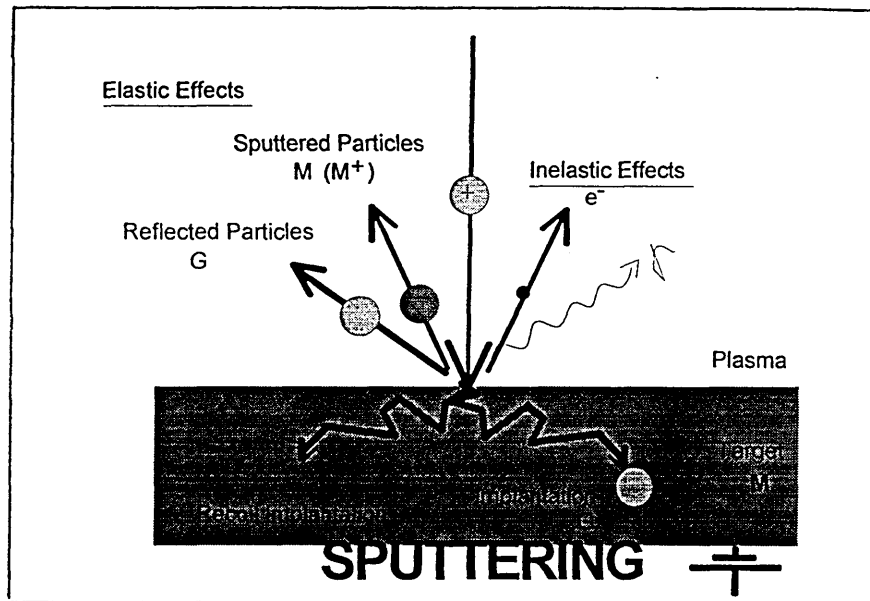


Figure 2.26: Sputter process on the target side during coating

In coating mode the target and substrate have to be considered. The process taking place on the target side is called sputtering. An incident ion causes elastic and inelastic effects (Figure 2.26). The sputtered particles move to the substrate side and can again cause elastic and inelastic effects. The important process concerns the particles condensing on the substrate surface as a coating grows (Figure 2.27).

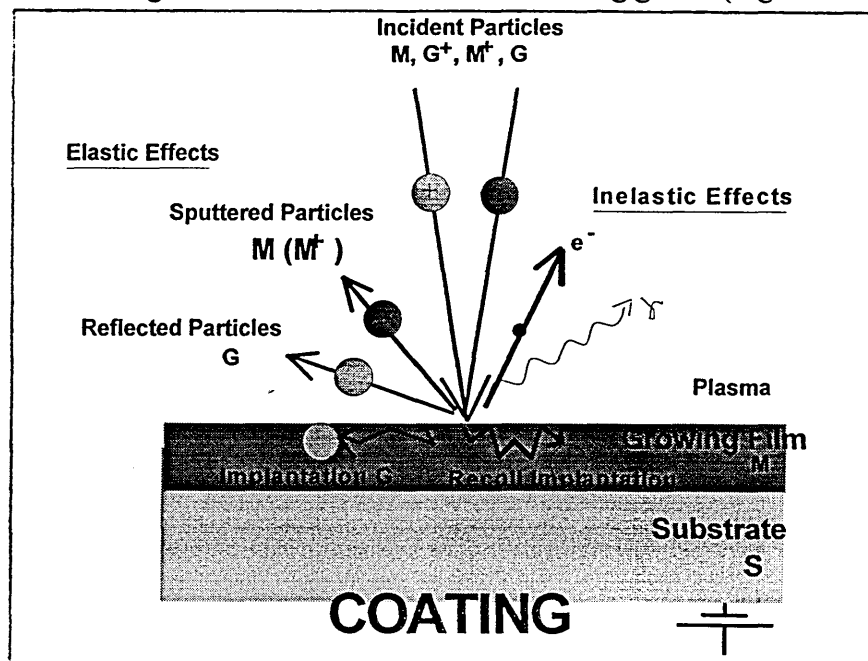


Figure 2.27: Coating process on the substrate side during coating

2.4.8 Coating Growth and Structure-Zone-Models

Metal atoms sputtered from the target arrive at the substrate at a certain rate. They strike the substrate surface and kinetic energy is transferred, the atoms are mounted loosely as adatoms. The adatoms are diffusing on the substrate surface. Energy exchange takes place with the crystal lattice, until the adatoms have low energy places or they are resputtered from the surface. If the arriving species are not re evaporating they can establish metastable

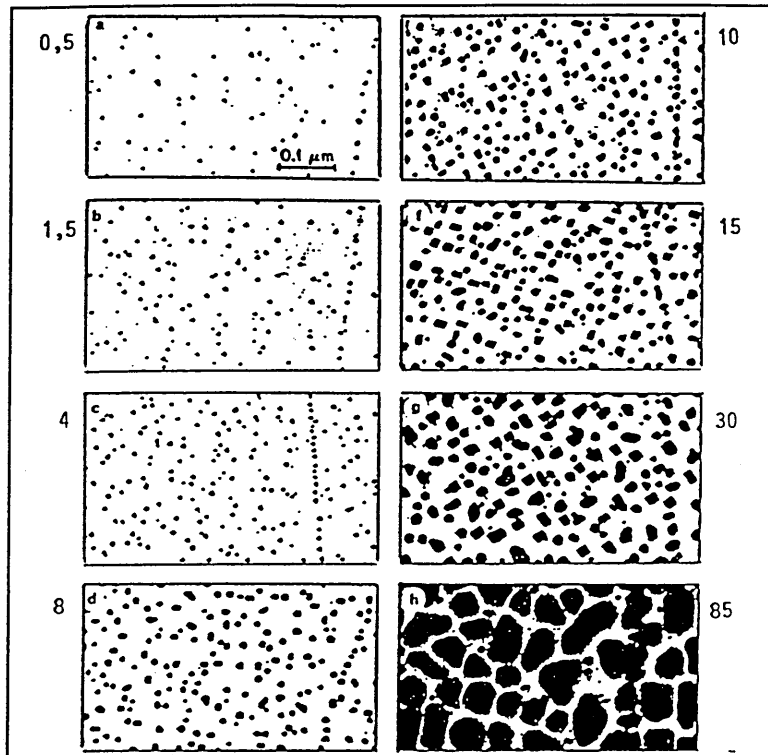


Figure 2.28: Coating Growth

clusters and condensed atoms are diffusing in the crystal lattice (volume diffusion). Once they have a critical cluster size the film will begin to grow around these sites as islands, which will expand across the surface until they meet adjacent islands (Figure 2.28). The nucleation is depending on the defect density. As the islands expand and their growth fronts meet, a grain boundary defect is generated and growth can then only continue vertically [54, 66]. In the first two nm the film properties and growth are determined.

The mobility of the adatoms is increasing with increasing temperature. The substrate temperature has a big influence on the coating structure. The exact nature of the columnar structure varies with different deposition conditions from porous, open-structure through a fine-grained, fibrous structure to

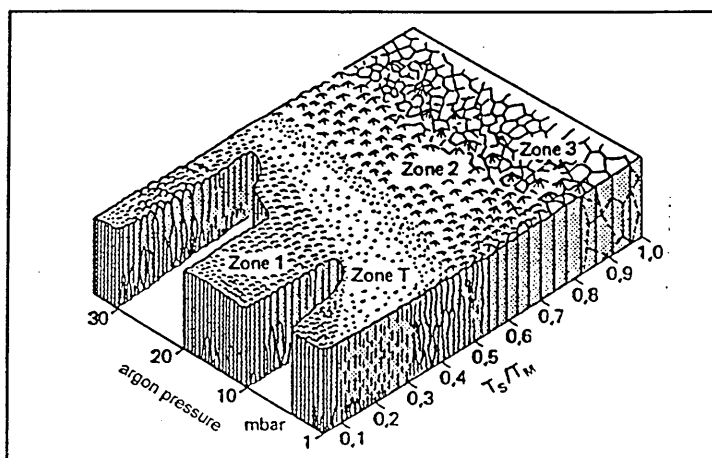


Figure 2.29: Thornton Diagram [67]

recrystallised densely packed columns. This influence was described for vacuum metallizing by *B A Movchan* and *A V Demchisin* and was further developed for sputtering by *JA Thornton* [67]. The Thornton diagram (Figure 2.29) shows the coating structure depending on the ratio of the substrate temperature T and the melting point of the coating material in Kelvin versus the argon pressure in mbar. The low temperature zone 1 structure corresponds to low adatom mobility and consists of widely spaced columns with domed or angular tops with a dark grey surface. Zone T consists of densely packed but poorly defined fibrous grains. In the area below T/T_m 0.75 there are nano-, micro- and macro columns and -hollows [57]. The mid temperature zone 2 structure corresponds to significant surface diffusion effects and consists of densely packed columns with a smooth surface. For the high temperature zone 3 structure, bulk diffusion and recrystallisation becomes the dominant process with smooth flat grains and grooved boundaries.

Messier et al showed, that the growth of the coating can be influenced by bombarding the substrate with high energy particles, leading to a higher movability of the adatoms. This can be realised

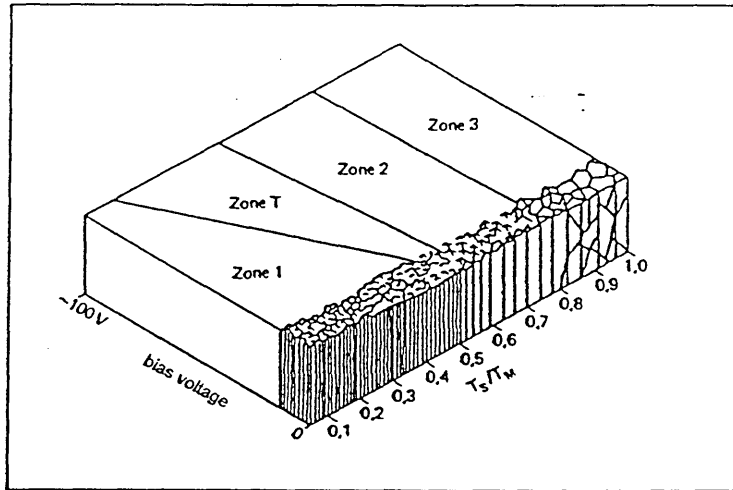


Figure 2.30: Messier diagram

by applying a bias voltage onto the substrate, resulting in dislocating the boundary between zone 1 and T to lower temperatures with increasing ion current density (Figure 2.30). [92].

2.5 Test Methods

2.5.1 Glow Discharge Spectroscopy

Glow Discharge Optical Emission Spectroscopy (GDOES) relies on excitation of atoms within the sample being analysed. Electrons pass over to a lower energy level during relaxation and emit radiation quanta with characteristic frequency and wavelength [68]. Hence excitation of different elemental atoms will give rise to the emission of characteristic spectral lines by which those elements may be identified. The intensities of the lines are proportional to the number of emitted quanta, and hence to the element concentration. This is the essence of atomic emission spectroscopy [54].

In the Glow Discharge Optical Emission Spectroscopy (GDOES) the sample to be analysed forms the cathode at one end. The hollow cylindrical anode is in a small vacuum chamber, filled with argon as a working gas. The other end of the vacuum chamber contains a window through which the photon emission is detected via a polychromator.

An applied voltage between the anode and the cathode causes ionisation. Those argon ions are then accelerated towards the cathode. On impact, kinetic energy is transferred which causes the sputtering of neutral cathode atoms (at a sputtering rate in the range of 10 to 100 nm per second) and secondary electrons (sustaining the discharge). The sputtered cathode atoms diffuse across the dark space into the negative glow region and are excited or ionised by collision with secondary electrons or argon ions. These excited atoms will emit characteristic line spectra.

The quantification of the sputtered depth from the sputtering time can be subsequently checked by surface profiling the sputter erosion craters after analysis and comparing with the glow discharge plots and can be calibrated using a surface profilometer or directly from available sputter yield data.

The determination of the chemical content from the emission line intensities is depending on the voltage, current, sputtering rate and chemical composition. Intensity calibration is performed using certified reference materials of known chemical composition.

The analysed composition is normalised to 100%, so it is important to know all the major elements present in the sample.

The characteristics of the Glow Discharge Emission Spectroscopy are given below:

-
- depth profiles of chemical composition
 - depth range from tens of nanometers to tens of microns
 - depth resolution can be as low as 5 to 10 nm
 - can cover all elements of the periodic table
 - simultaneous analysis of 40 elements
 - analysis is quantitative and accurate, provided suitable calibration samples available
 - ppm accuracy is possible
 - easy sample preparation, only flat surface necessary
 - area of analysis is 4 mm diameter
 - analysis can be very fast for routine precalibrated samples

2.5.2 Adhesion and Scratch Test

Adhesion is defined as "the state in which two surfaces are held together by interfacial forces which may consist of valence forces or interlocking forces or both" (ASTM D907-70). The nature of these bonding forces are van der Waals, electrostatic and / or chemical bonding forces which are effective across the coating-substrate interface. The practical adhesion is a macroscopic property which depends on chemical and mechanical bonding at the interface, residual stress and the presence of any stresses imposed [66].

Depending on the brittle / ductile properties of the coating and substrate a number of possible failure modes can occur in any application. If a break occurs at the interface it is termed adhesive failure, and if it occurs within the substrate or the coating it is named cohesive failure. A number of techniques have been developed in order to improve the adhesion, for example:-

- (i) pretreatments - cleaning and degreasing of components prior to loading coating systems
- (ii) in situ treatments - such as heating, plasma treatment, sputter cleaning. Higher process temperatures lead in general to better adhesion, caused by increased surface mobility, inter-diffusion and the formation of chemical bonds.
- (iii) bonding layers - to form strong interfacial phases, minimise interfacial stresses and getter contaminations [66].

At the present time there are no tests for the measurement of practical adhesion which fulfil requirements like easily adaptable to routine testing, relatively simple interpretation, amenable to standardisation, reproducibility, quantitative and directly related to coating reliability. All of the commonly used tests are destructive in nature [69, 70].

Methods of adhesion evaluation are eg. Pull-Off methods (ie tape test) and the scratch test. The methods used in this thesis are the scratch test and the indentation test, which are described in more detail below.

Scratch Adhesion Test

The scratch test was introduced by Heavens and was later developed by Benjamin and Weaver. In the scratch test, an indenter is drawn across the coated surface while a continuous or stepwise increasing normal load is induced (Figure 2.31). When the critical normal force F_c is reached, a failure event occurs which is detected by optical or other means. Provided that the observed event represents the loss of adhesion at the

coating-substrate interface, the critical load can be used as a qualitative measure of the coating-substrate adhesion [71]. The critical force value cannot be directly related to the strength of the coating-substrate interface. Coating thickness, substrate hardness, surface roughness, stylus radius, scratching speed, loading rate and gradual wear of the diamond stylus have a significant influence on F_c .

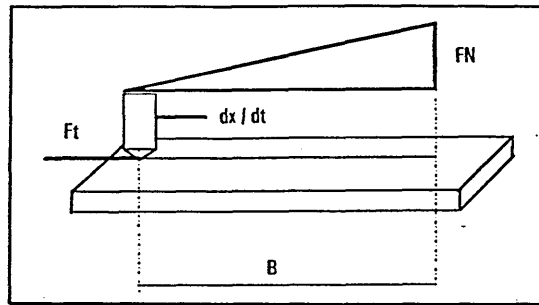


Figure 2.31: Scratch adhesion test

Identified mechanisms of coating damage and detachment are given in figure 2.32 [72] and figure 2.33 [73].

	Pronounced plastic deformation	PPD
	Stick-slip deformation	SSD
	External parallel cracking	EPC
	Internal transverse cracking	ITC
	External transverse cracking	ETC
	Coating debris removal	CDR
	Discontinuous chip removal	DCR
	Continuous chip removal	CCR
	Splinter-like parallel flaking	SPF
	Sideward lateral flaking	SLF
	Forward lateral flaking	FLF

Figure 2.32: Coating damages

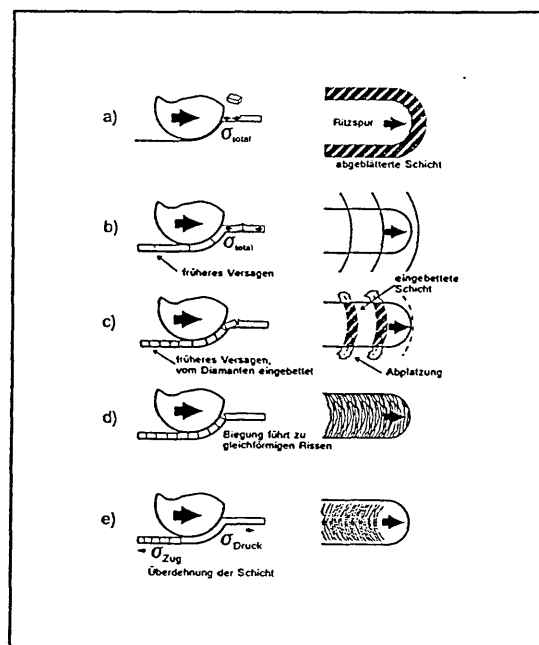
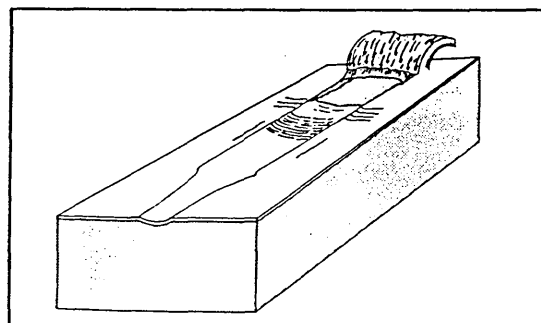


Figure 2.33: Failure of coatings

Figure 2.34: Schematic damage mechanism



The coating thickness and substrate hardness not only influence the critical normal force, but also have a strong effect on the occurrence and relative importance of the various coating damage mechanisms. As a result of the low mechanical resistance of the used brass substrate, the coating begins to be damaged at a low critical load. Figure 2.34 shows a schematic representation of the coating damage mechanism route for low composite hardness: external parallel cracking, internal transverse cracking and external transverse cracking. A typical part of a scratch test image obtained from an aluminium coated brass sample is shown in figure 2.35.

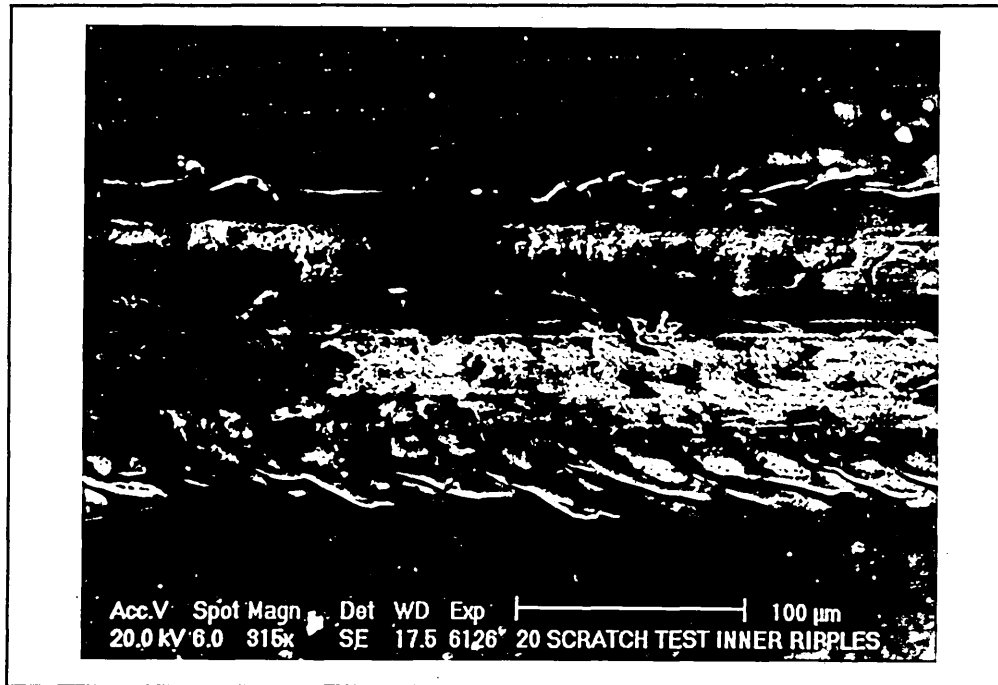


Figure 2.35: Typical part of a scratch test image

The use of the scratch test for the characterisation of ductile coating-substrate systems has been described previously by many authors. A modified scratch test for study of the adhesion of soft and ductile coatings was introduced by N Frey et al in 1994 [71]. It is based on the simultaneous measurement of the normal and tangential forces. The critical normal force is determined from the observation of a transition in the slope of the curve tangential force vs normal force. The applied

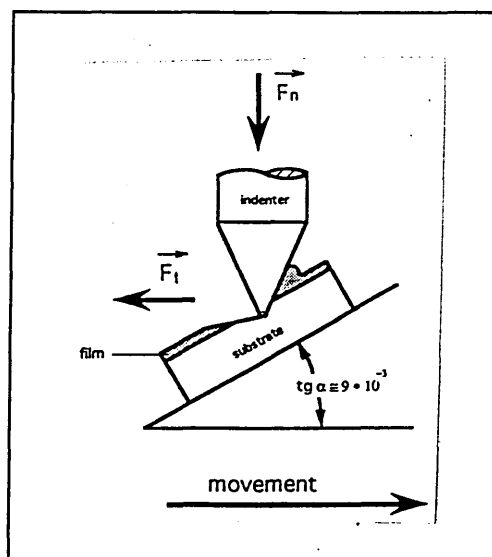


Figure 2.36: Modified scratch test

forces are smaller by two orders of magnitude than in the case of brittle coatings. The sample is inclined at an angle between 0.3° and 0.6° with respect to the horizontal (figure 2.36).

A further method to determine the failure point was the acoustic emission, which was recorded by a plotter as a function of the load applied [37]. It showed a well defined critical load on a CrN/Cr coatings system on brass.

2.5.3 Hardness

Hardness is the equivalent of the average pressure under the indenter, calculated as the applied load divided by the projected area of contact between the indenter and the sample [74, 88].

Generally the hardness of a bulk material is evaluated through the determination of the indentation size (diagonal). In fact, this measuring procedure is fast and simple. For thin films, functional coatings and surface modified layers however, to obtain correct hardness values, it is necessary to produce very small indentations. Accepted hardness measurements for thin coatings are Vickers and Knoop. The minimum limit for Vickers is a coating thickness of 3 μm , for Knoop 1.5 μm .

To measure the hardness of hard coatings without being influenced by the substrate, the maximum indentation depth must be below 10 % of the coating thickness. In the case of soft coatings, the maximum depth must be not more than 25 % of the coating thickness (ASTM STP 889, Philadelphia 47). This criteria is often difficult, if not impossible, to satisfy for coatings below 2 μm in thickness by means of conventional microhardness tests. The minimum loads which are commonly used in microhardness testing are of the order of 2 to 5 g. The smaller the size of the indentations, the better the surface preparation must be, since the precise optical evaluation of the diagonal becomes increasingly difficult. A measurement error of 10-15 % corresponds to an error in the hardness value of 20-30 %. Such errors can be avoided by using the indentation hardness principle, which was introduced by S I Bulychiev et al in 1976.

This method is recommended for coating thickness less than 5 μm : the universal hardness HU (ISO/TC 164/SC 3N 556, VDI/VDE 2626). It measures ultra-low load hardness under test load, based on penetration depth measurements during a loading and unloading cycle with specially shaped indentors. Based on the correlation between the indentation depth and the geometry of the indenter, a physically meaningful universal hardness number is derived: $HU = F / (26.43 h^2)$ in N/mm^2 . The hardness value HU is derived from the test load F and the indentation surface area, which is obtained from the indentation depth h. The application of the test load and the measurement of the indentation depth is based on technologies which have been developed to achieve test uncertainties of less than 1 %. In a single test cycle information are received about surface hardness and a hardness profile as a function of indentation depth in the layers close to the surface, elastic and plastic properties, and the creep behaviour of the material. The hardness profile is obtained from a single indentation point. This eliminates influences on the result through measurements at various points of the

surface area in question. The test is automated and free of any subjective operator influences [75].

Figure 2.37 shows schematically the process of indentation and relaxation as well as a test cycle. Upon unloading, the curve AP_{\max} represents the behaviour of a plastic material, the curve AO that of a fully elastic material, and the curve AB that of an elasto-plastic material. O is the point of physical contact between indenter and surface, A is the point of contact under maximum load, F_{\max} , B the point after total unloading. The unloading portion of the F/P diagram is used to determine the plastic depth, which allows evaluation of the microhardness HV and the Young's modulus E .

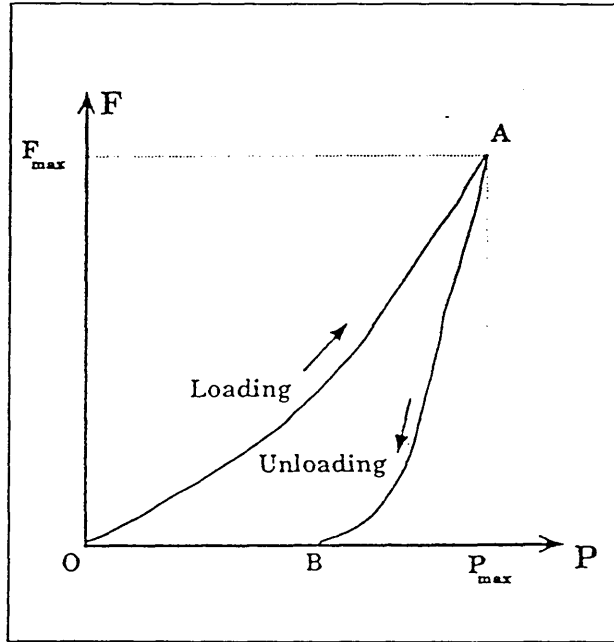


Figure 2.37: Schematic penetration of a complete loading and unloading cycle

2.5.4 Indentation Adhesion Test

During the indentation adhesion test the sample is submitted to a hardness testing with a diamond cone (Figure 2.38). Due to indentation crater, which is analysed under a light microscope, a qualitative statement about the adhesive strength and the ductility of the coating is received.

A diamond hardness indenter penetrates the sample surface. When a coated material is subjected to a localised normal load, the coating deforms. Figure 6.8a shows a Rockwell indentation in top view and figure 6.8b the indentation in cross section. It shows an adhesive coating down into the indentation, which leads in many cases to a pushing of the coating into the substrate and a significant stretching and a large membrane stress, respectively occurs.

If the load is extremely high like in the HRC test with 150 kg, not only adhesive but also cohesive failure occurs. Figure 6.9a shows a Rockwell indentation with adhesive failure mechanism along the edge as cracks and delaminations. The two circular delaminations around the indentation show cohesive failure mechanism within the substrate - coating interface region. Figure 6.9b shows the indentation in cross section. The coating is delaminating, as can be seen at the marked positions.

Rockwell indentations in soft coatings on soft brass substrate showed a totally different failure mechanism as described and classified in the DIN Fachbericht 39 (Classification of thin layers, 1993).

Hence the common Rockwell adhesion test was replaced by a Vickers adhesion test for soft coatings on soft substrate. The optimum load was found to be 2.5 kg. The produced indentation is observed using a light microscope at a magnification of 500 and 1000 times. The classification made is "good" or "bad" as described in chapter 3.5.5.

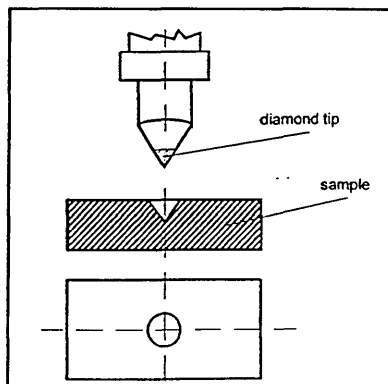


Figure 2.38: Scheme of Rockwell adhesion test

2.5.5 X-Ray Diffraction XRD

To determine the crystalline structure of coatings XRD was used. The samples are examined using monochromatic Cu K α radiation with a typical penetration depth of 20 μm . Using Bragg's law the reflected radiation is analysed using a spectrometer. The peaks derived from the crystalline lattice can be identified using ASTM or JCPDS reference cards. Using the equations given in chapter 3.5.7 information can be obtained about the texture, lattice parameter, macro and micro elongation as determined from the breadth of the x-ray reflections, tension and grain size.

Using a equation which was developed by Nelson and Riley the lattice parameter can be extrapolated, because the lattice parameters are not all the same for all reflections as known from literature caused by lattice distortions.

The Hall-Williamson equation is used to calculate the elongation and grain size.

Coatings may have a preferential orientation because of the preferred growth in certain lattice directions as shown in figure 2.39. The textures can be calculated from the reflection intensities.

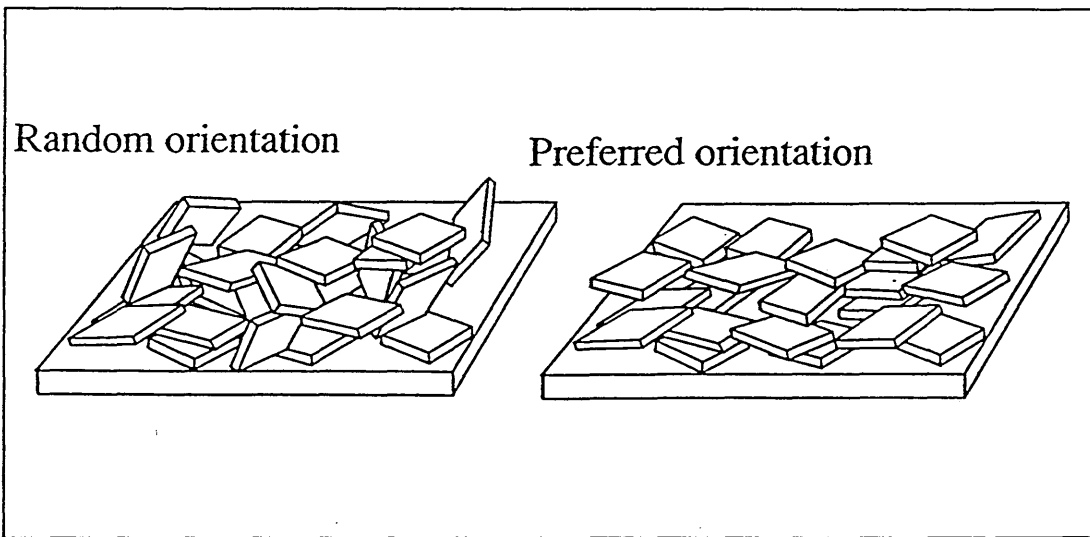


Figure 2.39: Random and preferred orientation

2.5.6 Corrosion Tests

For any specific problem, reliable and quick methods to assess the corrosion resistance are required. There are various kind of corrosion testing methods which are not standardised [77].

Industrial corrosion tests can be distinguished in long term-, short term and quick corrosion test. In long term tests the conditions are almost real, whereas in short term tests the temperature is enhanced or the chemical agent concentration is increased to get evaluateable results in a shorter time. The application of such results into the reality has to be done with great care and a combination of various tests is recommended [30]. Using quick corrosion tests totally different corrosion chemicals are used to shorten the examine time further more. This results are not transferable into the reality. If the coating is less noble than the substrate material, such corrosion tests are useless, because the substrate materials are cathodically protected. But still this test are used commonly to detect failures in the coatings. The industrial used corrosion tests for decorative parts are given below:

(i) Porosity test HNO_3 [5]

(ASTM B 735) Test method for porosity in gold coatings on metal substrates by nitric acid vapour

(ASTM B 765) Guide to the selection of porosity tests for electrodeposits and related metallic coatings

(EIA 364-53: Electronic Industries Assoc., Washington USA) Determines the magnitude of porosity and other surface defects inherent in application of gold contact finished and is to be used as an evaluation technique for their acceptability.

(ii) Salt spray tests (ISO 9227 / DIN 50 021 / BS 7479)

Specifies standard conditions for corrosion spray tests including salt spray testing:

NSS neutral salt spray test

AASS acetic acid salt spray test

CASS copper-accelerated acetic acid salt spray test

(iii) Sweat test (DIN 50 958 / DIN ISO 6425 / 1)

Testing of electroplated coatings; corrosion test of chromium plated parts according to the modified corrodokote test

BAM Bundesanstalt für Materialprüfung: Handschweißtest

(iv) Thioacetamide Test (TAA test) (BS 5466 Part 4 / ISO 4538)

[CH₃CSNH₂] Thioacetamide is a carcinogen. All contact with human skin should be avoided.

(v) KFW 2,0 S (DIN 50 018)

Testing in a saturated atmosphere in the presence of sulphur dioxide
(Kondenswasser-Wechselklimatetest)

(vi) NH₃ Test (DIN 50 916 Part 1, 2 / ISO 6957)

Testing of copper alloys; stress corrosion cracking test in ammonia, testing of tubes, rods and profiles

(vii) Kesternich test, following (BS 5466 Part 8 / DIN 50018)

[SO₂] test, which was also described by Clarke and Sansum as a two hour porosity test at 60 °C [78, 79].

(viii) bending as a plastic deformation and then corrosion test [36]

(ix) electrochemical corrosion tests (DIN 50918) which do not offer a correlation to technical results.

CHAPTER 3: Experimental Techniques

3.1 Diffusion Test

The loss of Zn from the surface and the diffusion of Zn into the barrier layers were investigated by heat treating uncoated and coated brass specimens at different temperatures up to 300 °C for different times. Samples were cooled down immediately after annealing in a freezer at -20°C to avoid further diffusion of Zn caused by the residual heat.

The equipment used was as shown in figure 3.1 and featured: (i) electrically heated oven (Carbolite Furnacer RHF 1200) with sensor to regulate the temperature to the set value, no air circulation and volume = 3.4 dm³, (ii) argon cylinder with flow rate regulator, (iii) thermocouple type K, (iv) digitizer to determine the temperature and (v) plotter to plot the temperature versus time.

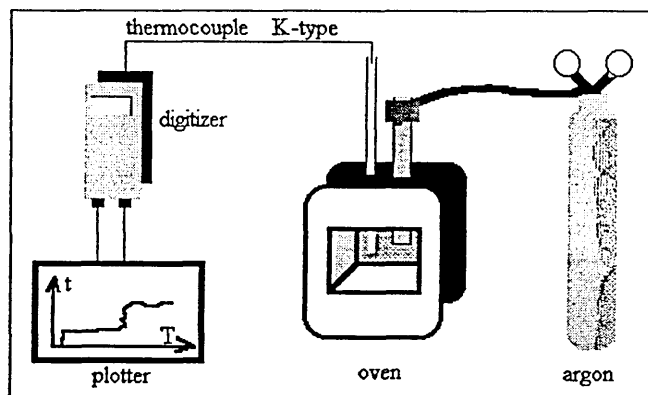


Figure 3.1: Equipment for diffusion annealing

Details of the heat treatments used are given below:

❶ Specimens are prepared to investigate the surface loss of Zn. 36 brass specimens were prepared as described in section 3.2 and heat treated using all combinations of temperatures and times. The temperatures and times investigated were: 50, 100, 150, 200, 250, 300 °C and 15, 30, 45, 60, 75, 90 min respectively.

The results obtained from these experiments are given in section 4.1.

❷ Specimens are prepared to investigate the Zn diffusion through the barrier layer. 12 brass specimens were prepared as described in section 3.2 and heat treated as follows: 5, 10, 15, 20, 25, 30, 35, 40, 45, 50, 55 and 60 min at 250 °C.

The results obtained from these experiments are given in sections 4.4.

The distribution of zinc in the heat treated specimens was investigated by both metallography and GDOES techniques (see sections 3.5.9 and 3.5.3 respectively)

3.2 Sample Preparation

Brass discs for use in the investigation of the mechanical and analytical properties of the thin PVD layers were prepared for coating by grinding, polishing and cleaning.

Brass sheets for use in the investigation of the adhesion behaviour (bending test) and brass rods to investigate the fracture characteristics were prepared for coating by polishing and cleaning.

The alternative, much simpler and more effective, electropolishing method is not possible to apply on brass with the high lead concentration in samples, used in the experiments described here.

3.2.1 Grinding and Polishing

Mechanical grinding and polishing of brass discs was performed using an automatic variable speed grinder-polisher machine BUEHLER Ecomet 3 with Automet 2 power head. The following steps were performed when preparing 6 samples in a single holder (table 3.1):

Preparation step	particle size	medium	force	speed	time	rotation	paper
(i)	240	SiC	30 lb	150	2	↺	
(ii)	washing						
(iii)	320	SiC	30 lb	240	2	↺	
(iv)	ultrasonic cleaning for 2 min						
(v)	3 μm	diamond	30 lb	240	4	↺	PSU
(vi)	3 μm	diamond	30 lb	240	4	↺	PSU
(vii)	ultrasonic cleaning for 2 min						
(viii)	1 μm	diamond	30 lb	250	2	↺	PSA
(ix)	ultrasonic cleaning for 2 min						
(x)	0.25 μm	diamond	by hand				PSA

Table 3.1: Grinding and polishing parameters

In contrast sheet and rod test pieces were polished by hand using a cloth impregnated with 1 μm diamond.

3.2.2 Precleaning

The precleaning behaviour of brass test pieces was intentionally investigated when they were subjected to different cleaning procedures.

(i) Polished with Sidolin®* until a bright finish was obtained followed by ultrasonic cleaning in acetone to remove polishing residues before hot air drying.

(ii) The standard pretreatment normally used in PVD coating is summarised in table 3.2:

step	function	medium	temp [°C]	ultra-sonics	time [min]
1	degreasing	2 % banner clean 16** in tap water	70	yes	3
2	rinse	tap water	RT	no	0.5
3	rinse	de ionised water	RT	yes	3
4	final rinse	de ionised water	RT	no	1
5	drying	hot air dryer	100	no	5-10

Table 3.2: cleaning parameters for the cleaning line

(iii) Ultrasonic cleaning in acetone followed by hot air drying

(iv) Cathodic degreasing [80] using a proprietary alkaline cyanide solution, Kleenax salt***, at 40 °C for 2 min using a cathodic current of 30 mA/cm². Following cathodic treatment test pieces were washed in distilled water, activated in 10% HCl, washed in distilled water, dipped in ethanol and quickly dried in hot air.

(v) Cathodic degreasing for 30 s at 8 V, followed by an anodic degreasing for 5 s at 4 V in an alkaline degreasing electrolyte: Henkel P 3 galvaclean 62, 50 g/l at 20 °C. Following cathodic and anodic treatment test pieces were washed in distilled water, activated in nitric acid 290 g/l for 30 s, washed in distilled water, dipped in ethanol and quickly dried in hot air [31]. For product data sheet see appendix.

* metal polish with 5 - 10% soap, ammoniumcitrat, alkohol, ammonia, polishgrains

** banner clean 16: isopropyl alcohol 20% with anionic and non-ionic surfactants

(Samuel Banner & Co. Ltd., Liverpool)

*** cyanide based degreaser (Canning, Birmingham)

(vi) Degreasing in Henkel RST at a concentration of 4 % at a temperature of 70 °C for 3 min with ultrasonic support or 10 min without ultrasonic support. For product data sheet see appendix. The method was finally applied to all experiments described here.

(vii) To remove smeared lead on the surface of brass specimens formed as a result of the polishing procedure.

Samples were etched as follows:

- (i) 30 s, 2 and 5 min in 280 g/l fluoroboric acid HBF_4
- (ii) 30 s, 2 and 5 min in 290 g/l nitric acid HNO_3

To investigate the removability of smeared Pb layers from the surface analysis was done as follows:

- (i) samples were electroplated with cyanidic Cu to protect the specimens surface for the depth profile made using GDOES in order to see an accumulation of Pb.
- (ii) X-ray mapping of the Pb $\text{M}\alpha$ line.
- (iii) optical microscope. Pb inclusions were made visible using a colour technique as described in [81], painting the surface with a marker pen. The best contrast was obtained using a blue water resistant OFREX OHP Permanent pen.

3.3 Cleaning in the PVD Chamber

The loss of Zn from the substrate surface and the changes in the surface roughness resulting from the cleaning procedures were investigated. The pretreatments used were argon ion etching, metal ion etching and a combined argon followed by a metal ion etch.

The brass specimens were prepared as described in section 3.2 and the distribution of Zn in their etched surfaces was determined by GDOES techniques (see section 3.5.3). The change in roughness of the surfaces following etching was measured as described in section 3.5.10.

Details of the cleaning treatments used are given below. The results obtained from these experiments are given in section 4.3.

3.3.1 Argon Ion Etching

Substrate cleaning was performed in the glow discharge mode with the shutters open, using a bias voltage of -800 V and a maximum temperature of 137 °C for 20 min. The target voltage was set at 120 V and the coil currents of all four targets were set to 5 A.

3.3.2 Metal Ion Etching

Substrate cleaning was done in the ion etching mode with the shutters closed, using a bias voltage of -600, -800, -1000 and -1200 V and a maximum temperature of 200 °C for 7 min. The target power was set at 1.8 kW with no coil current to any of the four targets.

3.3.3 Combined Argon and Metal Ion Etching

Argon ion etching was carried out initially with the shutters open, using bias and target voltages of -800 and 120 V respectively for 20 min. Subsequent metal ion etching of specimens was carried out for 1 min using bias voltages of -800, -1000 and -1200 V respectively with shutters closed.

3.4 Coating Processes in the PVD Chamber

Mechanical, analytical and structural properties as well as appearance of PVD coatings on brass substrates resulting from the coating procedures were investigated.

The brass specimens were prepared as described in section 3.2 and the distribution of Zn was determined by GDOES techniques (see section 3.5.3). The adhesion of the coatings was classified using the scratch adhesion test (see section 3.5.4), the indentation test (see section 3.5.5) and bending test (section 3.5.12). Coating thicknesses were determined by using the calotest, the step scan and GDOES techniques. Details are given in section 3.5.6. Coating structure was determined using XRD as described in section 3.5.7 and both topographical and cross section images were recorded using SEM (section 3.5.8) and metallographic techniques (section 3.5.9).

A typical procedure used to coat a specimen was as follows:

(i) **Pump down.** Pump out the chamber to a base pressure below 10^{-5} mbar. This would take typically 2 h, depending on how long the chamber had been left open. A leak rate below 10^{-3} mbar l s^{-1} was also obtained.

(ii) **Heating.** In order to eliminate water vapour the chamber was heated by in-built heating elements to an appropriate start temperature.

(iii) **Target sputter cleaning.** For every process target cleaning was carried out in glow discharge mode with the shutters closed for 15 min. The argon gas flow rate of 10 % resulted in a working pressure of 2.5×10^{-3} mbar. The target power was set at 4 kW with no bias voltage and no coil current to any of the four targets. Vertically mounted substrates were subjected to a two fold planetary rotation at a distance of 25 cm from the targets.

(iv) **Substrate cleaning.** Substrates were cleaned in ion etching or glow discharge mode with an argon gas flow rate of 10 % at a working pressure of 2.5×10^{-3} mbar. Etching voltage -800 V. Details are listed in table 6.2.

(v) **Coating.** The substrates were coated in UBM Mode with an argon gas flow rate of 8 % at a working pressure of 2.5×10^{-3} mbar.

Additional details concerning steps (iv) and (v) relating to specific processes are given below. Details are listed in table 6.2.

(vi) **Cooling down.** This would take typically 30 to 60 min.

3.4.1 Aluminium Diffusion Barrier (Al)

Substrate cleaning was carried out in either glow discharge mode or ion etching mode. In order to keep the specimen temperature as low as possible both the glow discharge and ion etching cleaning were carried out in an intermittent manner. Thus periods of cleaning were alternated with periods in which the specimens were allowed to cool. In each case cleaned specimens were allowed time to cool to a suitable temperature before the coating process started.

During processes, the effect of separate variations in coil current and temperature were investigated. The temperatures investigated were between 60 and 180 °C and coil current variations were made in the range of 4 x 1.5 A to 4 x 6 A. Typical coating parameters were a coating time of 40 or 60 min at a constant target power of 2 x 5 kW with an applied bias voltage of -50 V.

The results obtained from these experiments are given in section 4.4.1.

3.4.2 Aluminium - Niobium Diffusion Barrier (Al-Nb(X))

Substrate cleaning was carried out in the ion etching mode. In order to keep the specimen temperature below 138 °C the ion etch cleaning as well as the coating processes were carried out in an intermittent manner. As in the preparation of Al diffusion barrier layers, periods of cleaning and coating were alternated with periods in which the temperature of the specimens were allowed time to cool down to 100 °C.

The process was operated using a Nb target with different applied powers with a view to optimise the power required to produce shiny, dense, corrosion resistant and adhesive coatings. The power associated with the Nb target was 5, 10, 20 and 50 % of the total power associated with the two Al targets on the four runs respectively.

Additionally standard Nb coatings were produced on top of the Al-Nb(X) coatings as described in section 3.4.5 (ii).

The results obtained from these experiments are given in section 4.4.2.

3.4.3 Copper-Aluminium Diffusion Barrier (CuAl8)

Substrate cleaning was carried out in ion etching mode with a bias voltage of -800 V and a current of 80 A for 3 min. Various temperatures were used for the coating processes, carried out with 10, 15 and 20 kW target powers, -75 V bias voltage and a coil current of 2, 3 and 6 A to each target for 30 min and 60 min respectively. Additionally a standard Nb coating was deposited on top of some CuAl8 coatings as described in section 3.4.5 (ii) and stated in table 6.2.

The results obtained from these experiments are given in section 4.4.3.

3.4.4

Copper-Aluminium-Niobium Diffusion Barrier (CuAl8-Nb(X))

Substrate cleaning was carried out in ion etching mode with a bias voltage of -800 V and a current of 80 A for 3 min. The process was operated using a Nb target with different applied powers with a view to optimise the power required to produce shiny, dense, corrosion resistant and adhesive coatings. The power associated with the Nb target was 5, 10, 20 and 50 % of the power associated with the CuAl8 target on the four runs respectively.

Additionally standard Nb coatings were produced on top of the CuAl8-Nb(X) coatings as described in section 3.4.5 (ii). The results obtained from these experiments are given in section 4.4.4.

3.4.5 Niobium Coatings (Nb)

Substrate cleaning was performed in ion etching mode at 70 to 80 A arc current and an applied bias voltage of -800 V for 3 min.

Nb coatings were applied on

(i) pure brass using various temperature processes in combination with different bias voltages of -50, -75 and -100 V. The coil current was changed from 4x3, 4x4, 4x5 and 4x8 A in order to investigate the influence on the coating properties. The coating time was 60 minutes each with a target power of 10 kW. The results obtained from these are given in section 4.4.5.

EXPERIMENTAL TECHNIQUES

(ii) brass precoated with Al-Nb(X) and CuAl8-Nb(X) diffusion barriers as given in section 3.4.2 and 3.4.4. The Nb coatings were produced having a target power of 8 kW for the Al-Nb(X) coatings and 10 kW for the CuAl8-Nb(X) coatings. The applied bias voltage was -75 V and the coil current was 3 A on each target for a coating time of each 30 min. One process used the same parameters for a coating time of 60 min.

The specimen temperatures were allowed to increase until the processes ended.

3.5 Testing Methods

3.5.1 Sulphur Dioxide Corrosion Test

This corrosion test, a variation of the Kesternich test (BS 5466 Part 8 and BS 6670 Part 2 / DIN 50018) was developed by Clarke, Sansum and Leeds [78, 79, 82] as a quick means of monitoring the porosity, especially of noble metal coatings. In the present work the test was applied to PVD coated brass specimens which were exposed in a humid sulphur dioxide containing atmosphere in a 10 l chamber.

The volume of the solution is 1/40 of the test chamber = 250 ml. The mixture was made up from four volumes of 20% sodium thiosulphate (40 g / 200 ml H₂O) and one volume of 50/50 concentrated sulphuric acid / water solution (50 ml). This solution leads to a controlled test atmosphere which is approximately 10 % sulphur dioxide at 86 % relative humidity.

The standard exposure time used is 24 h, but in these tests the samples were exposed to attack for 72 h with visual observation every 24 h. Pore sites which developed during the test showed up as matt spots which consist of corrosion products. The development of corrosion products at the interface between the substrate and coating lead to its delamination. The occurrence of porosity, as indicated by the appearance of corrosion products, was evaluated during observations following test periods of 24, 48 and 72 h. This allowed to rank the porosity of different coatings.

3.5.2 Ammonia Porosity Test

Porosity and corrosion resistance was determined using a NH_3 porosity test which was described by Siemens / Belgium [83]. This test was developed as an effective porosity test for coatings on copper containing substrates.

PVD coated brass specimens were exposed in a humid ammonia containing atmosphere, which was generated in a desicator having a volume of 7 l. The solution used to generate the test atmosphere contained 350 g potassium citrate in 98 ml of water. This solution produces a controlled test atmosphere of approximately 63 % relative humidity. Powdered ammonium carbonate (140 g) contained in an open beaker was also present in the test chamber. Test specimens were placed above the solid and liquid reagents.

The standard exposure time for the test is 16 h. During the test the development of spots of blue corrosion products indicate the presence of pores. The formation of corrosion products during the test at the coating substrate interface lead to delaminations of the coating. The porosity of test samples was evaluated visually under 25 x magnification within a 24 h period following test. The potassium citrate solution can be used repeatedly for this test but a fresh portion of ammonium carbonate should be used for each test.

3.5.3 Glow Discharge Optical Emission Spectroscopy (GDOES)

Depth profiles of the chemical composition were measured using a glow discharge optical emission spectroscope Leco model GDS-750 QDP over a period of 100 s. The sample has to be at least as big as the O-ring seal, ie Ø 5 mm. The instrument was calibrated for determining quantitatively the depth profiles of Cu, Zn, O, C, N and Al. Instrument calibration was carried out using certified reference material of known chemical composition. A typical depth profile plot is shown in figure 3.2.

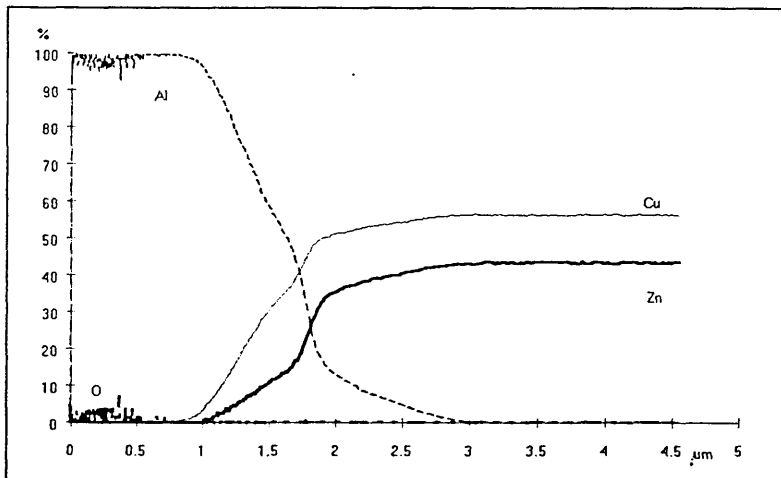


Figure 3.2: Original GDOES depth profile plot

Where appropriate the data from these plots were normalised upon a Cu + Zn value of 100% using purpose written Fortran programme. The normalised plot obtained from the data in figure 3.2, using the relationship $Cu' = (Cu \cdot 100) / (Cu + Zn)$ and $Zn' = (Zn \cdot 100) / (Cu + Zn)$, is shown in figure 3.3.

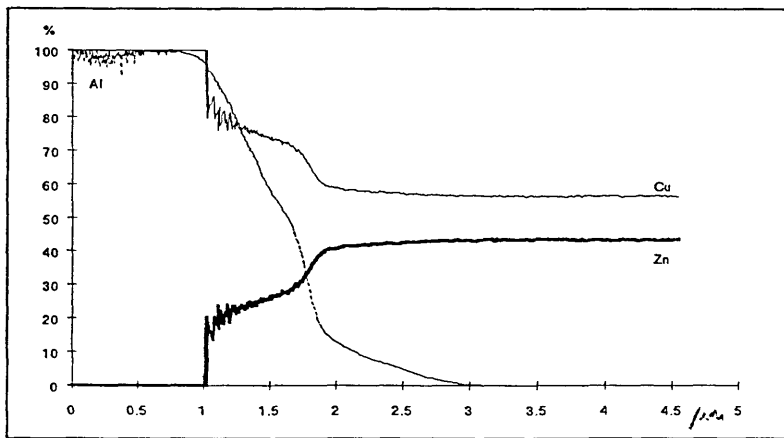


Figure 3.3: Normalized Cu and Zn lines

The line representing Al is unchanged in figure 3.3 from that in 3.2. Elimination of the line representing copper enables interdiffusion of the elements to be more easily represented by a block diagram (Figure 3.4).

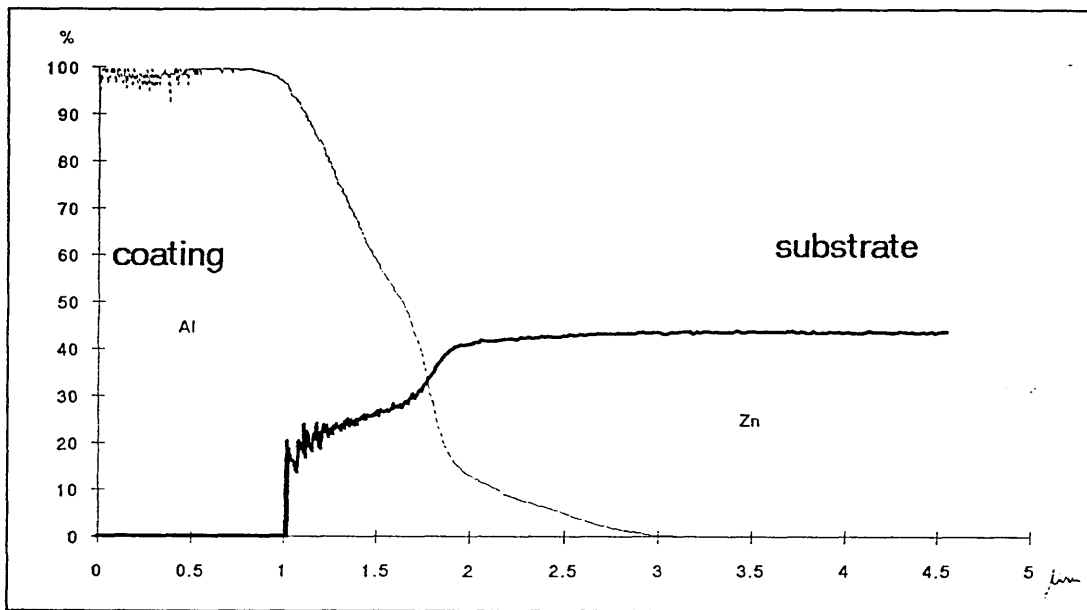


Figure 3.4: Block diagram

Figure 3.4 shows the coating (Al) and substrate (brass) interface as a vertical line and in addition shows the normalised component of the substrate (ie Zn in the brass). Furthermore the y-axis of the diagram simultaneously represents the percentages of the two metallic components being considered (ie in this case Al and Zn) having a value from 0 to 100 and from 100 to 0 % respectively. Thus at any point on the x-axis the two values add up to 100%.

3.5.4 Scratch Adhesion Test

Adhesion of coatings was classified using a Megatech Scratch Adhesion Tester model ST-200. The maximum force used in this test was 100 N, at a controlled loading rate of $F_N/d_t = 100 \text{ N/min}$. The scratch length used was 10 mm, at a table speed of $d_s/d_t = 10 \text{ mm/min}$. This is in line with the DIN Fachbericht 39 [73].

The DIN standard concerning hard coatings can not be applied on soft coatings due to their vastly different characteristics. Only with a few samples could a critical load be detected. This is the load where adhesive failure first takes place. A SEM is used to observe the scratch made by the indenter in secondary electron and back scatter electron images.

The shape of the scratch end can be classified into two types:

- (i) Coatings with good adhesion show straighter edges with a buckled end. Such a compressive surface buckling of a coating is shown in figure 6.18. Cross sections through the scratch at 20 and 80 N positions show that the coating is still adherent (figures 6.19 a and b).
- (ii) Coatings with poor adhesion show distorted edges with cracks and delaminations. Such a failure mechanism is shown in figure 6.20. Cross sections through the scratch at 20 and 80 N positions show that the coating is already partly delaminated at 20 N (figure 6.21 a) and completely delaminated at 80 N (figure 6.21 b).

3.5.5 Indentation Adhesion Test

A qualitative indication of the adhesive strength and ductility of the coating is also given by the indentation adhesion test. A method similar to the Rockwell adhesion test is used.

A Vickers indenter penetrates the coating-substrate system and leads to plastic deformation and upset material around the indentation. To avoid cohesive failure mechanisms in the coatings, the applied force must be at a certain level. Vickers indentation performs an optimum deformation of the brass substrate when a load of 25 N is applied.

Classification of the adhesion was performed using an optical microscope at magnifications of 500 and 1000 x. The two classifications are "good" (Figure 3.5) having no cracks or delaminations and "bad" (Figure 3.6) having cracks and delaminations respectively.

At least two measurements are necessary for good reproducibility.

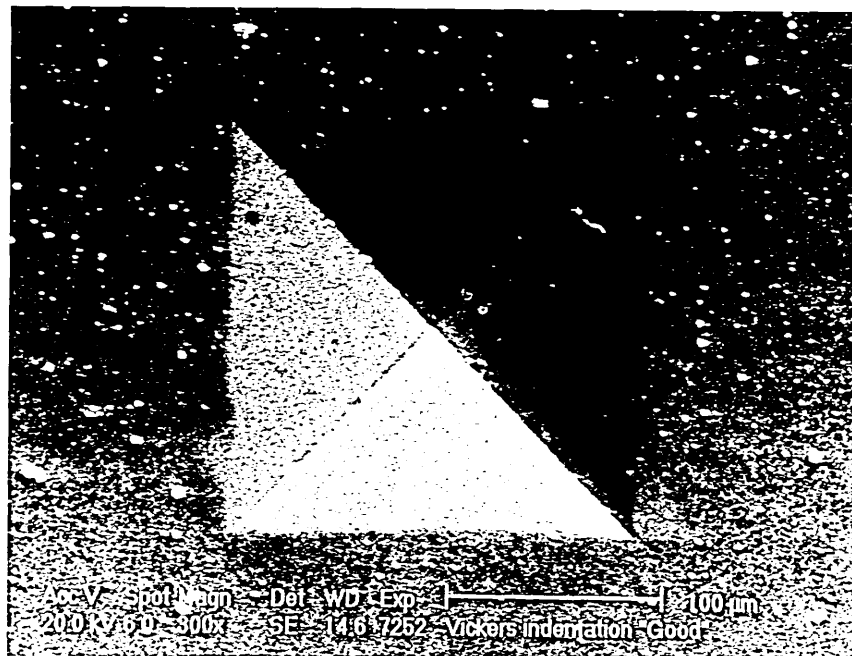


Figure 3.5: Vickers indentation, classification „good“, SEM 300x

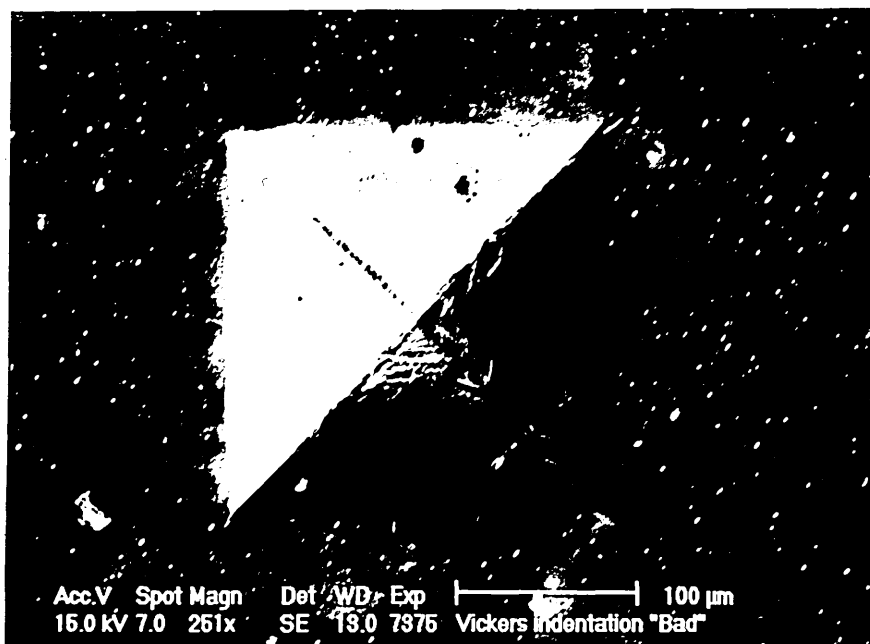


Figure 3.6: Vickers indentation, classification „bad“, SEM 300x

3.5.6 Coating Thickness Determination

The thicknesses of coatings were determined using two different methods:

(i) A ball-cratering instrument EIFELER NORD COATING GmbH model Caloprep. It is necessary to optimise various parameters, ie those associated with the preparation, grinding time, rotational speed and grinding lubricant, as well as the size of the sphere used to grind out a sharply defined crater. After formation the diameters of the craters are measured using an optical microscope fitted with an eyepiece containing a calibrated scale. The coating thickness, s , is then calculated from the diameters of the crater measured at the top (D) and bottom (d) of the coating using following equation (Figure 3.7).

$$s = \frac{1}{2} \left(\sqrt{4R^2 - d^2} - \sqrt{4R^2 - D^2} \right) \text{ where } s, d, D \text{ and } R \text{ (the sphere radius) are in mm}$$

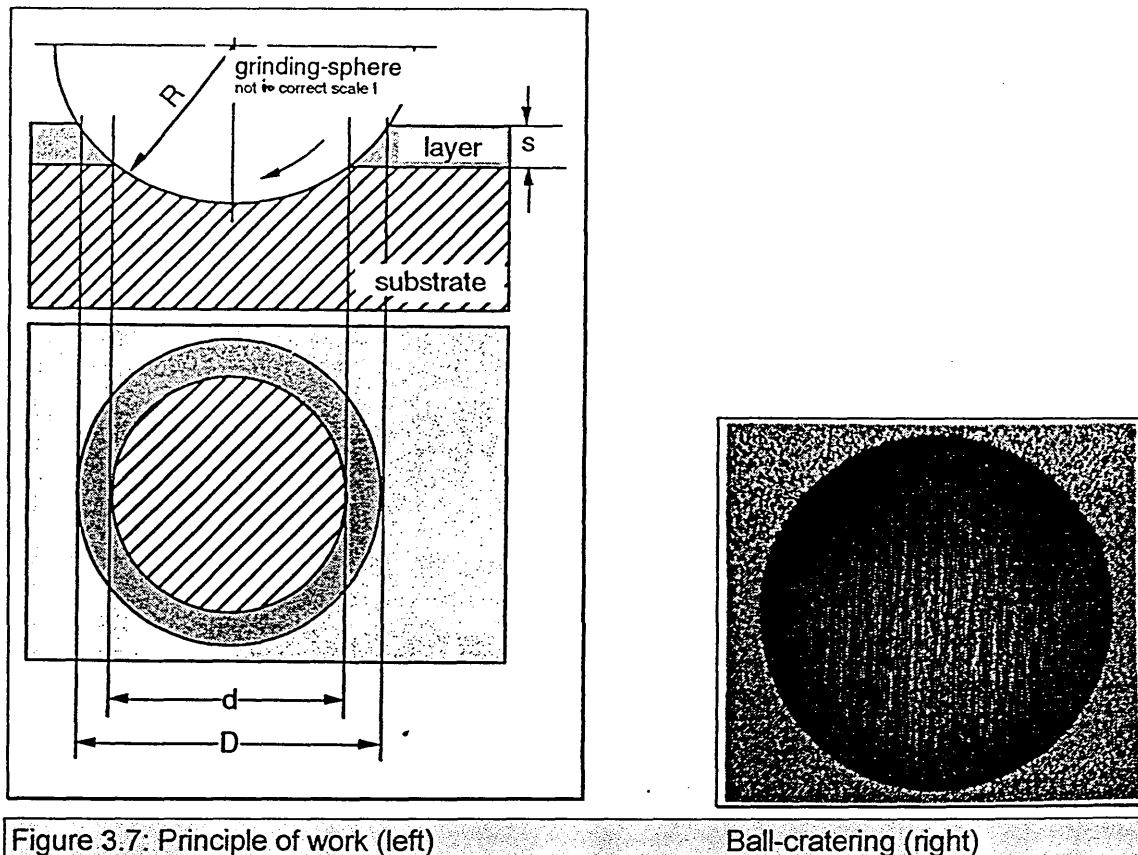


Figure 3.7: Principle of work (left)

Ball-cratering (right)

(ii) For the second method the specimens were partly blanked off by covering with a metal strip during coating. This procedure left a central part of the specimen's surface uncoated. The height difference between the coated and uncoated surface, measured with the Talysurf, gave coating thickness.

EXPERIMENTAL TECHNIQUES / TESTING METHODS

Very good agreement was obtained for thickness values determined by the above two methods. Furthermore GDOES depth profile measurements determined through the coating to the substrate confirmed the thickness values obtained by the other two methods.

3.5.7 X-Ray Diffractometry (XRD)

X-Ray diffraction plots were obtained using an X-Ray diffractometer Philips model PW1820 which is software controlled from a PC. The wavelength λ of the monochromatic Cu K α radiation is 1.54060×10^{-10} m. The optimum voltage was found to be 25 kV and the current 35 mA in order to obtain peaks from the thin coatings on brass. A typical X-Ray diffraction plot is shown in figure 3.8. The texture, lattice parameter, macro elongation, micro elongation, tension condition and grain size were calculated from the X-Ray diffraction plots using the methods set out below.

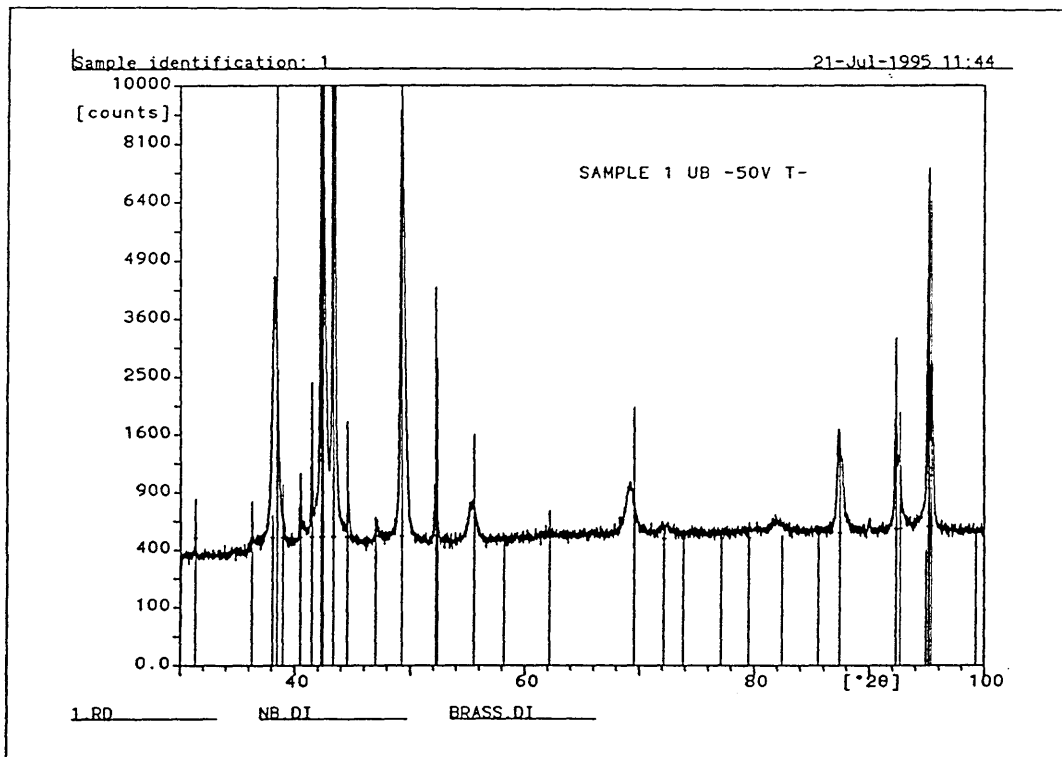


Figure 3.8: Typical X-Ray Diffraction plot

Using the Bragg equation

$$n\lambda = 2d \sin\theta \quad \dots 1$$

with n = integer value depending on the order

λ = wavelength of radiation

d = periodic spacing

θ = constructive diffraction angle

Positions of the obtained diffraction peaks were fitted by using a fitting routine. Those peaks coming closest to the calculated expected peaks are the real element peaks.

With the real element peaks the real d_{hkl} spacing can be calculated by

$$d = \frac{\lambda}{2 \sin(\theta)} \quad \dots 2$$

and the actual lattice parameter a by

$$a = d \cdot \sqrt{h^2 + k^2 + l^2} \quad \dots 3$$

with h , k and l are the Miller's indices. *Nelson* and *Riley* developed the equation

$$a = a_0 + b \cdot \left(\frac{\cos^2 \theta}{\sin \theta} \right) \quad \dots 4$$

with a = lattice parameter by Nelson-Riley

a_0 = real lattice parameter

b = constant (slope of straight line)

$(\cos^2 \theta / \sin \theta)$ = Nelson-Riley function

to calculate the lattice parameter by calculating the best least-squares straight line by

$$S = \sum d_i^2 = \sum (y_i - (mx_i + c))^2 \quad \dots 5$$

with d = vertical distance of P_i to best least-squares straight line

m = slope

c = intercept with y-axis

and minimising S with $\frac{\partial S}{\partial m} = 0$ and $\frac{\partial S}{\partial c} = 0$6

To determine elongations which can be derived by Bragg equation and grain size which was described mathematically by *Scherrer*, the Hall-Williamson relationship from *Rickerby* and *Gissler* is used [84]:

$$\frac{\beta \cdot \cos \theta}{\lambda} = \frac{1}{D} + \varepsilon \frac{4 \sin \theta}{\lambda} \quad \dots 7$$

with ε = elongation

D = grain size

and the true broadening $\beta = \sqrt{(B - b)\sqrt{B^2 - b^2}}$ [85]

... 8

with B = observed broadening

b = instrumental broadening.

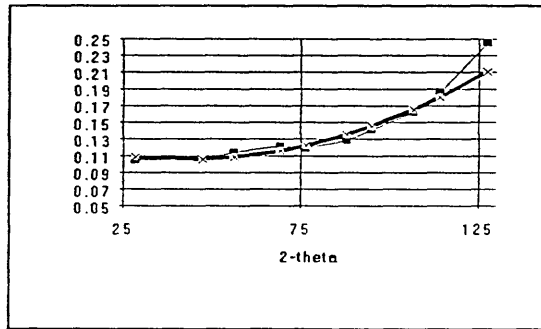


Figure 3.9: Instrumental broadening b

The instrumental broadening b is determined by a polynomial regression curve third order of the diffraction peak widths of silicon standards (Figure 3.9).

The preferred orientation was decided by texture percentages which were defined as:

$$T_{hkl} = \frac{\frac{I_{hkl}}{I_{ref_{hkl}}}}{\sum \frac{I_{hkl}}{I_{ref_{hkl}}}} \cdot 100[\%]$$

... 9

with I_{hkl} = measured diffraction intensity

$I_{ref_{hkl}}$ = reference diffraction intensity

The EXCEL work sheet to calculate those properties is given in the appendix using Nb as an example.

3.5.8 Scanning Electron Microscope SEM and Energy Dispersive X-Ray Analysis EDX

Structures and features of metallographic cross sections, fractures and topographical pictures were investigated using a Philips scanning electron microscope model XL40 with Windows driven software. Energy dispersive X-ray analysis was made using Link analysis hardware and software.

Fractures of the ductile PVD coated brass rods with a diameter of 8 mm were prepared as follows:

- (i) cut 3/4 of the diameter with a grinding blade
- (ii) cool down using liquid nitrogen
- (iii) fracture the 1/4 part of the rod using an Avery-Dension sharp impact tester with a maximum energy of 150 J.

3.5.9 Metallography

The cross sections of specimens, ground and polished, as previously described in section 3.2.1, were examined using the microscope. Prepared cross-sections of selected specimens hot mounted in BAKELIT® were examined metallographically following etching. The etchants used were those previously described [86] and were as follows:

- (i) *H S Rawdon and M G Lorentz* etchant contains 100 cm³ H₂O, 2.4 cm³ concentrated HCl and 0.3 g Fe(III)Cl₃
- (ii) *Klemm II* colour etchant which is made up using 100 ml of a stock solution (300 ml distilled H₂O, T=35 °C + 1 kg sodium thiosulphate) and 5 g di-potassium di-sulphite K₂S₂O₅.

All optical metallography was carried out using an Olympus model Vanox-T microscope.

3.5.10 Roughness Measurement

The surface topography and roughness profiles of specimens were measured using a Taylor Hobson roughness tester (model Form Talysurf - 120 L), which is a laser supported mechanical apparatus. Values were calculated for Ra, Rq, Rp, Rt and Rz. Additionally it was used to produce topographical images of a surface area 0.815 mm x 0.815 mm.

3.5.11 Microhardness Test

The hardness of coatings and hardness profiles were measured using a Fischer microhardness tester model Fischerscope H 100. The maximum applied force used in this test is 5 mN with the load being applied in 60 steps followed by unloading, again using 60 integral steps. The hardness measured under load is called Universal hardness HU. They are calculated from indentation depth by geometrical calculation of diagonals. The unit of HU is N/mm².

The hardness was also measured using a Mitutoyo hardness tester model MVK - G1 with an Knoop indenter and a load of 10 g.

3.5.12 Bending Test

Adhesion of coatings was examined using a bending test following DIN 50 111 "Technologischer Biegeversuch und Faltpfung". PVD coated soft annealed brass sheets were bent 90° and 180° with a radius of 3 mm. An optical microscope is used to observe the bend edges at a magnification of 10 times.

3.5.13 Colour Measurement

Colour of coatings was measured using a Dr. Lang colour difference tester "Micro Color". The diffuse reflection of the sample is determined at an angle of 8°. The used illumination source is a xenon flash light (DIN 5033, class D65).

The received colour can be represented by the CIELab system.

- (i) L, where L = 100 is white and L = 0 is black
- (ii) a*, where a* = 100 is red and a* = -80 is green
- (iii) b*, where b* = 100 is yellow and b* = -80 = blue

CHAPTER 4: Results

4.1 Diffusion Test of Uncoated Brass Substrate

Results for Metallographical Examinations

Metallographic examination of heat treated, uncoated brass samples showed bright grains of the α phase surrounded by grains of the darker β phase (Figure 6.1). The black dots seen are Pb inclusions. It can be further seen that the etching technique used showed up the twins and discolourations in the α phase associated with the Zn diffusion which had taken place during heat treatment. Figure 6.2 was obtained at a magnification of 3002x using the SEM and shows the twinning in the grains in more detail due to the use of an etchant.

Results obtained using GDOES

The results of GDOES investigations carried out on uncoated brass specimens heat treated for 90 min at 50, 100, 150, 200, 250 and 300 °C respectively show that a depletion of Zn had occurred at the surface (Figure 6.3). The concentration profiles obtained at all temperatures were similar to the schematic case shown in figure 6.5 and figure 6.4 shows the actual result obtained for a heat treated specimen.

A detailed analysis of the Zn concentration at different depths from the brass surfaces (see Figure 6.5) for samples heat treated for different combinations of time and temperature are given in figure 6.6. It can be seen that these results are generally similar except in the case of the profile obtained for the specimen treated at 50 °C for 15 min.

4.2 Precleaning of the brass substrate

Visual evaluation directly after precleaning

Visual evaluation of precleaned uncoated brass samples shows a slightly tarnished surface for the samples polished with Sidolin and ultrasonic cleaning in acetone due to etching effects caused by the ingredients of the metal polish. The samples cleaned with the MRI cleaning line with Banner cleaning detergent show a heavily tarnished surface due to chemical reactions with the anionic and non-ionic surfactants. The samples cleaned in ultrasonic tanks containing acetone show clean bright surfaces but are not totally degreased. The samples cleaned cathodically and anodically using Henkel P3 Galvaclean 62 show a slightly tarnished surface. Best result are from either the samples cleaned cathodically with the cyanide based degreaser Kleenax or with the Henkel RST degreaser, followed by pickling in 10% HCl and rinsing in deionised water. They show a bright shiny and totally degreased surface.

Visual evaluation after cleaning and coating in the PVD chamber

The samples polished with Sidolin and cleaned ultrasonically in acetone, the samples cleaned with the cleaning line and the samples cleaned using Henkel P3 Galvaclean 62 exhibit a tarnished surface after the cleaning and coating in the PVD chamber. The contaminations on the surfaces lead to arcing on the surface, resulting in irreversible arc tracks.

Samples cleaned cathodically with Kleenax or samples cleaned with the degreaser Henkel RST show excellent surfaces with no faults or damage, neither after the cleaning in the PVD chamber nor after the coating process.

Smearred Pb on the brass surface

GDOES depth profiling did not give any information about the Pb contribution on the sample surface. The optical microscope showed an attacked surface for all six etch experiments. Figure 6.7 shows the sample surfaces at a magnification of 500x after etching in HBF_4 and HNO_3 .

EDX mapping of Pb $\text{M}\alpha$ definitely showed Pb inclusions. However no signs of 'smearing' have been observed after polishing.

4.3 Cleaning in the PVD Chamber

4.3.1 Argon Ion Etching

Results obtained using GDOES

The results of GDOES investigations carried out on uncoated brass specimens argon-ion etched for 20 min at -800 V bias voltage show that a depletion of Zn had occurred at the surface. Surprisingly Al up to 10 at% was found within the first 200 nm below the surface. This result is not fully understood yet and may be correlated to a cross contamination side effect from Al material deposited during prior coating runs before the experiment described here was carried out. In parallel, oxygen was associated with the Al signal (Figure GDOES 1).

Results obtained from roughness measurement

Roughness measurements of argon-ion etched uncoated brass samples showed the same roughness characteristics as the untreated polished specimens as shown in table 6.1. Figure 6.10 shows the 3D roughness profile.

4.3.2 Aluminium Ion Etching

Results obtained using GDOES

The results of GDOES investigations carried out on uncoated brass specimens Al-ion etched for 7 min at -800 V bias voltage respectively show an increase in depletion of Zn with increasing bias voltage. In comparison with the argon ion etch, one finds at -800 V a reduced amount of depletion, obviously due to the much shorter etching time. Also no severe diffusion of Al into the brass material has been observed. (Figure GDOES 2).

Results obtained from roughness measurement

Roughness measurements of Al-ion etched uncoated brass samples showed gradually increasing roughness with increasing bias voltage. The results of these measurements are given in table 6.1. Figures 6.11 to 6.14 show the 3D roughness profiles.

4.3.3 Combined Argon- and Aluminium Ion Etching

Results obtained using GDOES

Uncoated brass specimens argon ion etched for 20 min at -800 V followed by Al-ion etching for 1 min at -800, -1000 and -1200 V bias voltages respectively showed Zn depletion from the surface in all cases. However at -1200 V bias voltage the Zn depletion depth is approximately 90 nm. This corresponds also with the penetration depth of Al (Figure GDOES 3).

Results obtained using roughness measurement

Roughness measurements of Al-ion etched uncoated brass samples showed an increasing roughness with increasing bias voltage. The detailed results obtained are given in table 6.1. Figures 6.15 to 6.17 show the 3 D roughness profiles.

4.4 Coating Processes

Results obtained from Scratch Adhesion Test

The results of the scratch adhesion tests show different failure mechanisms relative to those known for hard coatings on hard substrates. Following the standardised criteria there is an immediate failure of PVD coatings on brass. Failure mechanisms are plastic deformations and delaminations from the beginning. Standard procedures are not applicable. Therefore new examination criteria were specified. The coating behaviour at the end of scratches at a stylus load of 100 N is described in section 3.5.4 and shown in reference figures 6.18 to 6.21.

Selected results obtained from colour measurement

The results of the colour measurement obtained using a xenon flash light source (DIN 5033, D65) are given in figure 6.56. The CuAl8 coatings show a process temperature dependant colour appearance. The L value is increasing with decreasing temperature, whereas the a^* and b^* values are decreasing with decreasing temperature. The medium temperature CuAl8 ($L=80.15$, $a^*=6.35$, $b^*=32.34$) comes closest to the brass substrate colour. However the golden colour can not be compared with any of the gold standards 1N to 5N NIHS 03-50.

The pure Nb coating and Nb coatings on CuAl8Nb(5%) and AlNb(5%) coating show reduced L and increased a^* and b^* values compared to the pure Al coatings. The L values are increased for the Nb coatings on CuAl8Nb(5%) and AlNb(5%) compared to the pure Nb coatings, but the a^* and b^* are in the same range.

The matt Al coating shows a higher L value than the shiny Al coating.

Critical remarks on GDOES results obtained on Nb

The results of GDOES carried out on Nb coatings or Nb containing coatings show in general oxygen concentrations up to 10 at-% and Zn concentrations which depend on the Nb signal. Oxygen and Zn are artefacts of the GDOES method. A much more sensitive SNMS examination on Nb coated steel showed a very thin continuous oxide layer on top of the Nb coating. The oxygen concentration in the Nb coating below this oxide film was less less than 1 at-%. The detected Zn intensity is only a GDOES interference effect with the Nb signal; in reality there exists no Zn incorporation in the Nb layer as XRF analysis has proven.

4.4.1 Aluminium Diffusion Barrier

Visual evaluation after coating in the PVD chamber

Visual evaluation of Al coated brass samples show a white, temperature dependant surface appearance. Only samples treated with low arc current during ion etching, low bias voltage and low coil current resulting in a process temperature less than 138 °C have a shiny and brilliant coating. Samples treated with high arc current during ion etching, high bias voltage and high coil current resulting in a temperature higher than 138 °C show a milky and matt surface.

GDOES

GDOES investigations were carried out on Al coated brass specimens with various substrate cleaning and coating processes. A typical GDOES plot is given in figure GDOES 4. The Al coating shows an Al film with an oxygen concentration of around 2.5 at-%. The interface between the Al coating and the brass substrate shows diffusion of Zn and Cu from the brass substrate into the coating and Al diffusion from the coating into the substrate. At the interface there is an accumulation of oxygen.

Roughness measurement

Roughness measurements of Al coated brass samples showed no systematic characteristic concerning the substrate cleaning and coating processes. The matt surfaces showed an increase by a factor of 4 for the roughness values of $R_a=0.0474\text{ }\mu\text{m}$, $R_q=0.0646\text{ }\mu\text{m}$, $R_t=0.6179\text{ }\mu\text{m}$ and $R_z=0.5038\text{ }\mu\text{m}$.

Vickers adhesion test

Vickers adhesion tests of Al coated brass show the tendency of better adhesion for matt films with a process end temperature of more than 138 °C ("Good") and worse adhesion for shiny films, which were produced with a process end temperature of less than 138 °C ("Good" to "Bad"). The samples with the intermittent temperature profile, leading to a process temperature between 100 and 130 °C, showed good adhesion.

Coating thickness

The coating thicknesses are around 1.1 μm as determined by calotests.

Hardness measurements

A typical hardness-depth profile is given in figure 6.24. The increase of the hardness can be correlated to the appearance of Al.

Figure 6.31 shows the hardness of Al coatings as a function of the applied coil current, produced with a process start temperature between 70 °C and 100 °C. It shows a decreasing hardness with increasing coil current and a maximum in hardness at 2 A coil current. Figure 6.32 shows the hardness as a function of the process start temperature T_s and the end temperature T_f at a coil current of 4 x 6 A. With increasing ratio T_f / T_s , the hardness increases.

Corrosion tests

Figure 6.41 a-c shows the results of the ammonia porosity test. The samples show fine pores and an overall uniform attack. The sample produced at a temperature between 112 and 138 °C shows by far the best result (Figure 6.41 c).

The results of sulphur dioxide corrosion tests carried out on Al coated brass specimens from process 7 shows an attack of the surface area of 30 % after 24 h, 70 % after 48 h and 100 % after 72 h. Figure 46a shows the sample after 72 h with partly dissolved Al coating.

Diffusion tests

The result of diffusion tests carried out on samples from 3 different Al processes with different process temperatures showed barrier behaviour against Zn (figure 6.23 a). The barrier coating is penetrated by Zn after roughly 15 min to 50 % and after 30 min to 100 % at an annealing temperature of 250 °C.

Temperature profile during the coating process

Figure 6.40a shows the temperature profiles of Al processes with various start temperatures and process parameters.

Images from the SEM / TEM

Figure 6.49a shows the topography of a shiny Al coating. The fracture in figure 6.49b shows a dense structured coating and cohesive failure in the brass substrate. Figure 6.49c shows the topography of a matt Al surface. The faults on the surface are probably droplets; it is also possible to see some grain boundaries.

Figure 6.49d shows a TEM image of an Al coating at a magnification of 10 000x. The Al coating is fine grained (around 0.25 μm). With a higher magnification of 100 000x the Al grains show a high dislocation density (Figure 6.49e).

The TEM images are produced parallel to the coating surface, therefore no information on texture or equiaxed structure can be gained.

Scratch adhesion test

Scratch adhesion tests on samples with a matt appearance resulting from a high process temperature showed at 100 N a buckled coating as described in section 3.5.4, reflecting a relatively good adhesion. Scratch adhesion tests carried out on samples produced at temperatures up to 138 ° C resulting in a shiny surface showed delaminations at 100 N as described in section 3.5.4, but there is a trend to better adhesion with lower coil current.

Scratch adhesion tests were also performed with a modified scratch tester as described in chapter 2.5.2., which is especially suitable for ductile coatings on ductile substrates. The result was obtained using test angle $\text{tg}\alpha$ of $1 \cdot 10^{-2}^\circ$, an initial vertical displacement of 0.3 μm , a horizontal displacement of 2 mm in 2000 steps. Figure 6.22a shows the displacement in μm vs the tangential and normal force in N. Figure 6.22b shows the normal force vs the tangential force and figure 6.22c shows the distance vs tangential/normal force (friction coefficient). The transitions are not easy to find. However, a transition point can be correlated with the appearance of wrinkles on the micrograph at about 300 μm of the beginning of the scratch.

The scratch test method being a comparative method, the value of the force at the transition does not mean anything on its own, but has to be compared with other values measured on the same system.

Bending test

Al coated brass sheet samples showed good adhesion in the bending test. They have an orange peel appearance for the bending test at 90 ° and show in part delamination for the 180 ° test.

4.4.2 Aluminium-Niobium Diffusion Barrier + Niobium

Visual evaluation after coating in the PVD chamber

Visual evaluation of samples coated with AlNb(X) + Nb, where X stands for various Nb target powers, showed shiny and bright surfaces.

GDOES

The results of GDOES investigations carried out on brass coated with Al-Nb sputter alloyed coatings + Nb with increasing Nb target power of 0.5, 1, 2 and 5 kW show an increasing Nb concentration from 2 to 12.5 at-% (Figure 6.35).

A typical GDOES plot is given in figure GDOES 5 for the sample produced with 0.5 kW. The depth distribution of the elements shows increasing Al concentration towards the interface to the Al-Nb alloy layer. The interface between the Nb and Al-Nb alloy layer shows Nb diffusion into the Al-Nb alloy layer and Al diffusion into the Nb layer. One third of the intermediate Al-Nb alloy layer shows Nb diffusion from the Nb outer layer into the intermediate layer. The interface between the Al-Nb alloy interlayer and the brass substrate is very broad and shows Al and Nb diffusion into the brass substrate and Cu and Zn diffusion into the interlayer. The interface shows accumulated oxygen and Nb.

Figure GDOES 6 shows a typical GDOES plot for the sample produced with 5 kW. It shows a higher Nb concentration of around 12.5 at-% in the Al-Nb sputter alloy intermediate layer when compared to GDOES 5. The intermediate layer is totally penetrated with oxygen. The interface between the Al-Nb sputter alloy layer and the brass substrate shows no accumulation of oxygen and Nb.

Roughness measurement

Roughness measurements of AlNb(X) + Nb coated brass samples showed roughness values for all samples in the same range. Roughness values are $R_a=0.0432\text{ }\mu\text{m}$, $R_q=0.0662\text{ }\mu\text{m}$, $R_t=0.6868\text{ }\mu\text{m}$ and $R_z=0.4908\text{ }\mu\text{m}$.

Vickers adhesion test

Vickers adhesion tests of AlNb(X) + Nb coated brass show a tendency better adhesion for films with higher Nb concentration (all "Good").

Coating thickness

The coating thicknesses measured using the calo test increase with higher Nb target power (Figure 6.36) from 1.08 μm to 1.37 μm , because more material is deposited.

Hardness measurements

Typical hardness-depth profiles are given in figure 6.25 and 6.26 for samples produced at 0.5 and 5 kW Nb target power. In both cases the increase in hardness can be correlated to the presence of Nb in the coatings.

Figure 6.33 shows the hardness of AlNb(X) + Nb coatings as a function of the applied Nb target power. The hardness decreases from the poisoned state to the 0.5 kW Nb target power process. Afterwards it shows increasing hardness with increasing Nb target power from 169 to 294 HK 0.01.

Corrosion tests

Figure 6.42 a-e shows the results of the ammonia porosity test. The samples show massive pores at low Nb concentrations and fine pores at higher Nb concentrations connected to an overall uniform attack. The sample produced with 5 % Nb target power (Figure 6.42 b) showed delaminations (white lines).

The results of sulphur dioxide corrosion tests carried out on AlNb(X) + Nb coated brass specimen show an attack of the surface area of 20 % after 24 h. After 48 h the samples with the low Nb concentration are corroded up to 70 % and after 72 h to 100 %. The sample produced at 50 % Nb target power having the highest Nb concentration showed a corroded area of 30 % after 48 h and 100 % after 72 h. Figure 6.46 b, c shows the samples after 72 h with partly dissolved coating.

Diffusion tests

The barrier behaviour was massively improved compared to the pure Al coatings. All samples showed a Zn penetration of around 30 % after 20 min. The sample produced at 5 kW Nb target power was totally penetrated after 35 min, the sample with the highest Nb concentration was totally penetrated after 40 min at an annealing temperature of 250 ° C. (Figure 6.23a)

Temperature profile during the coating process

Figure 6.40b shows the temperature profiles of AlNb(X) processes with various start temperatures. The AlNb(X) intermediate layer was produced in the temperature range between 100 and 138 ° C.

Images from the SEM

Figure 6.50a shows the topography of an AlNb(5%) + Nb coating. The fracture in figure 6.50b shows a columnar structured coating and cohesive failure in the brass substrate. Figure 6.51a shows the topography of an AlNb(50%) + Nb coating. The fracture in figure 6.51b shows a dense structured coating and cohesive failure in the brass substrate.

Scratch adhesion test

Classification of the scratch ends at 100 N showed bad adhesion for the coating produced with 5 % Nb target power, better adhesion for the coatings produced at 20 and 50 % target power and best adhesion for the coating produced at 10 % Nb target power.

4.4.3 CuAl8 Diffusion Barrier

Visual evaluation after coating in the PVD chamber

Visual evaluation of samples coated with CuAl8 showed a shiny golden colour and bright surface. Depending on the thickness of the coatings there is a difference in the apparent colour as described in section 4.4.

GDOES

The results of GDOES show CuAl8 layers with 18 at-% Al (approx. 7 wt-%) and around 4 at-% Fe (approx. 3 wt-%). A typical GDOES plot is given in figure GDOES 7. The homogenous CuAl8 coating is totally penetrated by oxygen at a low level. The interface between the coating and the brass substrate shows Al and Fe diffusion into the substrate and Zn diffusion into the coating. There is an accumulation of oxygen at the interface.

Roughness measurement

Roughness measurements of CuAl8 coated brass samples showed roughness values of $R_a=0.0168\text{ }\mu\text{m}$, $R_q=0.0577\text{ }\mu\text{m}$, $R_t=1.2295\text{ }\mu\text{m}$ and $R_z=0.4599\text{ }\mu\text{m}$ for the samples coated for 1 h. The samples coated for 30 min showed roughness values of $R_a=0.0096\text{ }\mu\text{m}$, $R_q=0.0130\text{ }\mu\text{m}$, $R_t=0.1602\text{ }\mu\text{m}$ and $R_z=0.0985\text{ }\mu\text{m}$.

Vickers adhesion test

Vickers adhesion tests of CuAl8 coated brass showed good adhesion for all processes as described in section 3.5.5.

Coating thickness

The coating thicknesses were around $2.7\text{ }\mu\text{m}$ for the 1 h processes and around $1.4\text{ }\mu\text{m}$ for the 30 min processes. The result shows a linear time depending coating growth.

Hardness measurements

A typical hardness-depth profile is given in figure 6.27 for a sample coated for 1 h. The samples from the 1 h processes having a thicker coating have a hardness of 235 HK 0.01, whereas the samples from the 30 min process having a thinner coating have a hardness of 194 HK 0.01. This can be explained by the influence of the substrate.

Corrosion tests

Figure 6.43a-d shows the results of the ammonia porosity test. The samples with the thick coating (a, b) show a dense film, having only fine pores and an overall uniform attack. The thinner coatings (c, d) show massive porosity and a strong attack.

The CuAl8 samples produced at 15 kW with a bias voltage of -75 V and a coil current of 4 x 3 A for 60 min and an additional Nb layer for 30 and 60 min showed the best corrosion resistance results. Figure 6.43e shows the sample with the Nb layer produced for 30 min which has relatively few pores. Figure 6.43f shows the sample with the Nb layer produced for 60 min, having only a minimal amount of small pores.

The results of sulphur dioxide corrosion tests carried out on the CuAl8 coated brass specimen show an attack of the surface area of 100 % after 24 h (figure 6.47a). The coating loses its golden colour and the coating is also partly dissolved.

Diffusion tests

Figure 6.23b shows the Zn penetration versus the diffusion time at 250 °C. The samples produced at the low start temperature with a thin coating produced in 30 min showed worse diffusion behaviour with total penetration after 45 min. The sample produced at the medium temperature with a thick coating produced in 60 min showed the best penetration behaviour with complete penetration after 55 min.

Temperature profile during the coating process

Figure 6.40c shows the temperature profiles of CuAl8 processes with various start and end temperatures

Scratch adhesion test

A failure could be detected at around 20 N for the 1 hour process samples. Al samples show a compressive surface buckling of coatings at the scratch end at 100 N as described in 3.5.4.

Images from the SEM

Figure 6.52a shows the topography of a CuAl8 coating. The fracture in figure 6.52b shows a dense columnar structure coating and adhesive failure.

Bending test

Samples showed good adhesion in the bending test. They have an orange peel appearance for the bending test at 90 ° and stronger orange peel but no delamination in the 180 ° test.

4.4.4 Copper-Aluminium-Niobium Diffusion Barrier + Niobium CuAl8Nb(X)+Nb

Visual evaluation after coating in the PVD chamber

Visual evaluation of samples coated with CuAl8Nb(X) + Nb, where X stands for various Nb target powers, showed a shiny and bright surface. After approximately 5 min cooling in air the samples exhibited delamination and blistering.

GDOES

The results of GDOES investigations carried out on CuAl8Nb(X) + Nb coated brass specimens with increasing Nb target power of 0.5, 1, 2 and 5 kW show an increasing Nb concentration from 0.5 at-% to 6 at-%, from which a Nb concentration of approximately 1.2 at-% per 1 kW Nb target power can be calculated (Figure 6.35).

A typical GDOES plot is given in figure GDOES 8 for the sample produced with 0.5 kW. The outer Nb layer is homogeneous. The interface between the Nb and CuAl8 alloy layer shows a Nb diffusion into the CuAl8 alloy layer and Al, Cu and Fe diffusion into the Nb coating. The CuAl8 alloy layer shows a homogeneous concentration of Cu, Al and Fe. A small amount of oxygen penetrates the CuAl8 alloy layer. The interface between the CuAl8 alloy layer and the brass substrate shows accumulated Nb and oxygen. The Zn from the brass substrate diffuses across approximately 0.2 μm into the CuAl8 alloy layer and the Al and Fe from the CuAl8 alloy layer diffuses into the brass substrate.

Figure GDOES 9 shows a typical GDOES plot for the sample produced with 5 kW. Compared to GDOES 8 this GDOES shows a higher Nb concentration of around 6 at-% in the CuAl8 alloy interlayer.

Roughness measurement

Roughness measurements of CuAl8Nb(X) + Nb coated brass samples showed roughness for all samples in the same range. Roughness values are typically $R_a=0.013 \mu\text{m}$, $R_q=0.019 \mu\text{m}$, $R_t=0.30 \mu\text{m}$ and $R_z=0.17 \mu\text{m}$.

Vickers adhesion test

Vickers adhesion tests of CuAl8Nb(Nb) + Nb coated brass showed good adhesion for samples up to 2 kW Nb target power and bad adhesion for the sample with 5 kW Nb target power.

Coating thickness

The coating thicknesses measured using the calo test are increasing with higher Nb target power (Figure 6.36) from 1.38 μm to 1.59 μm .

Hardness measurements

A typical hardness-depth profile is given in figure 6.28 for a sample produced at 0.5 kW Nb target power. It shows an increasing hardness at a distance of 0.5 μm towards the physical surface. Figure 6.29 shows a hardness-depth profile for a sample produced at 5 kW Nb target power. There the hardness is increasing rapidly at a distance of 2 μm towards the physical surface. That shows compared with the GDOES results from figures GDOES 8 and 9 that the hardness is increasing due to the appearance of the Nb.

Figure 6.34 shows the hardness of CuAl8Nb(X) + Nb coatings as a function of the applied Nb target power. It shows increasing hardness with increasing Nb target power from 221 to 286 HK 0.01. Figure 6.34 also shows the start, intermediate and end temperatures of these processes. It seems that there is no influence of the temperature on the hardness.

Corrosion tests

Figure 6.44 a-e shows the results of the ammonia porosity test. The samples show a lot of fine pores at low Nb concentrations and only few big pores at higher Nb concentrations.

The results of sulphur dioxide corrosion tests carried out on CuAl8Nb(X) + Nb coated brass specimens show a 100% attack of the surface area after 24 h. Samples with low

Nb concentration show a lot of fine delaminations (figure 6.47b) and samples with high Nb concentration show massive delaminations (figure 6.47 c).

Diffusion tests

Figure 6.23c shows an improved diffusion barrier behaviour for CuAl8 alloy coatings with sputter alloyed Nb. The coating produced at 0.5 kW Nb target power lead to a total penetration of Zn after 40 min at a temperature of 250 °C. The sample produced at 5 kW Nb target power showed roughly only half this amount of Zn penetration during the first 30 min and a total penetration of Zn through the coating after 55 min at a temperature of 250 °C.

Temperature profile during the coating process

Figure 6.40d shows the temperature profiles of CuAl8Nb(X) + Nb processes with various start temperatures. The solid lines show the CuAl8Nb(X) processes, followed by the dashed lines for the Nb processes.

Scratch adhesion test

All samples showed compressive surface buckling of coatings at the scratch end of 100 N as described in chapter 3.5.4 with reference to figures 6.18 and 6.19. The samples tend towards better adhesion with decreasing Nb concentration.

Images from the SEM

Figure 6.53a shows the topography of a CuAl8Nb(5%) + Nb coating. The fracture in figure 6.53b shows a dense structureless coating and adhesive failure. Figure 6.54a shows the topography of a CuAl8Nb(50%) + Nb coating. The fracture in figure 6.54b shows a dense structured coating and adhesive failure.

Bending test

Samples show good adhesion in the bending test. They have an orange peel appearance for the bending test at 90 ° and stronger orange peel but no delamination in the 180 ° test.

4.4.5 Niobium Diffusion Barrier

Visual evaluation after coating in the PVD chamber

Visual evaluation of samples coated with Nb showed a silvery surface. After around 5 min cooling in air the samples showed delamination and blistering.

GDOES

A typical GDOES plot is given in figure GDOES 10. It shows a Nb coating with the oxygen and Zn artefacts of the GDOES method described in section 4.4. The interface shows a massive diffusion of Nb into the brass substrate and less diffusion of Cu and Zn into the Nb coating.

Vickers adhesion test

Samples produced at higher coil currents tend to better adhesion than samples produced at low coil currents.

Coating thickness

Coating thickness is decreasing with higher coil current from 0.48 μm to 0.39 μm (Figure 6.37).

Hardness measurements

A typical hardness-depth profile is given in figure 6.30. The hardness as a function of the applied coil current shows a slightly increasing hardness from 200 to 205 HK 0.01 at coil currents from 3 to 5 A and a decreasing hardness down to 187 HK 0.01 at 8 A coil current (figure 6.37). The hardness as a function of the temperature showed parabolic behaviour with a minimum of 200 HK 0.01 at the medium process temperatures (figure 6.38). The hardness as a function of the bias voltage showed decreasing hardness values with increasing bias voltage from 200 to 181 HK 0.01 (figure 6.39).

Corrosion tests

Figure 6.45 shows the ammonia corrosion test results. All samples are strongly attacked. Figure 6.45g shows a sample at a magnification of 2 x, where the delaminations can be seen.

The sulphur dioxide corrosion test shows strongly attacked surfaces after 24 h in figure 6.48. The attack increases with increasing bias voltage.

Diffusion tests

The best diffusion behaviour was found for the samples produced at a coil current of 4x5 A with a total penetration time of 55 min. The worst result was found for the sample produced at a coil current of 4x8 A with a total penetration time of 40 min (Figure 6.23d). The diffusion behaviour as a function of the process temperatures is given in figure 6.23e. It shows the best result for the sample produced at the lowest start temperature with a total penetration time of 55 min. Figure 6.23f shows the diffusion behaviour as a function of the applied bias voltage. Best results are obtained having a bias voltage of between -50 and -75 V.

Temperature profile during the coating process

Figure 6.40e shows the temperature profiles of Nb processes with various start and end temperatures.

XRD

The results are given below:

(i) properties as a function of the applied coil current (figure 6.37):

The grain size shows increasing grain size up to 5 A coil current from 35 to 218 nm and afterwards decreasing grain size down to 46 nm at a coil current of 8 A. The macro elongation is increasing with increasing coil current from 0.55 % at 3 A to 0.67 % at 8 A. The micro elongation is decreasing with increasing coil current from 0.53 % at 3 A to 0.34 at 8 A. The lattice parameter, a , shows values in the range 3.324 to 3.288 Å. The stress and stress / thickness is increasing with increasing coil current from -1.46 GPa to -1.79 GPa and -3.05 GPa/ μm to -4.59 GPa/ μm , respectively. The dependency of the orientation is shown in the bottom chart.

(ii) properties as a function of the temperature (figure 6.38):

The grain size as a function of the process temperatures shows a value of 100 nm for the low temperature process, 35 nm for the medium and 298 nm for the high temperature process. The macro elongation is decreasing with higher process temperatures from 0.66 % to 0.28 % and the micro elongation is increasing with higher process temperatures from 0.51 % to 0.59 %. The lattice parameter is between 3.316 and 3.328 Å. The stress and stress / thickness is decreasing with increasing process temperature from -1.75 GPa to -0.73 GPa and -3.36 GPa/μm to -1.30 GPa/μm, respectively. The dependency of the orientation is shown in the bottom chart.

(iii) properties as a function of the applied bias voltage (figure 6.39):

The grain size as a function of the applied bias voltage shows a maximum at -75 V with around 125 μm. The macro and micro elongation are increasing with increasing bias voltage and show a minimum at -75 V with around 0.31 % and 0.43 %, respectively. The lattice parameter is between 3.317 and 3.341 Å. The stress and stress / thickness is increasing with increasing bias voltage from -1.46 GPa to -2.72 GPa and -3.05 GPa/μm to -6.36 GPa/μm, respectively. They have a minimum at -75 V at -0.81 GPa and -1.69 GPa/μm, respectively. The dependency of the orientation is shown in the bottom chart.

Scratch adhesion test

All samples showed a mix of compressive surface buckling and delaminated coatings at the scratch end for 100 N load. Best results were obtained having a bias voltage of -75 V and a coil current of 4 x 3 A and -50 V bias with 4 x 3 A coil current at a start temperature of 150 °C, respectively.

Images from the SEM

Figure 6.55a shows the topography of a Nb coating. The fracture in figure 6.55 b shows a dense, almost structureless coating and adhesive failure.

Bending test

Samples showed bad adhesion in the bending test. They show massive orange skin for the bending test at 90 °C and delamination for the 180 ° test.

5. Discussion

Aluminium was originally thought to be the most promising candidate for corrosion and diffusion barriers between the substrate material, brass, and the actual corrosion barrier niobium. Mainly thermal considerations lead to this assumption. It was expected, that brass would show the temperature sensitivity, which has been confirmed by GDOES measurements (chapter 3.1 and 4.1). The low melting point of aluminium and therefore also the low critical temperature to form the necessary zone T structure of the Thornton diagram [67] were the driving forces when deciding to use aluminium as a barrier coating. 250 °C as critical maximum temperature is equal to a T/T_m ratio of 0.56. This means that the temperature level is reached which is already in the zone 2 range of the Thornton diagram. This indicates that the formation of rough surfaces of the condensed aluminium coating is very likely and that one of the main tasks of decorative coatings, namely high brilliance (high L^* values in the CIELAB colour scale) might be impossible to achieve. As one of the main results of this study, the conclusion may be drawn that pure aluminium fails as a diffusion and corrosion barrier due to the temperature problems. The practical experiments have shown that for 'shiny' and 'brilliant' aluminium surfaces substrate temperatures of 135 °C must not be exceeded when using the ABS machine even with low ionisation, for example with coil currents as low as 1.5 A (see chapter 3.4.1 and 4.4.1). As 1 to 2 µm of aluminium were needed to form an effective diffusion barrier, very long processes of either sputtering and / or ion etching periods were needed to fulfil this precondition. The duration of ion etching alone, keeping $T_{max} \leq 135$ °C, resulted in an etching time of four hours, with only 7 minutes of effective etching. The long cooling periods dramatically overshadowed the experiments.

With AlNb alloys the problem of the low melting point can be considerably reduced. The binary alloy phase diagrams show a liquidus / melting temperature of around 1650 °C at niobium concentrations of up to 12 at%. At a maximum allowable substrate temperature of 250 °C this will lead to a T/T_m ratio of 0.27, which is at the lower region of the Thornton diagram. However, as we did not have cast or powder metallurgically fabricated AlNb targets which would have allowed us to take full advantage of this situation, the success was only a partial one with the use of simple Al and Nb targets.

Having an appropriate ion bombardment, the zone T in the Messier diagram can be obtained which shows a smooth surface and a high brilliance of the applied coatings. Results of experiments confirmed that with increasing niobium concentration the

allowable substrate temperature is higher before the coatings become dull. Furthermore the diffusion barrier behaviour has definitely improved as compared to the pure aluminium coatings. This effect can be explained by the niobium atoms, which distort the base lattice caused by the different atom diameters. As explained in section 2.1.5.4.3 tetragonal NbAl₃ will be formed and influence the diffusion barrier behaviour positively (see chapter 2.1.5.1.1) [41].

In electroplating metallisation, copper is used as a diffusion barrier for zinc. To also take advantage of the positive corrosion properties of aluminium on the brass substrates observed in this work, copper-aluminium alloy coatings were produced as a logical consequence to improve the diffusion barrier and corrosion barrier behaviour. Technical bulk copper-aluminium alloys [42] show an optimum combination of high corrosion resistance in many aggressive media with mechanical properties above average compared to other copper based alloys [93]. Table 6.4 gives an overview on internationally available CuAl alloys. It should be mentioned, that copper-aluminium alloys can not be deposited by electroplating. For PVD this limitation does not exist of course. Nonetheless no PVD data have been published up to now, surprisingly. The high corrosion resistance can be explained by the oxide film on the surface, which is mainly aluminium oxide Al₂O₃ with some copper oxide. The corrosion behaviour is dependant on the structural constitution.

With a melting temperature of around 1045 °C and a process temperature of 250 °C a T/T_m ratio of 0.39 in the Thornton diagram is obtained. This would already lead to a dense coating, obviously without any ion bombardment. The coating will be further densified using ion bombardment to influence the coating growth. A shiny appearance was expected under such conditions and it was confirmed by the experiments.

The coatings show a temperature dependant colour in the golden range. With decreasing temperatures the L value increases up to 83 and the coatings change from a yellow-golden colour into a more white-golden colour. Principally these coatings could already act as decorative coatings on their own. The excellent adhesion of CuAl₈ coatings on brass, the corrosion resistance and the diffusion barrier behaviour and the relatively low target costs make this type of coating a promising candidate for an industrially used process.

The layer system can be completed by a niobium layer on top of the CuAl₈ layer. These samples showed by far the best corrosion results. There is still the adhesion problem of niobium coatings on the CuAl₈ caused by an interlayer formed between CuAl₈ and niobium mainly by contamination of CuAl₈ onto the niobium target during the CuAl₈ deposition. As can be learned from the DKI [42] it would also be worthwhile to investigate CuAl alloys with additions of Sn and Co to explore their

influence on the corrosion performance. In bulk materials these additives should improve the tarnishing behaviour. However, as these additional elements will be distributed statistically in the condensed material, it is a priori not sure, whether they can play the same beneficial role as in the bulk material.

The extremely chemically stable niobium is known for its superior corrosion resistance [41]. The reason is the formation of a passivating layer of niobium(V)oxide. Electrodeposition of niobium from aqueous electrolytes is not possible because niobium exists as complex ions which show very little ionisation, insufficient for successful cathodic deposition [41]. However, niobium can be deposited by PVD methods similar to its electrochemically related metal tantalum [90, 91, 94]. Having a melting point of 2467 °C and considering a maximum allowable deposition temperature of 250 °C a T/T_m ratio of only 0.19 is obtained, certainly too low to form a dense structure. Therefore this would lead to a porous structure, which could never act as a stable corrosion barrier. Consequently the ion bombardment plays a key role in order to obtain a dense structure in reference to the existence of the transition zone T in the Messier diagram. Earlier experiments showed, that dense niobium coatings can be deposited on steel at 400 °C and by using an appropriate bias voltage of -75 V, as proven by TEM work [90].

Results from this work show however, that it is indeed possible to optimise process parameters like coil current, bias voltage and especially the process temperature in such a manner that dense coatings may even be obtained at substrate temperatures as low as 250 °C. The important precondition for this successful approach was the minimisation of the internal stresses. There is a minimum in stresses having a low coil current of 4x3 A (figure 6.37) and a bias voltage of -75 V (figure 6.39). With increasing process temperature, the internal stresses are continuously decreasing (figure 6.38). Consequently the niobium layers must be produced at the highest allowable temperature for brass, ie 250 °C.

To obtain a niobium layer which is acting as a corrosion barrier an appropriate coating thickness of $> 0.5 \mu\text{m}$ is necessary. A minimisation of the compressive stress is therefore also very important in order to allow an increase of the coating thickness above $0.5 \mu\text{m}$ and to have a sufficient adhesion of the coatings. Optimisation in order to reduce the stresses and increase the adhesion is therefore very difficult.

Within the scope of this MPhil thesis the development of the niobium coatings has not been entirely completed; much more work is necessary in order to reduce the stresses further, especially if niobium thicknesses larger than $1 \mu\text{m}$ should be required.

It has to be mentioned also, that up to now only one very special corrosion test has been carried out. To satisfy the demands of the top quality decorative coating

standards, many more tests and even more severe corrosion tests have to be passed, before an industrial application of the technology proposed here becomes viable.

In particular complete decorative multilayer coating sequences on brass such as CuAl / Nb / TiN, CuAl / Nb / ZrN and CuAl / Nb / TiAlN have to be deposited and evaluated before a final conclusion can be drawn to rate the level of success realistically.

-
1. Brass can be coated directly by PVD, as long as special preparation methods and process features are followed.
 2. Brass substrates including lead as chip breakers should be machined carefully using sharp tools in order to avoid smeared lead which will worsen the adhesion. By polishing the brass smeared lead can be removed.
 3. Brass precleaning should be carried out using special detergents like the Henkel RST .
 4. The coating process start temperature should be between 100 and 120 °C. At the end of the process a temperature of 250 °C should never be exceeded.
 5. Substrate cleaning should be done with in situ substrate ion etching in a Hauzer HTC 1000-4 ABSTM with a bias voltage of -800 V and an arc current of 80 A for three minutes.
 6. Sufficient corrosion and diffusion barrier properties as well as sufficient adhesion were obtained using an intermediate layer made from a copper-aluminium(8%) alloy. However the deposition parameters have to be optimised carefully.
 7. 0.5 µm Niobium layers alone do not act as a sufficient corrosion barrier on brass. They display low adhesion caused by huge internal stresses.
 8. Scratch adhesion and Rockwell indentation tests are not directly applicable on the system soft brass + ductile coating. A new classification for both scratch and indentation tests has been developed.

References

- [1] A. H. Maslow
The Farther reaches of human nature
Penguin, 1976
- [2] U. Kopacz and S. Schulz
Society of Vacuum Coaters, 34th Annual Technical Conference Proceedings,
1991, 48-61
Industrial Applications Of Decorative Coatings - Principle And Advantages Of
The Sputter Ion Plating Process
- [3] Plasma Surface Engineering 1988 (DGM)
Editors: E. Broszeit, W.-D. Münz, H. Oechsner, H. Erhardt, S. Bastian,
and H. Petersen
H. Erhardt, S. Bastian and H. Petersen
Decorative Coatings by PVD
- [4] G. Kienel
Galvanotechnik, 1989, 80, 6, 1937-1940
Kombinationsschichten - hergestellt durch elektrochemische und PVD-Prozesse
- [5] U. Beck, G. Reiners, I. Urban, H. A. Jehn, U. Kopacz and H. Schack
Surface and Coatings Technology, 1993, 61, 1-3, 215-222
Decorative hard coatings: new layer systems without allergy risk
- [6] U. Kopacz, C. Daube and S. Schulz
Galvanotechnik, 1992, 83, 3, 844-848
Korrosionsschutz bei dekorativen harten Schichten durch Kombination von
PVD- und Galvanikbeschichtungen
- [7] A. S. Korhonen
Vacuum, 1994, 45, 10/11, 1031-1034
Corrosion of thin hard PVD coatings
- [8] U. Kopacz
Products Finishing, 1992, 56, 8, 72-73
Better Than Brass?
- [9] K. Schulze-Berge
Galvano-Verfahrenstechnik, 1989, 43, 5, 197-200
Galvanische Vorbehandlung in Kombination mit PVD-Deckschichten
- [10] H. Erhart
Galvanotechnik, 1990, 44, 2, 59-62
Kombination von Galvano- und PVD-Technik
- [11] ETA Fabriques d' Ebauches
Oberfläche surface, 1990, 31, 1-2, 29
Hartstoffschichten, die Uhren, Brillengestelle, Feuerzeuge und Schreibgeräte
besser schützen und verschönern
- [12] Wieland-Werke AG, Ulm
Wieland-Buch Kupferwerkstoffe, Wieland-Werke AG, Ulm, 1986, 5
- [13] W. Domke
Werkstoffkunde und Werkstoffprüfung, Cornelsen-Velhagen & Klasing, 1986,
10, 3-590-81220-6
- [14] MRI Information, SHU internal information
Typical Applications of XRF
- [15] F. C. Porter
Zinc Handbook, Properties, processing, use in design, 1991

- [16] B. Chapman
Science and technology of surface coating, NATO advanced study institute
1994
- [17] E. A. Brandes and G. B. Brook
Smithells Metals Reference Handbook, 7th. edition
- [18] Deutsche Gesellschaft für Galvano- und Oberflächentechnik
Anhang zu den Güte- und Prüfbestimmungen
Gütesicherung RAL - RG 660 Teil 3
- [19] H. A. Jehn
Galvanotechnik, 1991, 82, 9, 3023-3031
Verschleißaspekte dekorativer Schichten
- [20] R. Riedl
VDI-Tagung, 1993, 34-19-01
Dekoroberflächen: Anforderungsprofil für dekorative Anwendungen
- [21] R. Riedl
Galvanotechnik, 1989, 80, 10, 3391-3397
Hartstoffbeschichtung von Armbanduhren mit Farbanpassung an genormte Goldtöne
- [22] C. Daube
Dissertation: Aspekte des Korrosionsverhaltens von PVD-Hartstoffschichten am Beispiel der Systeme TiN und (TiAl)N
RWTH Aachen, 1990, 1
- [23] H. A. Jehn
VDI-Tagung, 1993, 34-19-01
Systemaspekte der Anwendung dekorativer Schichten von der Materialsauwahl bis zum Feldtest
- [24] W.-D. Münz
Society of Vacuum Coatings
36th annual Technical Proceedings 1993
Production of PVD Decorative Hard Coatings Using Multitarget UBM Coating Machines
- [25] P. J. Kay and C. A. Mackay
International Tin Research Institute, Greenford, 1979, 169-174
Barrier Layers Against Diffusion
- [26] E. Raub and K. Müller
Properties of metal deposits
1967, 186-197
- [27] Th. Emmerich
DA: thermisch stabile Diffusionsbarrieren
RWTH Aachen, 1992
- [28] M. R. Pinnel and J. E. Bennett
Metallurgical Transactions A, 1976, 7A, 629-635
Qualitative Observations on the Diffusion of Copper and Gold Through a Nickel Barrier
- [29] H. Schumann
Metallographie, VEB Deutscher Verlag für Grundstoffindustrie, 1989, 12, 152-915/69/89
- [30] H. A. Jehn and M. E. Baumgärtner
Surface and Coatings Technology, 1992, 54/55, 108-114
Corrosion studies with hard coating - substrate systems

- [31] Wieland-Werke AG
TF Oberflächenlabor
Empfehlung zur Vorbehandlung von bleihaltigem Messing zur galvanischen Beschichtung
- [32] K.-H. Knirsch and H. Sick
Metalloberfläche, 1982, 9, 36, 1-5
Haftfestigkeit galvanischer Nickelschichten auf bleihaltigem Messing
- [33] O. Kayser
PLATIN NRW 1994
Dekorative Hartstoffsichten durch PVD-Verfahren: Herstellung und Anwendung
Dekorative und verschleißschützende Beschichtungen durch Lichtbogenverdampfen
- [34] E. Kolawa, J. S. Chen, J. S. Reid, P. J. Pokela and M.-A Nicolet
J. Appl. Phys., 1991, 70, 3, 1369-1373
Tantalum-based diffusion barriers in Si/Cu VLSI metallizations
- [35] P. Madakson
J. Appl. Phys., 1991, 70, 3, 1374-1379
Interdiffusion, hardness, and resistivity of Cr/Cu/Co/Au thin films
- [36] S. Bastian
Galvanotechnik, 1990, 81, 8, 2706-2709
Die Entwicklung der Brille in sieben Jahrhunderten
- [37] D. Dubiel
Prakt. Met. 26, 1989, 26, 68-82
Characterization of Sputter Deposited Chromium Nitride Coatings
- [38] M. J. Park, A. Leyland and A. Matthews
Surface and Coatings Technology, 1990, 43/44, 481492
Corrosion Performance of Layered Coatings Produced by Physical Vapour Deposition
- [39] C.-K. Hu, S. Chang, M. B. Small and J. E. Lewis
Diffusion Barrier Studies for Cu
V-Mic Conf. CH 2337-4/86/0000-0181, 1986, 181-187
- [40] H. Yamagata, A. Inone and T. Masumoto
US Patent 5,366,564, Nov. 94
Hard Wear resistant film and method of production thereof
- [41] G. L. Miller
Tantalum and Niobium, Butterworths Scientific Publications, 1959, 1
- [42] Deutsches Kupfer Institut DKI, Nr. I.006
Informationsdruck: Kupfer-Aluminium Legierungen, Eigenschaften, Herstellung, Verarbeitung und Verwendung
- [43] H. A. Jehn and I. Pfeifer-Schäller
Galvanotechnik, 1993, 84, 10, 3283-3288
Korrosion von Hartstoffsichten Teil 1
- [44] W. Schröter, K.H. Lautenschläger and H. Bibrack
Taschenbuch der Chemie, Harry Deutsch 1990, 14, 3-87144-922-9
- [45] H. A. Jehn and I. Pfeifer-Schäler
Galvanotechnik, 1993, 84, 11, 3669-3675
Korrosion von Hartstoffsichten Teil 2
- [46] W. Siedel, VEB Deutscher Verlag für Grundstoffindustrie, Leipzig 1985, 1
Porosity in Electroless Ni Plating
Oberflächenvorbehandlung und metallische Beschichtungen

- [47] H. A. Jehn and I. Pfeifer-Schäler
Galvanotechnik, 1993, 84, 12, 4059-4064
Korrosion von Hartstoffschichten Teil 3
- [48] G. E. Murch and A. S. Nowick
Diffusion in Crystalline Solids
Academic Press Inc., 1984, 1, 0-12-522662-4, 530.41 MU
- [49] American Society for Metals
ASTM Handbook 28, 28-64
Principles of Heat Treatments of Nonferrous Alloys
- [50] G. H. Geiger and D. R. Poirier
Transport Phenomena in Metallurgy, Addison-Wesley, 1980, 1, 0-2010-2352-0
- [51] I. Knaur and W. Gust
Fundamentals of Grain and Interphase Boundary Diffusion, Ziegler-Press,
Stuttgart, 1989, 2
- [52] G. E. Murch and A. S. Nowick
Diffusion in crystalline solids, Academic Press, Inc., 1984, 0-12-522662-4
- [53] B. C. Scott
Trans. Inst. Met. Finish., 1987, 65, 3, 90-98
Zinc diffusion in tin coatings on brass
- [54] M. Ives
PhD-Thesis: Fundamental Studies of the PVD Technique
SHU 1994
- [55] Bhunshan and Gupta
Handbook of Tribology, Materials, Coatings and Surface Treatments
- [56] P. C. Johnson
Plating and Surf. Finishing, 1989, 76, 3, 30-33
PVD of thin films
- [57] H. Frey and G. Kienel
VDI, Dünnschichttechnologie, 1987
- [58] American Society for Metals
ASTM Handbook 18
Coating: PVD / CVD
- [59] American Society for Metals
ASTM Handbook 13
Corrosion: CVD / PVD
- [60] W.-D. Münz
Surface and Coatings Technology, 1991, 48, 81-94
The unbalanced magnetron: current status of development,
- [61] W.-D. Münz
Surface and Coatings Technology, 1993, 58, 205-212
The new way to hard coatings: Arc Bond Sputtering ABS Part II,
- [62] W.-D. Münz, D. Hofmann and K. Hartig
Thin Solid Films, 1982, 96, 79
- [63] W.-D. Münz and D. Hofmann
Metalloberfläche, 1983, 37, 279
- [64] W. D. Münz
Surface and Coatings Technology, 1992, 50, 169-178
The new way to hard coatings ARC Bond Sputterings: ABSTTM
- [65] W.-D. Münz
Beschichten von Hartstoffen, Das unbalancierte Magnetron, Stand der
Entwicklung heute, VDI, 1992

- [66] Editor: H. A. Jehn
Advanced Techniques for Surface Eng., Kluwer Academic Publishers, 1992,
1,0-7923-2006-9
- [67] J. A. Thornton
J. Vac. Sci. Technol., 1974, 11, 4, 666-670
Influence of apparatus geometry and deposition conditions on the structure and
topography of thick sputtered coatings
- [68] H. Kuchling
Taschenbuch der Physik, Harry Deutsch, 1989, 12, 3 8171 1020 0
- [69] P. R. Chalker, S. J. Bull and D. S. Rickerby
Materials Science and Engineering, 1991, A140, 583-592
A review of the methods for the evaluation of coating-substrate adhesion
- [70] E. Bergmann, F. Dupont and S. Steiger
Oberfläche surface, 1991, 32, 1-2, 8-12
Nécessité d'un concept système pour l'assurance qualité des revêtements PVD
- [71] N. Frey, P. Mettraux, G. Zambelli and D. Landolt
Surface and Coatings Technology, 1994, 63, 167-172
Modified scratch test for study of the adhesion of ductile coatings
- [72] P. Hedenqvist, M. Olsson and S. Jacobson
Surface and Coatings Technology, 1990, 41, 1, 31-49
Failure Mode Analysis of TiN-coated High-Speed Steel: In Situ Scratch
Adhesion Testing in the Scanning Electron Microscope
- [73] H. A. Jehn, G. Reiners and N. Siegel
DIN Fachbericht 39, 1993, 1
Charakterisierung dünner Schichten
- [74] H. E. Hintermann
Fresenius J Anal Chem, 1993, 346, 45-52
Characterization of surface coatings by the scratch Adhesion test and by
indentation measurements
- [75] Handbook Fischerscope 100, 10/91, 962-601
- [76] Philips, Information paper: X-Ray diffraction
- [77] W. H. Ailor
Handbook on corrosion testing and evaluation
John Wiley & Sons, 1971, 1, 0-471-00985-7
- [78] M. Clarke and A. J. Sansum
Transactions of the Institute of Metal Finishing, 1972, 50, 2, 11-14
A Two Hour Porosity test for Gold on Substrates of Copper, Silver and Nickel
- [79] G. W. Marshall, S. V. Allen, M. Tonks and D. Clayton
3rd international Conference on Advances in Coatings & Surface Engineering
For Corrosion and Wear Resistance, 1992
Subplate Effects Upon The Porosity Of Electrodeposited Gold
- [80] Canning, Birmingham
The Canning handbook
Surface Finishing, 1982
- [81] B. Langer
Praktische Metallographie, 1993, 30, 6, 312-314
Quantifying Inclusions in Materials - Determination of Slag inclusions in welds

- [82] M. Clarke and J. M. Leeds
Transactions of the Institute of Metal Finishing, 1968, 46, 81-86
A Sulphur Dioxide Porosity Test for Coatings of Gold and the Platinum Metals
on Substrates of Copper and its Alloys, Nickel, and Silver
- [83] Siemens
Belgium, N.V. EC B Q Oos, 18.06.90, F49-F6255
Prüfung auf Poren- und Rißfreiheit veredelter Oberflächen auf kupferhaltigen
Substraten
- [84] D. S. Rickerby
J. Vac. Sci. Technology, 1986, 6, 11/12
Internal Stress and adherence of TiN coatings
- [85] K. W. Andrews
Physical Metallurgy, Techniques and Applications, George Allen & Unwin
Ltd., London, Volume 1
- [86] M. Becker and H. Klemm
Handbuch der metallographischen Ätzverfahren
VEB Deutscher Verlag für Grundstoffchemie, 1984, 4, 152-915/67/84
- [87] American Society for Metals
Binary Alloy Phase Diagrams
ASTM Handbook 2
- [88] M. F. Doerner and W. D. Nix
J. Mater. Res. 1(4), 1986
A method for interpreting the data from depth-sensing indentation instruments
- [89] G. Hoffacker
mo Metalloberfläche, 1993, 47, 2, 62-65
Cu/Sn-Legierungen als Alternativen zu allergieauslösenden Ni-Überzügen
- [90] E.E. Saalagean, D.B. Lewis, J.S. Brooks, W.-D. Münz, I. Petrov and J.E. Greene
Combined steered arc-unbalanced magnetron grown niobium coatings for
decorative and corrosion resistance applications
Submitted to publish in Surface and Coatings Technology
- [91] J.H. Hsieh, R. Lee, R.A. Erck, G.R. Erck, G.R. Fenske, Y.Y. Su, M. Marek, R.F.
Hochmann, Surface and Coatings Technology, 1991, 49, 83
- [92] R. Messier, A.P. Giri and R.A. Roy
J. Vac. Sci. Technol., 1974, 11, 666
- [93] W.F. Smith
Foundations of materials science and engineering
Second Edition, McGraw-Hill, Inc. 1993
- [94] R. W. Berry, P. M. Hall and M. T. Harris
Thin film technology
Van Nostrand Reinhold Company, 1968

CHAPTER 6: Figures and Tables

NOTE:

The figures and tables in this chapter are the figures and tables mentioned in the text as 6.xx

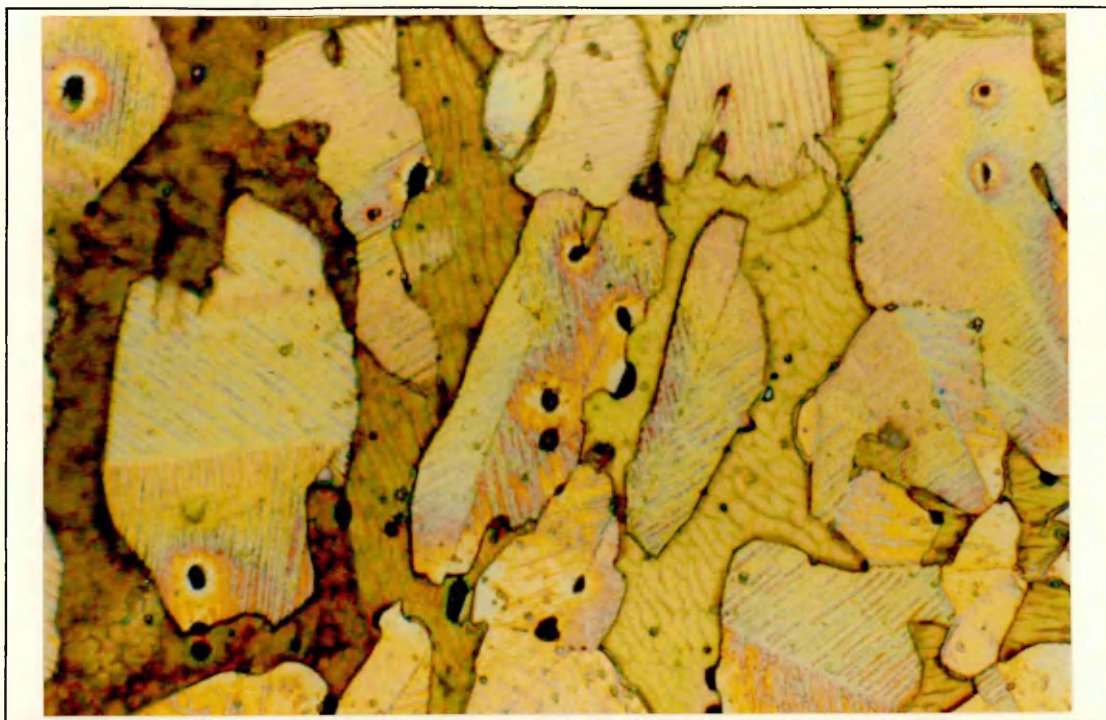


Figure 1: diffusion annealed brass substrate (90 min, 250 °C)
metallographic cross section close to the surface
magnification: 1000 x
colour etching etchant (II)

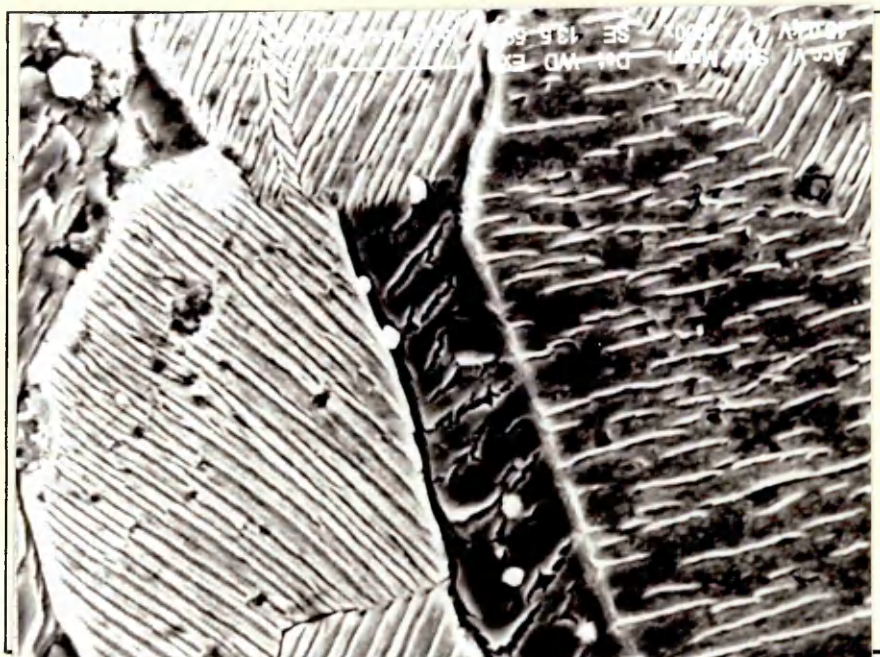


Figure 2: part of figure 1 under SEM magnification 3002 x

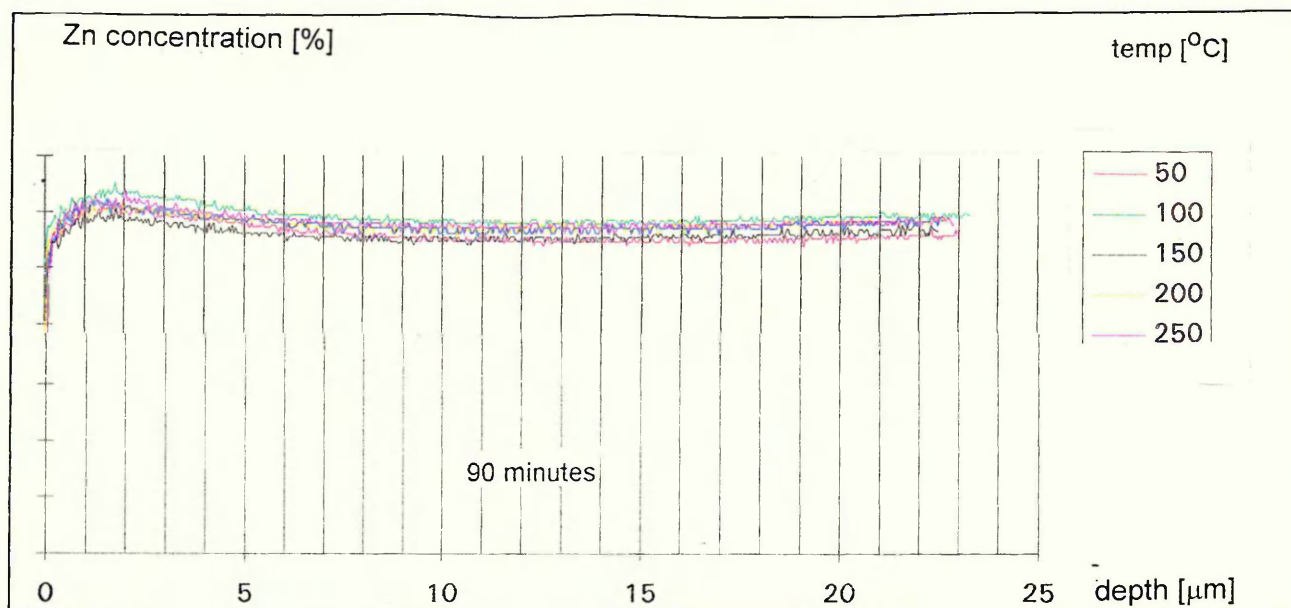


Figure 3: overlaid Zn graphs of diffusion annealed brass substrate at constant time of 90 minutes at various temperatures

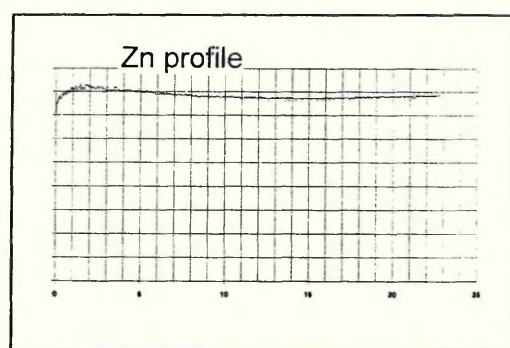


Figure 4: single Zn concentration profile at 90 min / 200 $^{\circ}\text{C}$

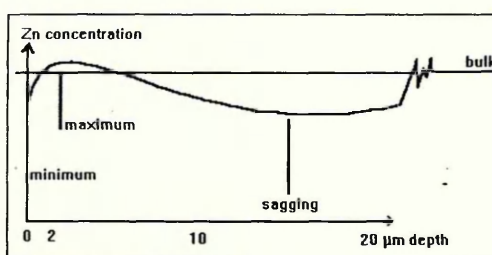


Figure 5: shows schematically figure 4 with marked positions at 0 μm : physical surface, minimum 2 μm : maximum Zn concentration around 15 μm : sagging of the curve

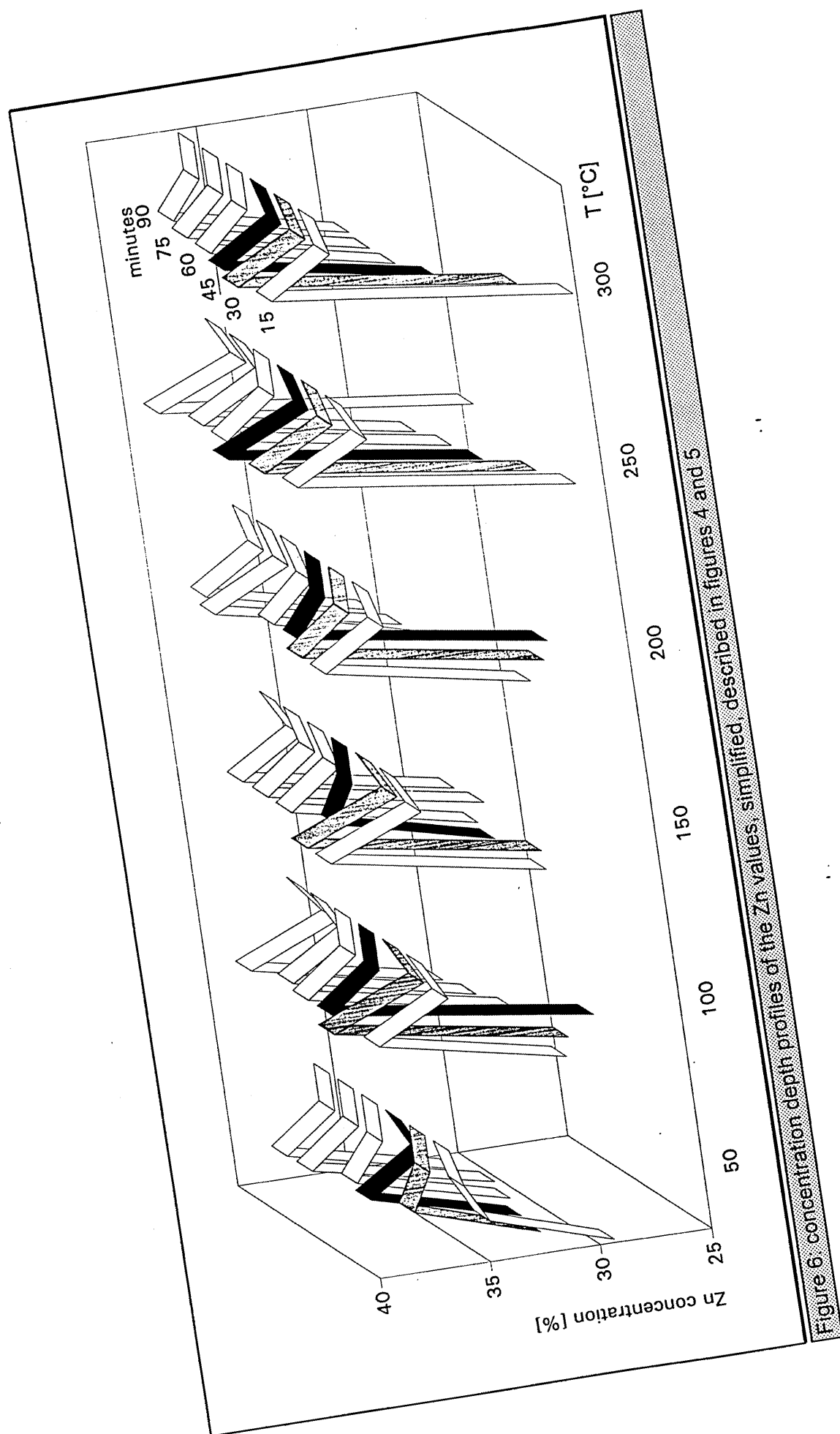


Figure 6. concentration depth profiles of the Zn values, simplified, described in figures 4 and 5

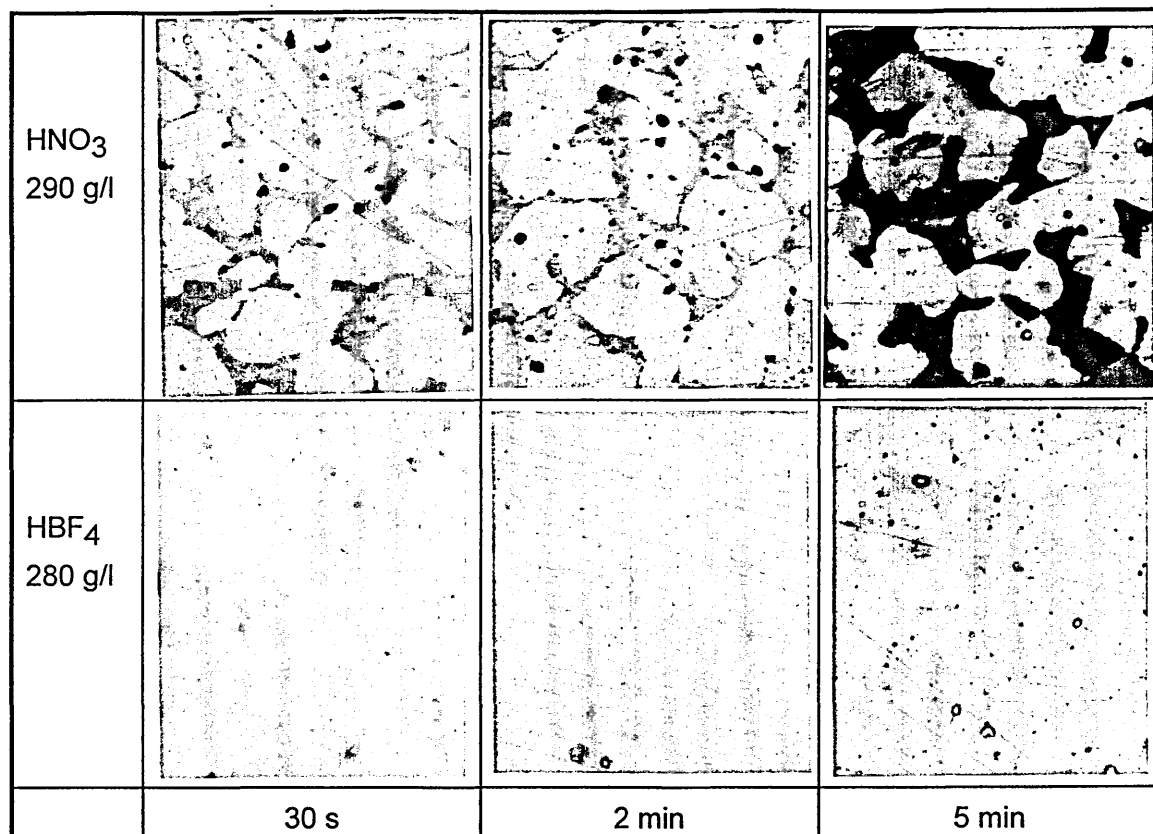


Figure 7: sample surfaces after etching in HNO₃ and HBF₄
(optical microscope, magnification 500 x)

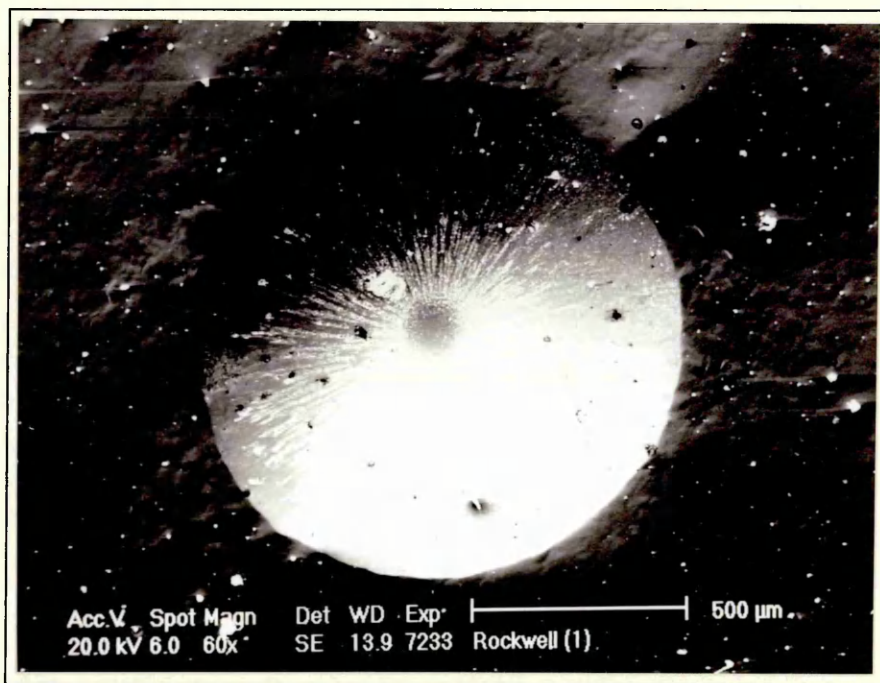


Figure 8a: Rockwell indentation with no failure

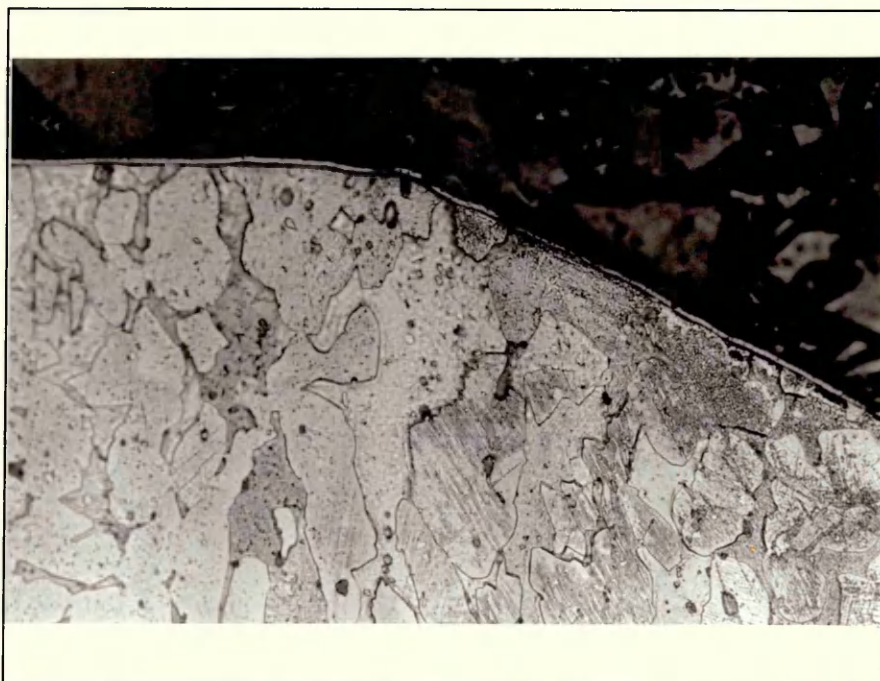


Figure 8b: Rockwell indentation with no failure in cross section (500 x)

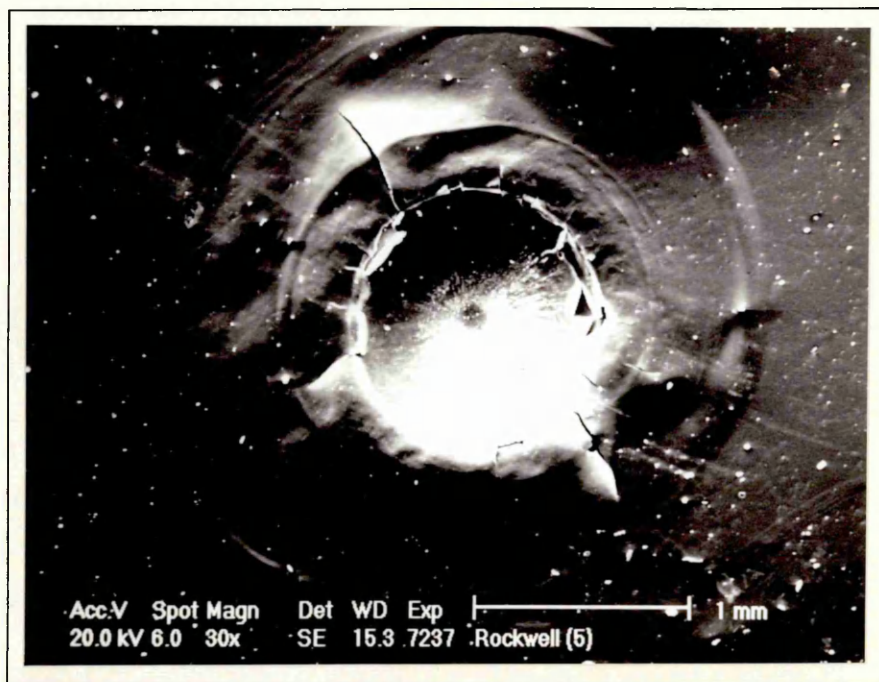


Figure 9a: Rockwell indentation with cohesive failure

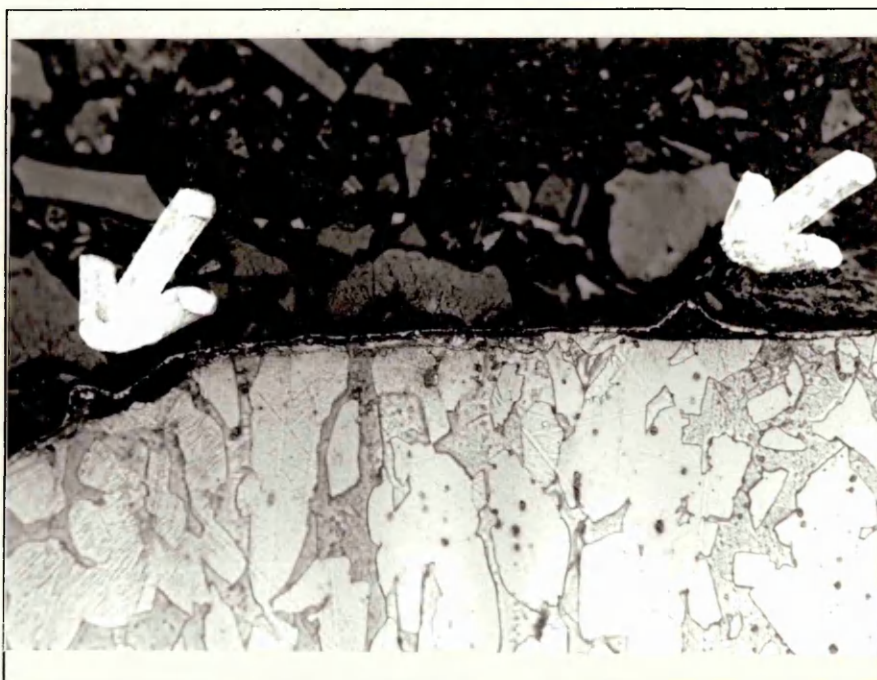


Figure 9b: Rockwell indentation with cohesive failure in cross section (500 x)

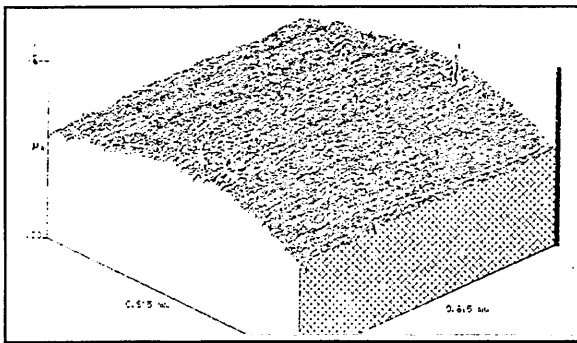


Figure 10: Argon Ion Etching, -600 V

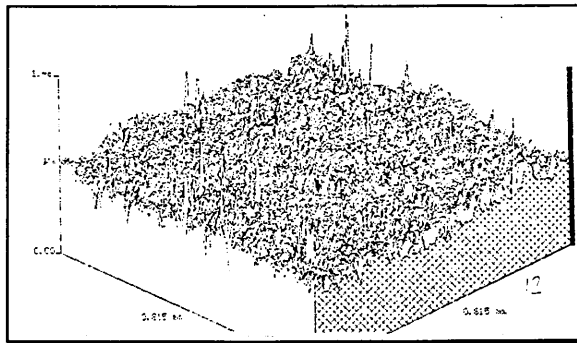


Figure 11: Metal Ion Etching, -600 V

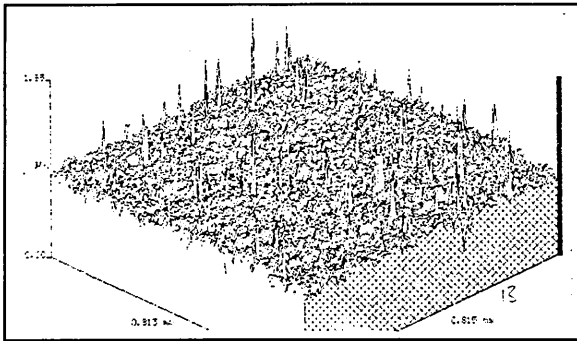


Figure 12: Metal Ion Etching, -800 V

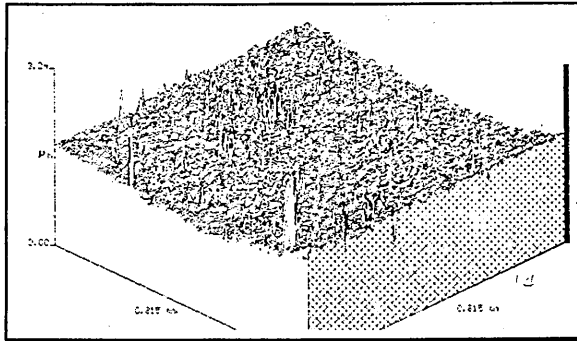


Figure 13: Metal Ion Etching, -1000 V

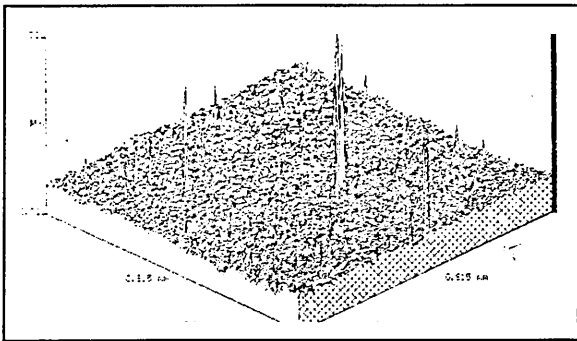


Figure 14: Metal Ion Etching, -1200 V

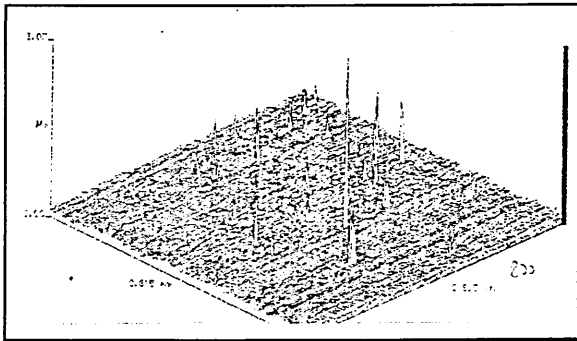


Figure 15: Combined Etching, -800 V

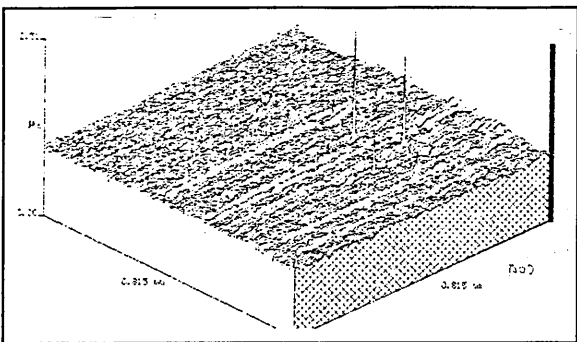


Figure 16: Combined Etching, -1000 V

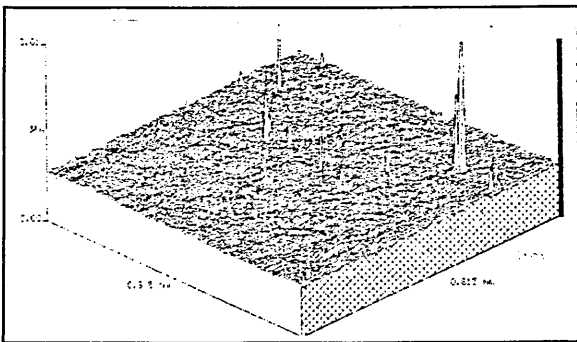


Figure 17: Combined Etching, -1200 V

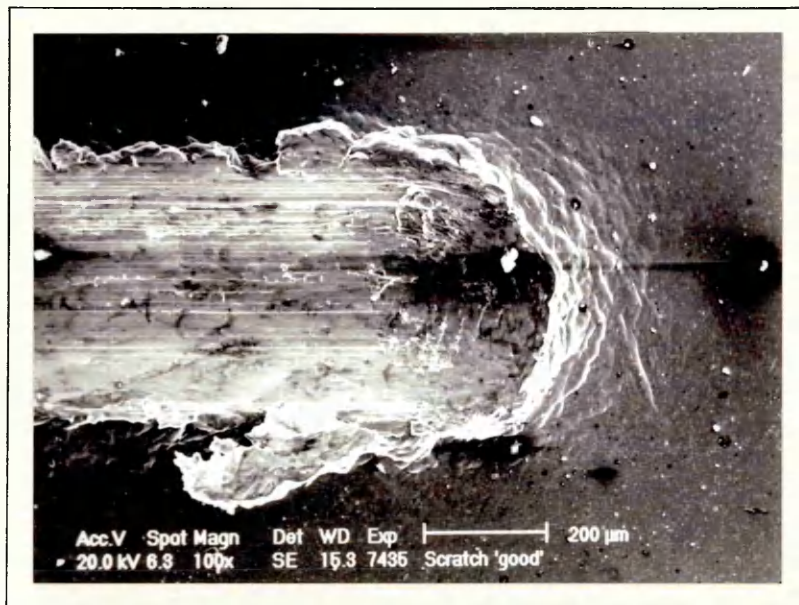


Figure 18: Scratch adhesion test, top view at 100 N, showing upset coating

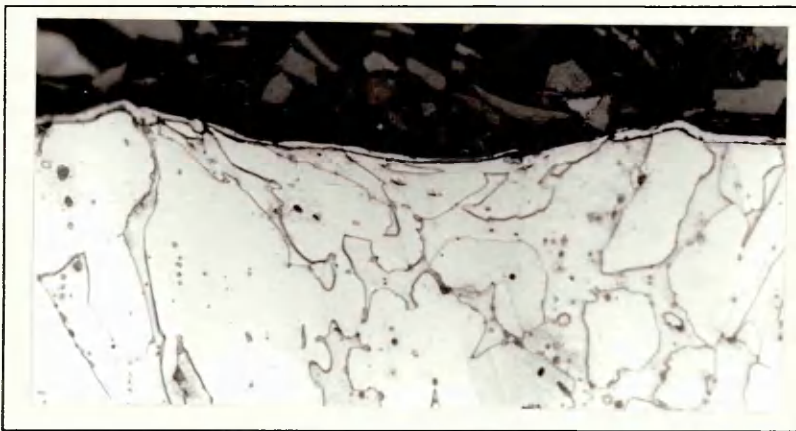


Figure 19a: Scratch adhesion test, cross section (500x), showing adhesive coating at 20 N

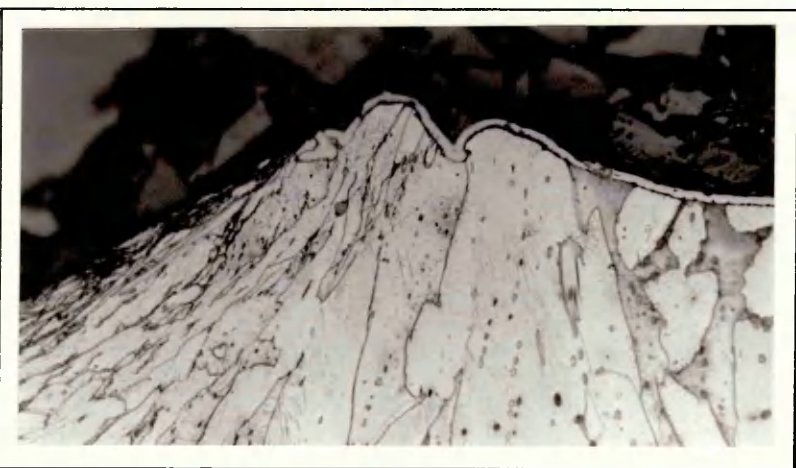


Figure 19b: Scratch adhesion test, cross section (500x), showing adhesive coating at 80 N

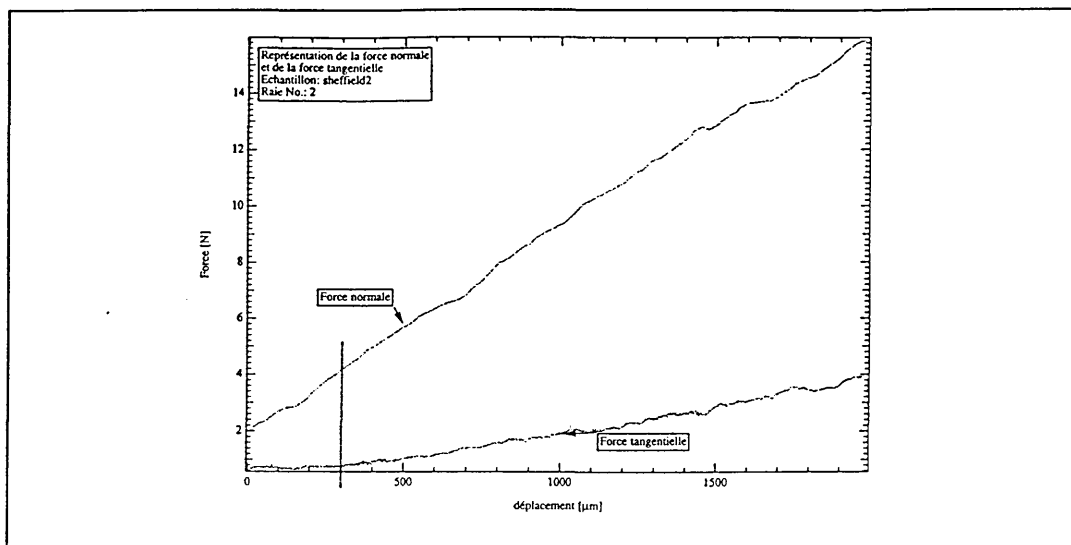


Figure 22 a: Scratch adhesion test, displacement vs tangential and normal forces

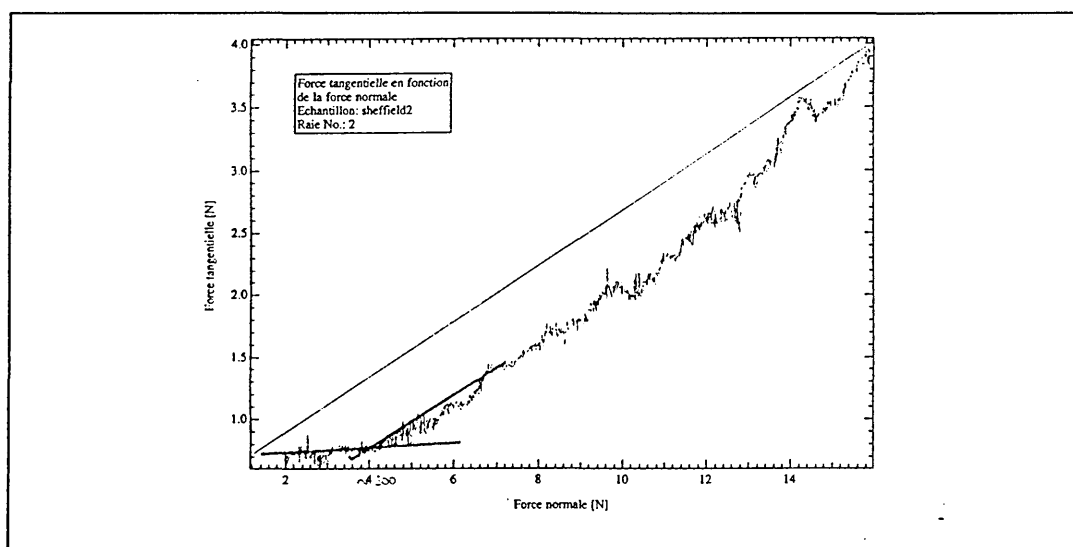


Figure 22 b: Scratch adhesion test, normal force vs tangential force

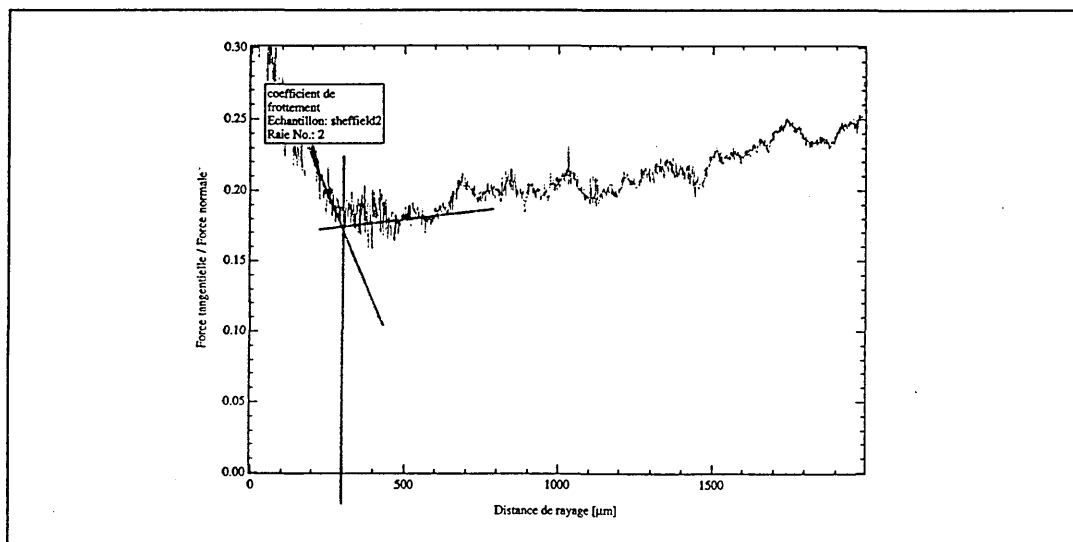


Figure 22 c: Scratch adhesion test, distance vs tangential force / normal force

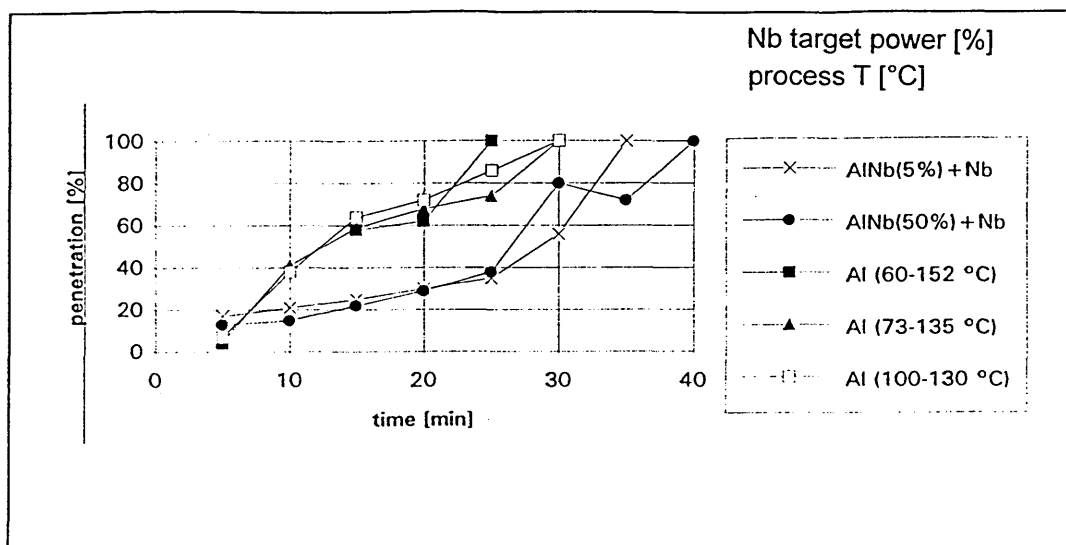


Figure 23 a: Diffusion of Zn in aluminium and AlNb(X)+Nb coatings

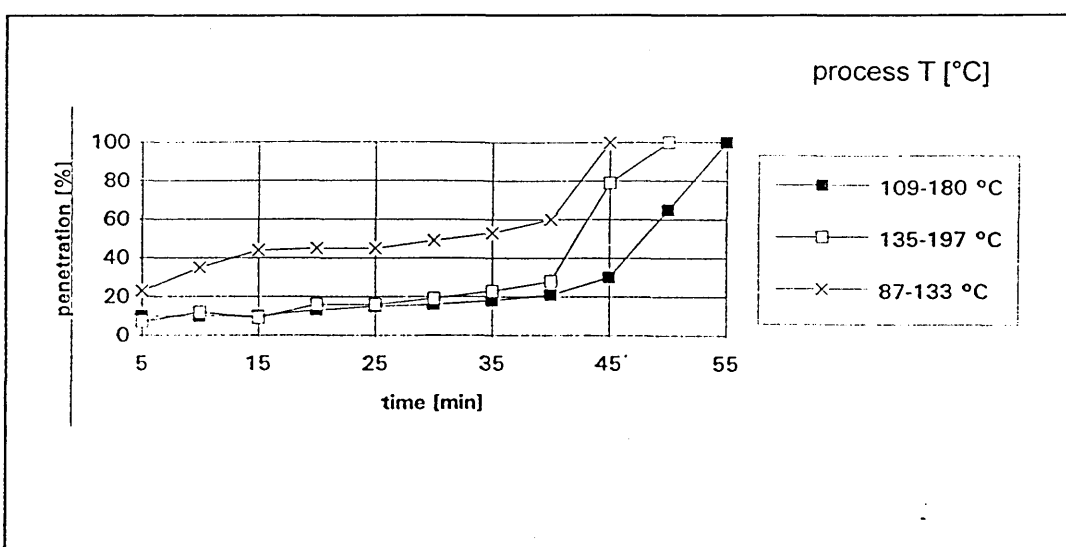


Figure 23 b: Diffusion of Zn in CuAl8 coatings

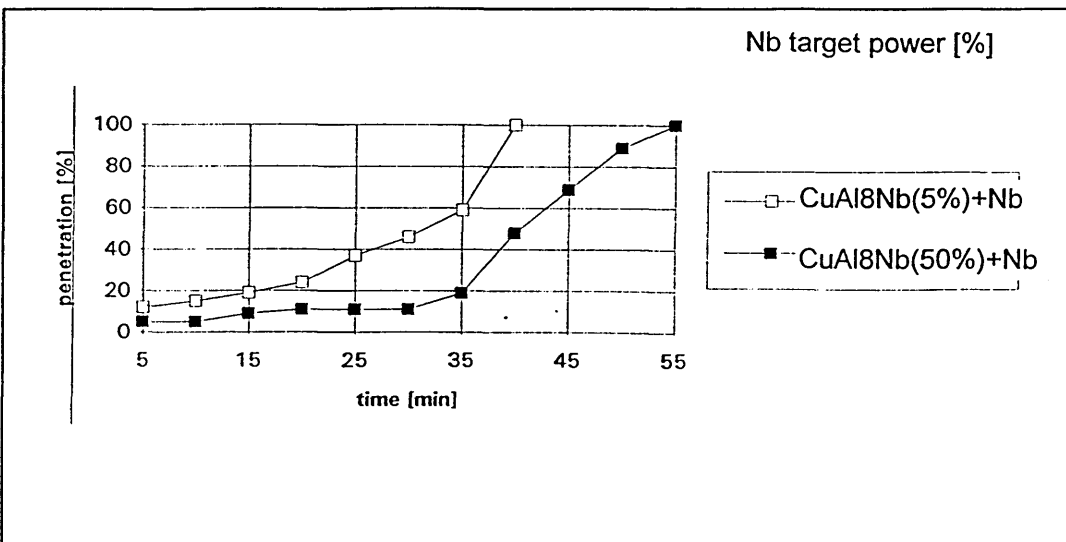


Figure 23 c: Diffusion of Zn in CuAl8(X)+Nb coatings

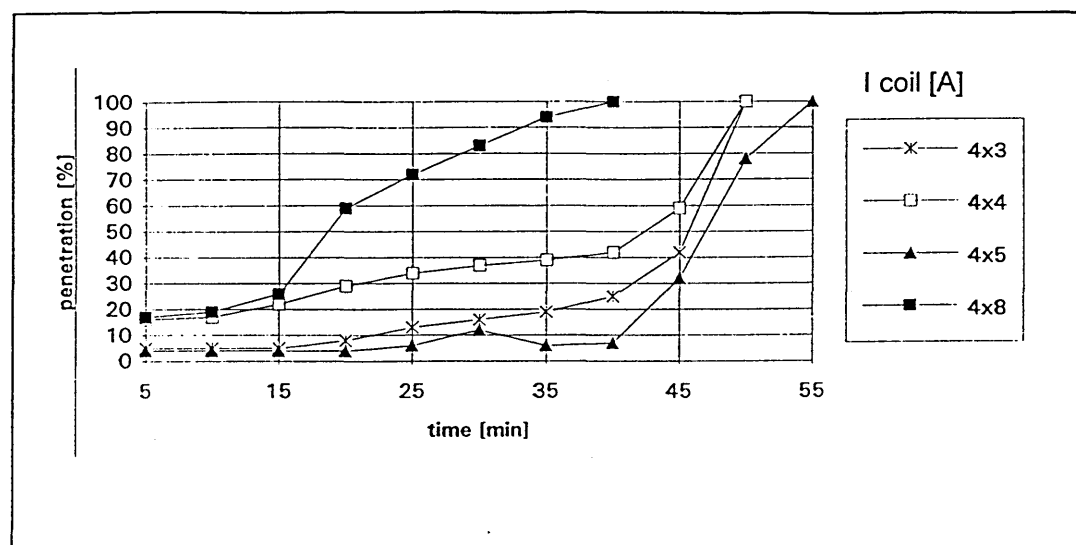


Figure 23 d. Diffusion of Zn in Nb coatings as a function of the applied coil current

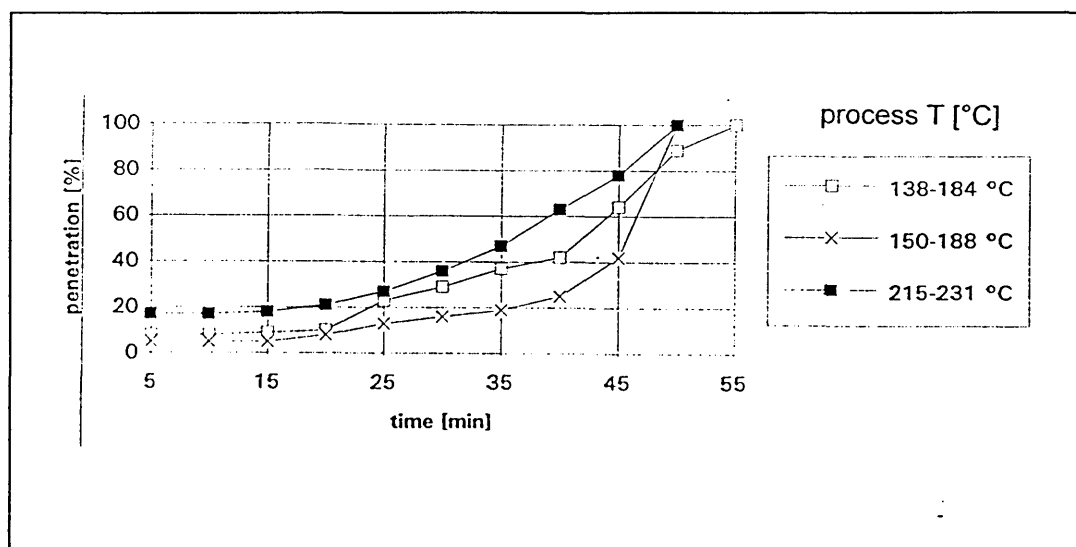


Figure 23 e. Diffusion of Zn in Nb coatings as a function of the temperature

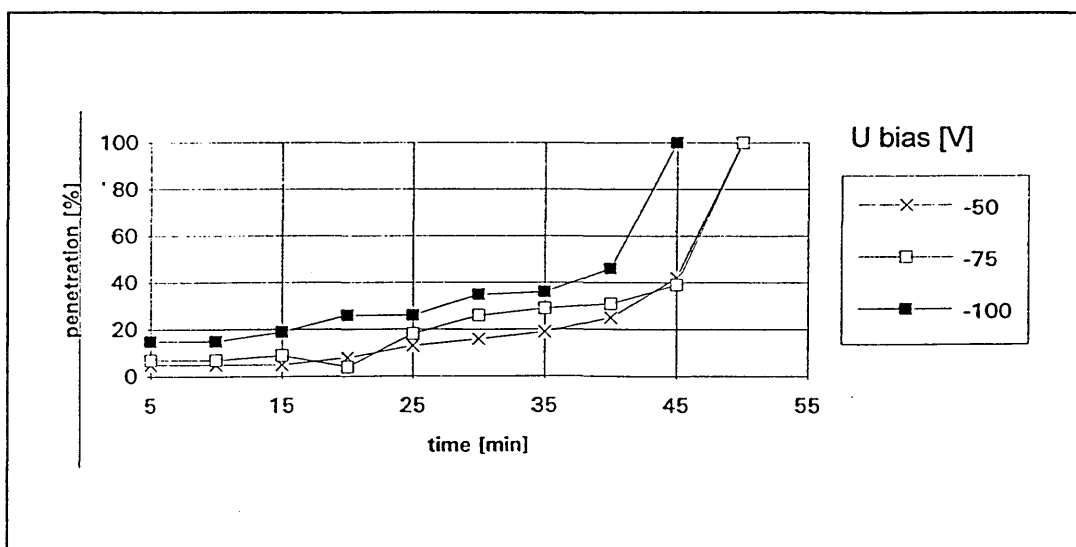


Figure 23 f. Diffusion of Zn in Nb coatings as a function of the applied bias voltage

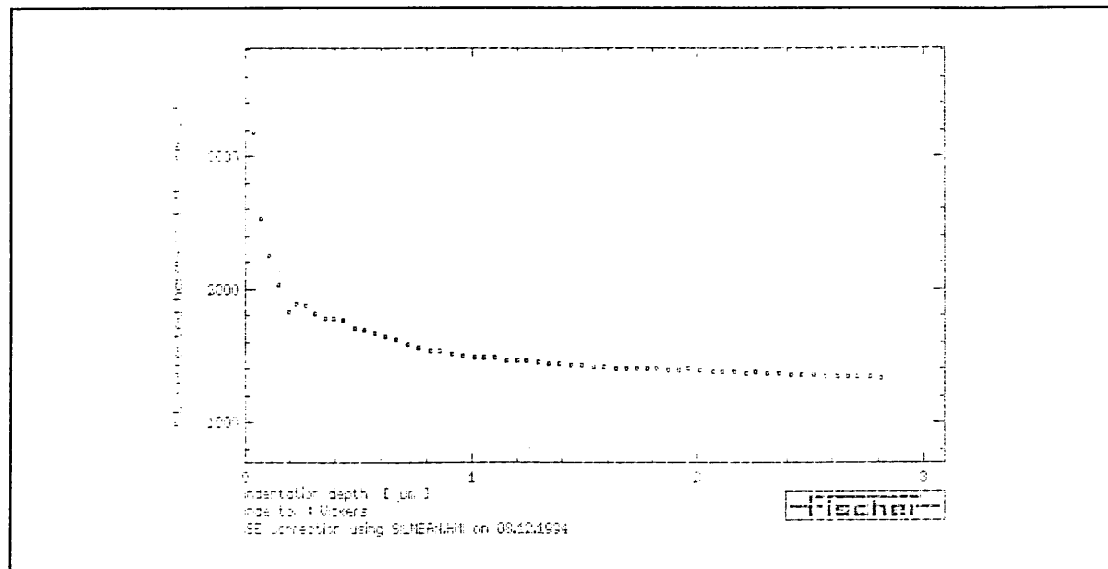


Figure 24: Hardness-depth profile of an aluminium coating on brass

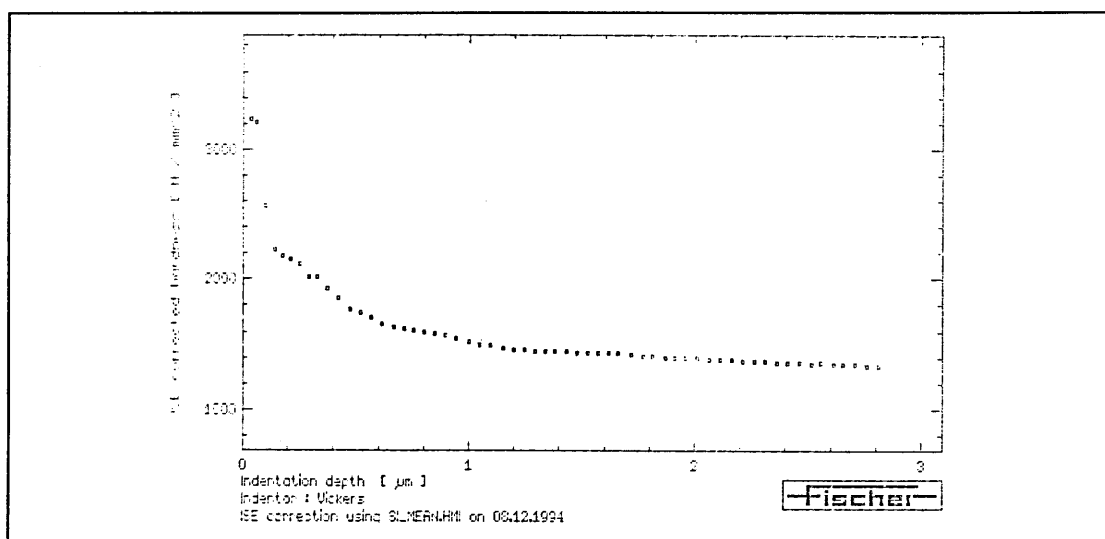


Figure 25: Hardness-depth profile of an AlNb(5%)+Nb coating on brass

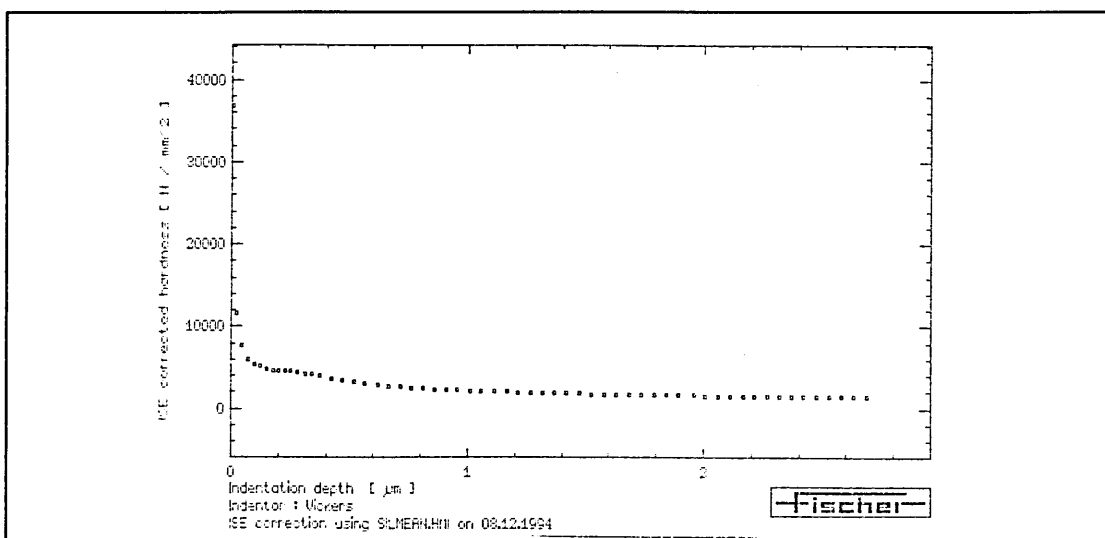


Figure 26: Hardness-depth profile of an AlNb(50%)+Nb coating on brass

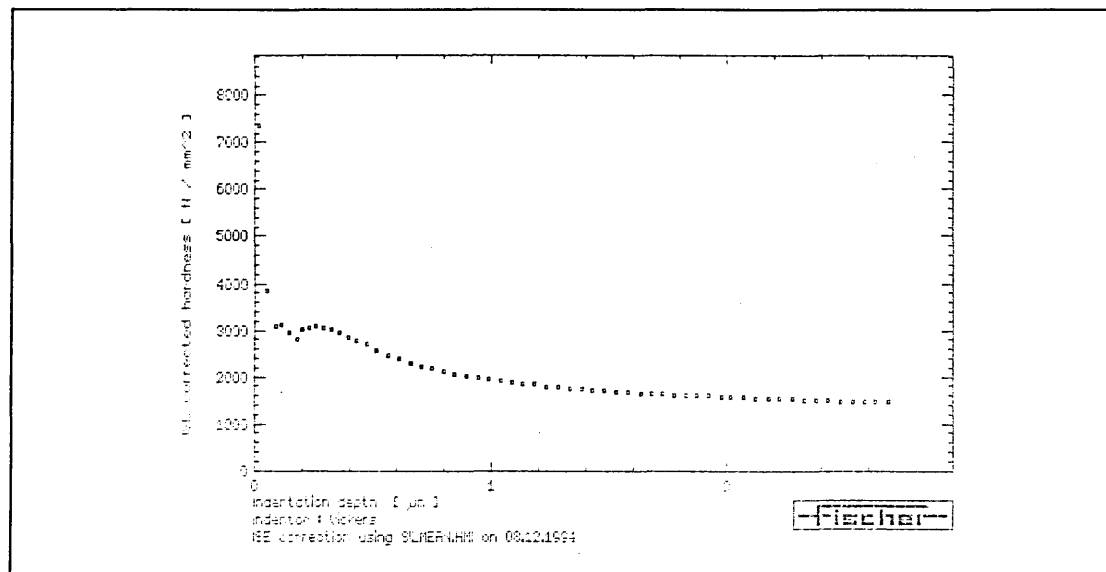


Figure 27: Hardness-depth profile of a CuAl8 coating on brass

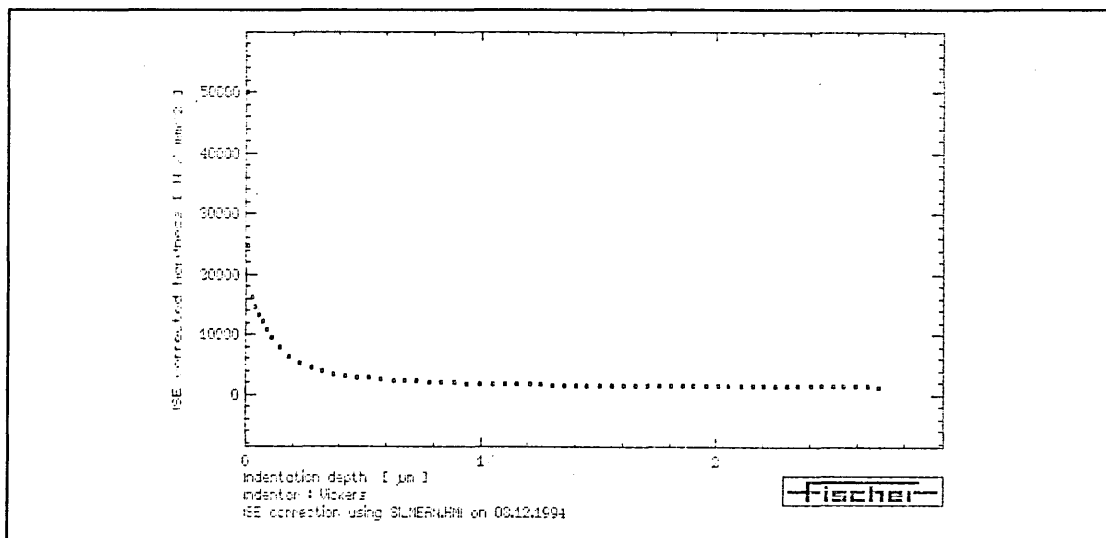


Figure 28: Hardness-depth profile of a CuAl8Nb(5%)+Nb coating on brass

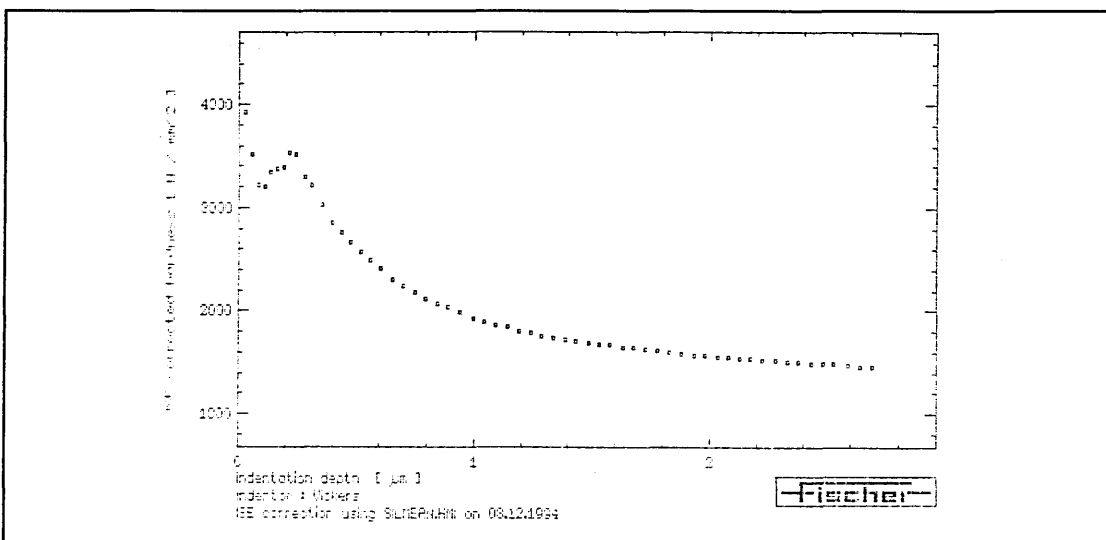


Figure 29: Hardness-depth profile of a CuAl8Nb(50%)+Nb coating on brass

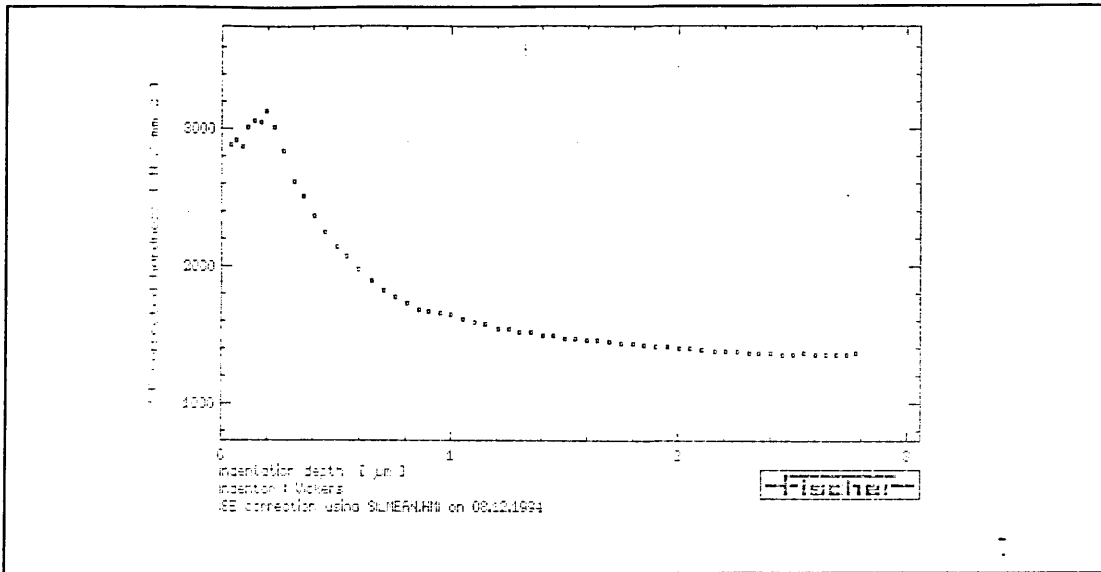


Figure 30. Hardness-depth profile of a niobium coating on brass

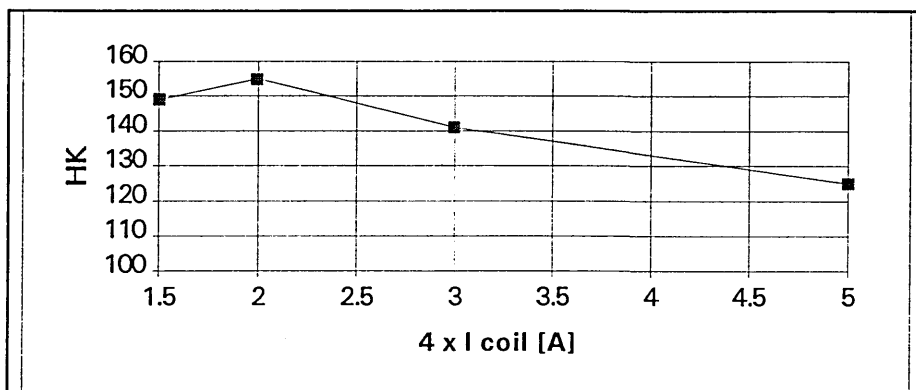


Figure 31: Hardness HK 0.01 of aluminium coatings as a function of the applied coil current (I_{coil}) at start temperatures between 70 and 100 °C

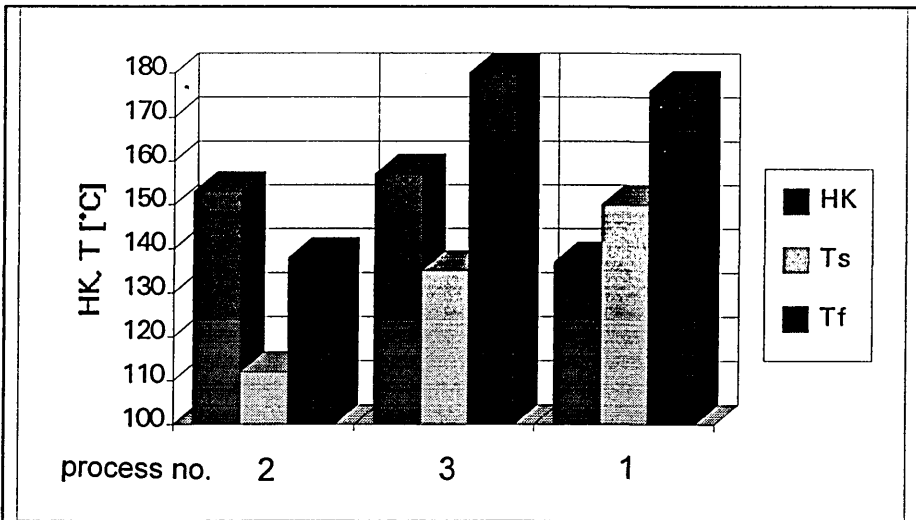


Figure 32: Hardness HK 0.01 of Al coatings as a function of the start and end temperatures T_s and T_f at an applied coil current of 4 x 6 A

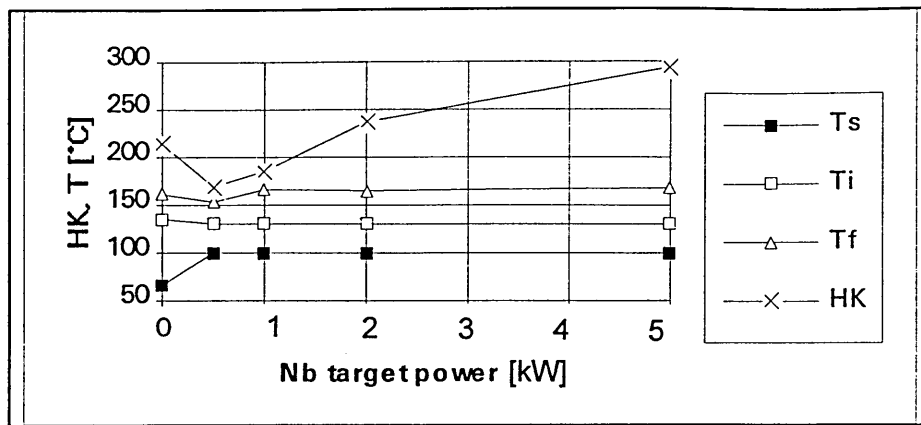


Figure 33: Hardness HK 0.01 of AlNb(X) + Nb coatings as a function of the applied Nb target power [%], showing the AlNbX start, Nb intermediate and end temperatures T_s , T_i and T_f .

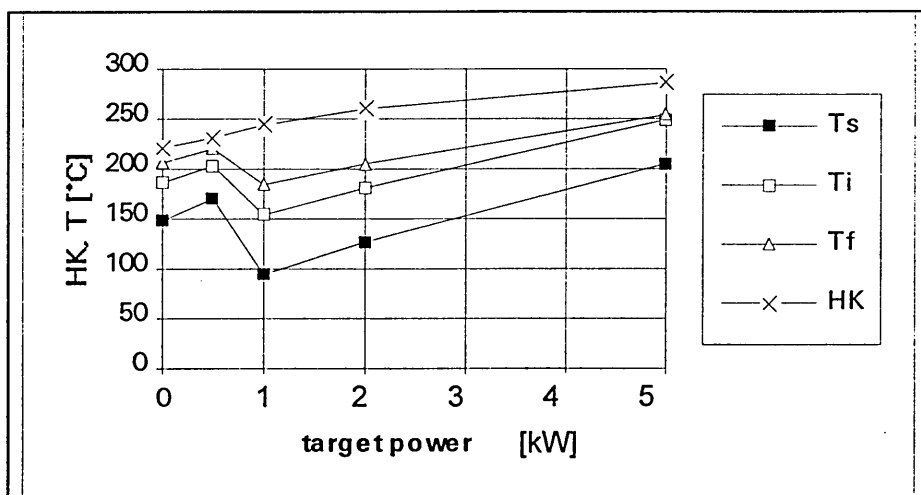


Figure 34: Hardness HK 0.01 of CuAl8Nb(X) + Nb coatings as a function of the applied Nb target power [%], showing the CuAl8NbX start, Nb intermediate and end temperatures T_s , T_i and T_f .

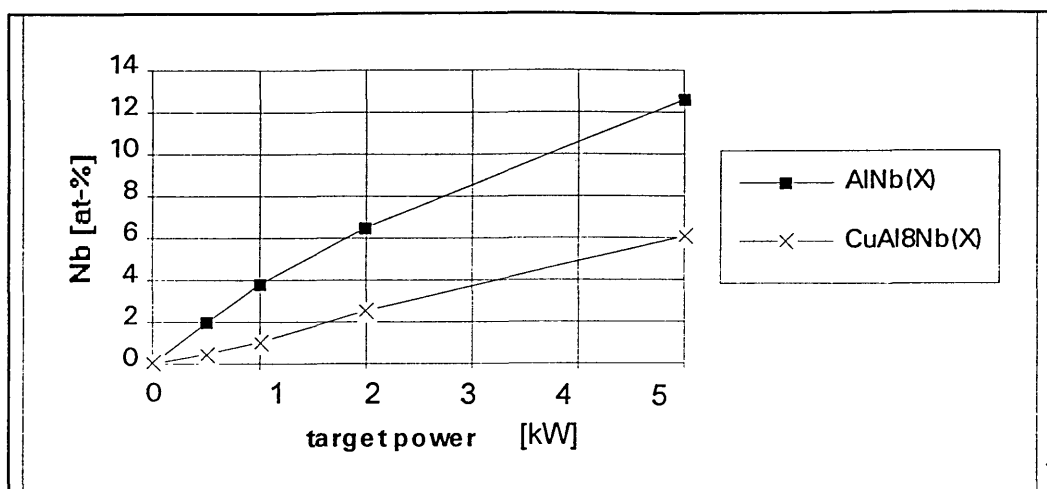


Figure 35: Niobium concentration [at-%] as a function of the niobium target power in percent of the total power associated with the Al and CuAl8 targets

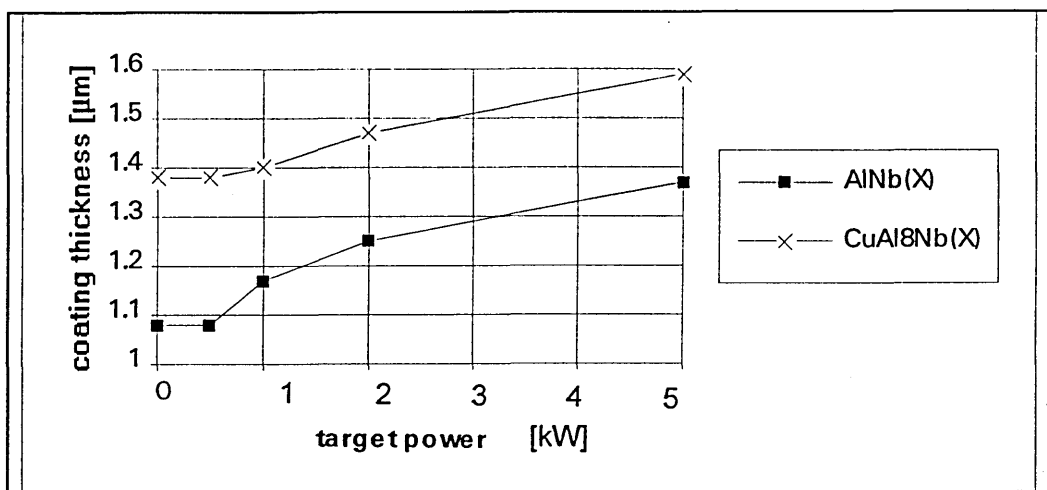


Figure 36: Coating thickness [μm] as a function of the niobium target power in percent of the total power associated with the Al and CuAl8 targets

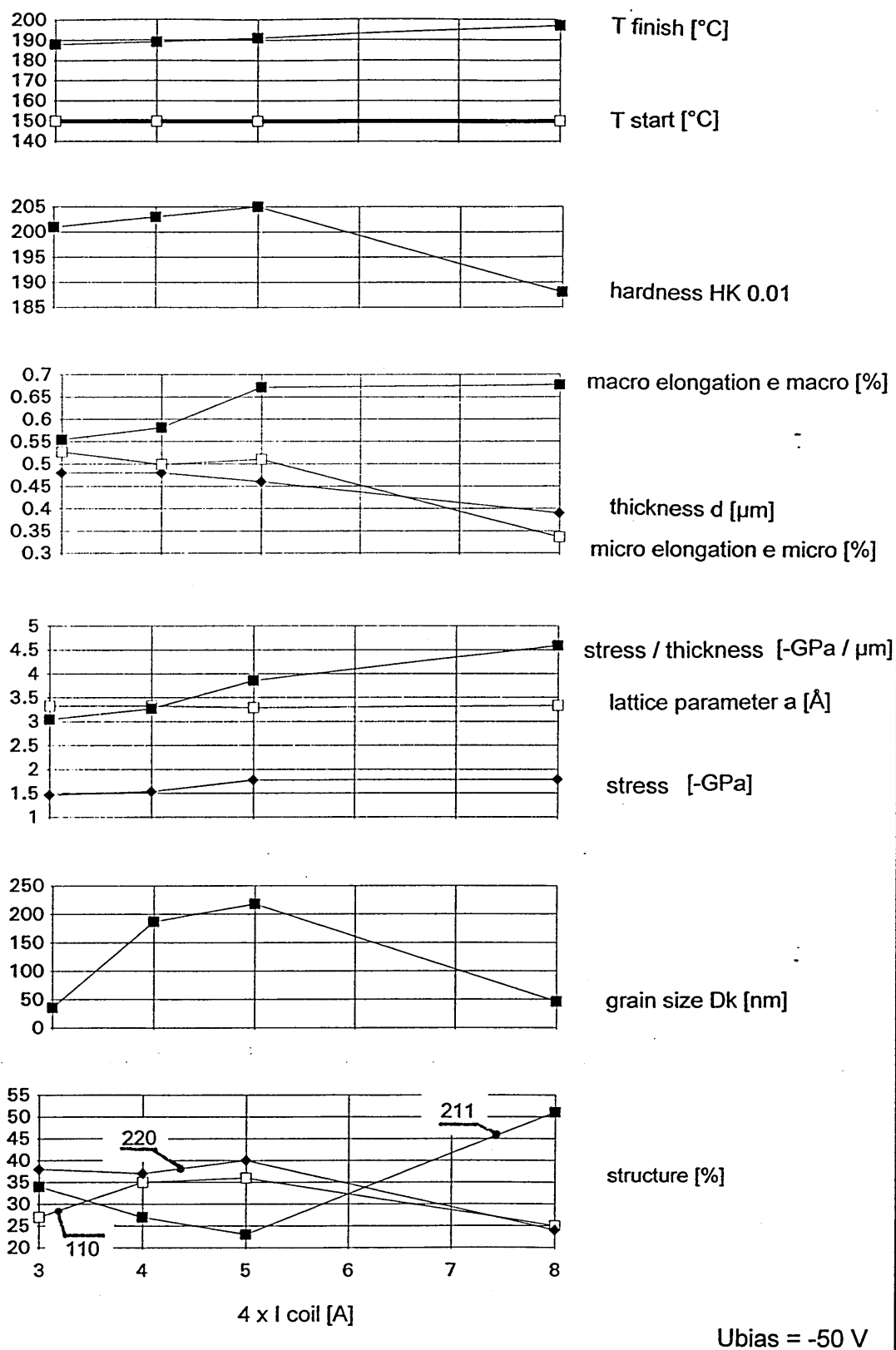


Figure 37: Properties of Nb coatings as a function of the applied coil current

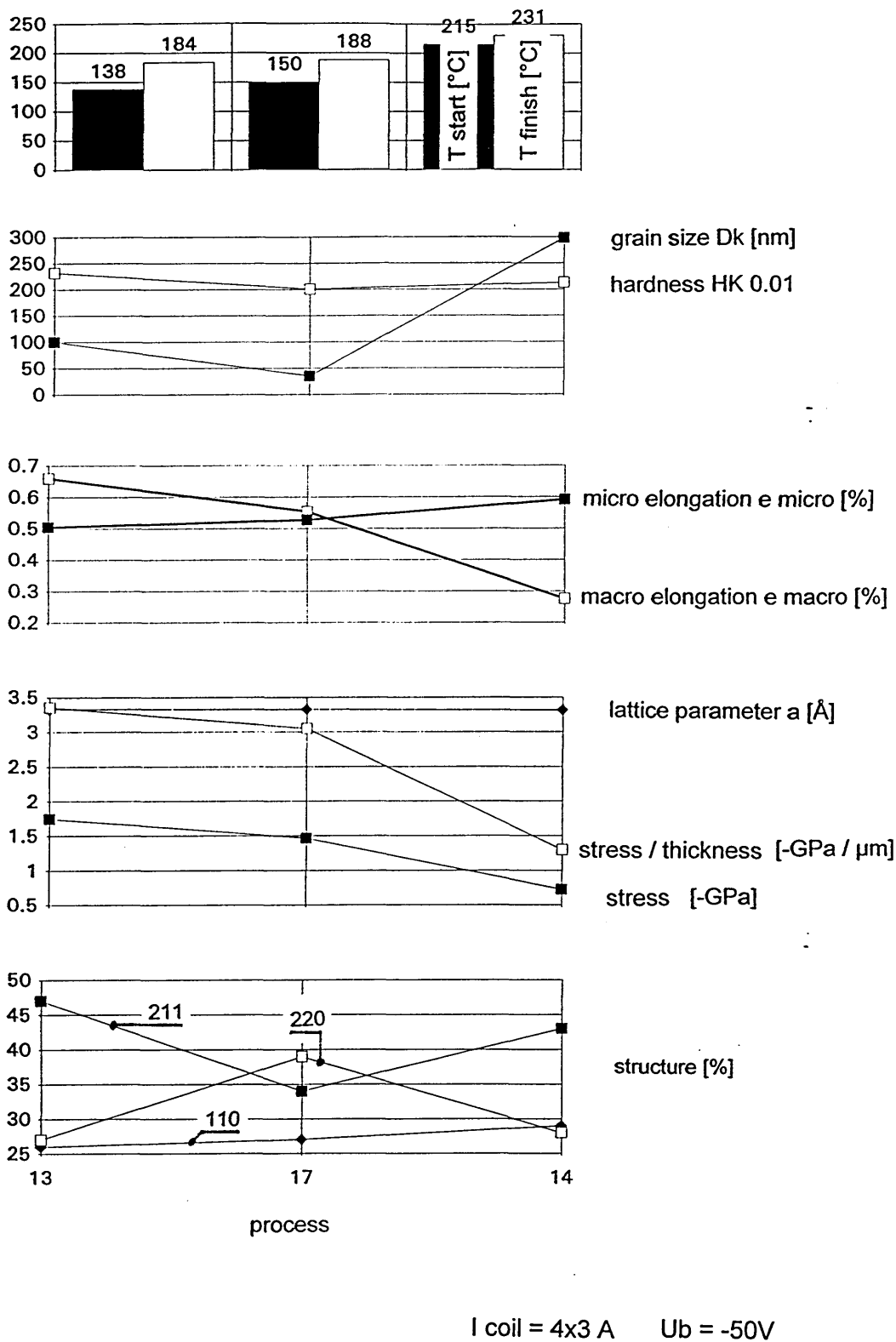


Figure 38: Properties of Nb coatings as a function of the temperature

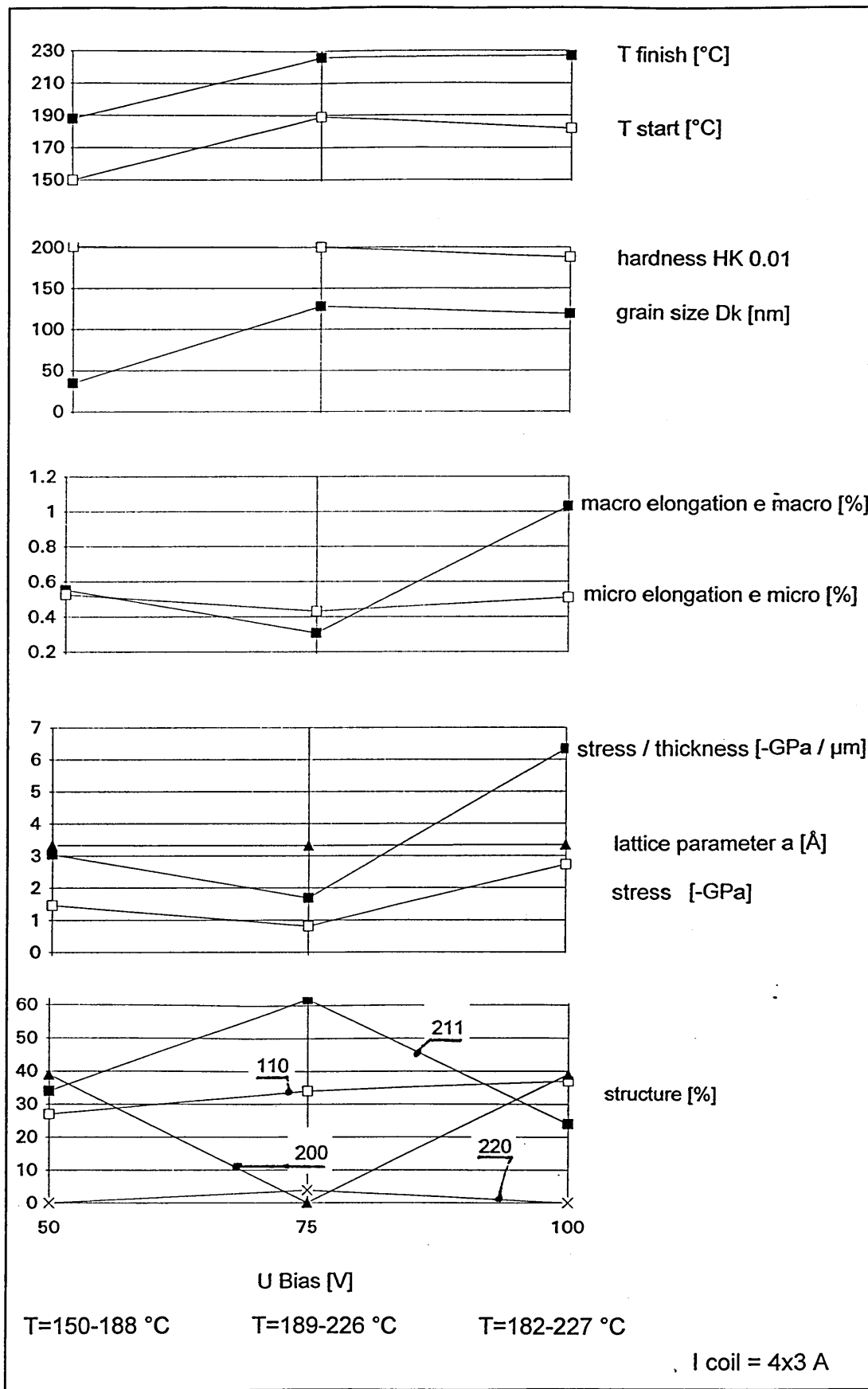


Figure 39: Properties of Nb coatings as a function of applied bias voltage

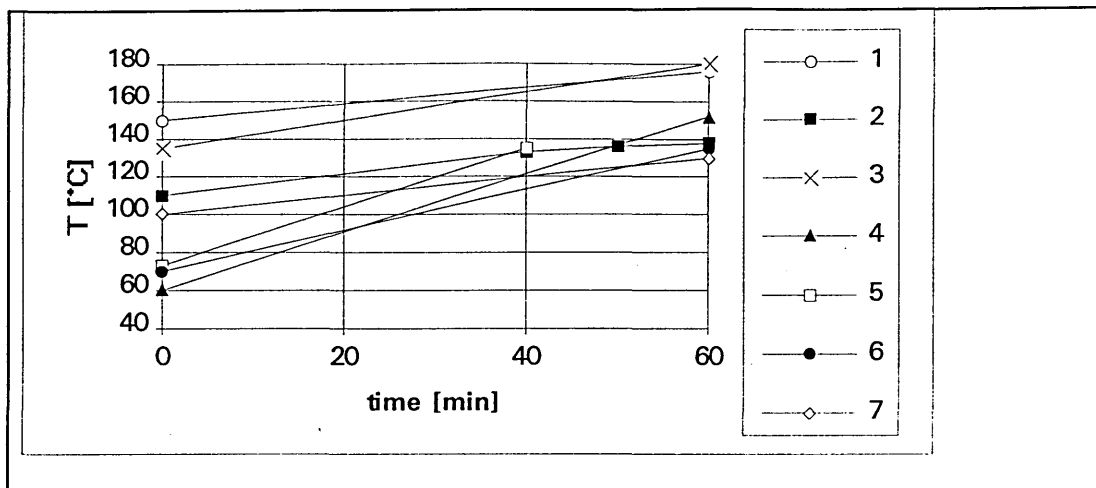


Figure 40 a: Temperature profile of aluminium coatings on brass

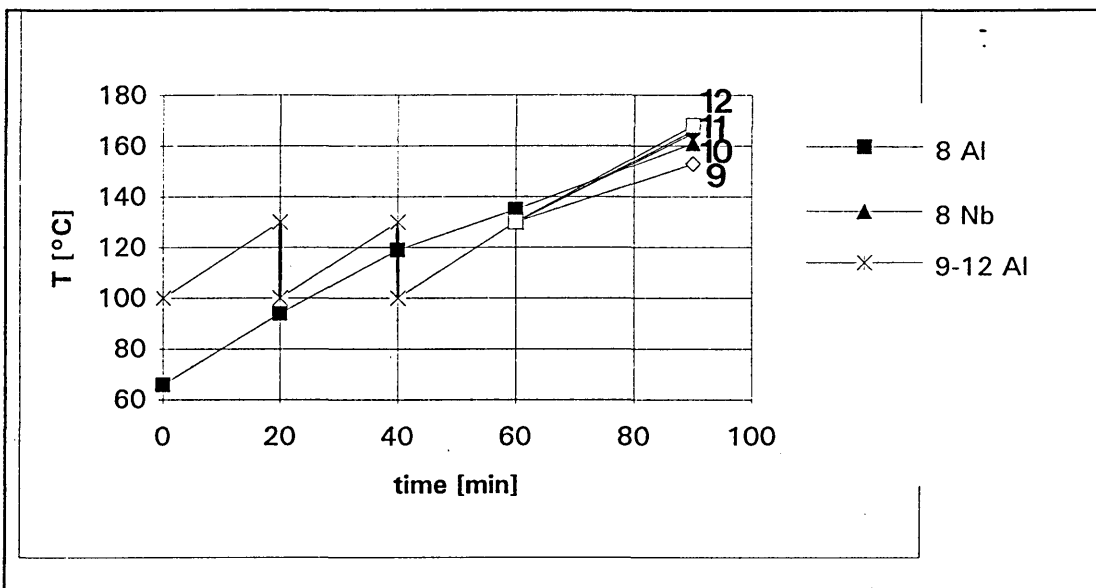


Figure 40 b: Temperature profile of AlNbX + Nb coatings on brass

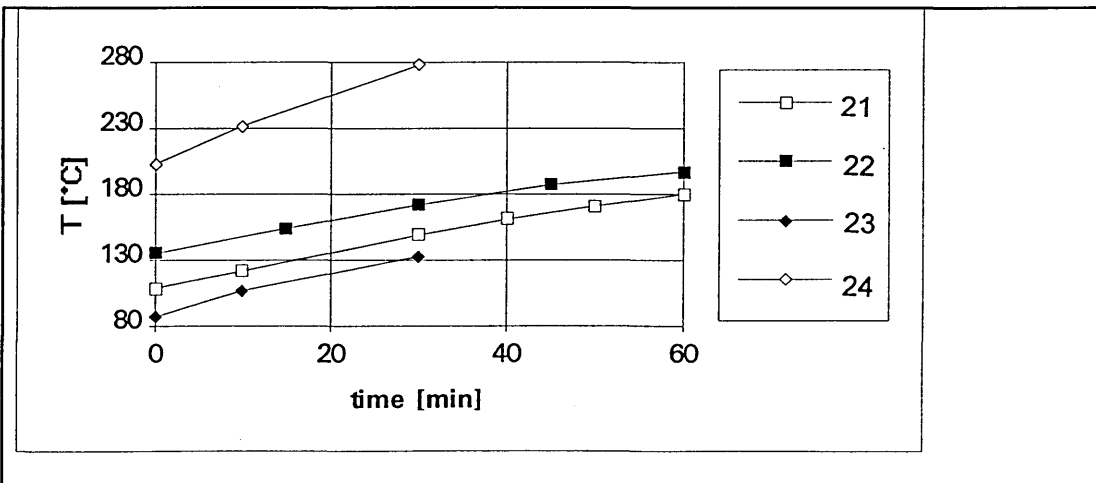


Figure 40 c: Temperature profile of CuAl8 coatings on brass

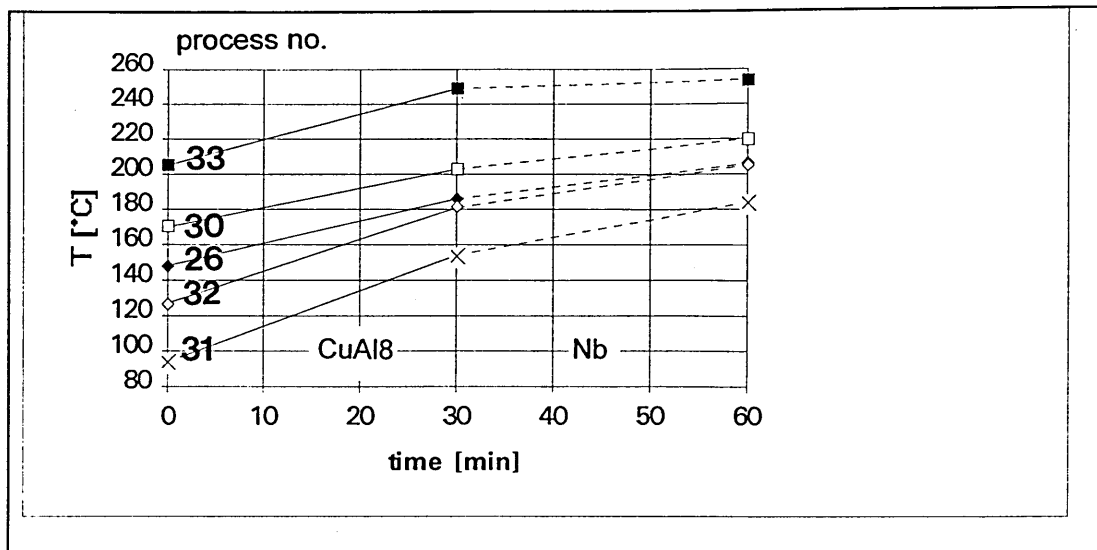


Figure 40 d: Temperature profile of CuAl8NbX + Nb coatings on brass

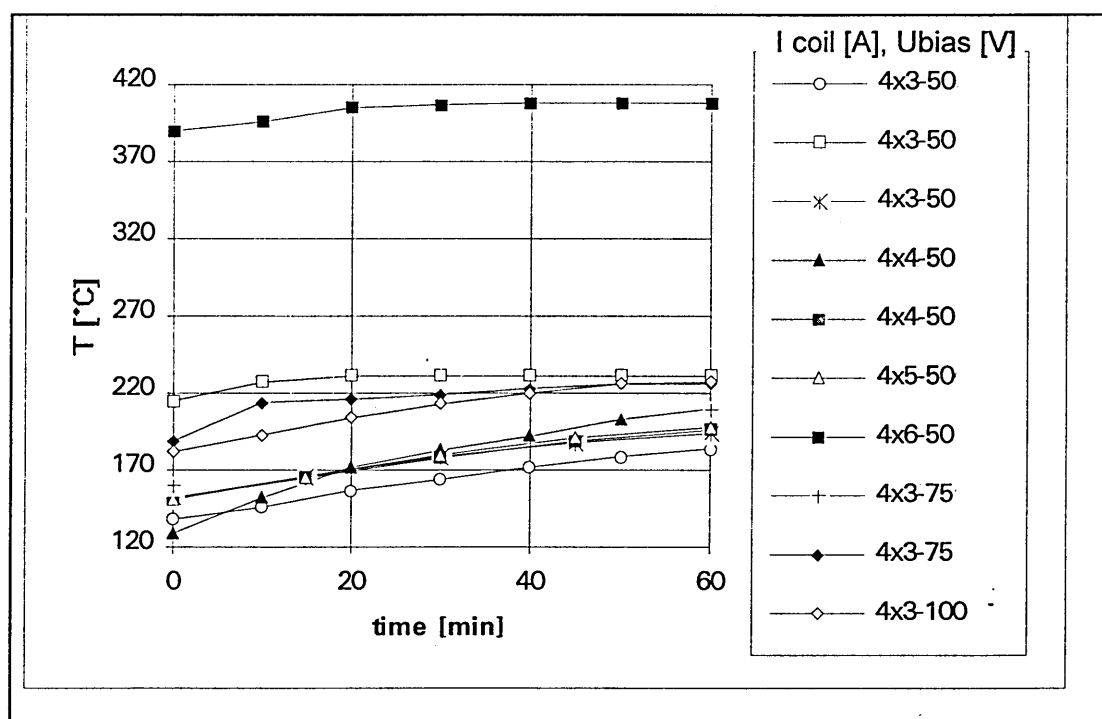


Figure 40 e: Temperature profile of niobium coatings on brass

AMMONIA POROSITY TEST (magnification 25 x)






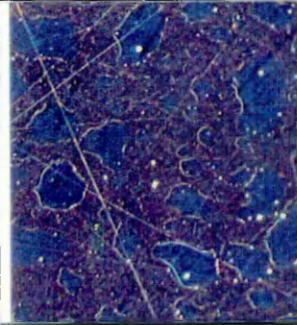



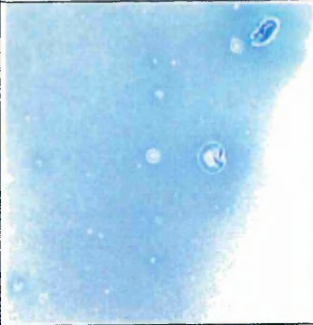
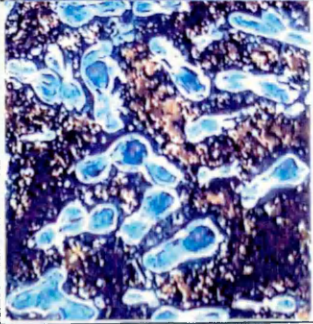

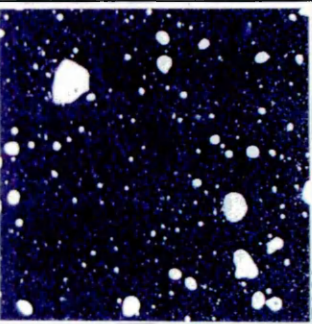
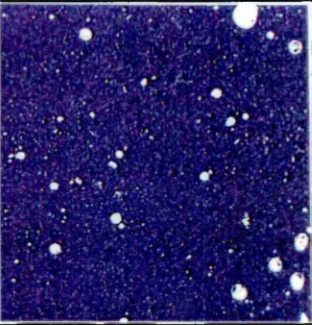
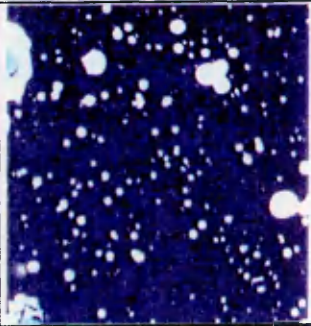
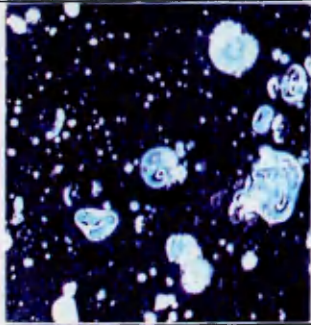
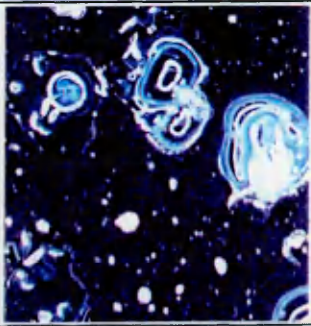
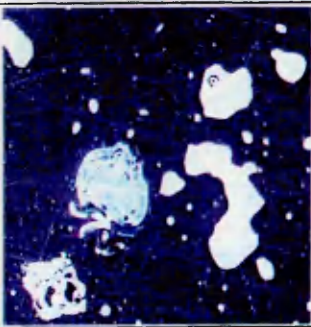
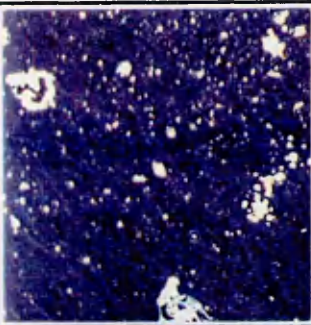
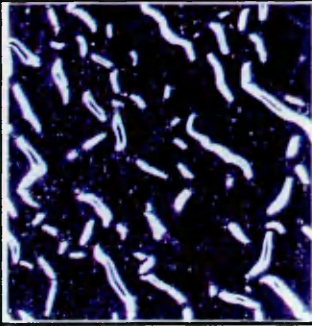
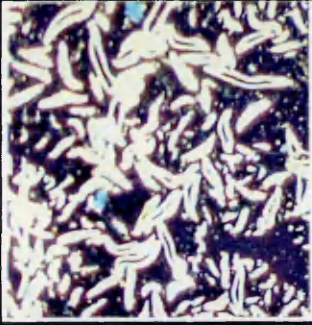

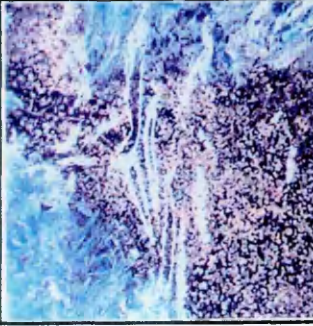
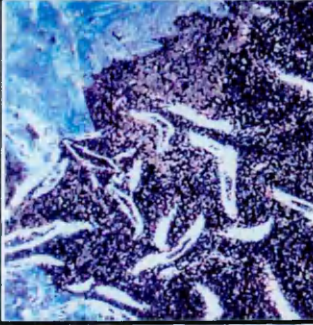
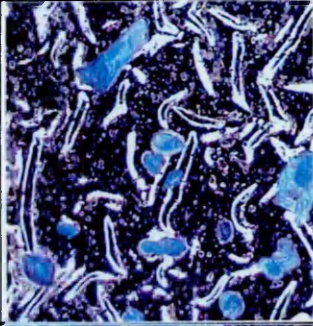

Figure 41: Al $U_b = -50\text{ V}$ $I_{\text{coil}} = 4 \times 6\text{ A}$			
	a) 1, $T=150-176\text{ °C}$	b) 2, $T=112-138\text{ °C}$	c) 3, $T=135-180\text{ °C}$

Figure 42: AlNbX+Nb $U_b = -50\text{ V}$ $I_{\text{coil}} = 4 \times 2\text{ A}$					
	a) 8, poisoned	b) 9, 5 %	c) 10, 10 %	d) 11, 20 %	e) 12, 50 %

<p>Figure 43: CuAl8</p> <p>Ub = -75 V I coil = 4x6 A</p>		a) 24, T=109-180 °C
		b) 25, T=135-197 °C
		c) 26, T=87-133 °C
		d) 27, T=203-278 °C

<p>CuAl8 + Nb</p> <p>CuAl8: P = 15 kW I coil = 4x3 A Ub = -75 V t = 60 min</p> <p>Nb: 10 kW 4x3 A -75 V</p>		e) Nb t = 30 min
		f) Nb t = 60 min

<p>Figure 44: CuAl8NbX + Nb</p> <p>Ub = -75 V I coil = 4x6 A</p>		a) 28, poised
		b) 29, 5 %
		c) 30, 10 %
		d) 31, 20 %
		e) 32, 50 %

<p>Figure 45: Nb</p> <p>I coil = 4x3 A</p> <p>Ub = -50 V</p>		a) 17, Ub = -50 V
		b) 22, Ub = -75 V
		c) 23, Ub = -100V
		d) 18, I coil = 4x4 A
		e) 19, I coil = 4x5 A
		f) 20, I coil = 4x8 A
		g) 17, magnification = 2x

SULPHUR DIOXIDE CORROSION TEST (magnification 1.1 x)

Figure 46:
Al,
AlNbX+Nb

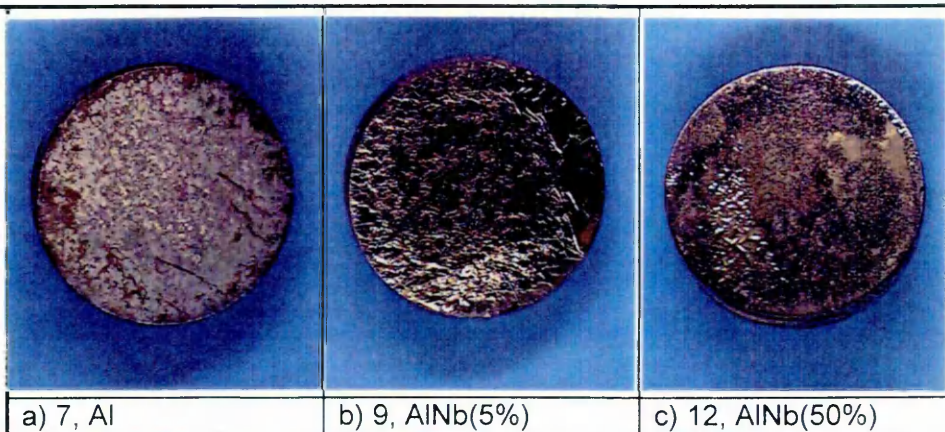


Figure 47:
CuAl8,
CuAl8Nb(X)
+Nb

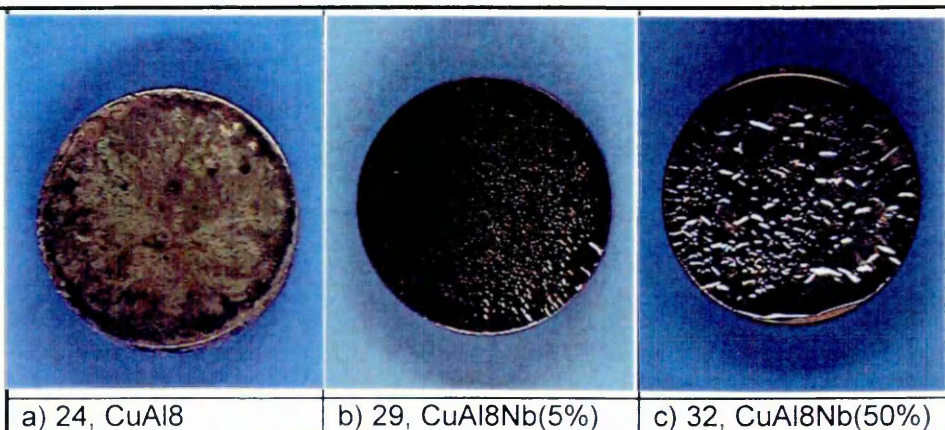
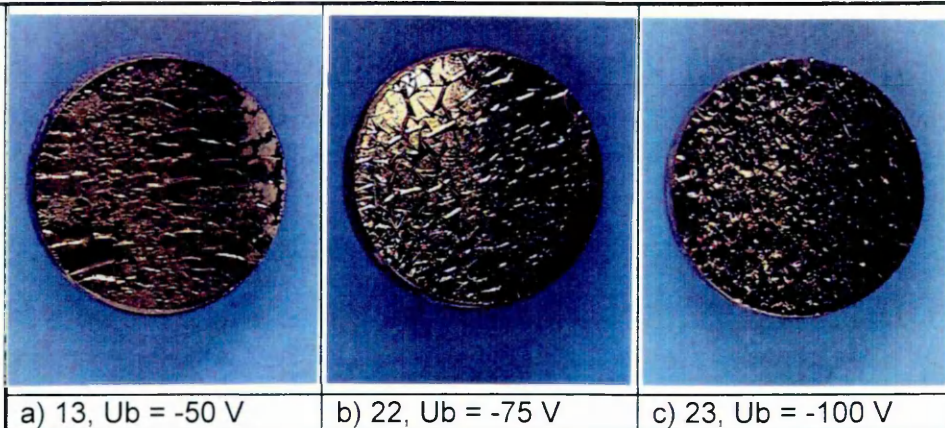


Figure 48:
Nb



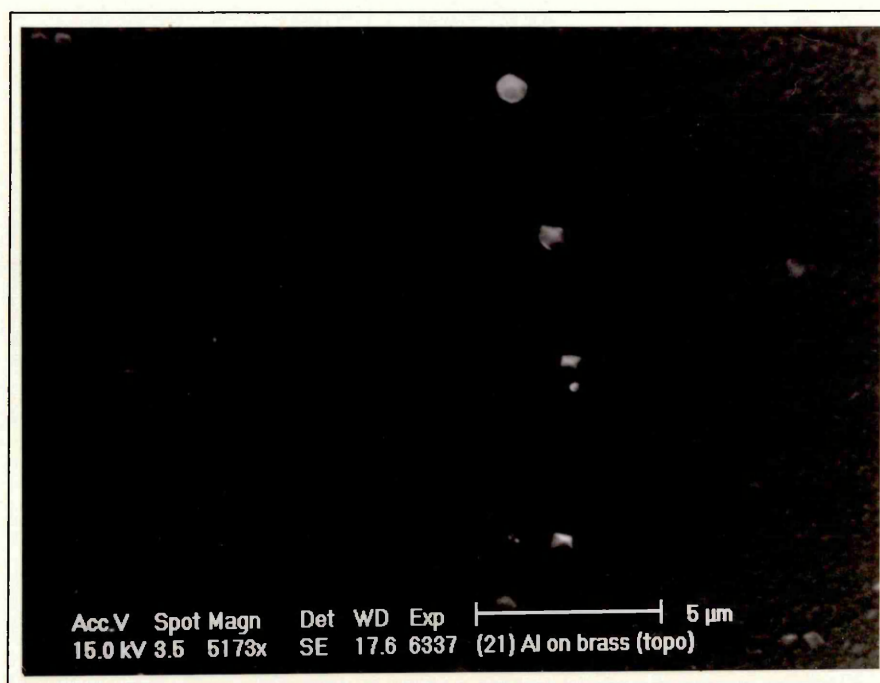


Figure 49 a: Surface topography of a shiny Al coating

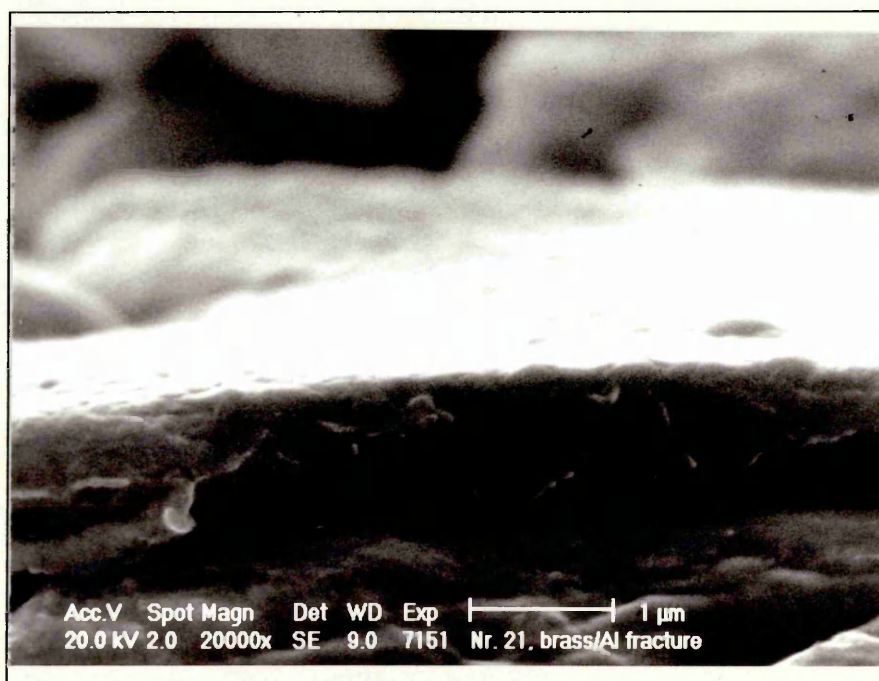


Figure 49 b: Fracture of an Al coating

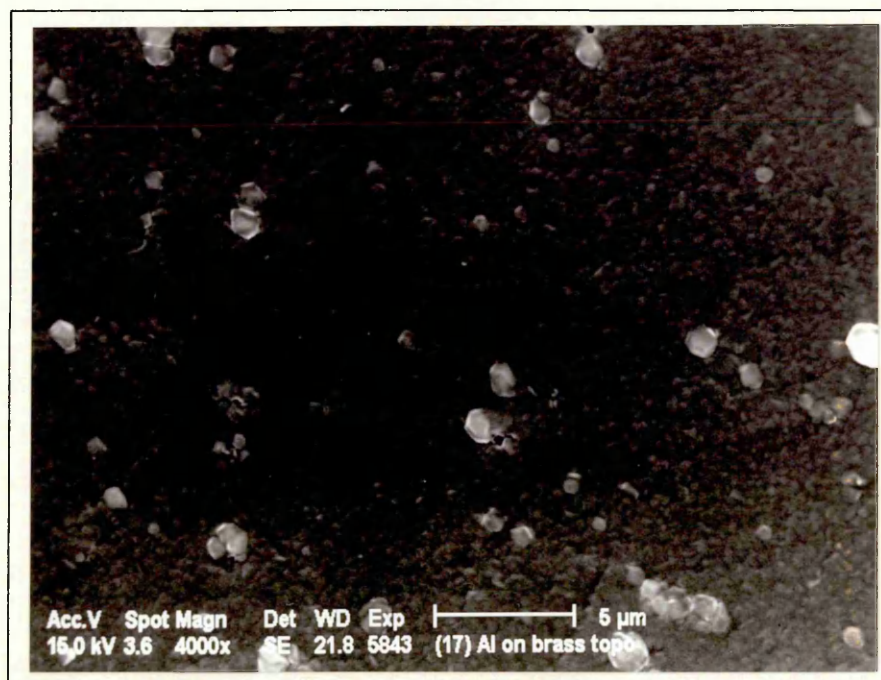


Figure 49 c: Surface topography of a matt Al coating

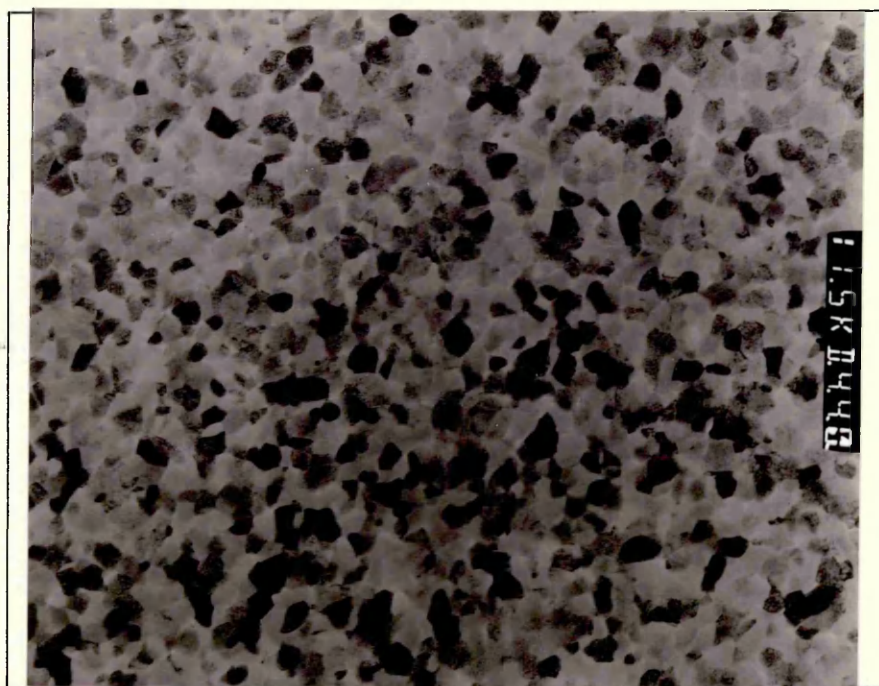


Figure 49 d: TEM image of an Al coating, Magn. 10 000 x

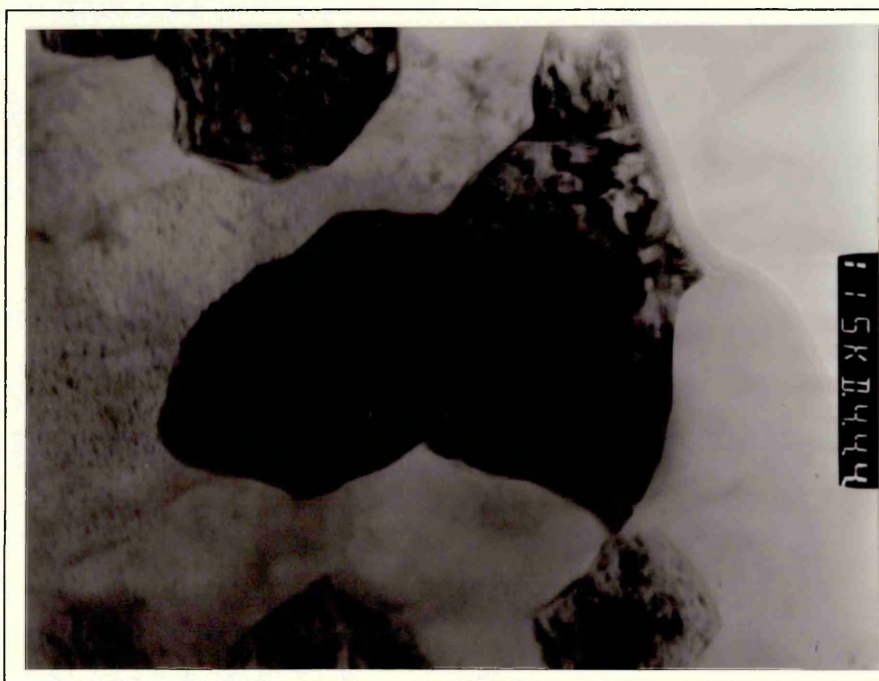


Figure 49 e: TEM image of an Al coating, Magn. 100 000 x

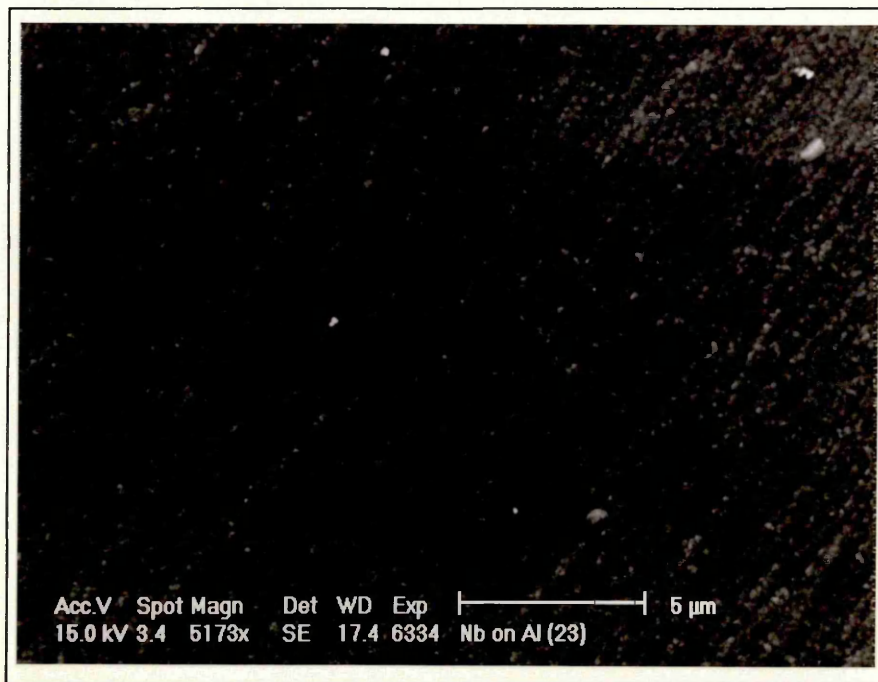


Figure 50 a: Surface topography of a AlNb(5%)+Nb coating

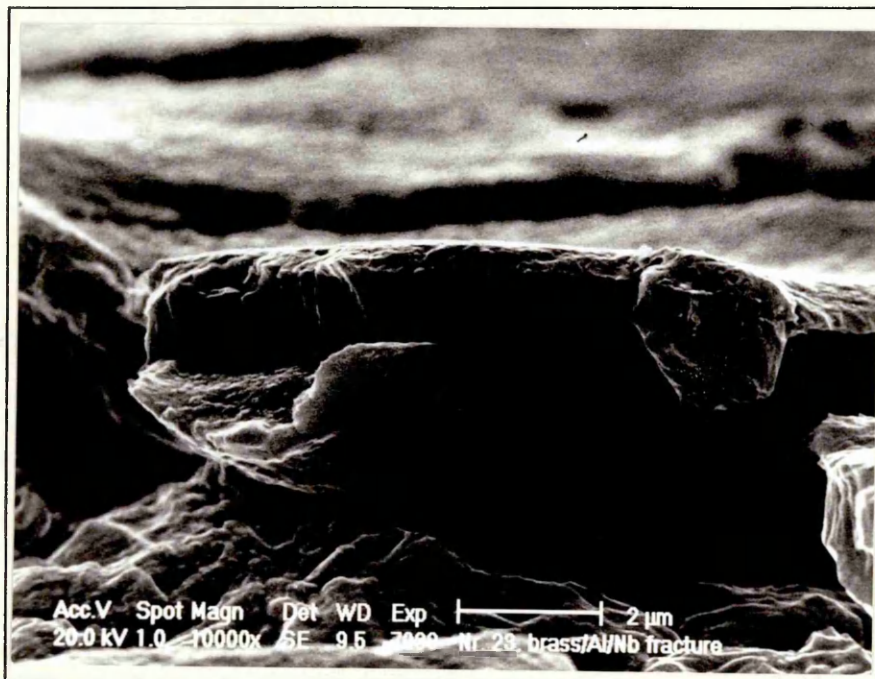


Figure 50 b: Surface topography of a AlNb(5%)+Nb coating

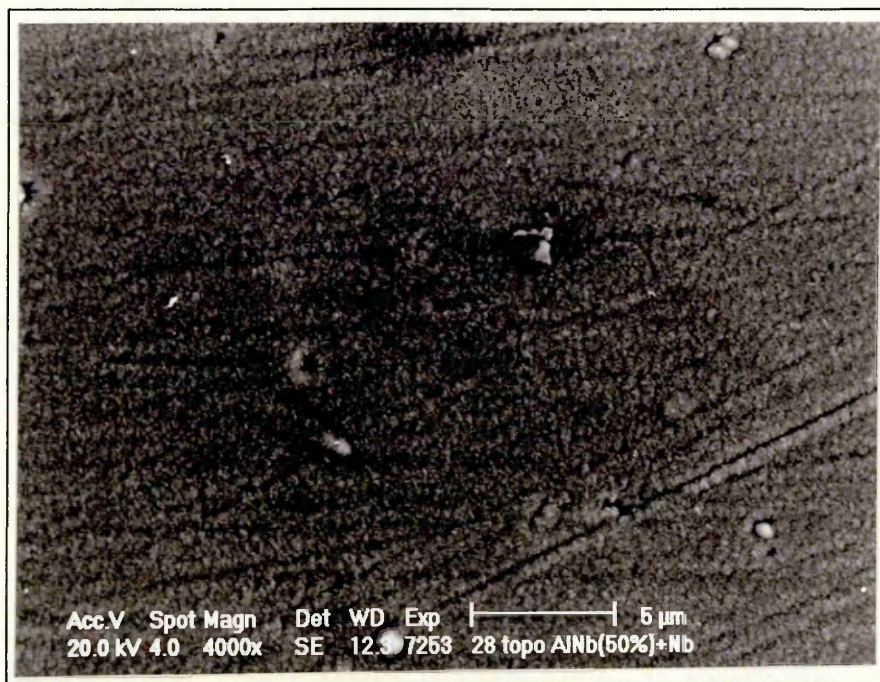


Figure 51 a: Surface topography of a AINb(50%)+Nb coating

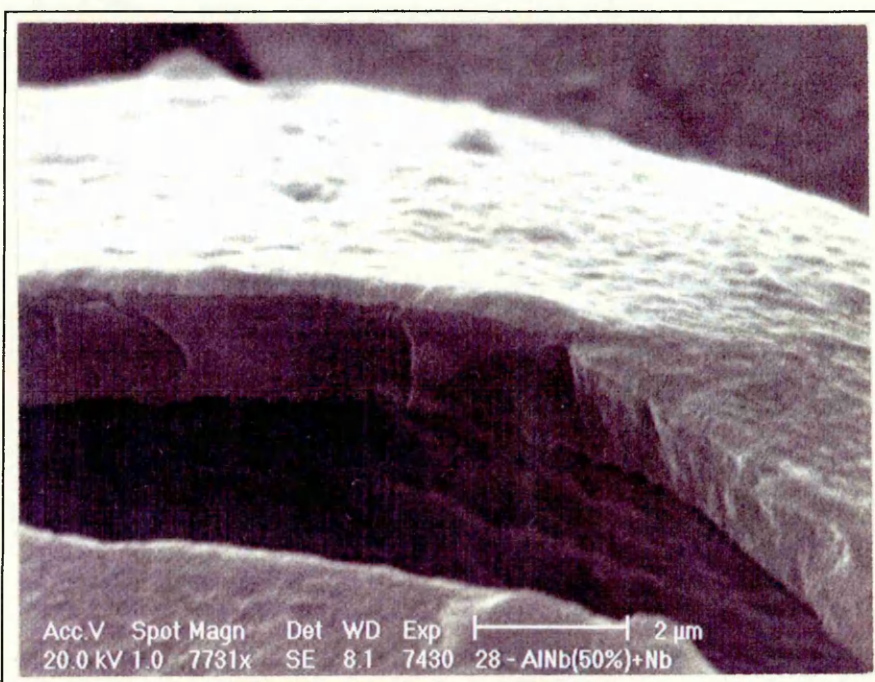


Figure 51 b: Surface topography of a AINb(50%)+Nb coating

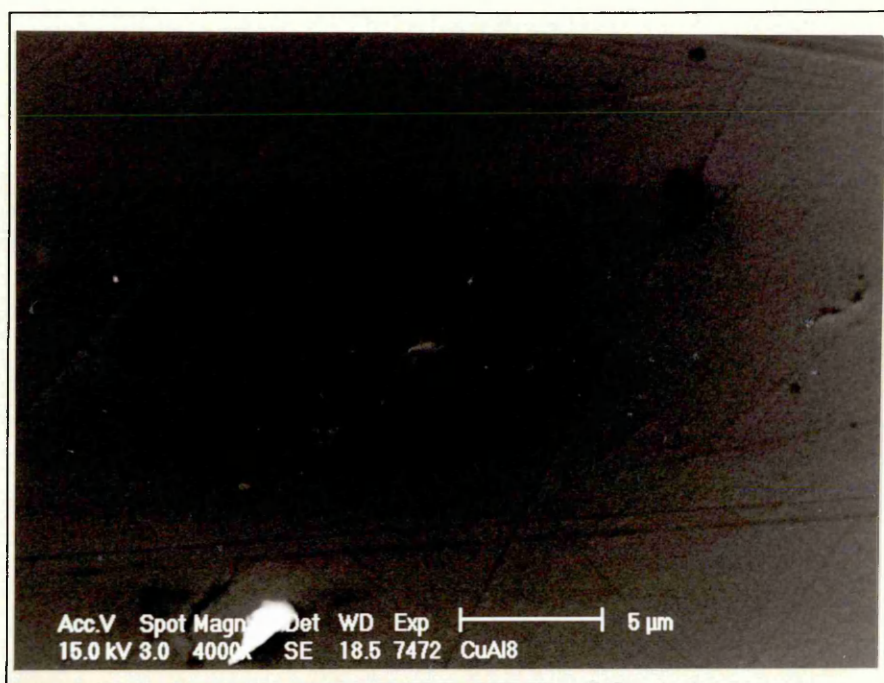


Figure 52 a: Surface topography of a CuAl8 coating

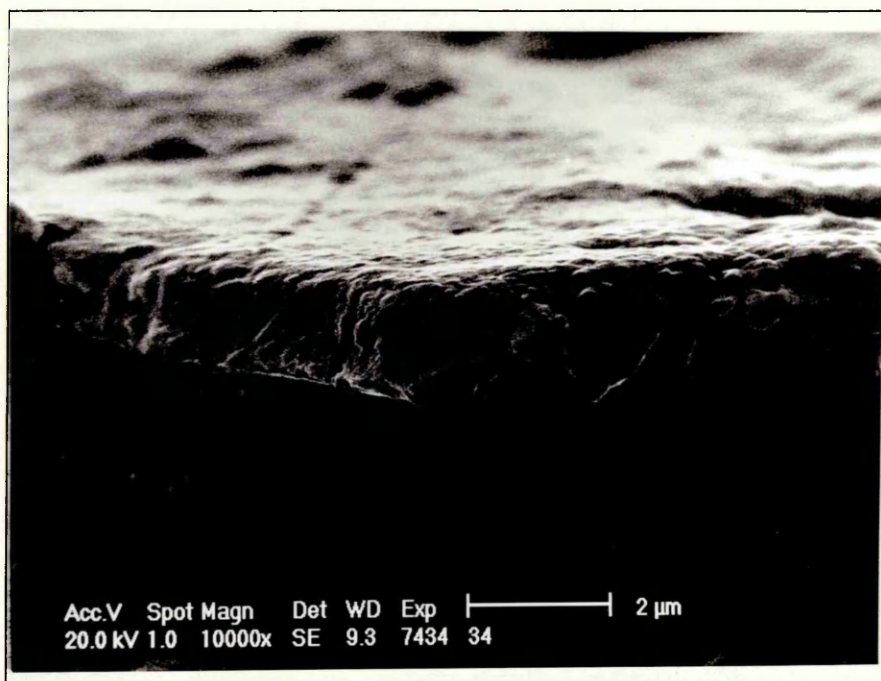


Figure 52 b: Surface topography of a CuAl8 coating

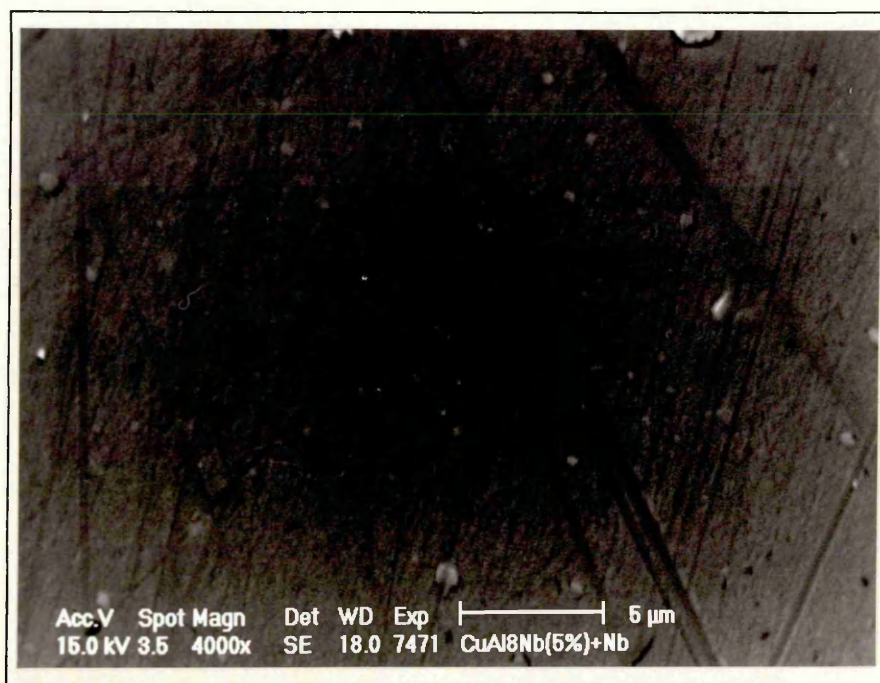


Figure 53 a: Surface topography of a CuAl8Nb(5%)+Nb coating

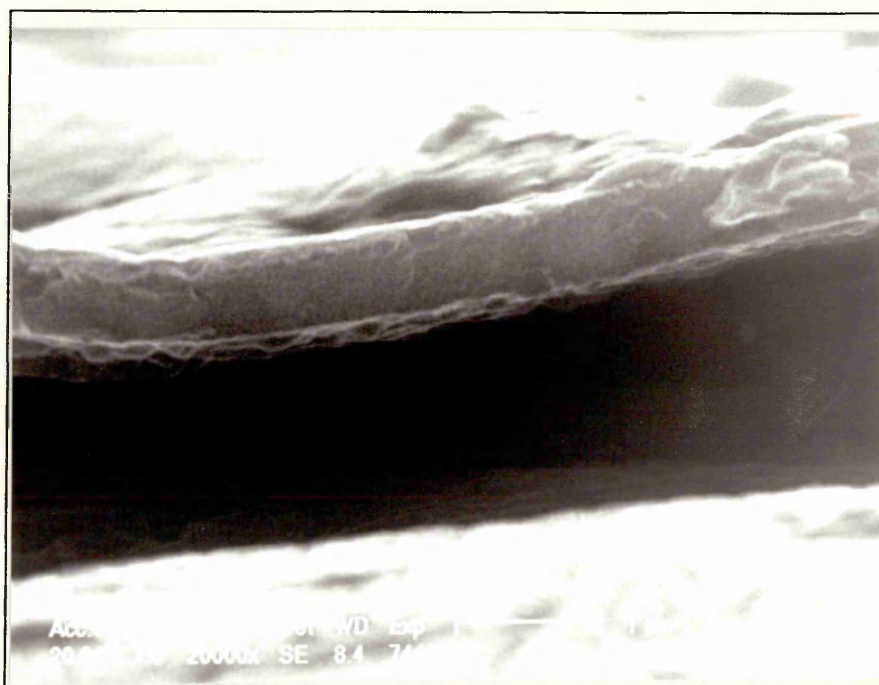


Figure 53 b: Surface topography of a CuAl8Nb(5%)+Nb coating

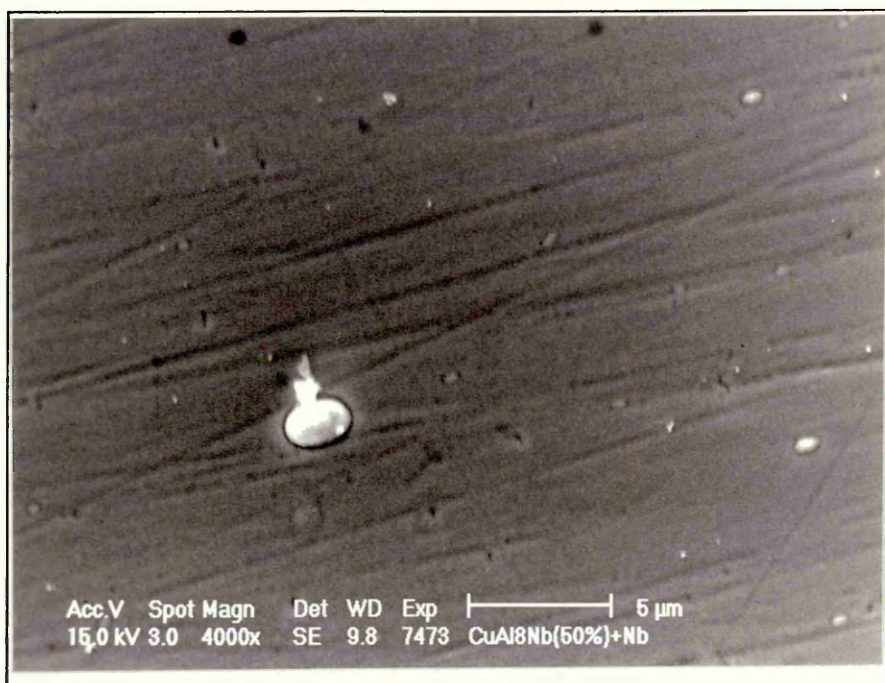


Figure 54 a: Surface topography of a CuAl8Nb(50%)+Nb coating

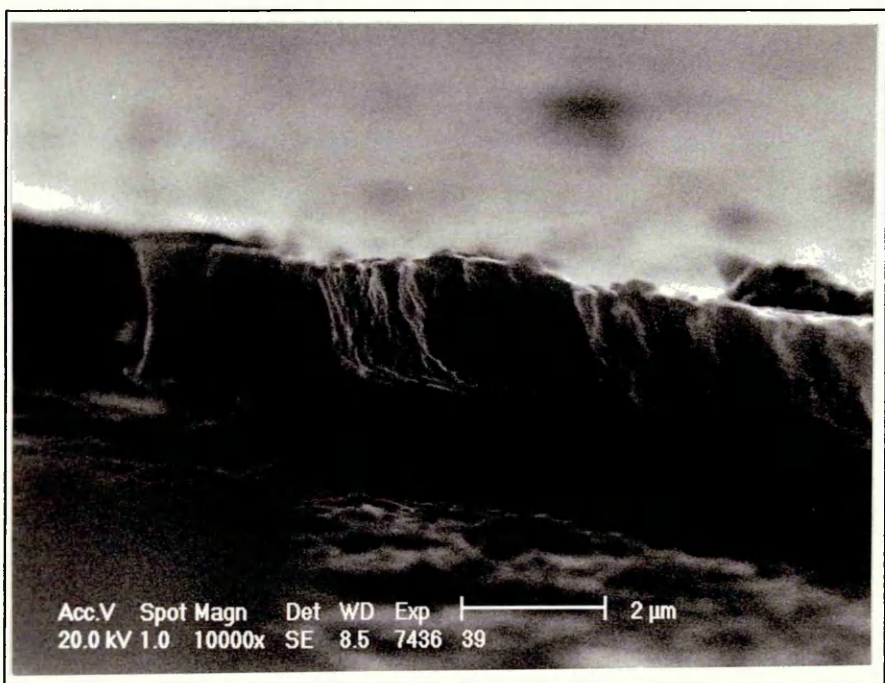


Figure 54 b: Surface topography of a CuAl8Nb(50%)+Nb coating

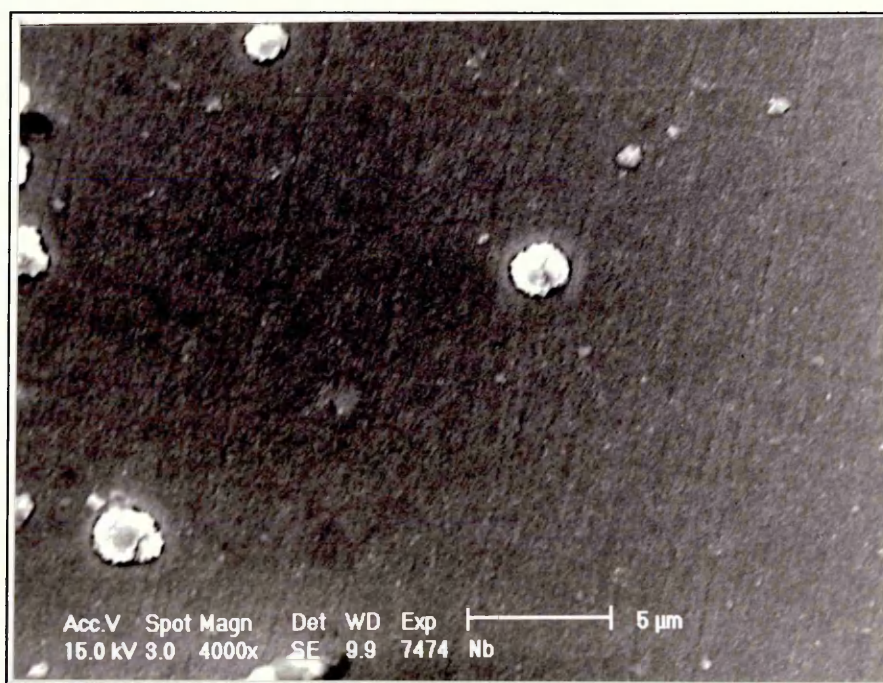


Figure 55 a: Surface topography of a Nb coating

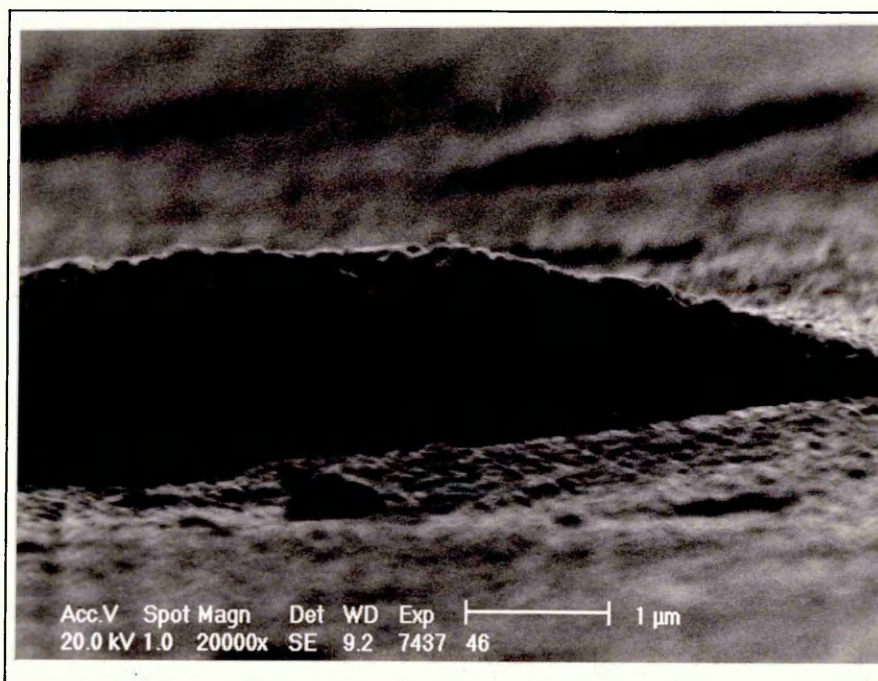


Figure 55 b: Surface topography of a Nb coating

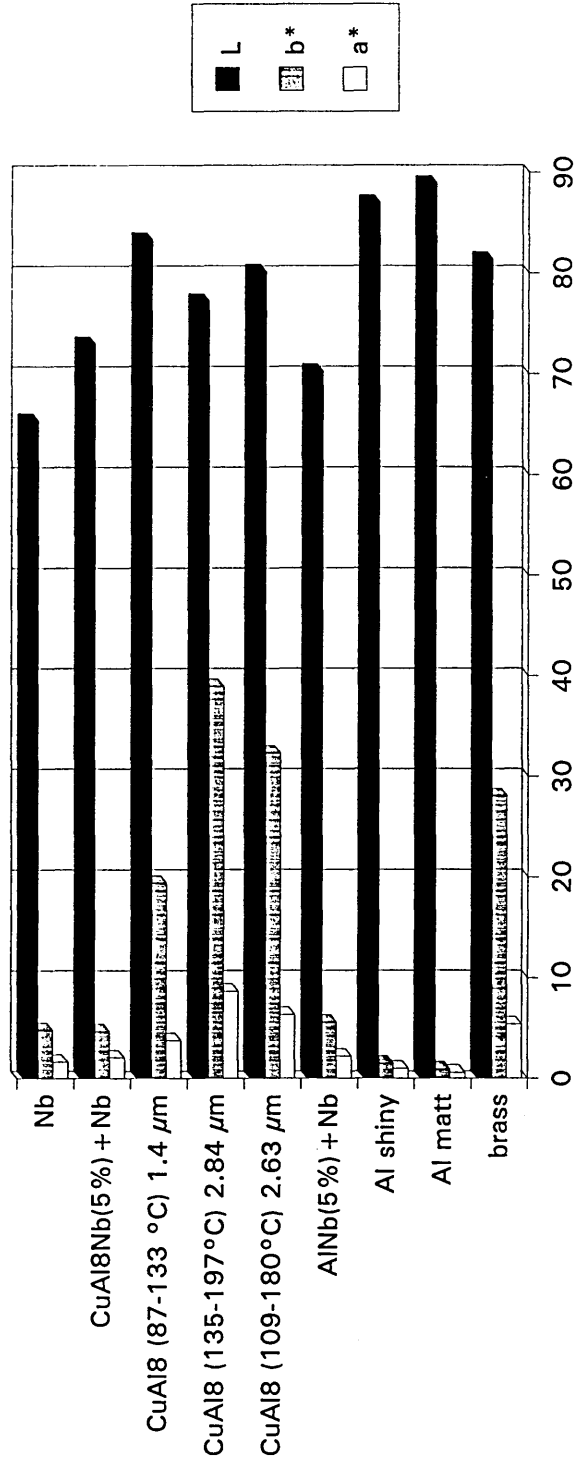
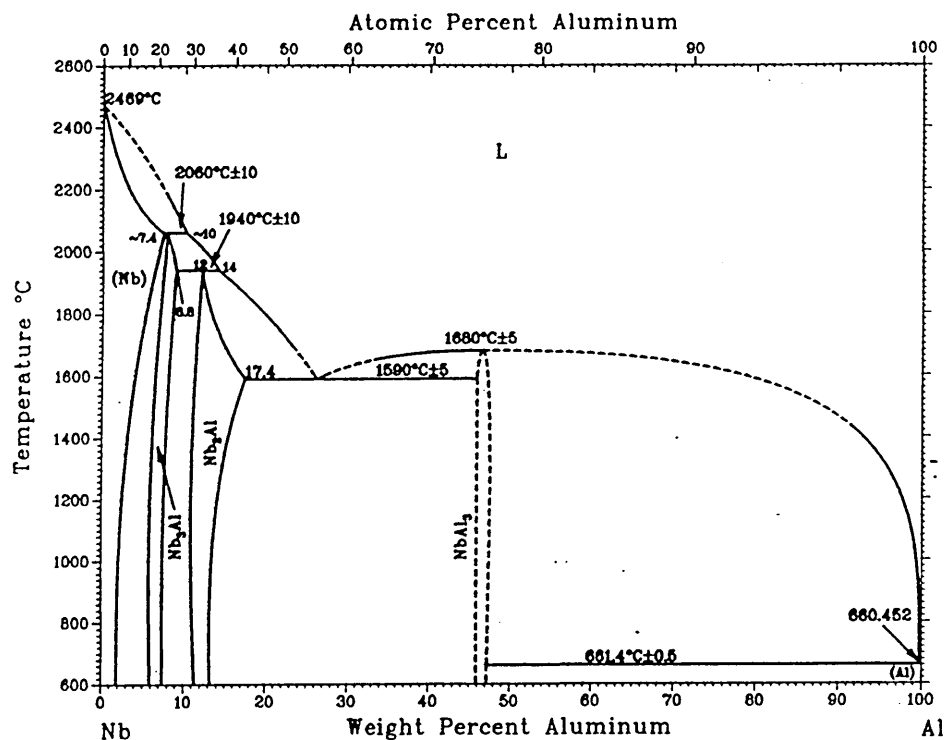


Figure 56 Colour measurements of Al, AlNb(X)+Nb, CuAl8, CuAl8Nb(X)+Nb and Nb coatings.
 L: 100 = white a*: -80 = green, 100 = red b*: -80 = blue, 100 = yellow

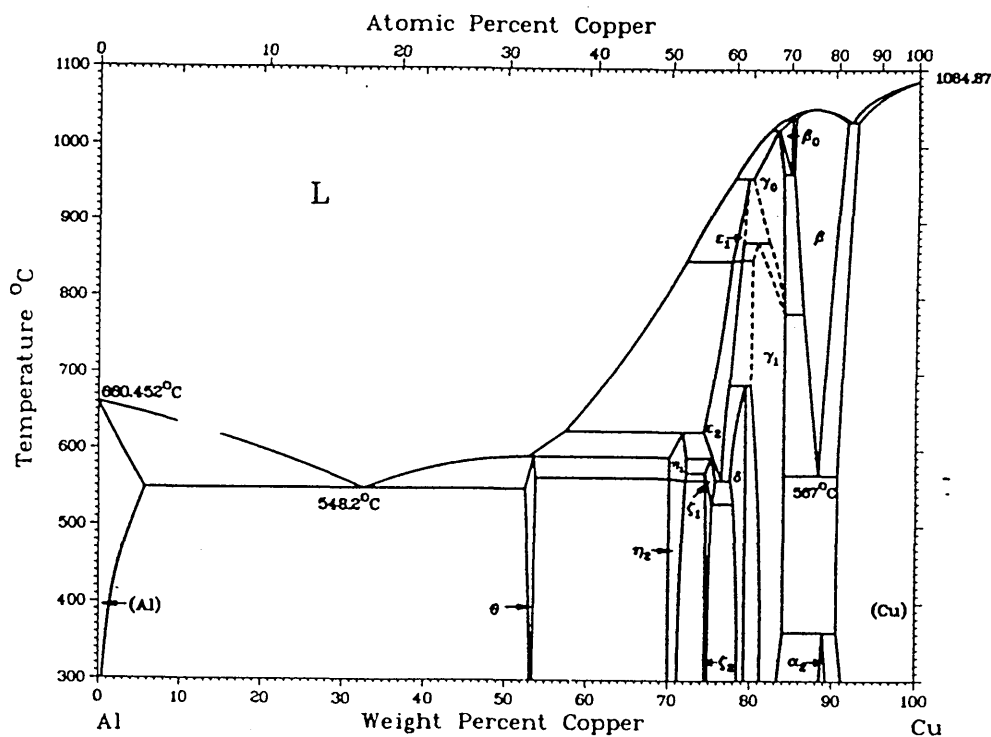
Al-Nb



Phase	Composition, wt% Al	Pearson symbol	Space group
(Nb)	0 to ~7.4	<i>cI2</i>	<i>Im</i> $\bar{3}m$
Nb ₃ Al	18.6 to 8.8	<i>cP8</i>	<i>Pm</i> $\bar{3}n$
Nb ₂ Al	11 to 17.4	<i>tP30</i>	<i>P4</i> ₂ <i>/mmn</i>
NbAl ₃	47	<i>tI8</i>	<i>I4/mmm</i>
(Al)	100	<i>cF4</i>	<i>Fm</i> $\bar{3}m$

Figure 57 a: binary phase diagram Al-Nb [87]

Al-Cu

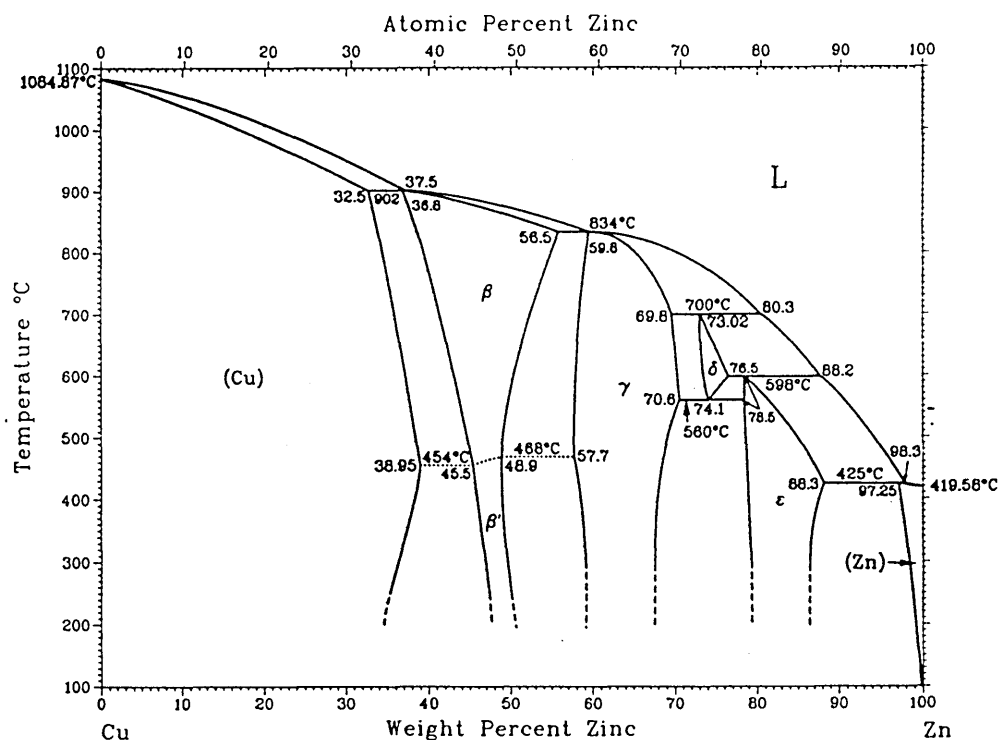


Phase	Composition, wt% Cu	Pearson symbol	Space group
(Al)	0 to 5.65	<i>cF4</i>	<i>Fm$\bar{3}m$</i>
θ	52.5 to 53.7	<i>tI12</i>	<i>I4/mcm</i>
η_1	70.0 to 72.2	<i>oP16</i> or <i>oC16</i>	<i>Pban</i> or <i>Cmmn</i>
η_2	70.0 to 72.1	<i>mC20</i>	<i>C2/m</i>
ζ_1	74.4 to 77.8	<i>hP42</i>	<i>P6/mmm</i>
ζ_2	74.4 to 75.2	(a)	...
ϵ_1	77.5 to 79.4	(b)	...
ϵ_2	72.2 to 78.7	<i>hP4</i>	<i>P6$_3$/mmc</i>
δ	77.4 to 78.3	(c)	<i>m</i>
γ_0	77.8 to 84	(d)	...
γ_1	79.7 to 84	<i>cP52</i>	<i>P$\bar{4}3m$</i>
β_0	83.1 to 84.7	(d)	...
β	85.0 to 91.5	<i>cI2</i>	<i>Im$\bar{3}m$</i>
α_2	88.5 to 89	(e)	...
(Cu)	90.6 to 100	<i>cF4</i>	<i>Fm$\bar{3}m$</i>
Metastable phases			
θ'	...	<i>tP6</i>	...
β'	...	<i>cF16</i>	<i>Fm$\bar{3}m$</i>
Al_3Cu_2	61 to 70	<i>hP5</i>	<i>P$\bar{3}m1$</i>

(a) Monoclinic? (b) Cubic? (c) Rhombohedral. (d) Unknown. (e) $D0_{22}$ -type long-period superlattice

Figure 57 b: binary phase diagram Cu-Al [87]

Cu-Zn



Phase	Composition, wt% Zn	Pearson symbol	Space group
α or (Cu)	0 to 38.95	<i>cF4</i>	<i>Fm</i> $\bar{3}$ <i>m</i>
β	36.8 to 56.5	<i>cI2</i>	<i>Im</i> $\bar{3}$ <i>m</i>
β′	45.5 to 50.7	<i>cP2</i>	<i>Pm</i> $\bar{3}$ <i>m</i>
γ	57.7 to 70.6	<i>cI52</i>	<i>I</i> $\bar{4}$ 3 <i>m</i>
δ	73.02 to 76.5	<i>hP3</i>	<i>P</i> $\bar{6}$
ε	78.5 to 88.3	<i>hP2</i>	<i>P</i> 6 ₃ / <i>mmc</i>
η or (Zn)	97.25 to 100	<i>hP2</i>	<i>P</i> 6 ₃ / <i>mmc</i>

Figure 57 c: binary phase diagram Cu-Zn [87]

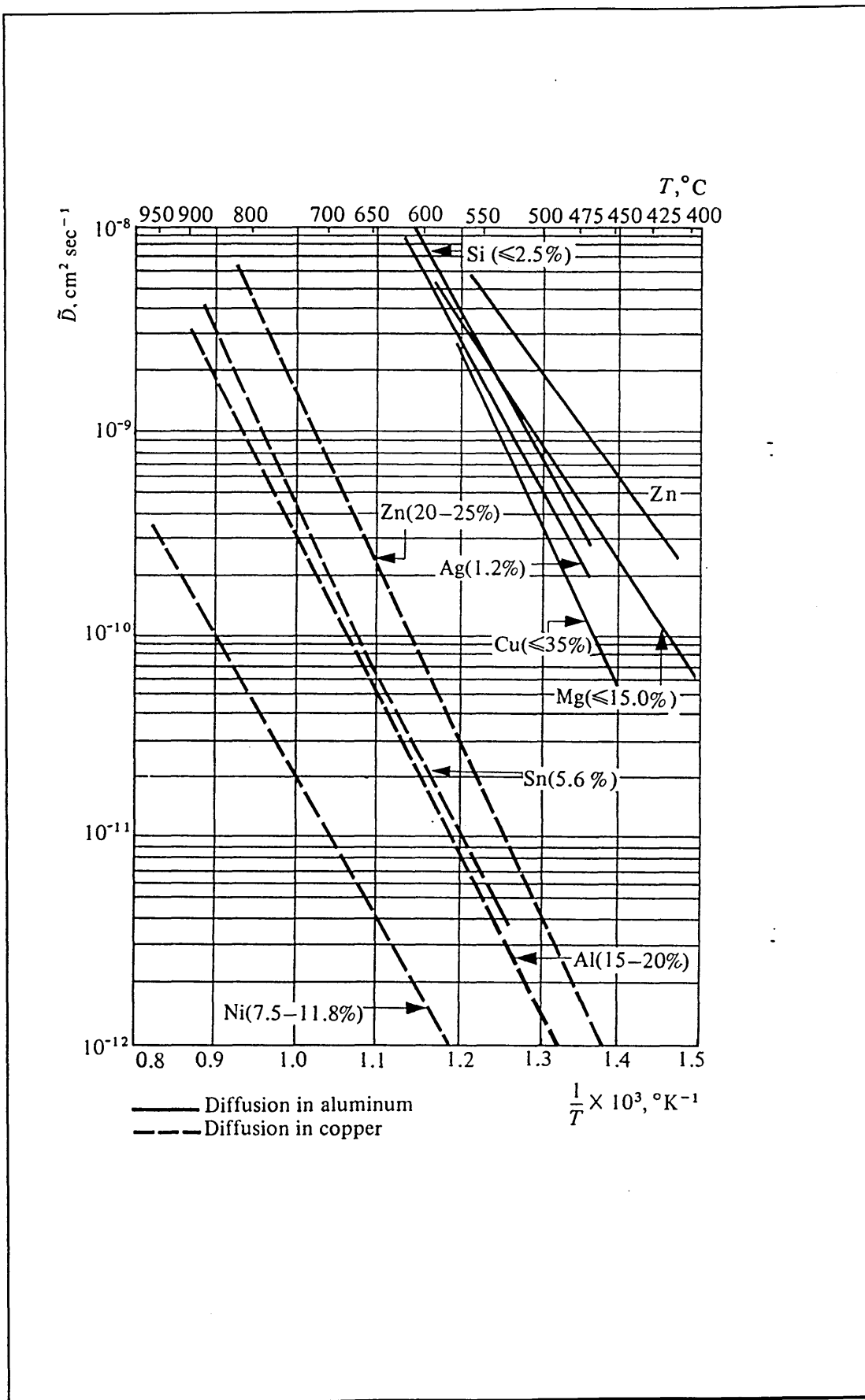
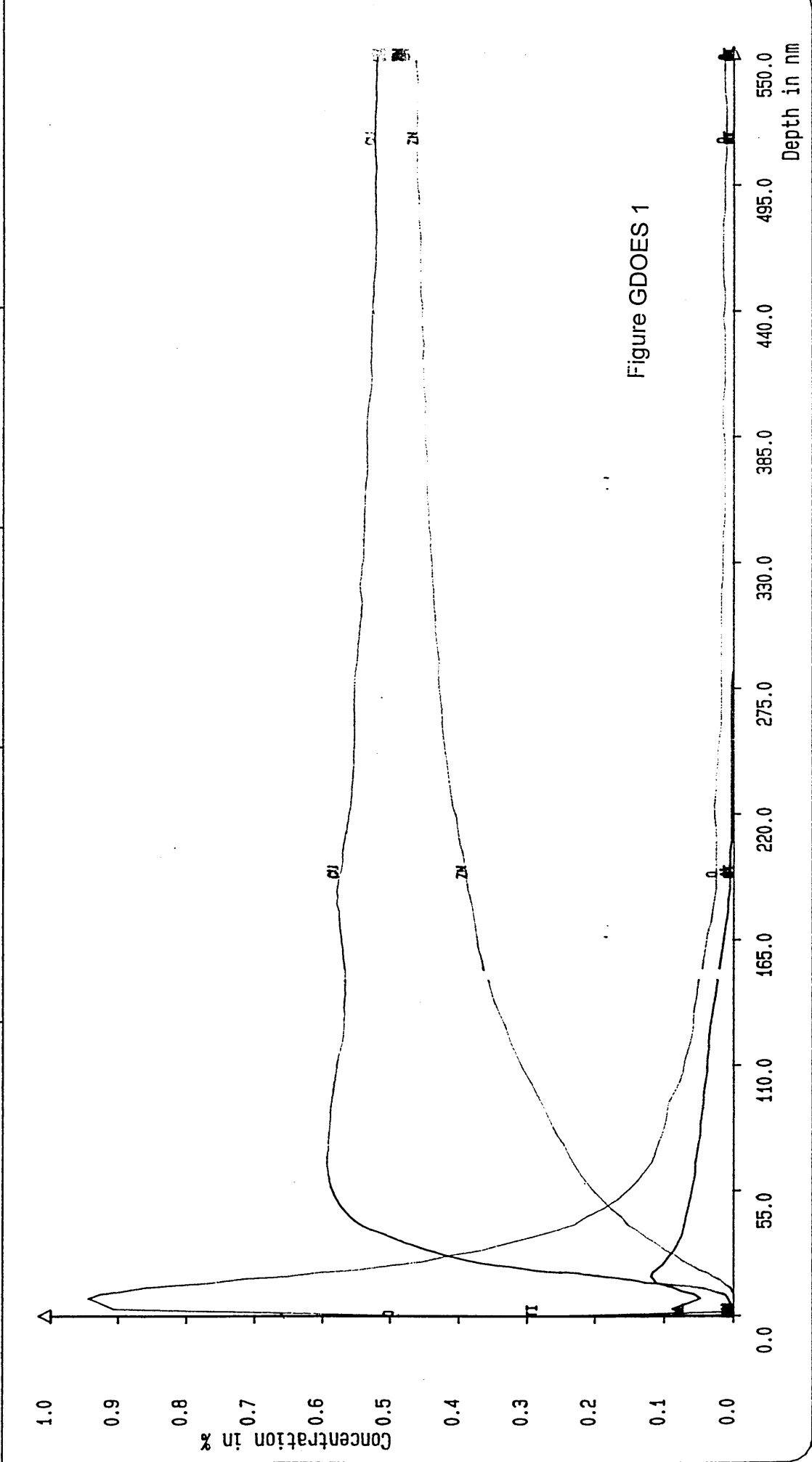


Figure 58: interdiffusion coefficients

MATERIALS RESEARCH INST. SHEFFIELD HALLAM UNIV. Tel. M.Ives (0742 533863)	DATE CLOCK 94-11-10 16:08 MTH.NAME PRESSURE PVDBRASS Endlevel EXITATION 700 V Control : 30 mA	Element: TI AL O N CU ZN	Range 100.0 % 100.0 % 100.0 % 100.0 % 100.0 % 100.0 %	V - Average : 694 V I - Average : 32.0 mA P - Average : 22.2 W ----- y-Axis = a%
	BR3B C:\LECO\SDPA\DATA\BR3B.ORE			



MATERIALS RESEARCH INST. SHEFFIELD HALLAM UNIV. Tel. M.Ives (0742 533863)	DATE CLOCK 95-01-19 16:34 MTH.NAME PRESSURE PVD BRASS Endlevel EXITATION 700 V Contr1 : 30 mA	Element Range AL 100.0 % O 100.0 % C 100.0 % CU 100.0 % Zn 100.0 %	V - Average : 657 V I - Average : 31.1 mA P - Average : 20.4 W y-Axis = a%
---	--	---	---

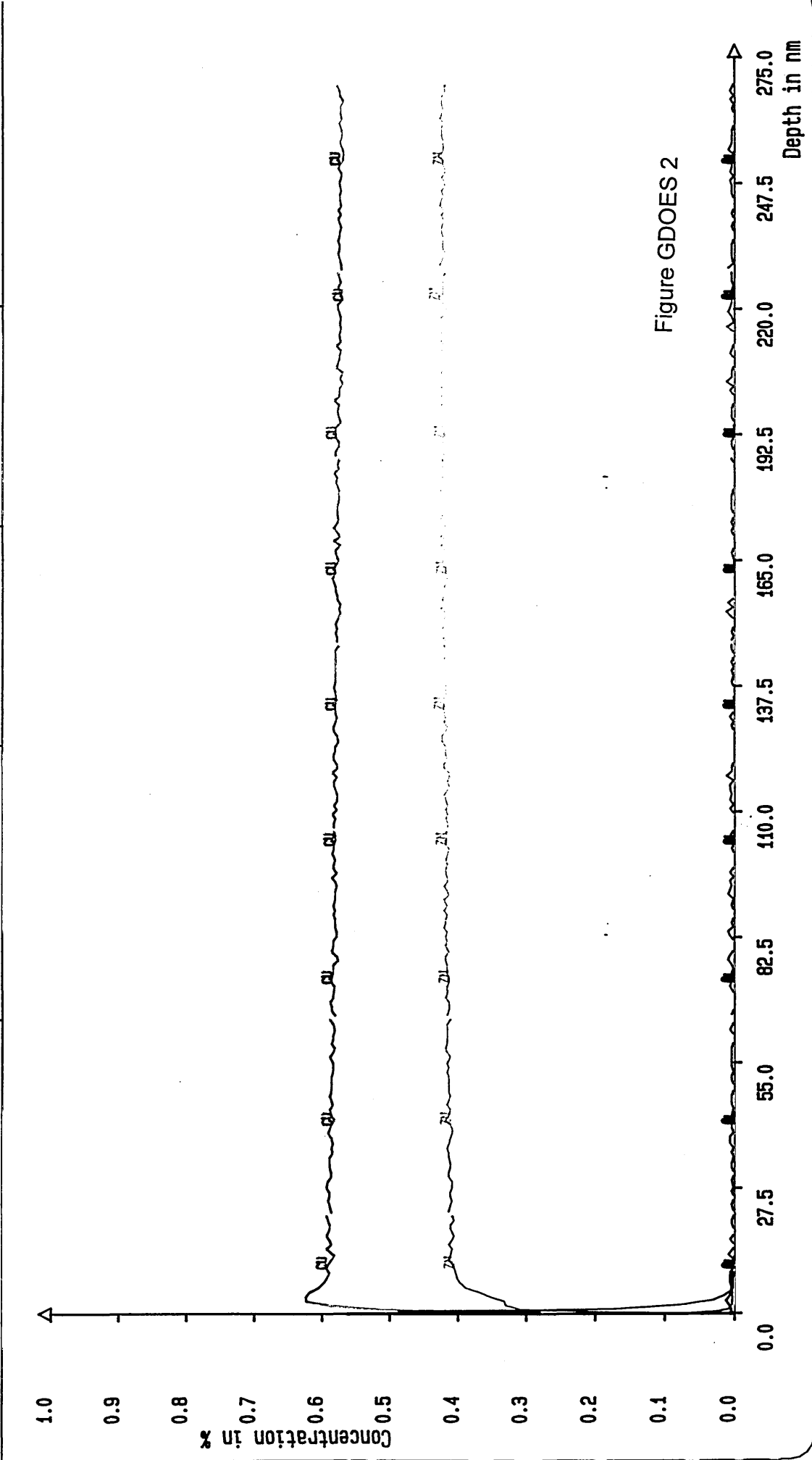


Figure GDOES 2

MATERIALS RESEARCH INST.
SHEFFIELD HALLAM UNIV.

Tel. M.Ives (0742 533863)

C:\LECO\SDPA\DATA\11A.0RH

DATE 00-00-00 00:00
CLOCK
MTH.NAME PRESSURE
PVD BRASS Endlevel
EXITATION
700 V Control : 30 mA

Element	Range
AL	100.0 %
O	100.0 %
C	100.0 %
CU	100.0 %
ZN	100.0 %

V - Average : 668 V
I - Average : 32.6 mA
P - Average : 21.8 W

y-Axis = a%

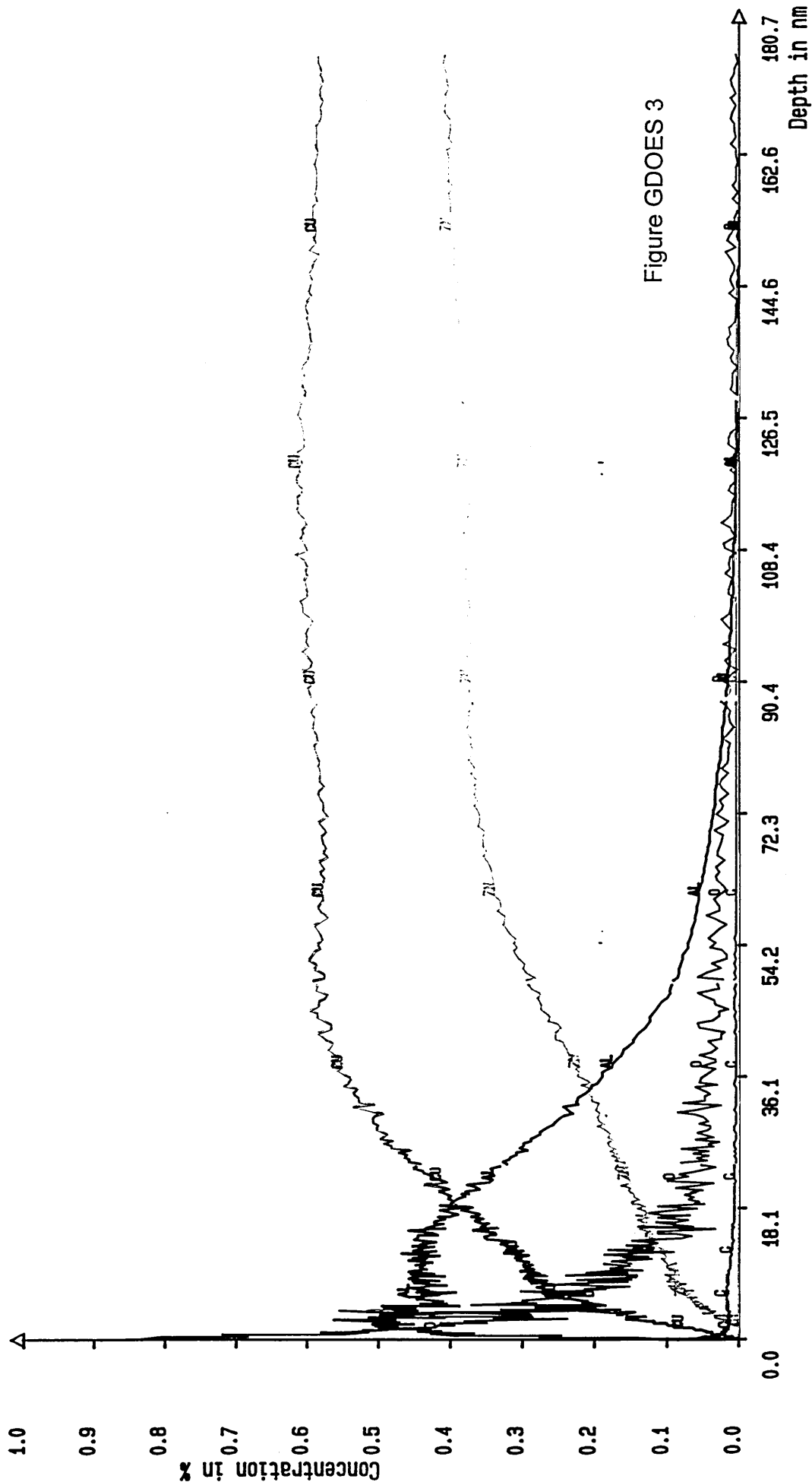


Figure GDOES 3

Materials Research Inst.
Sheffield Hallam Univ.

Tel. 0114 2533500

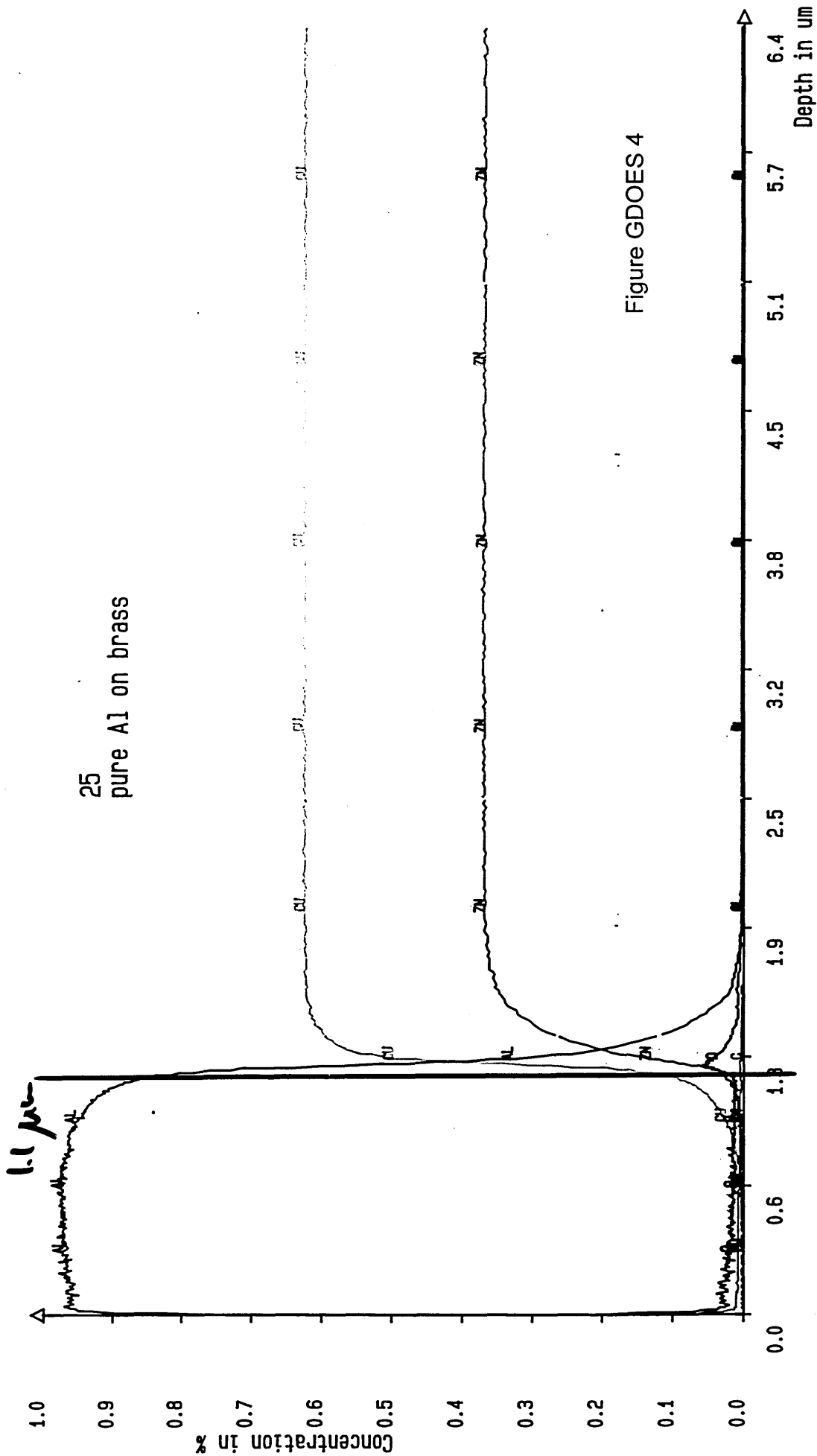
C:\LECO\SDPA\DATA\25.0RH

DATE 95-06-19 15:01
CLOCK
MTH.NAME PRESSURE
UNIQUNT Endlevel
EXITATION
700 V Contr1 : 30 mA

Element	Range
AL	100.0 %
O	100.0 %
C	100.0 %
CU	100.0 %
ZN	100.0 %

V - Average : 692 V
I - Average : 31.5 mA
P - Average : 21.8 W

y-Axis = a%



Materials Research Inst.
Sheffield Hallam Univ.

Tel. 0114 2533500

DATE 95-06-19

CLOCK 15:07

MTH.NAME PRESSURE

UNIQUNT Endlevel

EXITATION

700 V Contr1 : 30 mA

Element

AL

NB

O

C

CU

ZN

Range

100.0 %

100.0 %

100.0 %

100.0 %

100.0 %

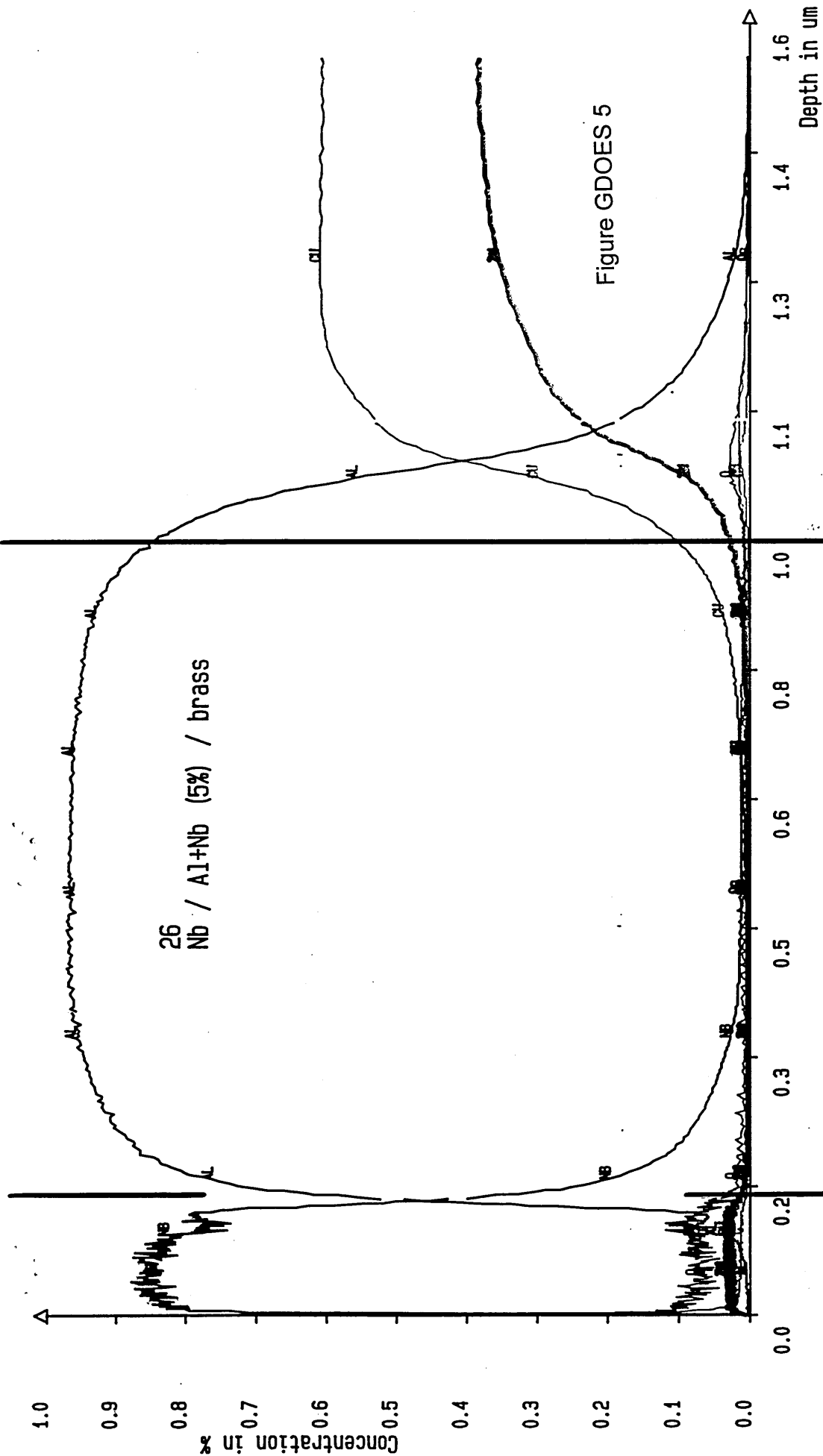
100.0 %

V - Average : 690 V

I - Average : 31.2 mA

P - Average : 21.6 W

y-Axis = a%



Materials Research Inst.
Sheffield Hallam Univ.

Tel. 0114 2533500

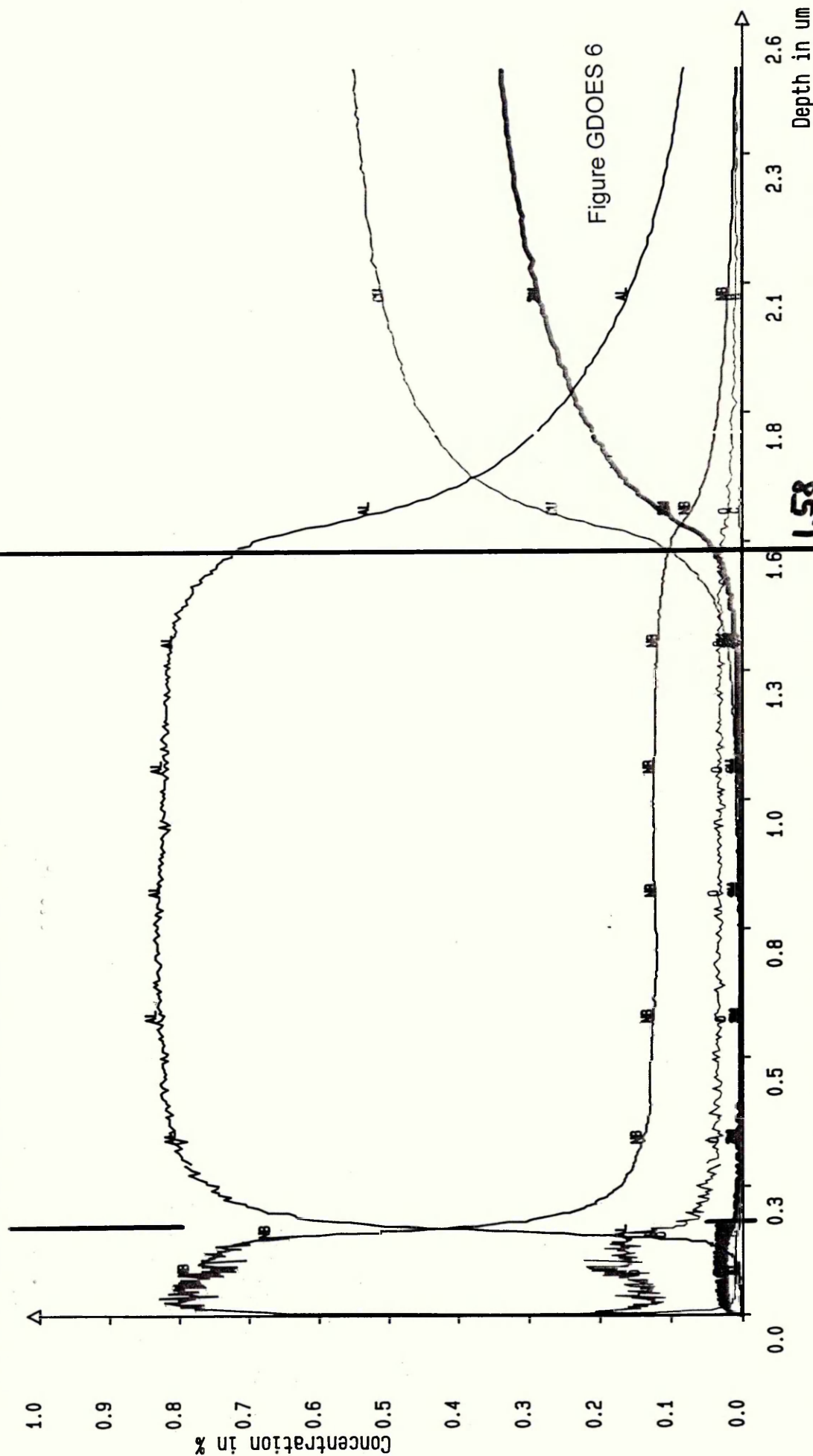
C:\LECO\SDPA\DATA\28.0RH

DATE 95-06-19 15:25
CLOCK 15:25
MTH.NAME PRESSURE
UNIQ.UANT Endlevel
EXITATION
700 V Contr1 : 30 mA

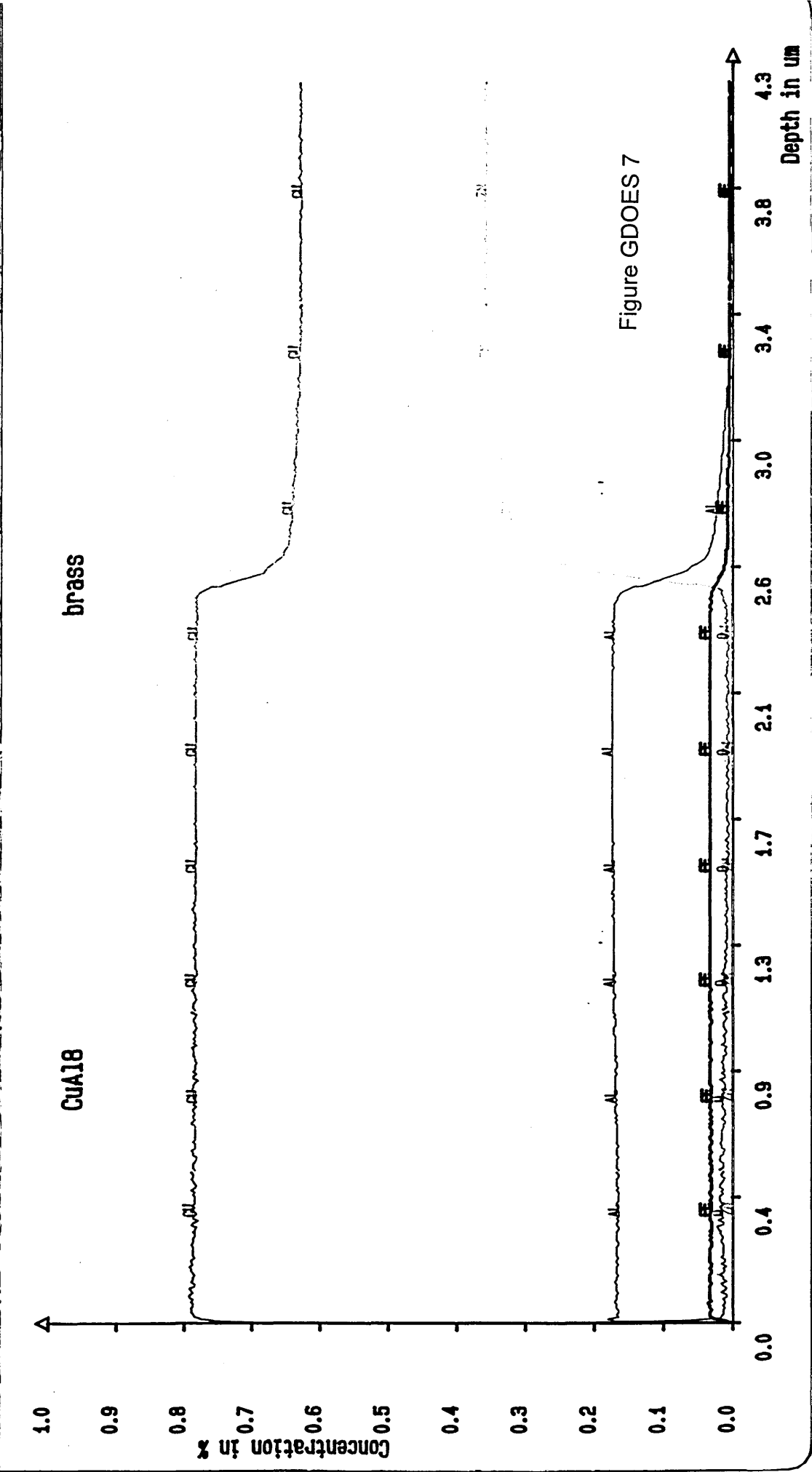
Element	Range
AL	100.0 %
NB	100.0 %
O	100.0 %
C	100.0 %
CU	100.0 %
ZN	100.0 %

V - Average : 691 V
I - Average : 31.2 mA
P - Average : 21.5 W

y-Axis = a%



Materials Research Inst. Sheffield Hallam Univ. Tel. 0114 2533500	DATE 95-07-20 CLOCK 10:29 MTH.NAME PRESSURE UNIQUE UNlevel EXITATION 700 V Contrl : 30 mA	Element FE AL O CU Zn	Range 100.0 % 100.0 % 100.0 % 100.0 % 100.0 %	V - Average : 681 V I - Average : 31.2 mA P - Average : 21.6 W y-Axis = a%
C:\LECO\SDPA\DATA\34.0HH				



Materials Research Inst.
Sheffield Hallam Univ.

Tel. 0114 2533500

C:\LECO\SDPA\DATA\39.00H

DATE 95-07-20 11:04

MTH.NAME PRESSURE

UNIQUEANT Endlevel

EXITATION

700 V Control : 30 mA

Element

FE

AL

NB

O

CU

ZN

Range

100.0 %

100.0 %

100.0 %

100.0 %

100.0 %

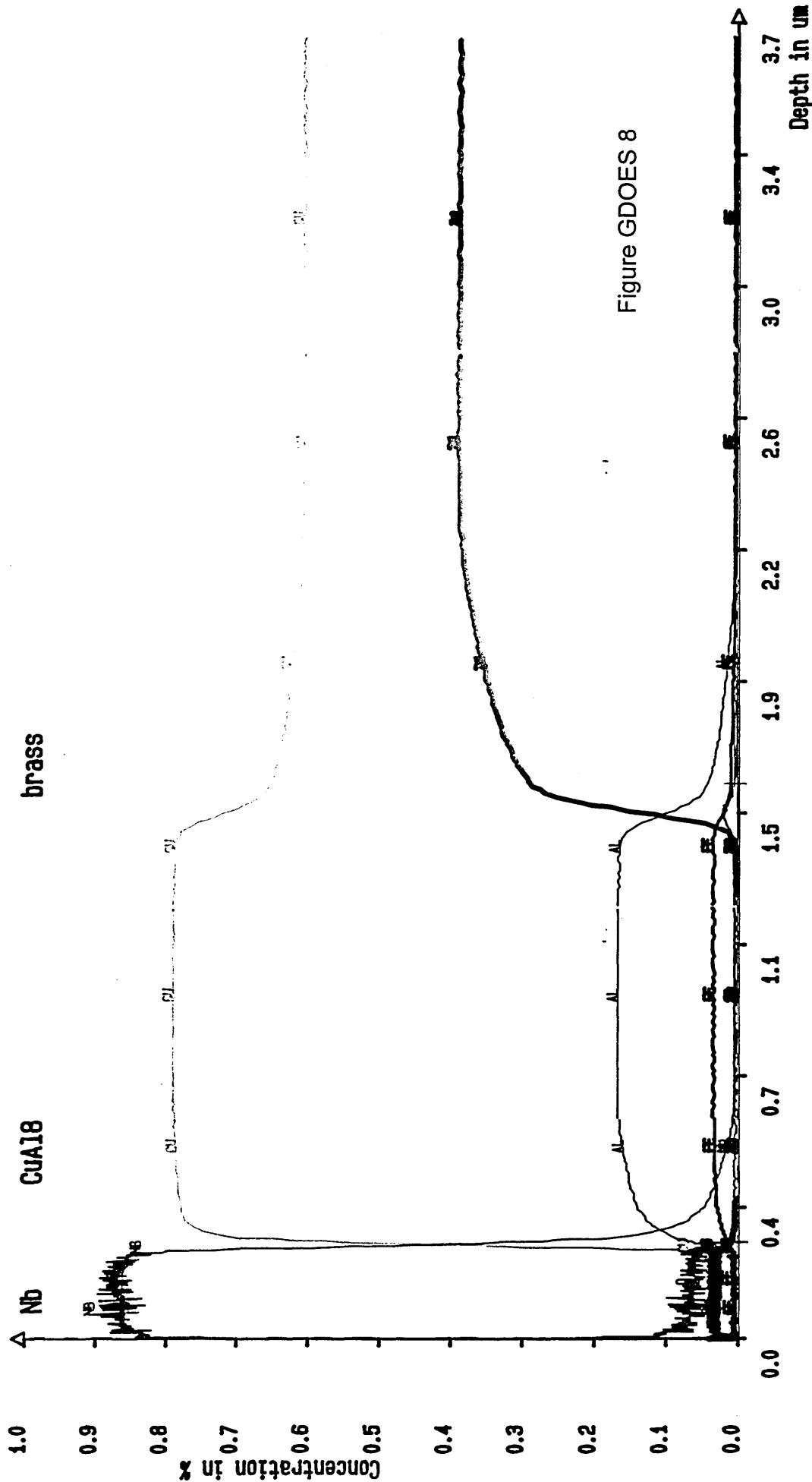
100.0 %

V - Average : 691 V

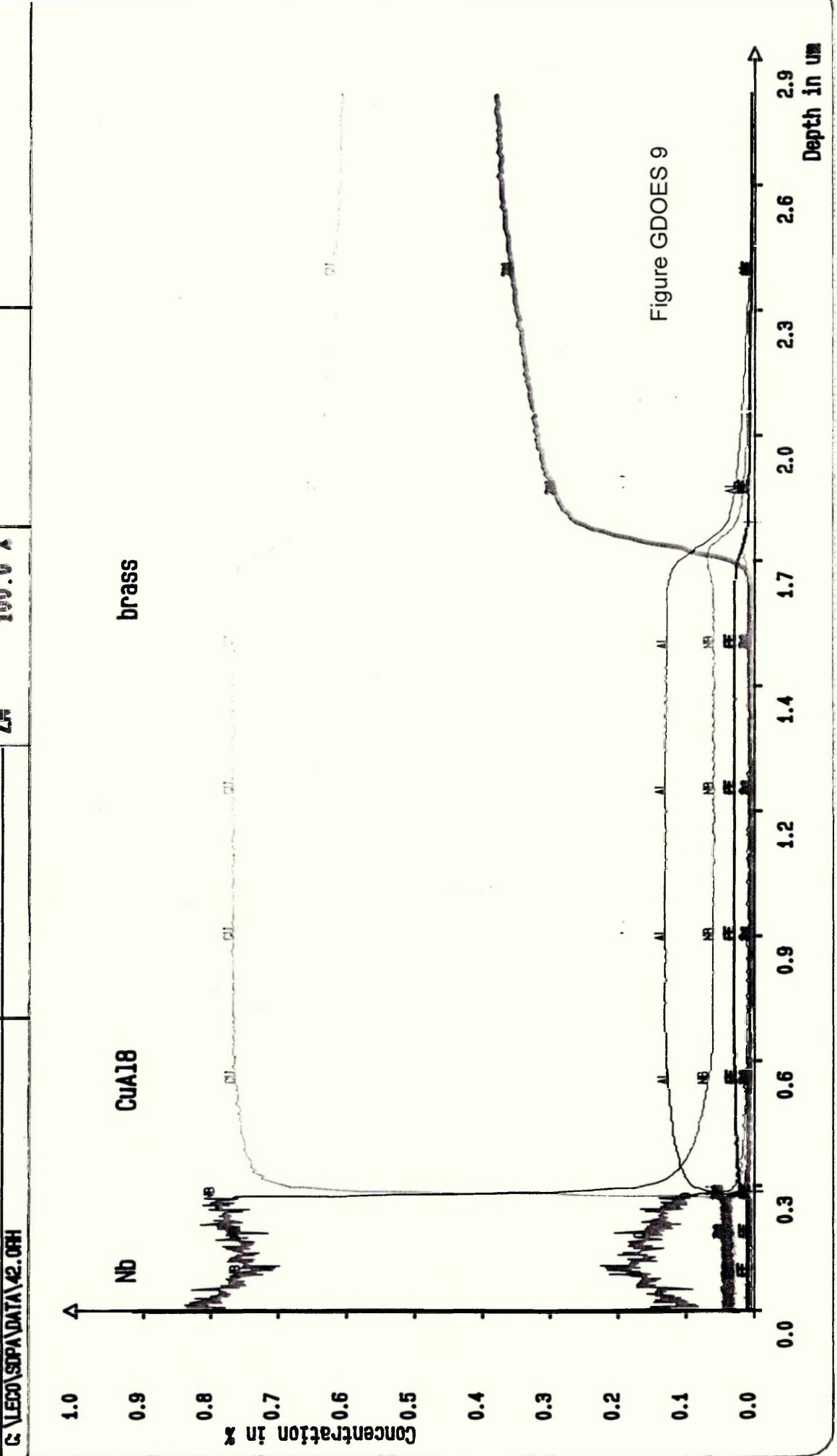
I - Average : 30.7 mA

P - Average : 21.2 W

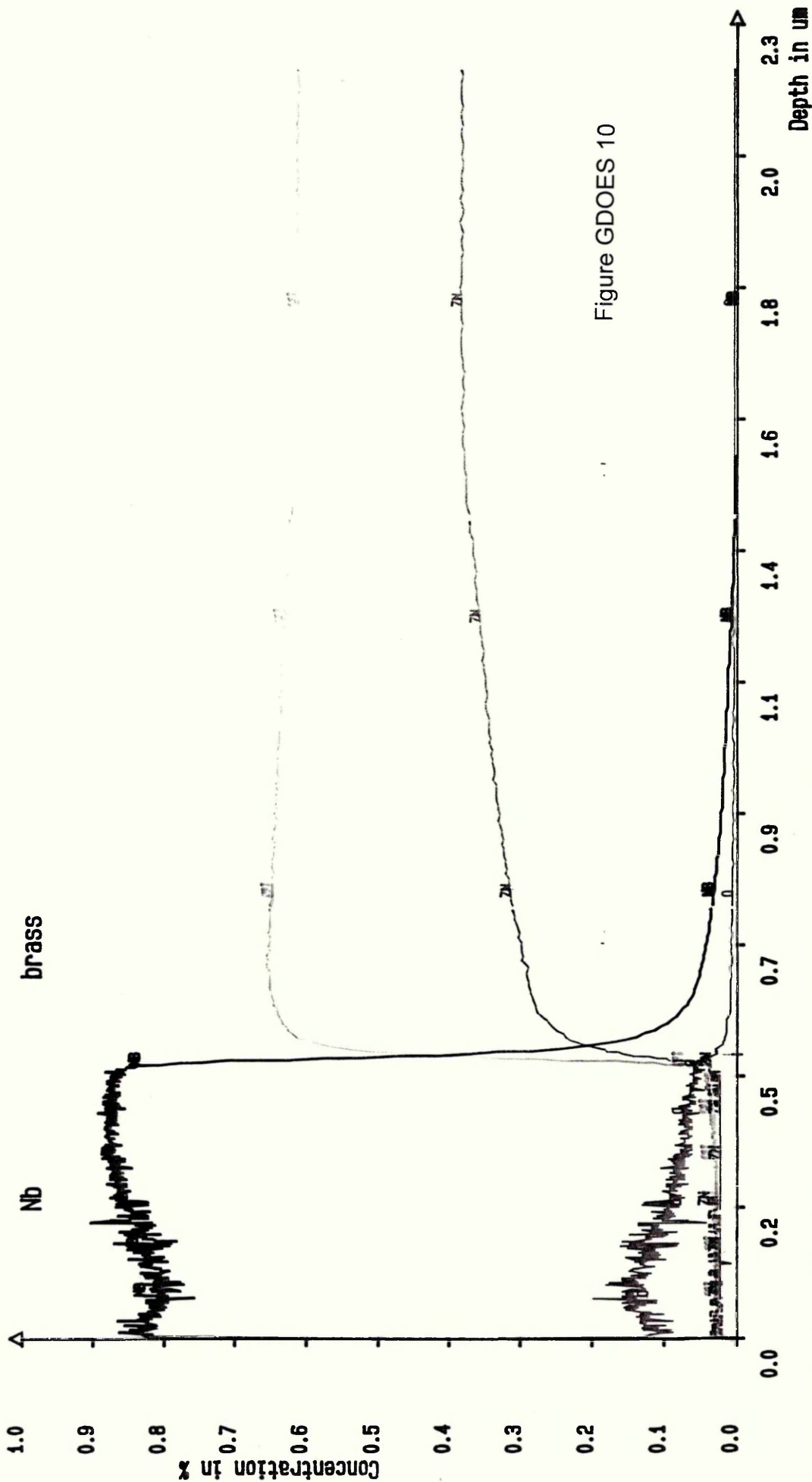
y-Axis = aX



<p>Materials Research Inst. Sheffield Hallam Univ.</p> <p>Tel. 0114 2533500</p>	<p>DATE 95-07-20 CLOCK 11:17 MTH.NAME PRESSURE UNIQUNT Endlevel EXITATION 700 V Control : 30 mA</p>	<p>Element FE AL NB O CU Zn</p> <p>Range 100.0 % 100.0 % 100.0 % 100.0 % 100.0 % 100.0 %</p>		<p>V - Average : 691 V I - Average : 31.2 mA P - Average : 21.6 W</p> <p>y-Axis = aZ</p>
---	---	--	--	--



Materials Research Inst. Sheffield Hallam Univ. Tel. 0114 2533500	DATE 95-07-20 CLOCK 10:25 MTH.NAME PRESSURE UNIQUE UNQUANT Endlevel EXITATION 700 V Contrl : 30 mA	Element NB 0 CU ZN	Range 100.0 % 100.0 % 100.0 % 100.0 %	V - Average : 691 V I - Average : 31.2 mA P - Average : 21.6 W
	y-Axis = a%			



Chap	Cleaning	Roughness [μm]			
		Ra	Rq	Rp	Rt
R 3.1	GD 20 min, -800 V	0.0148	0.0181	0.0533	0.1059
R 3.2	IE 7 min, -600 V	0.0465	0.0586	0.1586	0.4023
	IE 7 min, -800 V	0.0401	0.0524	0.1168	0.4750
	IE 7 min, -1000 V	0.0504	0.0936	0.6843	1.2489
	IE 7 min, -1200 V	0.0489	0.1581	1.4923	1.6106
R 3.3	GD 20 min, -800V + IE 1 min, -800V	0.0150	0.0194	0.1496	0.2375
	GD 20 min, -800V + IE 1 min, -1000V	0.0193	0.0241	0.0728	0.1948
	GD 20 min, -800V + IE 1 min, -1200V	0.0197	0.0246	0.1853	0.2636

Table 1. Roughness Characteristics of Ra, Rq, Rp and Rt depending on the cleaning process in the PVD-chamber, GD = Glow Discharge, IE = Ion Etching

No.	Description	Substrate Cleaning				Coating I				Coating II Niobium				Properties		Vickers adh.	Diffusion	Corr.-Test
		I [A]	U [V]	U Bias [V]	I coil [A]	t [min]	P [kW]	P Nb [kW]	U Bias [V]	I coil [A]	t [min]	P [kW]	U Bias [V]	I coil [A]	t [min]			
1	Al 150-176 °C	100		-1200		7	2x5			-50 4x6	60					(+)		(+)
2	Al 112-138 °C	100		-1200		4	2x5			-50 4x6	60					(+)		(+)
3	Al 135-180 °C	100		-800		7	2x5			-50 4x6	60					(+)		(+)
4	Al 60-152 °C	100	-120	-1200 4x3		20	2x5			-50 4x5	60					(+)	25'	(+)
5	Al 73-135 °C	100		-1200		7	2x5			-50 4x3	40					(+)	30'	(+)
6	Al 70-135 °C	100		-1200		7	2x5			-50 4x2	60					(+)		(+)
7	Al 100-130 °C	70		-800		3	2x5			-50 4x1.5	60					(+)	30'	(+)
8	Al + Nb	100		-1200		7	2x5			-50 4x2	60	8	-75 4x3		30	(+)		(+)
9	Al + Nb 5% + Nb	70		-800		3	2x5	0.5		-50 4x1.5	60	8	-75 4x3		30	(+)	35'	(+)
10	Al + Nb 10% + Nb	70		-800		3	2x5	1		-50 4x1.5	60	8	-75 4x3		30	(+)		(+)
11	Al + Nb 20% + Nb	70		-800		3	2x5	2		-50 4x1.5	60	8	-75 4x3		30	(+)		(+)
12	Al + Nb 50% + Nb	70		-800		3	2x5	5		-50 4x1.5	60	8	-75 4x3		30	(+)	40'	(+)
13	Nb 138-184 °C	70		-800		3				-50 4x3	60					(+)	55'	(+)
14	Nb 215-231 °C	70		-800		3				-50 4x3	60					(+)	50'	(+)
15	Nb 150-194 °C	80		-800		3				-50 4x3	60					(+)	50'	(+)
16	Nb 150-196 °C	80		-800		3				-50 4x4	60					(+)	50'	(+)
17	Nb 150-198 °C	80		-800		3				-50 4x5	60					(+)	55'	(+)
18	Nb 150-200 °C	80		-800		3				-50 4x8	60					(+)	40'	(+)
19	Nb 189-226 °C	75		-800		3				-75 4x3	60					(+)	50'	(+)
20	Nb 182-227 °C	70		-800		3				-100 4x3	60					(+)	45'	(+)
21	CuAl8 108-180 °C	80		-800		3	10			-75 4x6	60					(+)	55'	(+)
22	CuAl8 Nb I.E. 135-197 °C	80		-800		3	10			-75 4x6	60					(+)	50'	(+)
23	CuAl8 87-133 °C	80		-800		3	10			-75 4x6	30					(+)	45'	(+)
24	CuAl8 203-278 °C	80		-800		3	10			-75 4x6	30					(+)		(+)
25	CuAl8 141-265 °C	80		-800		3	20			-75 4x6 > 4x2	43					(+)		(+)
26	CuAl8 + Nb	80		-800		3	10			-75 4x6	30	10	-75 4x3		30	(+)		(+)
27	CuAl8 + Nb	80		-800		3	15			-75 4x3	55	10	-75 4x3		30	(+)		(+)
28	CuAl8 + Nb	80		-800		2	15			-75 4x3	60	10	-75 4x3		60	(+)		(+)
29	CuAl8 + Nb	80		-800		3	20			-75 4x2	30	10	-75 4x3		30	(+)		(+)
30	CuAl8 + Nb 5% + Nb	80		-800		3	10	0.5		-75 4x6	30	10	-75 4x3		30	(+)	40'	(+)
31	CuAl8 + Nb 10% + Nb	80		-800		3	10	1		-75 4x6	30	10	-75 4x3		30	(+)		(+)
32	CuAl8 + Nb 20% + Nb	80		-800		3	10	2		-75 4x6	30	10	-75 4x3		30	(+)		(+)
33	CuAl8 + Nb 50% + Nb	80		-800		3	10	5		-75 4x6	30	10	-75 4x3		30	(+)	55'	(+)

Table 2. Process parameters and summary of results

Sample ident =
 Further info =
 Kappa list = 16-Feb-95 Channel list = 22-Dec-94
 Calculated as : Elements Spectral impurity data : Teflon-----
 X-ray path = Vacuum Film type = No supporting film
 Case number = 4 Unknown Mass/Area (multi-element mono-layer)
 Eff.Diam = 24 mm Eff.Area = 452.2 mm2
 KnownConc = 0 %
 Rest = 0 %
 Dil/Sample = 0
 Viewed mass = ?
 Sample height = 0 mm

< means that the concentration is < 50 ppm

<2e means that Conc < 2 x StdErr

Z	wt%	StdErr	Z	wt%	StdErr	Z	wt%	StdErr
SumBe..F	0	0.38	29 Cu	89.8	3.6	51 Sb	<2e	
11 Na	<		30 Zn	<		52 Te	<	
12 Mg	<2e		31 Ga	<		53 I	<	
13 Al	7.4	0.1	32 Ge	<		55 Cs	<2e	
14 Si	<		33 As	<		56 Ba	<2e	
15 P	<		34 Se	<		SumLa..Lu	0.07	0.37
16 S	<		35 Br	<		72 Hf	<	
16 So	<		37 Rb	<		73 Ta	<	
17 Cl	<		38 Sr	<		74 W	<	
18 Ar	0.007	0.002	39 Y	<		75 Re	<	
19 K	<		40 Zr	<		76 Os	<	
20 Ca	<		41 Nb	<		77 Ir	<	
21 Sc	0.008	0.003	42 Mo	<2e		78 Pt	<	
22 Ti	<		44 Ru	<		79 Au	<	
23 V	<		45 Rh	<		80 Hg	<	
24 Cr	<		46 Pd	<2e		81 Tl	<	
25 Mn	<2e		47 Ag	<		82 Pb	<	
26 Fe	2.78	0.08	48 Cd	<		83 Bi	<	
27 Co	<		49 In	<2e		90 Th	<	
28 Ni	<		50 Sn	<		92 U	<	

==== Light Elements =====

==== Noble Elements =====

===== Lanthanides =====

4 Be		44 Ru	<	57 La	<
5 B		45 Rh	<	58 Ce	<2e
6 C		46 Pd	<2e	59 Pr	<
7 N		47 Ag	<	60 Nd	<
8 O		75 Re	<	62 Sm	<2e
9 F	<	76 Os	<	63 Eu	<2e
		77 Ir	<	64 Gd	<
		78 Pt	<	65 Tb	<2e
		79 Au	<	66 Dy	<
				67 Ho	<
				68 Er	<
				69 Tm	<
				70 Yb	<
				71 Lu	<

KnownConc= 0

REST= 0

D/S= 0

Calculated Mass/Area =

9.92 mg /4.52 cm2

21.9 g/m2 CountPrec = 0.5%

Table 3. XRF analysis of the CuAl8 target

Deutschland	International	Vereinigte Staaten von Amerika (USA)	Großbritannien	Frankreich	
Kupfer-Aluminium-Knetlegierungen					
DIN 17665	ISO ¹⁾ 428	UNS ²⁾ Alloy No.	ASTM ³⁾	BS ⁴⁾	NF ⁵⁾
			Alloy No.	neue Bezeichnung	alte Bezeichnung
CuAl5As	CuAl5As	C 60800	B 111 (608); B 359 (608); B 395 (608)	—	CuAl6 U-A6
CuAl8	CuAl8	C 61000	B 169 (610)	—	CuAl8 U-A8
CuAl8Fe3	CuAl8Fe3	C 61400	B 150 (614); B 169 (614) B 171 (614); B 432 (614)	CA 106 2874; 2875	CuAl7Fe2 U-A8Fe
CuAl9Mn2	CuAl9Mn2	—	—	—	CuAl9Mn2 U-A9M
CuAl9Ni3Fe2	CuAl9Ni3Fe2	—	—	—	CuAl9Ni3Fe2 U-A9N3Fe
CuAl10Fe3Mn2	CuAl10Fe3Mn2	C 62300	B 124 (623); B 150 (623) B 283 (623)	CA 105 2874	CuAl9Fe3Mn2 CuAl11Fe3Mn2 U-A9Fe3 U-A11Fe3
CuAl10Ni5Fe4	CuAl10Ni5Fe4	C 63200	—	CA 104 2872, 2874, 2875	CuAl9Ni5Fe3Mn U-A10N
CuAl11Ni6Fe5	—	—	—	—	CuAl11Ni5Fe5 U-A11N5Fe
Kupfer-Aluminium-Gußlegierungen					
DIN 1714	ISO ¹⁾ 1338	UNS ²⁾ Alloy No.	ASTM ³⁾	BS ⁴⁾	NF ⁵⁾
			Alloy No.	neue Bezeichnung	alte Bezeichnung
G-CuAl10Fe	CuAl10Fe3	C 95200	B 148-9A; B 271-9A; B 505	AB 1 1400	CuAl9Fe3 U-A9Fe3
G-CuAl9Ni	—	—	—	—	CuAl9Ni3Fe U-A9N3Fe
G-CuAl10Ni	CuAl10Fe5Ni5	C 95800	—	AB 2 1400	CuAl9Ni5Fe U-A9N5Fe
G-CuAl11Ni	—	—	—	—	CuAl11Ni5Fe U-A11N5Fe
G-CuAl8Mn	—	—	—	—	—

Table 6.4: CuAl alloys

APPENDIX



P3-galvaclean 62

Elektrolytische Entfettung, Entrostung und Aktivierung

Anwendungsgebiete:	Elektrolytische Entfettung und Aktivierung von Stahl bei anodischer Polarisation. Entfernung von Rost und geringen Zunderbelägen bei wechselnder Polarisation.
Zusammensetzung:	Alkalien Carbonate Phosphate
Aussehen:	Pulver
Schüttgewicht:	ca. 1200 g/l
Arbeitsverfahren:	Elektrolytische Behandlung
Badansatz:	Das Pulver wird dem auf ca. 40 – 50 °C vorgewärmten Wasser langsam unter Umrühren zugegeben. Das Bad darf erst dann in Betrieb genommen werden, wenn sich der Reiniger vollständig aufgelöst hat. Nach der Entfettung muß vor einer weiteren Oberflächenveredlung eine Wasserspülung der Werkstückoberfläche erfolgen.
Anwendungskonzentration:	50 – 200 g/l
Anwendungstemperatur:	20 – 70 °C
Behandlungszeit:	1 – 15 min, je nach Stärke des Oxidbelages
Stromdichte:	5 – 20 A/dm ²
Titrierfaktor:	4,4 g/(l * ml) bei Titration von 5 ml Badlösung mit 0,5 n HCl gegen Methylorange
Schaumverhalten:	nicht schaubildend
pH-Wert:	13,5 +/- 0,2 in einer Lösung von 10 g/l
Elektrische Leitfähigkeit:	44 mS/cm in einer Lösung von 10 g/l bei 20 °C Temperaturkoeffizient: 1,84 %/°C
Behältermaterial:	Stahl
Abwasserbehandlung:	Für 1 kg P3-galvaclean 62 werden 4,5 kg 25 %ige Schwefelsäure zur Neutralisation benötigt.

Aufgrund der während des Waschvorgangs eingeschleppten Verunreinigungen des Reinigungsgutes ist eine Abwasserbehandlung oder ggf. Entsorgung entsprechend den örtlichen Einleiterrichtlinien notwendig.



RST

Issue 1 ; page 1 of 2
Revision Date:
27 February 1995

PRODUCT DATA SHEET

GENERAL PURPOSE HOT SOAK CLEANER FOR ALL METALS

1. COMPOSITION AND PROPERTIES

RST is a very cost effective hot soak cleaner, which does not contain free caustic alkali and can safely be used on sensitive metals such as aluminium and its alloys.

RST is a highly efficient silicate-buffered alkaline powder product containing polymeric phosphates and a combination of wetting agents.

RST is suitable for use on all metals and has good water softening and 'wetting out' properties.

Product Uses

RST has been developed for heavy-duty soak and agitated immersion cleaning for all metals, including aluminium and zinc and their alloys. It is particularly suitable for removing pressing oils, cutting oils and lapping pastes, and produces excellent results on ground or polished surfaces.

RST does not affect the alloys of aluminium, copper, tin or zinc, and may be used to clean different metals simultaneously. RST may give a slight dulling to mirror polished aluminium if used over an extended contact time.

When used at 90°C, RST will strip alkaline-sensitive paints from light metal substrates.

RST has very good emulsifying properties and is an ideal product for soak and agitated immersion of used parts in engines and gear boxes encrusted in oil and road dirt before stripping and reconditioning.

2. PHYSICAL PROPERTIES

Appearance	:	White powder
Reaction	:	Alkaline
pH (1% soln)	:	ca 12

3. METHOD OF USE

Initial make-up

RST dissolves readily in water above 50°C.

Concentration

1-4%

Temperature

60-90°C

Contact time

For agitated immersion cleaning, generally between 3 and 10 minutes, depending on the soil to be removed. Static immersion will usually need longer contact times.

For mirror finished aluminium, do not exceed 3 minutes.

4. HANDLING PRECAUTIONS

When using the working solutions avoid contact with skin and eyes. Wear rubber gloves and goggles. When handling the product, avoid inhaling dust.

5. EFFLUENT

Used RST must not be discharged to the main drainage without neutralisation, filtration of solids, and removal of any separating oil. Discharge of residual liquid to main drainage may require prior consent.

NOTE Each kg of RST will require approximately 2-5kg of 25% by weight sulphuric acid of, must be undertaken before the neutralisation

6. SOLUTION CONTROL

Titrate 50mls of RST solution against N/10 HCl using Methyl orange as the indicator.

Concentration % RST = mls N/10 HCl x 0.16

7. FURTHER INFORMATION

Full information on the hazards and safe handling of the product as supplied is given in the Material Health & Safety Data Sheet which must be read and understood by everyone handling or using this product.

The details given in this data sheet reflect our current technical knowledge and experience, and are not a legally binding assurance of characteristics or suitability for a specific purpose. Users must satisfy themselves that there are no circumstances requiring additional information or safety precautions relating to details given herein and must not practise or use any patented invention or trademark without prior approval.



Material Health & Safety Data Sheet.

1. Identification of Preparation and Company

Product **RST**

Intended Use

Powdered product used diluted with water for metal cleaning.

Supplier Henkel Metal Chemicals
Eton House
Waterside Drive
Langley
Berks SL3 6EZ
Tel: 01753 811108

24 Hour Emergency Tel: 0181-312 0291 (Quoting Reference CE1)

2. Composition/Information on Ingredients

Contains sodium silicate and organic surfactants.

CAS No.	Hazardous ingredient	%	Symbol	Risk Phrases
13472-30-5	Sodium Silicate	40	C	R34

3. Hazards Identification

Caustic alkaline mixture which is corrosive to all parts of the body. Eye contact may cause severe irritation.

4. First Aid Measures

4.1 Skin Contact

Drench the affected area with water and continue thorough washing with soap and water. Get medical attention if irritation or a skin rash develops.

4.2 Eye Contact

Flush eyes with large quantities of cool water holding eyelids apart. Continue irrigation for at least 10 minutes.

Caustic alkaline solutions are very damaging to the eyes.

GET MEDICAL ATTENTION IMMEDIATELY.

4.3 If Swallowed

Rinse mouth with water.

Give copious quantities of water to drink.

DO NOT INDUCE VOMITING

GET MEDICAL ATTENTION IMMEDIATELY

4.4 Inhalation

Move to fresh air.

Keep affected person warm and rested.

5. Fire Fighting Measures

Non flammable.

6. Accidental Release Measures

Do not contaminate drains.

Collect solid residues and place in polythene bags, refer to a specialist waste contractor for safe disposal.

Any small residues should be hosed to drain with plenty of water.

7. Handling & Storage

Avoid inhaling the dust. Handle only in conditions of good ventilation.

Avoid all contact with skin and eyes

Wear the personal protective equipment (PPE) specified in Section 8.

When handling follow good industrial hygiene practices.

8. Exposure Controls/Personal Protection

When handling the products wear PVC or rubber gloves and eye protection.

Wear a dust mask to BS 2091.

Environmental controls must be adequate to maintain atmospheric concentration below the OES otherwise respiratory protection must be worn.

9. Physical and Chemical Properties

Appearance - white or off white powder.

pH of 1% solution 12 -13.

Infinitely soluble in water.

10. Stability and Reactivity

Avoid contact with acids

11. Toxicological Information

Strongly alkaline caustic product which may cause chemical burns and ulcerations if skin contact is prolonged or treatment is delayed.

Eye contact is particularly serious and may cause permanent damage.

Inhalation of dust can cause serious injury to the respiratory tract and mucous membranes.

12. Ecological Information

There is no experimental data available for this product.

Non-selectively toxic to plants.

The product should not be allowed to enter drains or watercourses.

13. Disposal Considerations

Under the Control of Pollution (Special Waste) Regulations 1980, if this product has to be disposed of it must be classed as "Special Waste". Disposal must be in accordance with these Regulations and with the general requirements of the Control of Pollution Act 1974 preferably by a Specialist Waste Disposal Contractor.

The Environmental Protection Act 1990 introduces new controls on the disposal and deposit of waste. The Regulations and Guidance given under this Act introduce a 'Duty of Care' which must be observed.

14. Transport Considerations

Conveyance Classification

SI (UN) Number :1759

Packing Group :II

ADR Classification :8 item 41b

IMDG Classification :8

Emergency Schedule (EMS) Number :8-06

15. Regulatory Information

Named Substance : Sodium Silicate

Hazard Classification :Corrosive

Risk Phrases :R35

Safety Phrases :S2-26-37/39

16. Other Information

EH40 Occupational Exposure Limits - published annually by UK Health & Safety Executive.

The Control of Substances Hazardous to Health Regulations 1988 (SI 1988:1657).

Protection of Eyes Regulations 1974 published by HMSO.

This Data Sheet has been written in accordance with EC Directive 88/379/EEC.

All information is given in good faith but users must satisfy themselves that there are no circumstances requiring additional information or precautions or the verification of details given herein.

EXCEL Worksheet: Calculation of PVD-Coating properties

valid for the Phillips PW1820 diffractometer, Materials Research Institute

Sheffield Hallam University

wavelength X-ray radiation:

Material:

JCPDS-ICDD Card number:

modulus of elasticity:

POISSON value:

reference lattice parameter:

Reference Values

h	k	l	d-spacing
1	1	1	2.338
2	2	0	1.431
3	1	1	1.221
2	2	2	1.169
3	3	1	0.9289

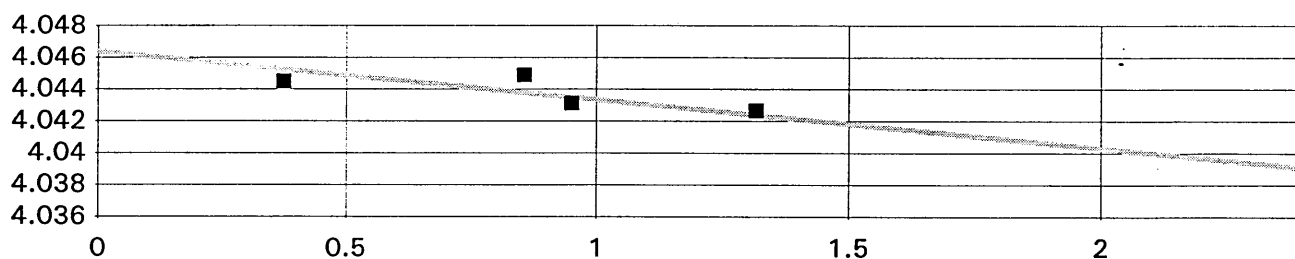
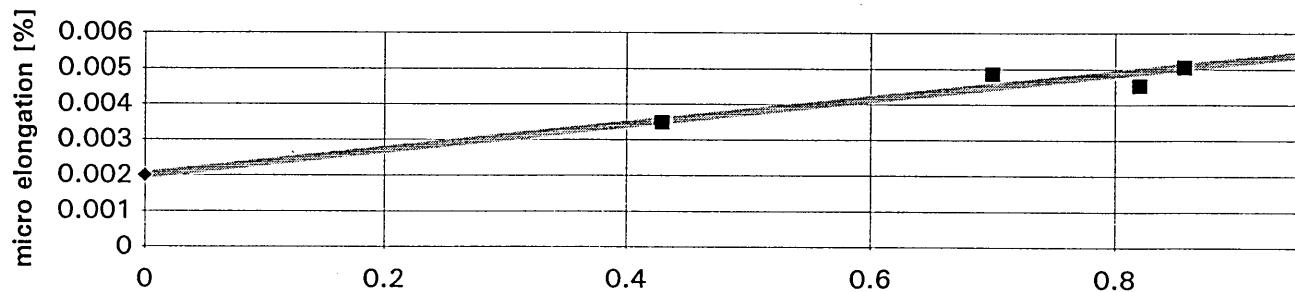
Nelson-Riley function:

macro elongation:

micro elongation:

tension condition:

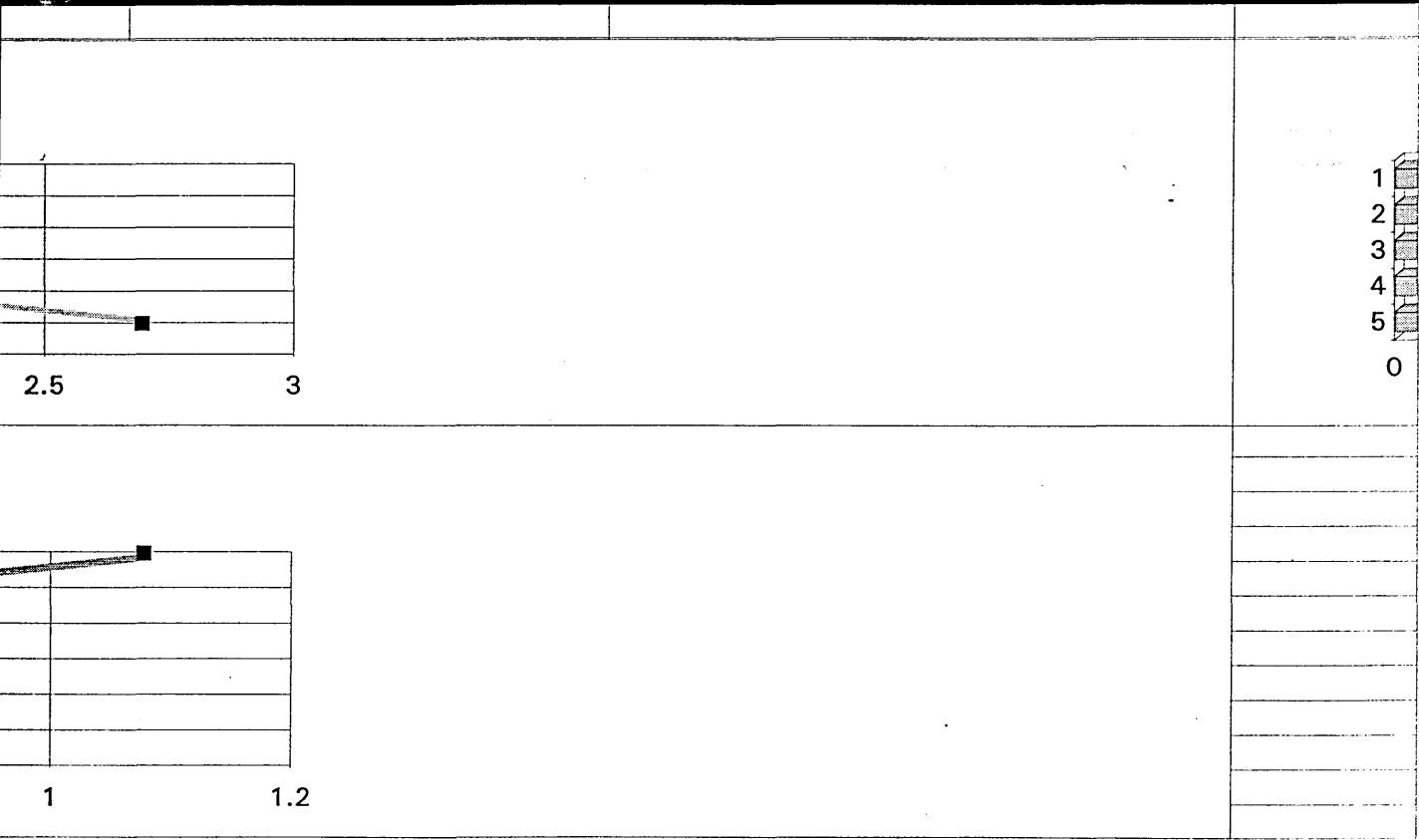
grain size:

Nelson-Riley Function**Hall-Williamson Function**

λ	1.54056	E-10 m	
	Al		
	4-787		
E	72000	N/mm^2	
μ	0.34		
a	4.0494	E-10 m	

		Fitted User Values	
intensity	peak	peak	broadening width
100	= 2*(ASIN(\$G\$5/(2*D16)))*180/PI()	38.587	0.38
47	= 2*(ASIN(\$G\$5/(2*D17)))*180/PI()	65.221	0.58
22	= 2*(ASIN(\$G\$5/(2*D18)))*180/PI()	78.377	0.598
24	= 2*(ASIN(\$G\$5/(2*D19)))*180/PI()	82.551	0.677
7	= 2*(ASIN(\$G\$5/(2*D20)))*180/PI()	112.23	1.045

	a =	= INTERCEPT(\$N\$16:\$N\$20,\$M\$16:\$M\$20)	
	ϵ =	= (G22-G11)/G11 * 100	%
	ϵ =	= T15/2 * 100	%
	$\sigma_1 + \sigma_2$ =	= (G9/G10) * G23 * (-1)/100	N/mm^2
	Dk =	= 1/(U15 * 10)	nm



[illegible]

[illegible]

Nelson-

Riley

graph

=INTERCEPT(\$N\$16:\$N\$20,\$M\$16:\$M\$20)

=J16*SQRT(A16^2+B16^2+C16^2)	=SLOPE(\$N\$16:\$N\$20,\$M\$16:\$M\$20)*M16+\$O\$15
------------------------------	---

=J17*SQRT(A17^2+B17^2+C17^2)	=SLOPE(\$N\$16:\$N\$20,\$M\$16:\$M\$20)*M17+\$O\$15
------------------------------	---

=J18*SQRT(A18^2+B18^2+C18^2)	=SLOPE(\$N\$16:\$N\$20,\$M\$16:\$M\$20)*M18+\$O\$15
------------------------------	---

=J19*SQRT(A19^2+B19^2+C19^2)	=SLOPE(\$N\$16:\$N\$20,\$M\$16:\$M\$20)*M19+\$O\$15
------------------------------	---

=J20*SQRT(A20^2+B20^2+C20^2)	=SLOPE(\$N\$16:\$N\$20,\$M\$16:\$M\$20)*M20+\$O\$15
------------------------------	---

[illegible]

[illegible]

EXCEL Worksheet: Calculation of PVD-Coating properties

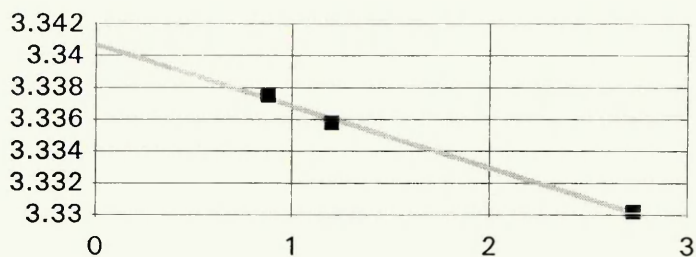
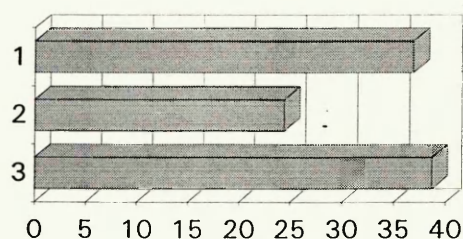
valid for the Phillips PW1820 diffractometer, Materials Research Institute

Sheffield Hallam University

wavelength X-ray radiation:	λ	1.54056	E-10 m
Sample:	Nb on brass (32)		
coating thickness		0.43	μm
Material:		Nb	
JCPDS-ICDD Card number:		35-789	
modulus of elasticity:	E	104900	N/mm ²
POISSON value:	μ	0.397	
reference lattice parameter:	a	3.3066	E-10 m

Reference Values						Fitted User Values				TEXTURE [%]
h	k	l	d-spacing	intensity	peak	peak	broadening width	intensity area	d real	
1	1	0	2.3379	100	38.47385	38.187	0.527	3024.4	2.35479919	36.882619
2	1	1	1.3499	20	69.58695	68.891	0.989	400.72	1.36182805	24.434266
2	2	0	1.1688	5	82.45262	81.504	1.16	158.6	1.17998819	38.683116

Nelson-Riley function:	a =	3.340691	
macro elongation:	ϵ =	1.031006	%
micro elongation:	ϵ =	0.509463	%
tension condition:	$\sigma_1 + \sigma_2$ =	-2724.244	N/mm ²
grain size:	Dk =	119.0164	nm
			-6.33545167 GPa / μm

Nelson-Riley Function**Texture****Hall-Williamson Function**